

THE UNIVERSITY OF MICHIGAN  
INDUSTRY PROGRAM OF THE COLLEGE OF ENGINEERING

CALCULATION OF GAMMA RAY SCINTILLATION DETECTOR  
EFFICIENCIES AND PHOTOFRACTIONS BY MONTE CARLO METHODS

Bernard J. Snyder

A dissertation submitted in partial fulfillment  
of the requirements for the degree of  
Doctor of Philosophy in the  
University of Michigan  
Department of Nuclear Engineering  
1965

May, 1965  
IP-706

Doctoral Committee:

Assistant Professor Glenn F. Knoll, Chairman  
Assistant Professor Ziyaeddin Akcasu  
Professor Dietrich H. Vincent  
Associate Professor Franklin H. Westervelt

Dedicated to the Memory  
of my Father

Jesse Snyder



## ACKNOWLEDGEMENTS

The subject of this investigation was first suggested to the author by Dr. Geza L. Gyorey, who served as chairman of the doctoral committee in the initial stages of the work. It is a pleasure to acknowledge the assistance of Dr. Knoll, as chairman of doctoral committee throughout most of this investigation. The other members of the committee offered aid during various stages of the work, for which the author is appreciative.

Many helpful conversations were held with K. Wainio who, as a colleague of the author, gave assistance in formulating part of the Monte Carlo programs. The cooperation of the staff of the University of Michigan Computing Center, in particular F. Little, contributed to the successful completion of this research. The author is grateful for financial assistance provided by three Atomic Energy Commission Pre-doctoral Fellowships; and the Industry Program, College of Engineering, The University of Michigan.

I wish to express my appreciation for the assistance given by my family, in particular my mother. Finally, I will be forever indebted to my wife, Sondra, for her unselfish help and encouragement.



TABLE OF CONTENTS

	<u>Page</u>
ACKNOWLEDGEMENTS.....	iii
LIST OF TABLES.....	viii
LIST OF FIGURES.....	xi
 CHAPTER	
I INTRODUCTION.....	1
A. Gamma Ray Scintillation Spectrometry.....	3
B. Absolute Total Efficiency.....	6
C. Absolute Peak Efficiency.....	8
D. Photofraction.....	10
E. Intrinsic Total and Intrinsic Peak Efficiencies..	11
F. Calculation of the Absolute Total Efficiencies and Photofractions.....	11
II CALCULATION OF THE ABSOLUTE TOTAL EFFICIENCY.....	13
A. Definition of Absolute Total Efficiency ( $\epsilon_{AT}$ ).....	13
1. Isotropic Point Kernel for $\epsilon_{AT}$ .....	15
2. $\epsilon_{AT}$ for On-axis Point Sources.....	20
3. $\epsilon_{AT}$ for Disk and Cylindrical Volume Sources.....	22
4. Geometry Factors.....	23
B. Calculation of $\epsilon_{AT}$ .....	24
C. Checks Applied to Calculated $\epsilon_{AT}$ Results.....	24
D. Results of $\epsilon_{AT}$ Calculations.....	30
1. On-axis Point Sources.....	31
2. Off-axis Point Sources.....	37
3. Disk Sources.....	43
4. Cylindrical Volume Sources.....	49
E. Other Factors Effecting $\epsilon_{AT}$ .....	56

TABLE OF CONTENTS (CONT'D)

	<u>Page</u>
F. Accuracy of $\epsilon_{AT}$ Results.....	60
G. Extrapolation of Tabulated Results.....	63
1. Other Crystal Sizes.....	63
2. Other Source Energies.....	64
III APPLICATION OF MONTE CARLO TECHNIQUES TO CALCULATION OF PHOTOFRACTIONS.....	68
A. Principles of Monte Carlo Calculations.....	68
1. Cumulative Probability Technique.....	72
2. Rejection Techniques.....	74
B. Path Length Sampling.....	77
C. Gamma Interactions.....	78
1. Photoelectric Absorption.....	79
2. Compton Scattering.....	80
3. Pair Production.....	81
D. Secondary Gammas and Electrons.....	81
E. Typical Histories.....	83
IV DETAILS OF THE MONTE CARLO CALCULATIONS FOR PHOTOFRACTIONS.....	86
A. Source Geometries Considered.....	86
1. Isotropic Source Routines.....	87
a. Solid Crystal - Point Source.....	89
b. Well Crystal - Point Source.....	91
c. Extension to Other Isotropic Sources.....	97
2. Collimated Beam Sources.....	98
B. Gamma Interactions.....	99
1. Interaction Processes Considered.....	99
2. Secondary Gamma Treatment.....	100



TABLE OF CONTENTS (CONT'D)

	<u>Page</u>
3. Photoelectric Events.....	101
4. Compton Events.....	102
5. Pair Production Events.....	103
C. Approximation of Electron Transport.....	105
D. Bremsstrahlung Production.....	110
E. Escape Routines.....	119
F. Termination Categories.....	120
G. Photofraction Standard Deviation.....	121
H. Absorption and Scattering in the Source.....	123
V RESULTS FROM THE MONTE CARLO CALCULATIONS.....	129
A. Comparison of Experimental and Calculated Results.....	129
1. Solid Crystals.....	130
2. Well Crystals.....	135
B. Effects of Bremsstrahlung and Electron Escape on Photofraction.....	139
C. Effect of Geometry on Photofractions.....	140
1. Isotropic Sources.....	140
2. Collimated Beam Sources.....	144
3. Comparison of Solid and Well Crystal Photofraction.....	147
D. Comparison of Monte Carlo and Integration Results.....	147
E. Photofractions Calculated for NaI.....	150
F. Photofractions for Materials other than NaI.....	151
VI CONCLUSIONS.....	155
A. Summary of Results.....	155
1. Absolute Total Efficiencies ( $\epsilon_{AT}$ ).....	155
2. Photofractions.....	156

TABLE OF CONTENTS (CONT'D)

	<u>Page</u>
B. Application of Results.....	157
C. Extension of Results.....	157
 APPENDICES	
A DERIVATION OF EXPRESSIONS FOR THE ABSOLUTE TOTAL EFFICIENCY.....	159
B SERIES SOLUTION FOR THE TOTAL EFFICIENCY.....	171
C DERIVATION OF KAHN'S METHOD FOR SAMPLING FROM THE KLEIN-NISHINA FORMULA.....	175
D WELL CRYSTAL ESCAPE ROUTINE.....	178
E INSTRUCTIONS FOR COMPUTER PROGRAMS FOR CALCULATION OF THE ABSOLUTE TOTAL EFFICIENCY AND PHOTOFRACTIONS..	186
F METHOD OF SELECTING FROM A UNIFORM AZIMUTHAL DISTRIBUTION OF DIRECTIONS.....	200
G TABULATED VALUES FOR ABSOLUTE TOTAL EFFICIENCIES.....	204
REFERENCES.....	226

LIST OF TABLES

<u>Table</u>		<u>Page</u>
II-1	Comparison of $\epsilon_{IT}$ Values for Point Sources on Centerline of Solid Crystals.....	25
II-2	Comparison of $\epsilon_{AT}$ Values for Point Sources on Centerline of 2 x 2 Inch Solid Crystal.....	26
II-3	Comparison of $\epsilon_{AT}$ Values for Point Sources on Centerline of 3 x 3 Inch Well Crystal.....	26
II-4	Comparison of $\epsilon_{AT}$ Values for Disk Sources on Centerline of 3 x 3 Inch Solid Crystal.....	29
II-5	Comparison of Solid Angles Subtended by Two Inch Diameter Solid Crystal at Off-axis Points.....	30
II-6	Isotropic Point Source Off Crystal Axis at Radial Distance = M, 3 x 3 Inch Solid Crystal.....	36
II-7	Isotropic Point Source Off Crystal Axis at Radial Distance = M, 2 x 2 Inch Solid Crystal.....	36
II-8	$\epsilon_{AT(M)}/\epsilon_{AT(M=0)}$ for 2 x 2 Inch Solid Crystal, at 1.0 MeV.....	37
II-9	Isotropic Point Source Off Crystal Axis at Radial Distance = M, 8F8 Well.....	42
II-10	Isotropic Point Source Off Crystal Axis at Radial Distance = M, 3 x 3 Inch Well Crystal.....	42
II-11	Total Gamma Ray Sections in Pure NaI, From References 20, 21, Used in Evaluating $\epsilon_{AT}$ .....	63
III-1	Fraction of Primary Interactions.....	84
III-2	Fraction of the 1000 Interacting Gammas That Have Exactly X Scatterings Prior to Absorption.....	84
III-3	Fraction of the 1000 Interacting Gammas That Have Exactly X Scatterings Prior to Escape.....	85

LIST OF TABLES (CONT'D)

<u>Table</u>		<u>Page</u>
III-4	Typical Pair Production Events.....	85
IV-1	Integration of the Differential Bremsstrahlung Spectra for NaI.....	114
IV-2	Absolute Total Efficiencies, Source Self Absorption and Scattering Included, 2 x 2 Inch Solid Crystal.....	123
IV-3	Absolute Total Efficiencies, Source Self Absorption and Scattering Included, 8F8 Well Crystal.....	128
V-1	Broad Beam Photofractions, 2 x 2 Inch Solid Crystal...	135
V-2	Comparison for Point Source, $\epsilon_{IP}$ , 3 x 3 Inch Well Crystal.....	136
V-3	Comparison for Point Source, $\epsilon_{AP}$ , 3 x 3 Inch Well Crystal.....	137
V-4	Comparison for Point Source, $\epsilon_{AP}$ , 5 x 5 Inch Well Crystal.....	137
V-5	Comparison for Point Source, $\epsilon_{AP}$ , 8F8 and 7F8 Well Crystals.....	138
V-6	Effect of Electron and Bremsstrahlung Losses on Photofractions, Isotropic Point Sources.....	139
V-7	Source Geometry Effect on Photofractions, 3 x 3 Inch Solid Crystal.....	143
V-8	Source Geometry Effect on Photofractions, 8F8 Well Crystal.....	143
V-9	Solid Crystal Photofractions, Isotropic Point Source on Axis.....	150
V-10	Well Crystal Photofractions, Isotropic Point Source on Axis.....	151

## LIST OF FIGURES

<u>Figure</u>		<u>Page</u>
I-1	Idealized Differential Spectrum for Gamma Ray Spectrometer.....	3
II-1	Solid Crystal Geometry.....	16
II-2	Well Crystal Geometry.....	17
II-3	$\epsilon_{AT}$ Variation with Radial Distance from Solid Crystal Axis (.662 MeV).....	27
II-4	$\epsilon_{AT}$ Variation with Radial Distance from Solid Crystal Axis (.075 MeV).....	28
II-5	$\epsilon_{IT}$ for 2 x 2 Inch Solid Crystal.....	32
II-6	Effect of Moving Point Source Axially from 2 x 2 Inch Solid Crystal.....	33
II-7	Effect of Moving Point Source Axially in 8F8 Well Crystal.....	34
II-8	Increase in $\epsilon_{AT}$ of Well Crystal (8F8) for Non-central Point Source.....	40
II-9	$\epsilon_{AT}$ Variation with Disk Diameter of 8F8 Well Crystal.....	44
II-10	$\epsilon_{AT}$ Variation with Disk Diameter for 12AW12-W2 Well Crystal.....	45
II-11	$\epsilon_{AT}$ Variation with Disk Position for 8F8 Well Crystal.....	46
II-12	$\epsilon_{AT}$ Variation with Disk Radius.....	48
II-13	$\epsilon_{AT}$ Variation with Cylindrical Volume Source Height for 8F8 Well Crystal.....	50
II-14	$\epsilon_{AT}$ Variation with Volume Source Height for 8F8 Well Crystal.....	51

LIST OF FIGURES (CONT'D)

<u>Figure</u>		<u>Page</u>
II-15	$\epsilon_{AT}$ Variation with Volume Source Height for 12AW12-W2 Well Crystal.....	52
II-16	$\epsilon_{AT}$ Variation with Volume Source Height for 2 x 2 Inch Solid Crystal.....	53
II-17	$\epsilon_{AT}$ Variation with Source Cylinder Radius.....	54
II-18	$\epsilon_{AT}$ Variation with Well Diameter.....	57
II-19	$\epsilon_{AT}$ Variation with Well Height.....	58
II-20	$\epsilon_{AT}$ versus Well Size.....	59
II-21	$\epsilon_{AT}$ Variation with Energy for 8F8 Well Crystal.....	65
II-22	$\epsilon_{AT}$ Variation with Energy for 7F8 Well Crystal.....	66
II-23	$\epsilon_{AT}$ Variation with Energy for 2 x 2 Inch Solid Crystal.....	67
III-1	Flow Diagram for Monte Carlo Calculation of Photofractions.....	70
IV-1	Electron Transmission in NaI.....	107
IV-2	Bremsstrahlung Spectra from an Electron Slowing Down in Sodium Iodide.....	111
V-1	Photofraction versus Energy for 3 x 3 Inch Solid Crystal.....	132
V-2	Effect on Photofraction of Electron and Bremsstrahlung Escape from 3 x 3 Inch Solid Crystal..	141
V-3	Effect on Photofraction of Electron and Bremsstrahlung Escape from 8F8 Well Crystal.....	142
V-4	Variation of Solid Crystal Photofraction with Collimation.....	145

LIST OF FIGURES (CONT'D)

<u>Figure</u>		<u>Page</u>
V-5	Photofraction (Relative to Narrow Beam) Variation with Collimation for 3 x 3 Inch Solid Crystal.....	146
V-6	Absolute Peak Efficiencies for Collimated Sources Compared with Experiments of Jarczyk.....	148
V-7	Photofractions for Solid and Well-Type Crystals.....	149
V-8	Ratio of NaI Photofraction to CsI or CaI <sub>2</sub> Photofraction for 8F8 Well Crystal.....	152





## CHAPTER I

### INTRODUCTION

The investigation described in this dissertation is concerned with the calculation of gamma ray scintillation crystal detector efficiencies. As gamma ray detectors, scintillation crystals are superior to gas-filled detectors in their ability to measure the total energy of incident gamma rays, and their much higher gamma detection efficiency. Hofstadter<sup>(1)</sup> first suggested the use of NaI(Tl) as a gamma scintillation detector in 1948, and this material has remained the most important to date. The high density of NaI ( $3.667 \text{ gm/cm}^3$ ) and high atomic number ( $Z=53$ ) of iodine account for its superior gamma ray detection characteristics over gas-filled detectors.

The scintillation crystal can totally absorb the energy of an incident gamma ray, making possible a measurement of source energies, and use of the crystal detector in gamma ray spectrometry. Gas-filled detectors are not suitable for energy measurements, since total absorption of high energy gammas is negligible. Recent application of cooled germanium diode detectors in gamma ray spectroscopy show outstanding resolution characteristics, but are limited to much smaller volumes and efficiencies than readily available NaI crystals.

Calculation of efficiencies for gas-filled detectors is considerably more difficult, and probably less accurate than efficiency calculations for large volume solid medium detectors. The difficulties arise because of the mechanism for gamma interactions with a gas-filled

detector. The primary means of gamma detection is through the gas ionization produced by secondary electrons formed when a gamma interacts in the solid detector wall. The variations in range and energy of these electrons introduces considerable uncertainty in the calculation of the gas-filled detector efficiency.<sup>(2)</sup> Also, the sensitive volume of these detectors may be difficult to define accurately. However, the scintillation crystal efficiency is more readily calculated, as will be discussed subsequently. Once the efficiency of a given crystal has been obtained, another crystal of the same size will have exactly the same theoretical efficiency. The precise definition of the scintillation crystal sensitive volume insures reproducibility of the efficiency, independent of the electronic counting system.

Since scintillation crystals are the most widely used gamma ray detectors, the present calculations of detection efficiencies are useful in a variety of applications. Right circular cylinders, with and without a coaxial cylindrical well, are the specific crystal shapes used almost exclusively in gamma ray counting. Therefore, this investigation has concentrated exclusively on these two crystal shapes. Knowledge of the detection efficiency is required to obtain a quantitative measurement of the absolute gamma ray source emission intensity ( $I_\gamma$ ). Determination of the absolute source strength is required in many applications such as quantitative activation analyses, and absolute neutron flux measurements. The source strength may be related to the absolute disintegration rate of an isotope source if the decay scheme is known.

If the appropriate efficiency ( $\epsilon$ ) of a gamma ray detector is known, experimental observation of the count rate (C.R.) will give the absolute source strength ( $I_\gamma$ ).

$$I_\gamma = C.R./\epsilon \quad (1.1)$$

A. Gamma Detector Scintillation Spectrometry

Consider a monoenergetic point source of gamma rays of energy  $E_0$ , located such that some of the emissions interact with a scintillation crystal. If the differential count rate of the detector is observed with a pulse height spectrometer, it may appear idealized as  $H(E)$  in Figure I-1 below. The differential spectrum of emitted energy is as  $G(E)$ .

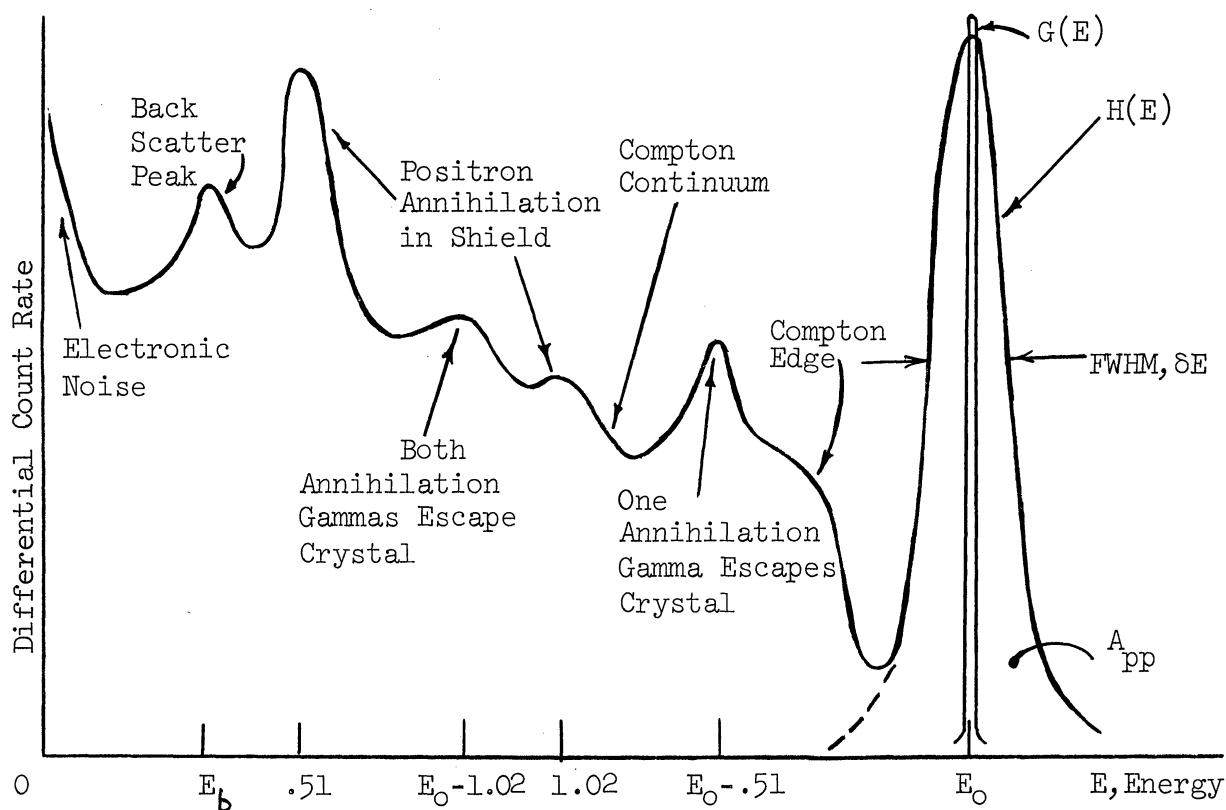
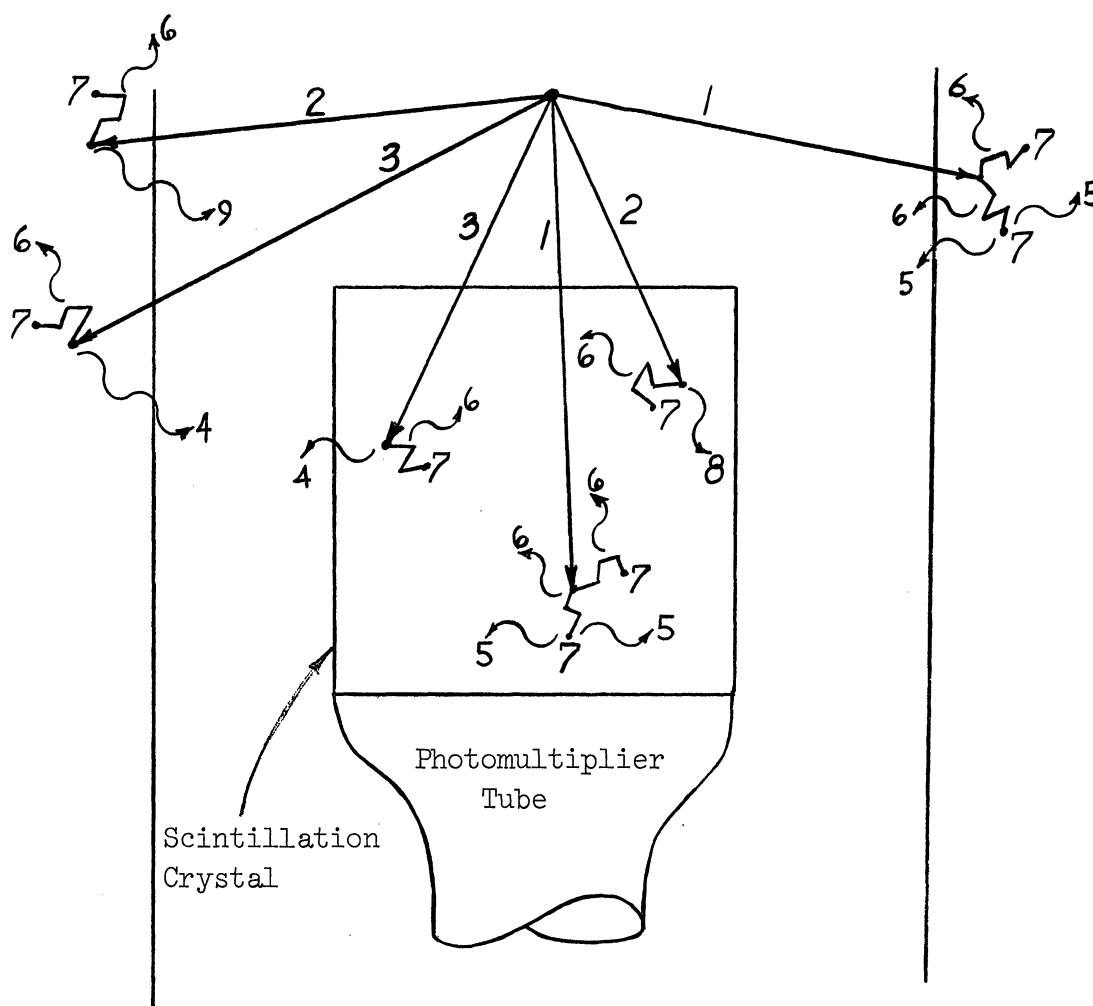


Figure I-1. Idealized Differential Spectrum for Gamma Ray Spectrometer.

The interactions which may contribute to the observed spectrum are depicted in the following sketch and are identified below.



Gamma rays from the source may have any one of three primary interactions in the crystal or surrounding media. Labeled rays from the source indicate these possible initial events:

1. Pair production event
2. Photoelectric absorption event
3. Compton scattering event.

These initial events give rise to the following secondaries, as labeled in the above sketch:

4. Compton scattered gammas
5. Positron annihilation photons (.51Mev)
6. Bremsstrahlung
7. Electrons
8. Iodine K x-ray
9. X-rays from surrounding media.

Other radiation may be present from the source, or background, which further complicates the observed spectrum.

The important features of the spectrum shown in Figure I-1 are as follows. The peak at  $E_0$  corresponds to total absorption of the source gamma within the crystal, and is conventionally defined as the photopeak. In addition to primary photoelectric events, the total absorption peak has contributions from successive events in the crystal which eventually result in total absorption of the source energy. Since these successive events occur within the crystal resolving time ( $0.25 \times 10^{-6}$  sec. in NaI<sup>(2)</sup>), the energy deposited in each event is assumed to give a single output pulse. For energies below  $E_0$ , the observed continuum is due to gammas that deposit less than the total source energy in the crystal. For example, gammas which undergo an initial Compton event frequently are scattered from the crystal with only part of the source energy, in the form of electron kinetic energy, being absorbed in the crystal. This process is the major source of the observed continuum, which is conventionally called the Compton continuum.

Superimposed on the Compton continuum may be found a number of peaks which are identified on the figure. The backscatter peak at  $E_b$  is due to Compton events in the material surrounding the crystal which result in near  $180^\circ$  scattering of the gamma into the crystal. The peaks which may be observed at  $E_0 - .51$  Mev and  $E_0 - 1.02$  Mev are due to initial pair production events within the crystal in which respectively one, or both positron annihilation gammas escape from the crystal. Also, positron annihilation in material surrounding the crystal may give rise to peaks at .51 and 1.02 Mev, if either, or both annihilation gammas are subsequently absorbed in the crystal. In some systems, peaks due to low energy x-rays may be seen near the region of electronic noise. The gamma emission intensity and observed total integral count rate are related to the differential spectra by:

$$I_\gamma = \int_0^\infty G(E) dE$$
$$C.R. = \int_{E(\text{disc.})}^\infty H(E) dE$$
(1.2)

where  $E(\text{disc.})$  is the discrimination level of the counting system.

#### B. Absolute Total Efficiency

Identifying the total area under the experimentally observed pulse height spectrum  $A_T$  with the total integral count rate, C.R.,

at zero discrimination level we have:

$$A_T = \int_0^{\infty} H(E) dE \quad (1.3)$$

and making further definitions:

$A_T^*$  = ideal total area, i.e., the total area under the ideal pulse height spectrum that would be obtained if no attenuating and scattering effects were present due to material surrounding the crystal (e.g. shielding) or due to gamma interactions within the source,

$\epsilon_{AT}$  = absolute total efficiency associated with the ideal total area, i.e., the fraction of gammas emitted from the source which interact with the crystal at least once and transfer energy to the crystal,

Equation (1.1) becomes:

$$I_{\gamma} = A_T^* / \epsilon_{AT} \quad (1.4)$$

From the above equations, if  $A_T^* = A_T$  and  $\epsilon_{AT}$  can be calculated, one should be able to determine the source intensity in gammas emitted per second from the observed integrated total count rate. In practice however,  $A_T^* \neq A_T$ , i.e., the ideal total area is not the observed total integrated count rate because of the perturbing effects of material surrounding the crystal and source self-absorption and scattering. As defined,  $\epsilon_{AT}$  is associated with  $A_T^*$  rather than  $A_T$ , because interactions of the source gammas with anything other than the

scintillation crystal are ignored. For example, the backscatter peak usually observed in a pulse height spectrum is not taken into account. In addition, the observed total area may include pulses due to positron annihilation in the shield as well as pulses at low energy due to electronic noise. The observed total area is not a parameter uniquely related to the absolute source emission intensity, but it also depends on the presence of other materials and the electronic system. For a given experimental arrangement, it is concluded that calculation of  $I_\gamma$  from  $A_T$  is not feasible, and one must seek another measurable quantity that can be accurately reproduced for any experimental arrangement.

C. Absolute Peak Efficiency

Instead of  $A_T$ , we will make use of the integrated pulse height under the photopeak (see Figure I-1). Making the definitions:

$A_{PP}$  = photopeak area, i.e., the experimentally observed area of the pulse height spectrum under the photopeak,

$\epsilon_{AP}$  = absolute peak efficiency, i.e., the fraction of gammas emitted from the source which interact with the crystal such that their total energy is transmitted to the crystal.

Physically,  $A_{PP}$  measures the number of source gammas incident on the crystal whose total energy is absorbed in the crystal. An implicit assumption made here is that the differential pulse height spectrum is proportional to the spectrum of energy deposition in the crystal. Investigations of this proportionality have been made by various workers, e.g. Verheijke,<sup>(3)</sup> Engelkemeir<sup>(4)</sup> and for most applications the assumption has been shown to be justified.



When the photopeak is clearly defined  $A_{pp}$  may be measured by direct summation of the appropriate portion of the differential spectrum. For cases when the spectrum is more complex and the photopeak is not as clearly defined,  $A_{pp}$  is conventionally obtained by assuming the photopeak to be a Gaussian curve. Based on this assumption, it can be shown that

$$A_{pp} = \frac{1}{2} \sqrt{\frac{\pi}{\log_e 2}} C_m \delta E$$

where  $C_m$  = maximum of the photopeak (at  $E_0$ )

$\delta E$  = full width of the photopeak at half maximum (FWHM).

When a source gamma ray has an interaction before entering the crystal (i.e., scattering in the detector shielding) some of its energy will be lost, preventing deposition of its total energy within the crystal and thus it will not be counted under the full energy peak. The photopeak area serves the purpose of providing a readily measurable quantity which can be related uniquely to the absolute source intensity. For a given geometry, and source intensity and energy,  $A_{pp}$  remains constant (assuming no change in the amount of shielding interposed directly between the source and the crystal) independent of changes in the counting system or the amount and position of external materials. For identical geometries and crystal sizes, the pulse heights may differ between two crystals and another photomultiplier may give different resolution, but the total number of counts under the photopeak does not depend upon pulse height or resolution.

The photopeak area is solely a measure of those source gammas which are totally absorbed in the crystal, and is reproducible since the experimental arrangement has essentially no effect  $A_{pp}$ .

D. Photofraction

From the above definitions of  $\epsilon_{AP}$  and  $A_{pp}$ , one may write:

$$I_{\gamma} = A_{pp} / \epsilon_{AP} \quad (1.5)$$

Since  $A_{pp}$  can be experimentally determined uniquely,  $I_{\gamma}$  may be obtained if  $\epsilon_{AP}$  can be calculated. Conventionally  $\epsilon_{AP}$  is not calculated directly, but rather is determined by the following:

$$I_{\gamma} = \frac{A_{pp}}{\epsilon_{AP}} = \frac{A_T^*}{\epsilon_{AT}} \quad (1.6)$$

$$\epsilon_{AP} = \epsilon_{AT} \left( \frac{A_{pp}}{A_T^*} \right) \quad (1.7)$$

where

$A_{pp}/A_T^*$  = peak-to-total ratio, or photofraction.

$\epsilon_{AP}$  is divided into these two factors primarily because  $\epsilon_{AT}$  can be obtained from explicit analytical expressions (see Chapter II), while the photofraction must be calculated by simulation of the transport of particles through the crystal by Monte Carlo methods (see Chapter III).

E. Intrinsic Total and Intrinsic Peak Peak Efficiencies

It will be convenient to define two other efficiencies, which have the solid angle dependence removed:

$\epsilon_{IT}$  = intrinsic total efficiency, the fraction of source gammas incident upon the crystal that interact with the crystal at least once and transfer energy to the crystal, and

$\epsilon_{IP}$  = intrinsic peak efficiency, the fraction of source gammas incident upon the crystal which interact with the crystal such that their total energy is transmitted to the crystal.

Thus we have,

$$\epsilon_{AT} = \frac{\Omega}{4\pi} \epsilon_{IT}$$

$$\epsilon_{AP} = \frac{\Omega}{4\pi} \epsilon_{IP}$$

where

$\Omega$  = mean solid angle subtended by the crystal at the source.

F. Calculation of the Absolute Total Efficiency and Photofraction

In the present work  $\epsilon_{AT}$  is calculated directly from analytic expressions (Chapter II). The quantity  $A_{pp}/A_T^*$ , known as the peak to total ratio or photofraction, is calculated by Monte Carlo methods for practical cases of interest (Chapter III). The photofraction

represents the ratio of the number of gammas that are completely absorbed, including all secondary radiation, to the number of source gammas that interact at least once. Calculation of the photofraction is performed by simulating with Monte Carlo methods the successive physical processes which an incident gamma undergoes. An analytical treatment involving solution of the problem is entirely impractical on account of the mathematical complexity of interactions, multiple secondary particles, and geometry. It should be noted that calculation of  $\epsilon_{AT}$  can also be done by the Monte Carlo process, but to obtain results with an accuracy equivalent to that obtained by numerical integration of the analytic expressions would require excessive computer time.

## CHAPTER II

### CALCULATION OF THE ABSOLUTE TOTAL EFFICIENCY

#### A. Definition of Absolute Total Efficiency ( $\epsilon_{AT}$ )

As previously defined in Chapter I, the absolute total efficiency,  $\epsilon_{AT}$ , is the probability that a gamma ray emitted from the source will interact with, and deposit some of its energy in the crystal.  $\epsilon_{AT}$  is considered here to be the product of two independent probabilities. First, the probability that the source gammas are incident upon the crystal surface and second, the probability that those gammas will interact with the crystal. These two probabilities are respectively the geometry factor,  $\Omega/4\pi$ , and the intrinsic total efficiency,  $\epsilon_{IT}$ . Making the definitions:

$\Omega$  = solid angle subtended by the crystal at the source

$$\frac{\int_{\Omega} (1 - e^{-\tau x}) d\Omega}{\int_{\Omega} d\Omega} = \text{probability that gammas incident upon the crystal will interact with the crystal} = \epsilon_{IT}$$

where,

$x(\Omega)$  = path length in the crystal extrapolated in the direction of emission of a source gamma

$\tau(E)$  = total gamma ray cross section (without coherent scattering) for the crystal material

$E$  = energy of the monoenergetic source gammas

one obtains,

$$\epsilon_{AT} = \frac{\Omega}{4\pi} \frac{\int_{\Omega} (1 - e^{-\tau x}) d\Omega}{\int_{\Omega} d\Omega} = \frac{\Omega}{4\pi} \cdot \epsilon_{IT}$$

and finally,

$$\epsilon_{AT} = \frac{1}{4\pi} \int_{\Omega} (1 - e^{-\tau x}) d\Omega. \quad (2.1)$$

It should be noted that the coherent (Rayleigh) scattering cross section has been removed from the total cross section values used. This process occurs only at the lowest energies, where photoelectric absorption predominates. For gamma energies above about .20 MeV in NaI, the cross section for Rayleigh scattering is negligible. Below this energy, the photoelectric cross section is approximately 10-50 times greater than the Rayleigh cross section. Even when a coherent scattering event occurs, the photon is scattered by the atomic electron cloud and the entire atom recoils, so that only a slight change in direction and energy of the photon occurs.

Equation (2.1) forms the basis for all calculations of  $\epsilon_{AT}$ . For perfectly collimated monodirectional photon beams parallel to the cylinder axis, Equation (2.1) reduces to:

$$\epsilon_{AT} = \epsilon_{IT} = 1 - e^{-\tau H} \quad (2.2)$$

where  $H$  = axial length traveled through the crystal cylinder. In Equation (2.1), the element of solid angle  $d\Omega$ , can be written as:

$$d\Omega = \sin \theta d\theta d\phi = -d\mu d\phi$$

Referring to Figures II-1 and II-2, the definitions are made:

$\theta$  = polar angle

$\mu = \cos \theta$

$\phi$  = azimuthal angle

and Equation (2.1) becomes:

$$\epsilon_{AT} = \frac{1}{4\pi} \int_{\phi} d\phi \int_{\mu} \left[ 1 - e^{-\tau x(\mu, \phi)} \right] d\mu \quad (2.3)$$

For both the well and solid crystals, the extrapolated path length,  $x(\mu, \phi)$  is a complicated function, which is discontinuous at the edges of the crystal and well. Solution of Equation (2.3) for an isotropic point source a distance,  $m$ , from the crystal axis for either the well or solid crystal provides a point kernel which can, in principle, be integrated to determine  $\epsilon_{AT}$  for any arbitrary source. The analysis here considered point sources, an isotropic disk source of zero thickness, or an isotropic cylindrical volume source of finite thickness. These point kernels are derived in Appendix A, using the definitions of Figures II-1 and II-2. The results are summarized here.

1. Isotropic Point Kernel for  $\epsilon_{AT}$

For a solid crystal:

$$\epsilon_{AT} (\text{off-axis pt.}) = \frac{1}{2\pi} \int_{-\frac{\pi}{2}}^{\frac{\pi}{2}} d\phi \left[ \int_{\mu_1}^1 F_1(\mu, \phi) d\mu + \int_{\mu_2}^{\mu_1} F_2(\mu, \phi) d\mu \right] \quad (2.4)$$

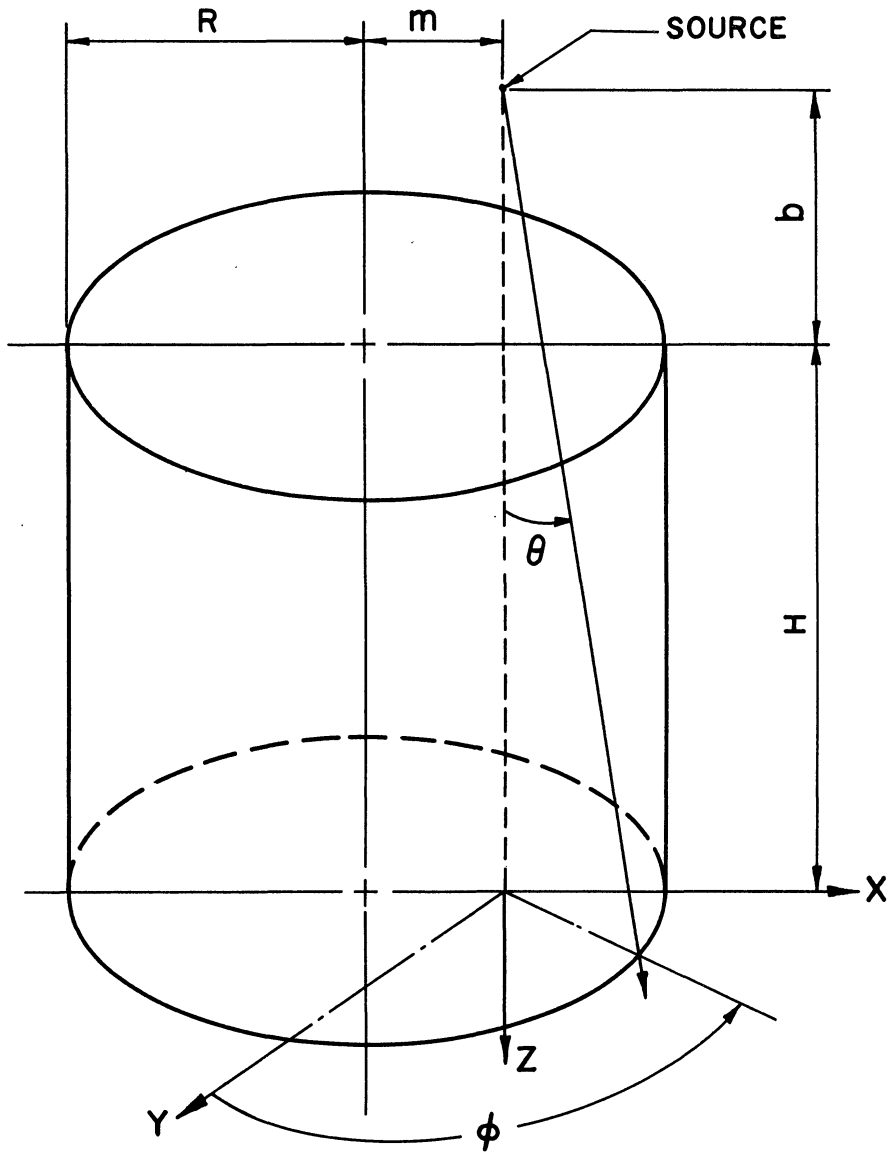


Figure II-1. Solid Crystal Geometry.



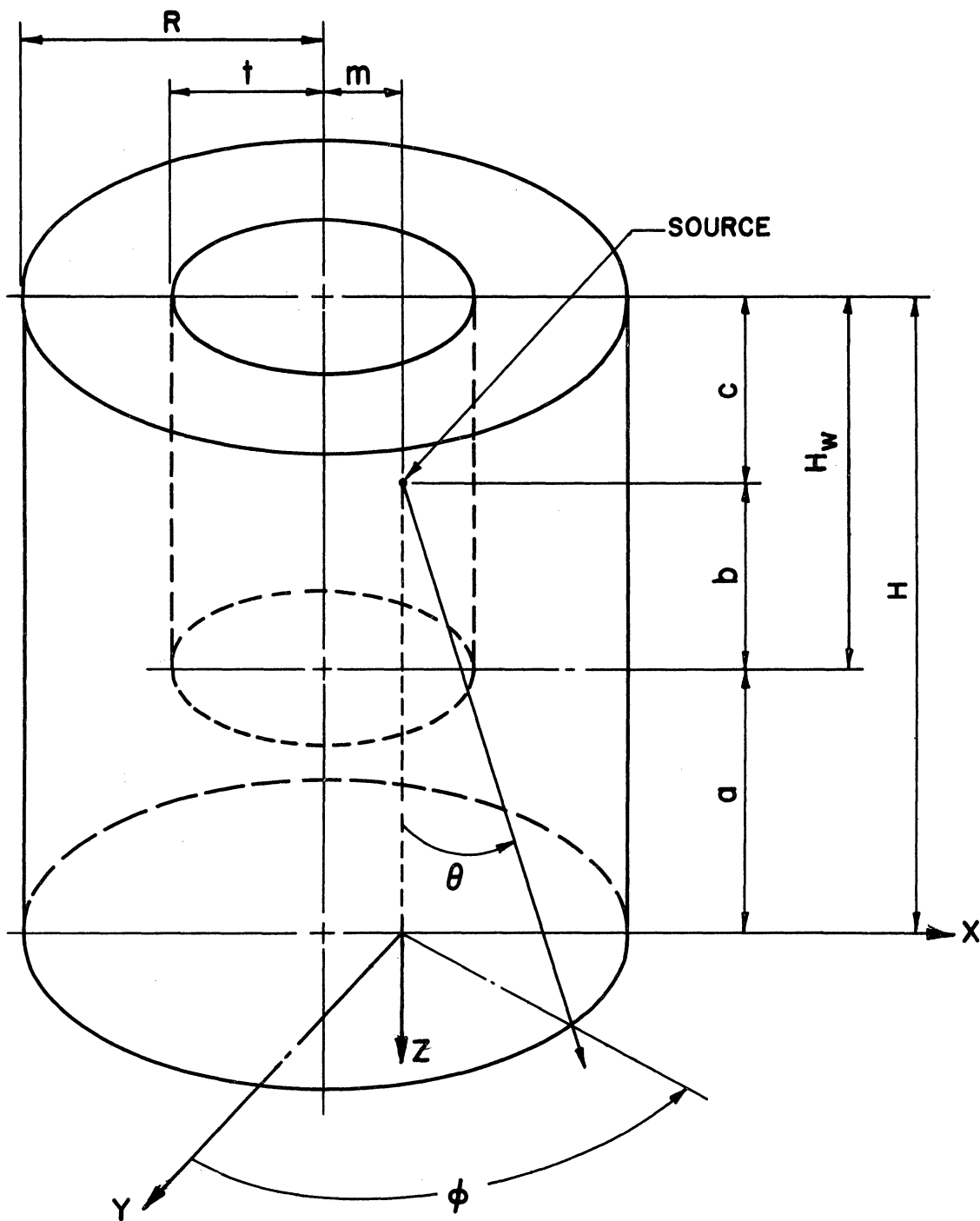


Figure II-2. Well Crystal Geometry.

where

$$\mu_1 = (H+b) / [(H+b)^2 + S^2]^{1/2}$$

$$\mu_2 = b / (b^2 + S^2)^{1/2}$$

$$F_1(\mu, \phi) = 1 - \exp(-\tau H / \mu)$$

$$F_2(\mu, \phi) = 1 - \exp\left[-\tau \left( \frac{S}{\sqrt{1-\mu^2}} - \frac{b}{\mu} \right)\right]$$

$$S = -m \sin \phi + \sqrt{R^2 - m^2 \cos^2 \phi}$$

For a well crystal, with the point source within the well:

$$\epsilon_{AT}(\text{off-axis pt.}) = \frac{1}{2\pi} \int_{-\pi/2}^{\pi/2} d\phi \left[ \int_{\mu_1}^1 F_1(\mu, \phi) d\mu + \int_{\mu_2}^{\mu_1} F_2(\mu, \phi) d\mu + \int_{\mu_3}^{\mu_2} F_3(\mu, \phi) d\mu + \int_{\mu_4}^{\mu_3} F_4(\mu, \phi) d\mu \right] \quad (2.5)$$

As discussed in Appendix A, the functions  $F_2$ ,  $\mu_1$ , and  $\mu_2$  depend on the inequalities:

$$\text{Case 1: } \frac{S_1}{b} < \frac{S_2}{a+b}$$

$$\text{Case 2: } \frac{S_1}{b} > \frac{S_2}{a+b}$$

where

$$S_1 = -m \sin \phi + \sqrt{t^2 - m^2 \cos^2 \phi}$$

$$S_2 = -m \sin \phi + \sqrt{R^2 - m^2 \cos^2 \phi}$$

The results are:

$$F_1 = 1 - \exp(-\tau a / \mu)$$

$$F_3 = 1 - \exp\left[-\tau \left(\frac{S_2 - S_1}{\sqrt{1 - \mu^2}}\right)\right]$$

$$F_4 = 1 - \exp\left[\tau \left(\frac{c}{\mu} + \frac{S_1}{\sqrt{1 - \mu^2}}\right)\right]$$

$$\mu_3 = -\frac{c}{\sqrt{c^2 + S_2^2}}$$

$$\mu_4 = -\frac{c}{\sqrt{c^2 + S_1^2}}$$

and for Case 1:

$$\frac{S_1}{b} < \frac{S_2}{a+b}$$

$$F_2 = 1 - \exp\left[-\tau \left(\frac{a+b}{\mu} - \frac{S_1}{\sqrt{1 - \mu^2}}\right)\right]$$

$$\mu_1 = \frac{b}{\sqrt{S_1^2 + b^2}}$$

$$\mu_2 = \frac{a+b}{\sqrt{(a+b)^2 + S_2^2}}$$

or for Case 2:

$$\frac{S_1}{b} > \frac{S_2}{a+b}$$

$$F_2 = 1 - \exp\left[-\tau \left(\frac{S_2}{\sqrt{1-\mu^2}} - \frac{b}{\mu}\right)\right]$$

$$\mu_1 = \frac{a+b}{\sqrt{(a+b)^2 + S_2^2}}$$

$$\mu_2 = \frac{b}{\sqrt{S_1^2 + b^2}}$$

Equations (2.4) and (2.5) are the desired point kernels for an off-axis point isotropic source for solid and well crystals, respectively. Any desired isotropic source geometry can be obtained from these equations, and in particular, the symmetrically located point, disk, and cylindrical volume sources are considered.

## 2. $\epsilon_{AT}$ for On-axis Point Sources

The point source on the crystal axis equation for  $\epsilon_{AT}$  is obtained by letting  $m = 0$  in Equations (2.4) and (2.5), and performing the integration over  $\phi$ . The results are:

For a solid crystal:

$$\epsilon_{AT}(\text{on-axis pt.}) = \frac{1}{2} \left[ \int_{\mu_1}^1 F_1(\mu) d\mu + \int_{\mu_2}^{\mu_1} F_2(\mu) d\mu \right] \quad (2.6)$$

where

$$\mu_1 = \frac{H+b}{\sqrt{(H+b)^2 + R^2}}$$

$$\mu_2 = \frac{b}{\sqrt{b^2 + R^2}}$$

$$F_1(\mu) = 1 - \exp(-\tau H/\mu)$$

$$F_2(\mu) = 1 - \exp\left[-\tau \left( \frac{R}{\sqrt{1-\mu^2}} - \frac{b}{\mu} \right)\right]$$

These results have been previously obtained. (5,6)

For a well crystal, with the point source within the well:

$$\epsilon_{AT}(\text{on-axis pt.}) = \frac{1}{2} \left[ \int_{\mu_1}^1 F_1(\mu) d\mu + \int_{\mu_2}^{\mu_1} F_2(\mu) d\mu + \int_{\mu_3}^{\mu_2} F_3(\mu) d\mu + \int_{\mu_4}^{\mu_3} F_4(\mu) d\mu \right] \quad (2.7)$$

where

$$F_1(\mu) = 1 - \exp(-\tau a/\mu)$$

$$F_3(\mu) = 1 - \exp\left[-\tau \left( \frac{R-t}{\sqrt{1-\mu^2}} \right)\right]$$

$$F_4(\mu) = 1 - \exp\left[\tau \left( \frac{c}{\mu} + \frac{t}{\sqrt{1-\mu^2}} \right)\right]$$

$$\mu_3 = - \frac{c}{\sqrt{c^2 + R^2}}$$

$$\mu_4 = - \frac{c}{\sqrt{c^2 + t^2}}$$

and when

$$\frac{t}{b} < \frac{R}{a+b}$$

$$F_2(\mu) = 1 - \exp\left[-\tau \left(\frac{a+b}{\mu} - \frac{t}{\sqrt{1-\mu^2}}\right)\right]$$

$$\mu_1 = \frac{b}{\sqrt{t^2 + b^2}}$$

$$\mu_2 = \frac{a+b}{\sqrt{R^2 + (a+b)^2}}$$

or when

$$\frac{t}{b} > \frac{R}{a+b}$$

$$F_2(\mu) = 1 - \exp\left[-\tau \left(\frac{R}{\sqrt{1-\mu^2}} - \frac{b}{\mu}\right)\right]$$

$$\mu_1 = \frac{a+b}{\sqrt{R^2 + (a+b)^2}}$$

$$\mu_2 = \frac{b}{\sqrt{t^2 + b^2}}$$

Expressions for a point source on the crystal axis, but outside the well, are given in Appendix A.

### 3. $\epsilon_{AT}$ for Disk and Cylindrical Volume Sources

The expression for a homogeneous isotropic disk source of radius  $g$ , located with its center on the crystal axis, is also derived in Appendix A and is given by:

$$\epsilon_{AT}(\text{disk}) = \frac{2}{g^2} \int_0^g m \cdot \epsilon_{AT}(\text{off-axis pt.}) dm \quad (2.8)$$

The expression is derived in Appendix A for a homogeneous isotropic cylindrical volume source of radius  $g$  and height  $(b_2-b_1)$ , located with its axis along the crystal axis. The source cylinder axial distances are measured from the same plane as  $b$ , given in Figures II-1 and II-2 ( $b_2 > b_1$ ).

$$\epsilon_{AT}(\text{vol.}) = \frac{2}{g^2(b_2-b_1)} \int_{b_1}^{b_2} db \int_0^g m \cdot \epsilon_{AT}(\text{off-axis pt.}) dm \quad (2.9)$$

#### 4. Geometry Factors

For the point source on the crystal axis, it is easily shown that the geometry factor,  $\frac{\Omega}{4\pi}$  is given by:

For solid crystal:

$$\frac{\Omega}{4\pi} = \frac{1}{2} \left( 1 - \frac{b}{\sqrt{b^2 + R^2}} \right) \quad (2.10)$$

For well crystal, source inside well:

$$\frac{\Omega}{4\pi} = \frac{1}{2} \left( 1 + \frac{c}{\sqrt{c^2 + t^2}} \right) \quad (2.11)$$

For well crystal, source outside well:

$$\frac{\Omega}{4\pi} = \frac{1}{2} \left( 1 - \frac{c}{\sqrt{c^2 + t^2}} \right) \quad (2.12)$$

## B. Calculation of $\epsilon_{AT}$

It is not possible to obtain solutions of Equations (2.4 - 2.9) in any closed-form analytical expressions, nor can these integrals, in general, be reduced to the form of any known tabulated functions. For a restricted number of special cases, series solutions have been found by Grosjean, Reference 7 and the unpublished derivation of N. McCormick given in Appendix B. Complete solution of these equations was carried out by numerical integration techniques on the Michigan IBM-7090 Digital Computer, using a Gaussian quadrature formula. Tabulations of calculated results are given in Appendix G. The computational algorithms used for the centerline point, disk and volume, and off-axis point sources are designated the BURP-1,2,3 Computer Programs, respectively. Operating instructions for use of these computer programs are given in Appendix E.

## C. Checks Applied to Calculated $\epsilon_{AT}$ Results

Numerous independent methods are available to ascertain the proper operation of these computer programs. Since considerable computational data are available for solid crystals, with point and disk sources,<sup>(5,6,8-13)</sup> direct comparisons are possible with other calculations for these source geometries. Only one published article<sup>(14)</sup> gives any results for right circular cylindrical crystals with a coaxial cylindrical well. Reference 14 gives data for only one crystal size. Comparisons were made with these references and agreement within all significant figures (usually three) was obtained, except for the calculations of Reference 11. These references generally used numerical integration



techniques based on the trapezoidal rule, using a small number of sub-intervals, since the computations were performed on older, smaller capacity machines than the IBM-7090. There are two reasons for the slight disagreement with the results of Reference 11. First, Reference 11 uses somewhat different cross sections, and second, the integration was performed by a different technique (Monte Carlo). However, since the maximum difference was less than 0.25%, no significant discrepancy is indicated for the different approaches taken by Reference 11 and the present computer programs. Tables II-1, II-2, and II-3 give some of the comparisons made for  $\epsilon_{IT}$  and  $\epsilon_{AT}$  for centerline point sources. Figures II-3 and II-4 compare some of the results obtained for off-axis points with that of Reference 5.

TABLE II-1  
COMPARISON OF  $\epsilon_{IT}$  FOR POINT SOURCES  
ON CENTERLINE OF SOLID CRYSTALS

Energy MeV	$\epsilon_{IT}$		Crystal Size, cm.		Source Height b, cm.
	Present Calc.	Reference	Dia.	Ht.	
0.2	.5491	.55 (10)*	3.81	.635	0.7
1.0	.1157	.12 (10)	3.81	.635	3.0
1.0	.0715	.07 (10)	3.81	.3175	1.5
2.0	.0798	.08 (10)	3.81	.3175	0.3
0.32	.7793	.7773 (11)**	7.62	7.62	11.0
0.661	.6284	.6277 (11)	7.62	7.62	11.0
4.43	.3973	.3976 (11)	7.62	7.62	9.3
7.48	.3997	.3995 (11)	7.62	7.62	9.3

\* Plotted values  
\*\*Tabulated values

TABLE II-2

COMPARISON OF  $\epsilon_{AT}$  VALUES FOR POINT SOURCES  
ON CENTERLINE OF 2 x 2 IN. SOLID CRYSTAL

Energy MeV	$\epsilon_{AT}$		Source Height b, cm.
	Present Calc.	Reference(5)	
0.01	.01539	.01539	10.0
0.129	.10605	.10619	3.0
1.10	.04118	.04119	3.0
2.04	.8233 x 10 <sup>-4</sup>	.823 x 10 <sup>-4</sup>	100.0
2.04	.5877 x 10 <sup>-2</sup>	.585 x 10 <sup>-2</sup>	10.0
2.04	.03343	.03344	3.0
5.50	.02940	.02940	3.0
7.90	.02994	.02995	3.0

TABLE II-3

COMPARISON OF  $\epsilon_{AT}$  VALUES FOR POINT SOURCES  
ON CENTERLINE OF 3 x 3 IN. WELL CRYSTAL

Energy MeV	$\epsilon_{AT}$		Source Height b, cm.
	Present Calc.	Reference(14)	
0.010	.9800	.980	0.0
0.10	.9712	.971	0.5
0.30	.6989	.699	2.0
0.60	.6203	.620	0.0
1.00	.0831	.0832	6.81
1.00	.01737	.0174	13.81
2.00	.4048	.405	0.0
3.00	.3314	.332	0.5
5.00	.3169	.317	0.5
5.00	.3551	.355	0.0

Well size: 7/8 in. dia. x 1-1/2 in. deep

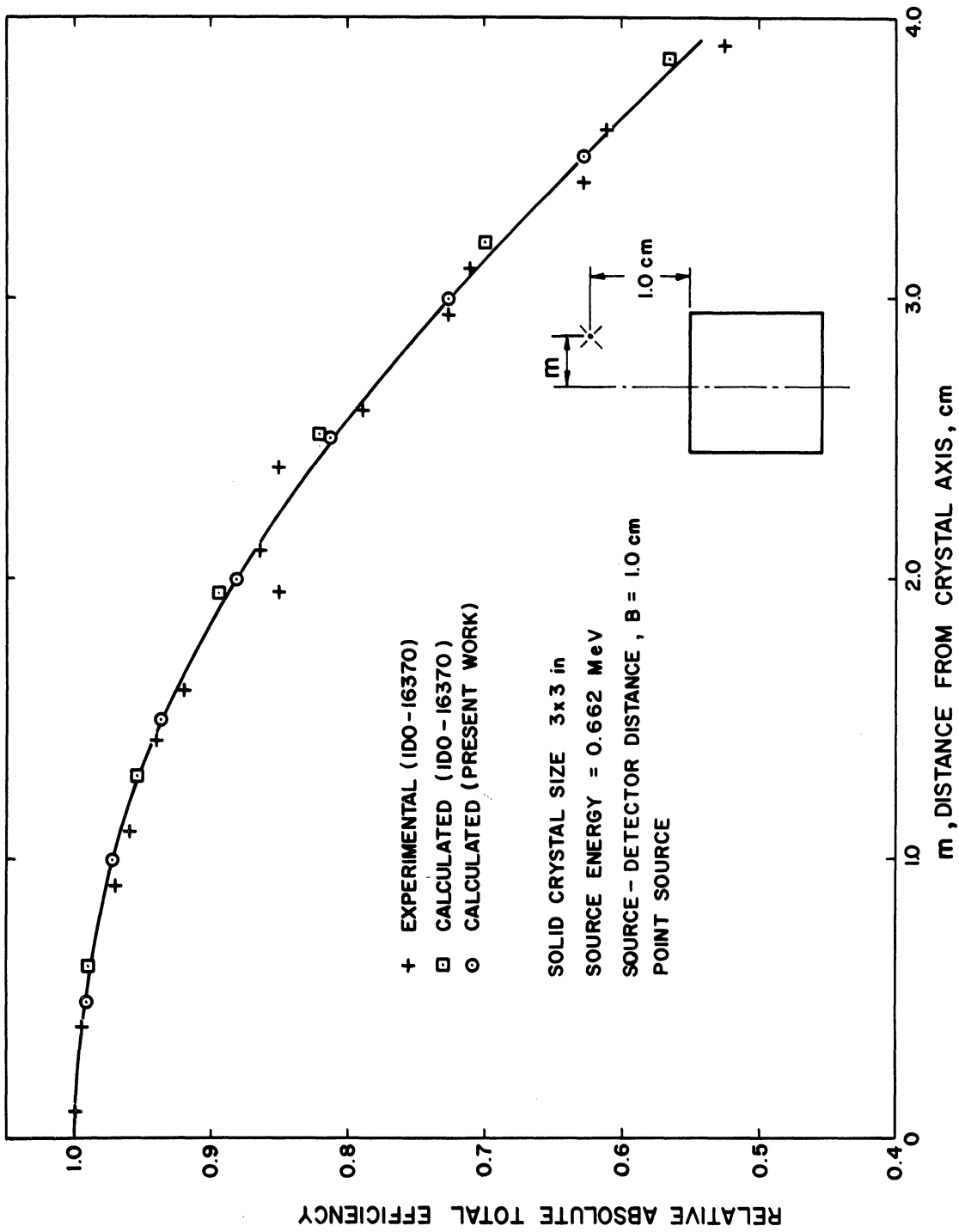


Figure II-3.  $\epsilon_{AT}$  Variation with Radial Distance from Solid Crystal Axis (.662 MeV).

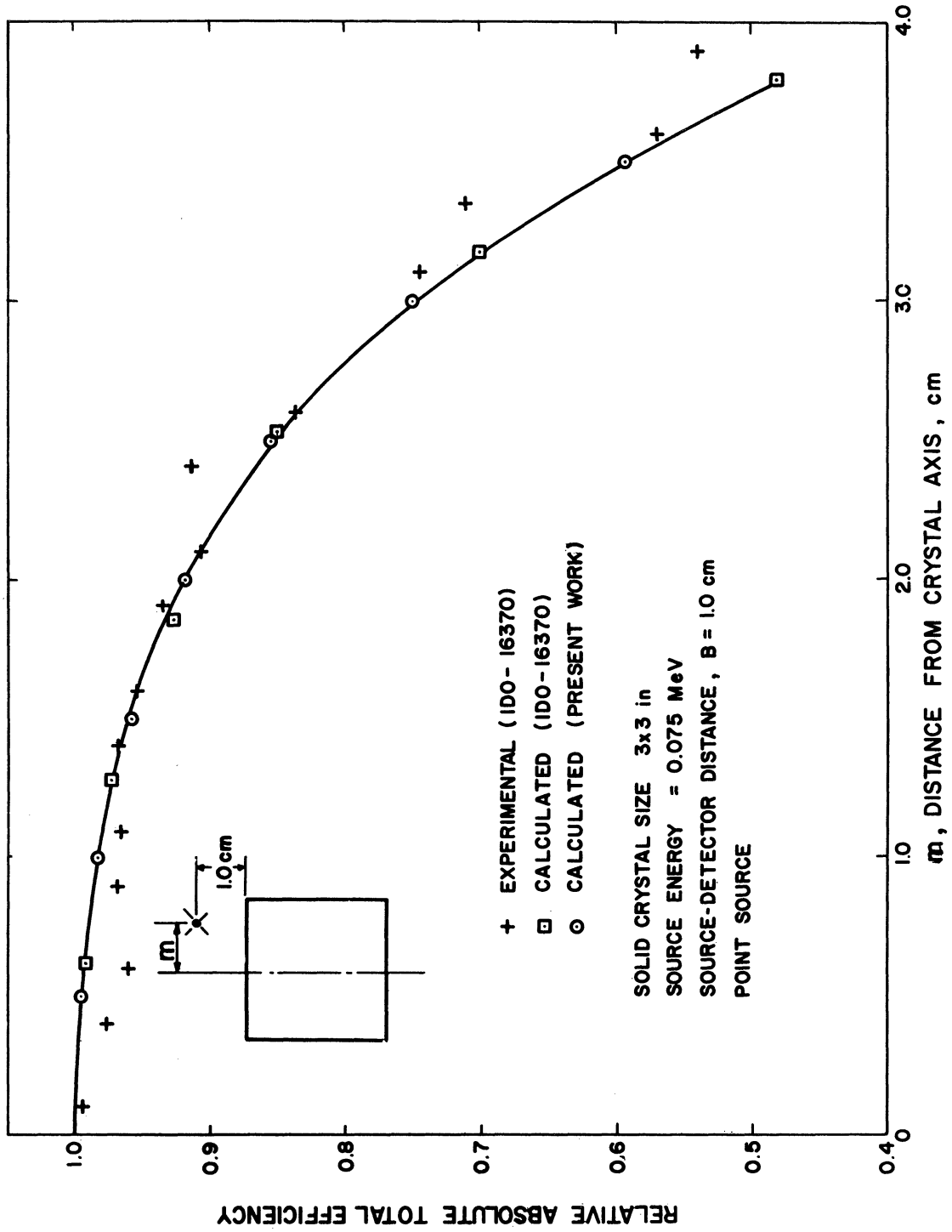


Figure II-4.  $\epsilon_{AT}$  Variation with Radial Distance from Solid Crystal Axis (.075 MeV).

An independent check is provided for disk sources with solid crystals by the tabulations of Reference 5.\* Table II-4 gives some of the comparisons made. In addition, Reference 15 provides some tables of the geometry factor for off-axis point sources. Since the present calculation of  $\epsilon_{AT}$  reduces to calculations of  $\frac{\Omega}{4\pi}$  for large values of the total cross section,  $\tau$ , a direct comparison is possible. Table II-5 presents this comparison. Another check on the proper calculation of  $\epsilon_{AT}$  for disk and volume sources is the asymptotic results obtained when the disk or cylindrical volume is made progressively smaller compared with the results obtained for the point source on the axis. As discussed later in this chapter, when the variation of  $\epsilon_{AT}$  with the size of a distributed source is investigated, correct asymptotic values are obtained.

TABLE II-4  
COMPARISON OF  $\epsilon_{AT}$  VALUES FOR DISK SOURCES  
ON CENTERLINE OF 3 x 3 IN. SOLID CRYSTAL

Energy MeV	$\epsilon_{AT}$		Disk Radius G, cm.	Source Height b, cm.
	Present Calc.	Reference(5)		
0.0484	.36105	.36119	1.905	1.0
0.0484	.03201	.03206	1.905	10.0
0.081	.35804	.35954	1.905	1.0
0.129	.34713	.34856	1.905	1.0
0.212	.31189	.31250	1.905	1.0
0.566	.21269	.21291	1.905	1.0
0.129	.08557	.08591	2.857	5.0
7.9	.03173	.03194	3.086	5.0

\*Reference 5 contains an error in Appendix III (Table VI) page 59. The heading at the top of this table specifies a value of R (disk radius), when actually this is r (crystal radius), in accordance with the authors' notation.

TABLE II-5

COMPARISON OF SOLID ANGLES SUBTENDED BY  
2 IN. DIA. SOLID CRYSTAL AT OFF-AXIS POINTS

Present Calc.	$\Omega/4\pi$	Source Distance		Source Height
	Reference(15)	Off-axis	m, cm.	b, cm.
.082065	.08206	0.635		3.81
.002479	.002479	0.635		25.4
.024781	.02479	1.27		7.62
.052270		0.5		5.08
.050758		1.0		5.08
.049529	.04956	1.27		5.08
.048364		1.50		5.08
.045257		2.00		5.08
.041650		2.50		5.08

D. Results of  $\epsilon_{AT}$  Calculations

Having performed all of these checks on the proper operation of the BURP-1, 2, and 3 computer programs, various detailed calculations were made, the results of which can be used for laboratory applications. In Chapter V, it is pointed out that changes in source geometry have only a small effect on the photofractions, whereas, the values of absolute total efficiency are strongly dependent upon these changes. In order to show the geometrical dependence of  $\epsilon_{AT}$ , a number of different calculations have been performed as follows:

- (a) Solutions for on-axis point sources for well and solid crystals
- (b) Effect of moving a point source from the crystal axis
- (c) Determination when a disk source can be considered a point source

- (d) Variations in  $\epsilon_{AT}$  with disk size and disk axial position
- (e) Determination when a thin cylindrical volume source can be considered a disk source
- (f) Variation in  $\epsilon_{AT}$  with the size of cylindrical volume sources
- (g) Effects on  $\epsilon_{AT}$  of crystal and well size, and thallium concentration.

All of the data of this chapter are for NaI(Tl) crystals; some data for other scintillation materials used for gamma ray detection (i.e., CsI and CaI<sub>2</sub>) are given in Appendix G.

#### 1. On-axis Point Sources

As will be shown later in this chapter, the two and three-dimensional sources of small enough extent can be well-represented by an on-axis point source. Therefore, the tabulation of results in Appendix G for on-axis point sources covers most of the commonly-used well crystals. The compilations are primarily for well crystals, since a considerable amount of data is available for solid crystals, (5,6,8-13) and except for Reference 14 no data is available for well crystals. Some calculations for 2 x 2 in. and 3 x 3 in. solid crystals, with on-axis point sources, are given to supplement those of the references.

Assuming the source to be a point on the crystal axis, Figures II-5, II-6, and II-7 show the variation in efficiency as the source-crystal distance is increased. Figure II-5 shows the intrinsic total efficiency,  $\epsilon_{IT}$  for a solid crystal, while Figures II-6 and II-7 are

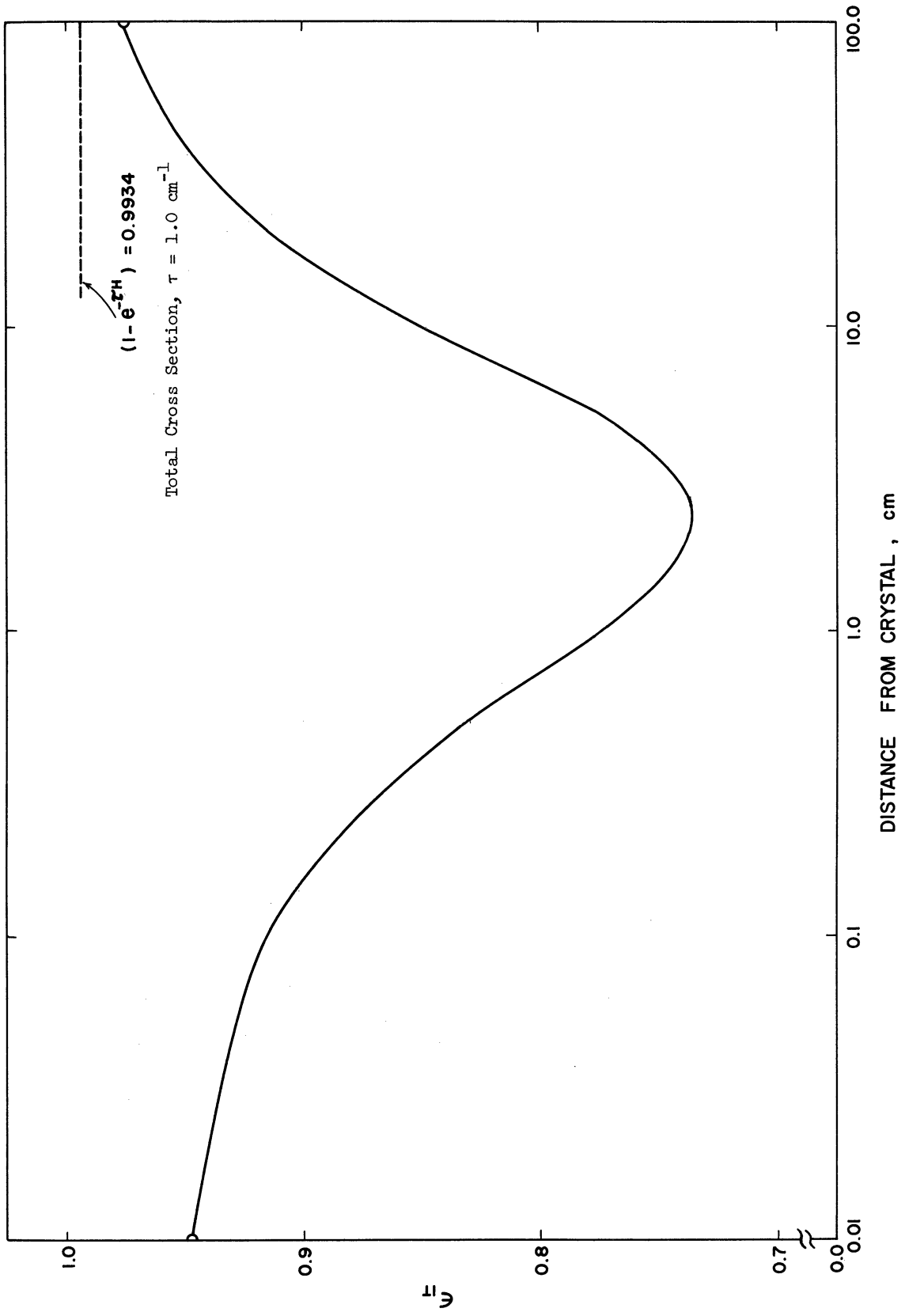


Figure II-5.  $C_{II}$  for 2 x 2 In. Solid Crystal.



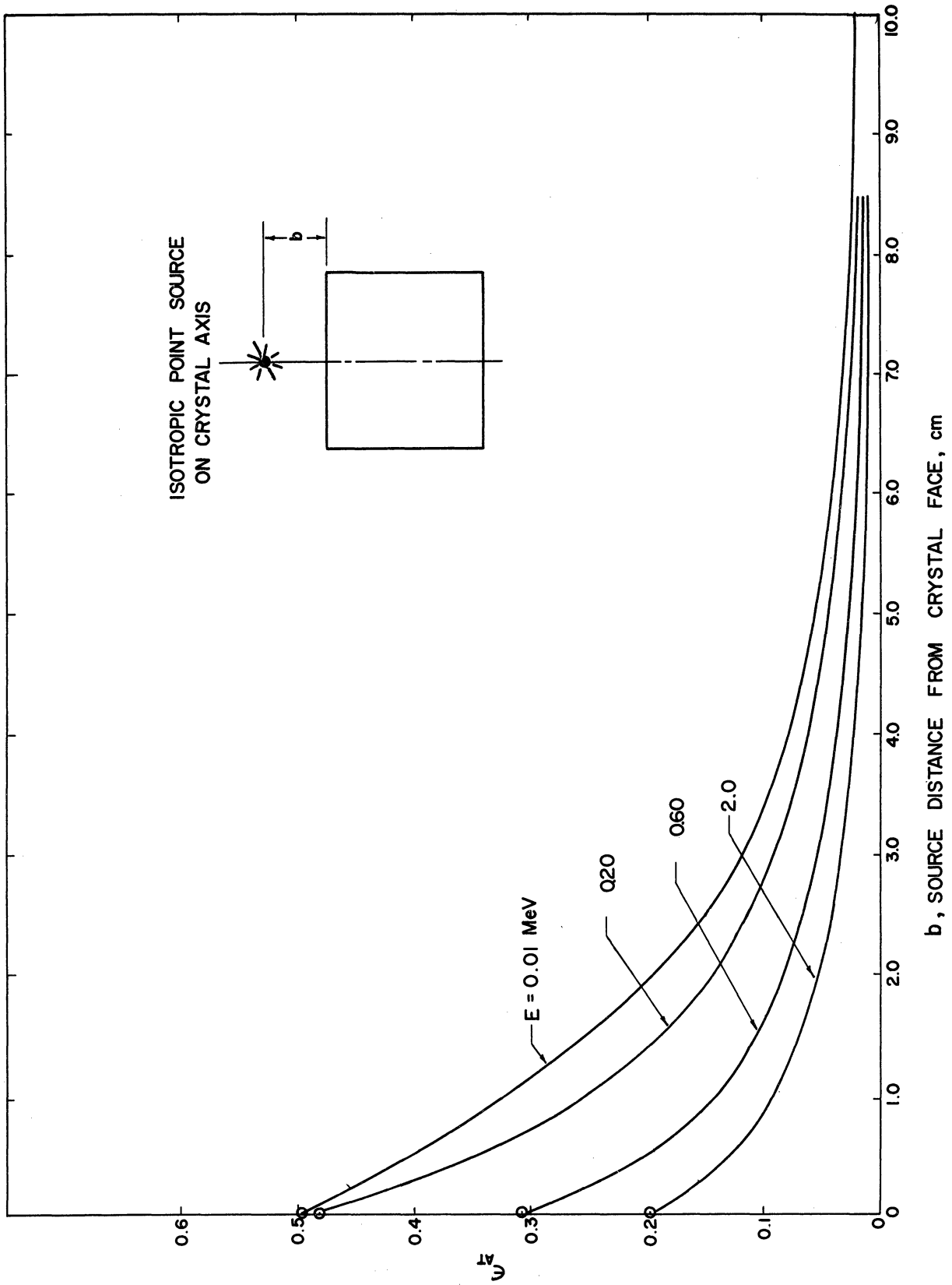


Figure II-6. Effect of Moving Point Source Axially from 2 x 2 In. Solid Crystal.

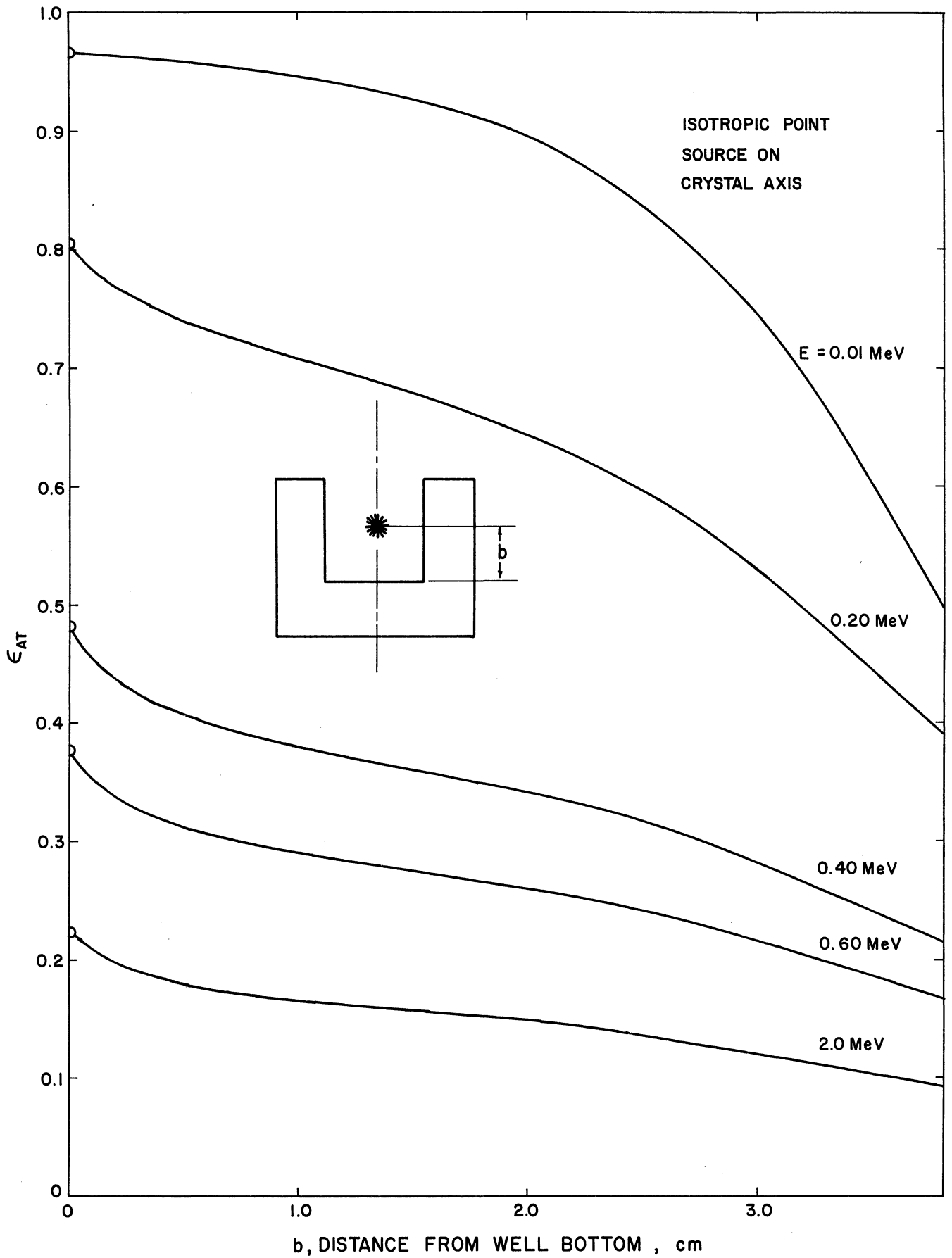


Figure II-7. Effect of Moving Point Source Axially in  $8F8$  Well Crystal.

for the absolute total efficiency,  $\epsilon_{AT}$  for solid and well crystals, respectively. These figures are plotted for two commonly used crystals, the Harshaw Chemical Company Well Crystal No. 8F8 (2 in. dia. x 2 in. ht., with 1-1/8 in. dia. x 1-1/2 in. deep well)<sup>(16)</sup> and a 2 x 2 in. solid cylindrical crystal. Figure II-5 is interesting because with the solid angle dependence removed ( $\epsilon_{IT} = \frac{\epsilon_{AT}}{\Omega/4\pi}$ ), the effect of variation of the extrapolated path length,  $x(\mu)$ , with source-crystal distance is more clearly evident. The average path length in the crystal is longest for very large and very small source-crystal distances because few gammas escape out the cylindrical surface. As this distance increases from zero to infinity, the intrinsic efficiency decreases rapidly, passing through a minimum at a distance equal to approximately the crystal diameter, and then increasing again as the distance increases further. Other investigations have shown this same trend.<sup>(12,17)</sup> Increasing the source distance from the crystal causes the divergence of the gamma rays from an isotropic point source to become a smaller effect, until finally the rays are essentially monodirectional. The latter effect can also be seen in Figure II-5 as the intrinsic efficiency asymptotically approaches the value calculated from Equation (2.2). Figures II-6 and II-7 show that a significant change in  $\epsilon_{AT}$  can result from only a slight axial movement of the point source.

TABLE II-6

ISOTROPIC POINT SOURCE OFF CRYSTAL AXIS AT RADIAL DISTANCE=M  
3 x 3 IN. SOLID CRYSTAL

D = 7.620000

H = 7.620000

B = 1.000000

ENERGY	M= .00	.10	.20	.50	1.00	1.50
.010	.3731	.9998	.9994	.9961	.9838	.9609
.015	.3731	.9998	.9994	.9961	.9838	.9609
.020	.3731	.9998	.9994	.9961	.9838	.9609
.030	.3728	.9998	.9994	.9960	.9832	.9595
.040	.3731	.9998	.9994	.9961	.9838	.9608
.050	.3730	.9998	.9994	.9960	.9835	.9601
.060	.3727	.9998	.9994	.9959	.9830	.9592
.080	.3706	.9998	.9993	.9958	.9827	.9583
.100	.3675	.9998	.9993	.9956	.9819	.9563
.150	.3550	.9998	.9992	.9946	.9778	.9472
.200	.3341	.9997	.9990	.9937	.9740	.9392
.300	.2887	.9997	.9989	.9929	.9714	.9341
.400	.2571	.9997	.9989	.9929	.9712	.9341
.500	.2351	.9997	.9989	.9929	.9713	.9346
.600	.2205	.9997	.9989	.9929	.9715	.9352
.800	.2001	.9997	.9989	.9930	.9719	.9360
1.000	.1857	.9997	.9989	.9931	.9722	.9367
1.500	.1622	.9997	.9989	.9932	.9726	.9378
2.000	.1496	.9997	.9989	.9933	.9729	.9385
3.000	.1380	.9997	.9989	.9933	.9732	.9391
4.000	.1236	.9997	.9989	.9933	.9732	.9395
5.000	.1325	.9997	.9989	.9934	.9733	.9394
6.000	.1325	.9997	.9989	.9934	.9733	.9394
8.000	.1345	.9997	.9989	.9933	.9732	.9395
10.000	.1377	.9997	.9989	.9933	.9732	.9391
15.000	.1466	.9997	.9989	.9933	.9730	.9386
20.000	.1540	.9997	.9989	.9932	.9728	.9385
30.000	.1656	.9997	.9989	.9932	.9726	.9377

TABLE II-7

ISOTROPIC POINT SOURCE OFF CRYSTAL AXIS AT RADIAL DISTANCE=M  
2 x 2 IN. SOLID CRYSTAL

D = 5.080000

H = 5.080000

B = 1.000000

ENERGY	M= .00	.10	.20	.50	1.00	1.50
.010	.3168	.9995	.9980	.9871	.9450	.8619
.015	.3168	.9995	.9980	.9871	.9450	.8617
.020	.3168	.9995	.9980	.9870	.9444	.8604
.030	.3152	.9995	.9979	.9867	.9433	.8585
.040	.3167	.9995	.9979	.9869	.9441	.8600
.050	.3160	.9995	.9979	.9867	.9435	.8589
.060	.3146	.9995	.9979	.9867	.9432	.8582
.080	.3111	.9995	.9978	.9862	.9413	.8543
.100	.3059	.9994	.9977	.9854	.9383	.8487
.150	.2833	.9993	.9974	.9833	.9311	.8375
.200	.2528	.9993	.9972	.9826	.9292	.8369
.300	.2019	.9993	.9973	.9831	.9318	.8454
.400	.1722	.9993	.9974	.9836	.9343	.8516
.500	.1534	.9994	.9974	.9840	.9358	.8554
.600	.1415	.9994	.9975	.9842	.9368	.8578
.800	.1257	.9994	.9975	.9846	.9381	.8609
1.000	.1150	.9994	.9976	.9848	.9390	.8629
1.500	.0983	.9994	.9976	.9851	.9403	.8660
2.000	.0897	.9994	.9976	.9853	.9410	.8675
3.000	.0819	.9994	.9977	.9854	.9416	.8689
4.000	.0790	.9994	.9977	.9854	.9418	.8694
5.000	.0783	.9994	.9977	.9855	.9418	.8695
6.000	.0783	.9994	.9977	.9855	.9418	.8695

## 2. Off-axis Point Sources

No data have been previously available which indicate the effect on  $\epsilon_{AT}$  of moving a point source radially from the axis of a well crystal. The BURP-3 Computer Program, described in Appendix E, was written to investigate the off-axis effect for both well and solid crystals. Reference 5 gives the results from a limited study of the off-axis effect on  $\epsilon_{AT}$  for solid crystals only.

Figures II-3 and II-4 indicate the effect on the efficiency of moving an isotropic point source from the crystal axis. These figures are for a 3 x 3 in. solid NaI(Tl) crystal, with 0.662 and 0.075 MeV sources at  $b = 1.0$  cm. from the crystal, and give a comparison of results from the present work and Reference 5. For solid crystals the trend of decreasing  $\epsilon_{AT}$ , as a point source is moved radially from the crystal axis, has been observed in all calculations with this program. Figures II-3 and II-4 indicate such a trend, and as can be seen, agreement of the present work with experimental and independent calculations<sup>(5)</sup> is excellent. Table II-6 gives the results of calculation for a 3 x 3 in. crystal, with the point source located at  $b = 1.0$  cm. from the crystal, over the energy range 0.01 - 6.00 MeV. Table II-7 gives a similar calculation for a 2 x 2 in. crystal. In both of these tables, the column labeled  $m = 0$  gives the absolute total efficiency for the point source on the crystal axis. For other values of  $m$ , the efficiencies are given relative to the on-axis efficiencies i.e., these are values of  $\epsilon_{AT}(m)/\epsilon_{AT}(m = 0)$ . The relative decrease in  $\epsilon_{AT}$  with varying off-axis distance,  $m$  is not the same at all source heights,  $b$  measured from the face of the

solid crystal. In fact as the data of Table II-8 show, at a given off-axis distance, the ratio  $\epsilon_{AT}(m)/\epsilon_{AT}(m = 0)$  goes through a minimum a short distance from the crystal and then approaches 1.0 as the source height,  $b$  is increased. Thus the magnitude of the effect is reduced further from the crystal. This is, of course, a very similar trend as that previously seen for calculated values of  $\epsilon_{IT}$  for a solid crystal, Figure II-5. The data of Table II-8 are for  $\epsilon_{AT}$  and thus the effect of solid angle decrease, as the source-crystal distance is increased, is included.

TABLE II-8

$\epsilon_{AT}(m)/\epsilon_{AT}(m = 0)$  FOR 2 x 2 IN. SOLID  
CRYSTAL,  $E = 1.0$  MeV

$b$ , cm.	$m = .5$ cm.	$m = 1.0$ cm.	$m = 2.0$ cm.
.1	.989	.949	.763
.5	.985	.940	.745
1.0	.986	.940	.759
2.0	.989	.950	.812
5.0	.996	.976	.913
10.0	.999	.992	.970

Two conclusions from these data for solid crystals are evident. First, in order to use the tabulated values for point sources on the crystal axis, the sources must be located accurately on the crystal axis. Second, the accuracy of this location is more critical close to the solid crystal face. Quantitatively, a 1.0 MeV source located 0.1 cm. from a 2 x 2 in. crystal must be positioned within 0.5 cm. of the crystal axis

for an error of less than 1% if the centrally located point source values for  $\epsilon_{AT}$  are used. If the source-crystal height is 10.0 cm., the radial location need be accurate only within 1.0 cm. of the crystal axis for the same error in applying centrally located point source values of  $\epsilon_{AT}$ . The above positioning requirements have been investigated at energies other than 1.0 MeV and are typical for energies in the range of laboratory sources.

The effect of moving a point source radially from the axis of a well crystal is shown by Figure II-8 for the Harshaw Chemical Company Crystal No. 8F8.<sup>(16)</sup> The effect for the well crystal is seen to be just opposite to that for the solid crystal, i.e.,  $\epsilon_{AT(m)}/\epsilon_{AT(m=0)} > 1.0$ , for  $m > 0$ . For the source within the crystal, two factors combine to cause the observed increase in efficiency as the point is moved from the crystal axis. First, the solid angle subtended at a point source by the top of the well decreases as the point moves off the axis<sup>(15)</sup> and as shown in Table II-5, and thus fewer gammas escape the well without striking the crystal. Second, the average path length in the crystal increases as the source moves off the axis, for well crystal dimensions presently used in practice. Since the geometry factor for most well crystals with the source located near the well bottom is close to unity, the first factor does not contribute as significantly as the second. The second factor was observed by computer analysis of the four integrands which make up the multiple integrals of Equation (2.5). In general the rate of increase in efficiency is less at the bottom of the well than in the upper portions (see Figure II-8)

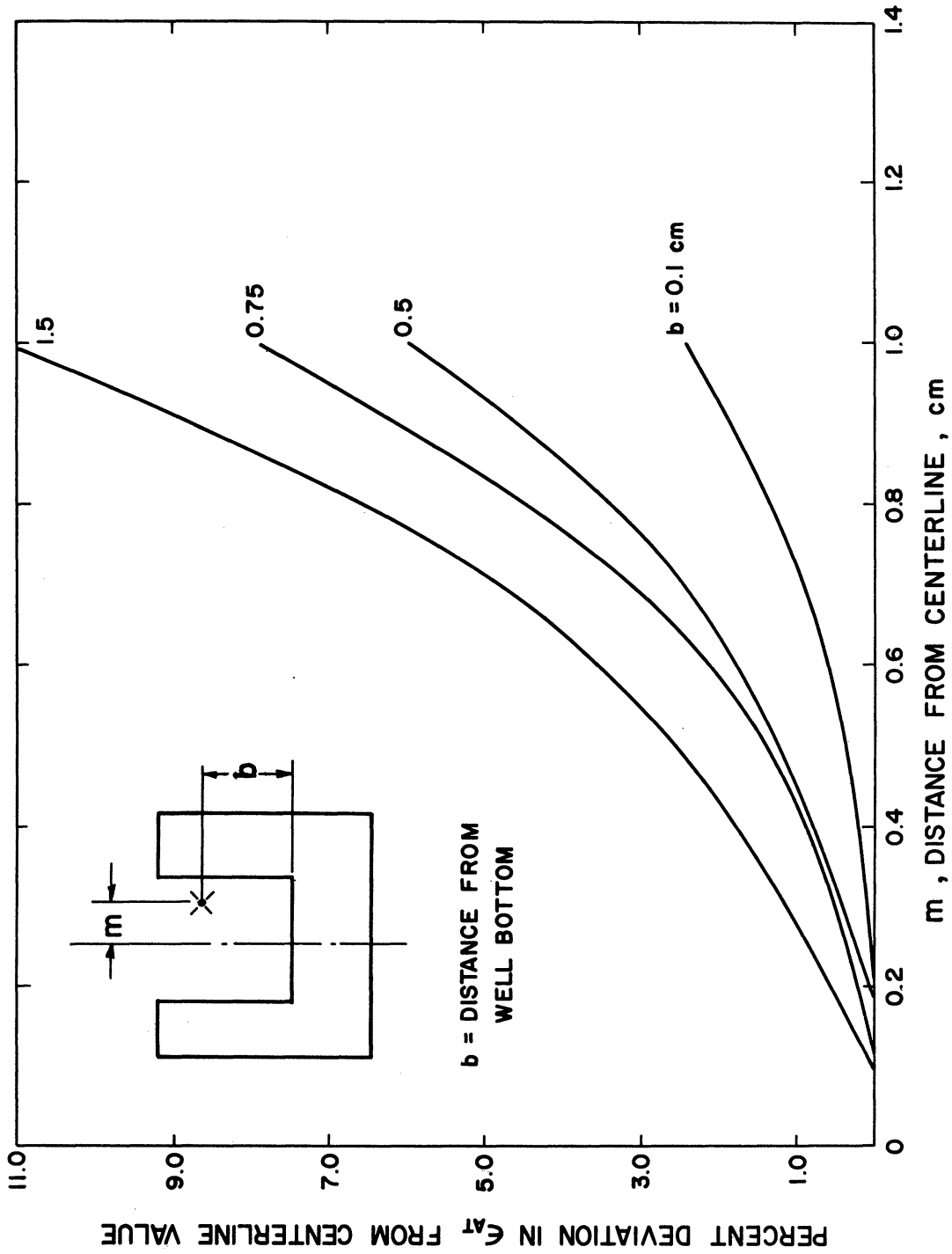


Figure II-8. Increase in  $C_{AT}$  of Well Crystal ( $8\mu\text{F}$ ) for Non-central Point Source. [Energy = 1.0 MeV.]



because the geometry factor influences the results more near the top of the well where  $\frac{\Omega}{4\pi}$  deviates considerably from unity. From the results given in Figures II-3 through II-8, it is evident that axial position variation for a point source has a greater influence on  $\epsilon_{AT}$  than radial position variation. For comparison with the solid crystal, the requirements for accurate location of a 1 MeV point source in an 8F8 well crystal in order to use on-axis values for  $\epsilon_{AT}$  are as follows, for an error of less than 1%. For  $b = 0.1$  cm. (see Figure II-2),  $m$  must be less than 0.7 cm. from the axis. For  $b = 3.0$  cm.,  $m < .3$  cm. is required. Again, these positioning requirements are typical over the energy range of laboratory sources. Tables II-9 and II-10 give results for well crystals. The point source is located at various off-axis radial distances,  $m$ , and at a fixed axial distance from the bottom of the well,  $b = 0.2$  cm. This value for  $b$  is typical of the crystal canning and reflector thickness of available detectors.<sup>(16)</sup> Table II-9 is for the Harshaw Crystal No. 8F8, and Table II-10 is for the 12AW(12)-W1 Harshaw Crystal, 3 x 3 in., with 0.791 in. dia. x 1.5 in. deep well. By reference to these tables it is evident that fairly accurate radial location of a point source is essential if on-axis data for  $\epsilon_{AT}$  are used. For counting measurements in which sources are just dropped into a well counter, the usually assumed reproducibility of source-detector geometry is not justified for precise work. A possible procedure, when an accurate radial positioning device is not available, would be to place the sources at the corner of the well where the location is more likely to be reproducible. Then by reference to data such as given in Tables II-9 and II-10, suitable correction can be applied to the on-axis values for  $\epsilon_{AT}$ .

TABLE II-9

ISOTROPIC POINT SOURCE OFF CRYSTAL AXIS AT RADIAL DISTANCE=M  
8F8 WELL

D = 5.080000                      H = 5.080000                      B = .200000  
WD = 2.857500                      WH = 3.810000

ENERGY	M = 0	.10	.20	.50	1.00	1.42
.010	.9649	1.0000	1.0001	1.0008	1.0031	1.0058
.015	.9649	1.0000	1.0001	1.0008	1.0030	1.0058
.020	.9649	1.0000	1.0001	1.0008	1.0030	1.0058
.030	.9644	1.0000	1.0001	1.0008	1.0032	1.0060
.040	.9648	1.0000	1.0001	1.0008	1.0030	1.0058
.050	.9646	1.0000	1.0001	1.0008	1.0031	1.0059
.060	.9642	1.0000	1.0001	1.0009	1.0032	1.0061
.080	.9633	1.0000	1.0001	1.0009	1.0034	1.0064
.100	.9612	1.0000	1.0002	1.0010	1.0039	1.0073
.150	.9065	1.0001	1.0004	1.0024	1.0101	1.0258
.200	.7691	1.0001	1.0006	1.0037	1.0175	1.0574
.300	.5473	1.0002	1.0008	1.0050	1.0256	1.0973
.400	.4384	1.0002	1.0008	1.0056	1.0291	1.1148
.500	.3761	1.0002	1.0009	1.0059	1.0309	1.1243
.600	.3395	1.0002	1.0009	1.0061	1.0320	1.1298
.800	.2932	1.0002	1.0009	1.0063	1.0333	1.1366
1.000	.2633	1.0002	1.0010	1.0064	1.0342	1.1410
1.500	.2190	1.0002	1.0010	1.0066	1.0354	1.1473
2.000	.1970	1.0002	1.0010	1.0067	1.0360	1.1505
3.000	.1778	1.0003	1.0010	1.0068	1.0365	1.1532
4.000	.1718	1.0003	1.0010	1.0068	1.0367	1.1542
5.000	.1691	1.0003	1.0010	1.0069	1.0368	1.1544
6.000	.1691	1.0003	1.0010	1.0069	1.0368	1.1544

TABLE II-10

ISOTROPIC POINT SOURCE OFF CRYSTAL AXIS AT RADIAL DISTANCE=M  
3 x 3 IN. WELL CRYSTAL

D = 7.620000                      H = 7.620000                      B = .200000  
WD = 2.857500                      WH = 3.810000

ENERGY	M = 0	.10	.20	.50	1.00	1.42
.010	.9649	1.0000	1.0001	1.0008	1.0031	1.0058
.015	.9649	1.0000	1.0001	1.0008	1.0031	1.0058
.020	.9649	1.0000	1.0001	1.0008	1.0030	1.0058
.030	.9646	1.0000	1.0001	1.0008	1.0030	1.0058
.040	.9649	1.0000	1.0001	1.0008	1.0030	1.0058
.050	.9648	1.0000	1.0001	1.0008	1.0030	1.0057
.060	.9645	1.0000	1.0001	1.0008	1.0031	1.0058
.080	.9634	1.0000	1.0002	1.0009	1.0035	1.0064
.100	.9618	1.0000	1.0002	1.0010	1.0039	1.0071
.150	.9520	1.0001	1.0003	1.0016	1.0061	1.0116
.200	.9116	1.0001	1.0004	1.0026	1.0109	1.0249
.300	.7752	1.0002	1.0006	1.0040	1.0181	1.0509
.400	.6733	1.0002	1.0007	1.0045	1.0212	1.0640
.500	.6041	1.0002	1.0007	1.0048	1.0229	1.0715
.600	.5595	1.0002	1.0008	1.0050	1.0239	1.0758
.800	.4989	1.0002	1.0008	1.0052	1.0251	1.0812
1.000	.4572	1.0002	1.0008	1.0054	1.0259	1.0847

### 3. Disk Sources

The discussion so far has been restricted to sources which are small enough to be considered mathematically as a point. Of obvious interest then is determination of when a distributed, homogeneous source can be considered a point source. Considering the isotropic source is a disk, with its center located on the axis of the crystal, calculations were made for  $\epsilon_{AT}$  as the disk diameter was decreased, at a fixed distance from the bottom of the well. Results for 8F8 and 12AW(12)-W2 crystals are shown in Figures II-9 and II-10, respectively. Tabulated results for these crystals, plus others, with disk sources are given in Appendix G. The 12AW(12)-W2 well crystal is 3 x 3 in., with 1-1/8 in. dia. x 1-1/2 in. deep well. Two facts are evident from these curves. First, as the disk diameter goes to zero, the results from the disk source computer program (BURP-2) reduce to those independently calculated by the point source program (BURP-1). This provides another check of the proper calculation with these programs. Second, over the range of energy  $.01 \leq E \leq 2.0$  MeV, and for both the 2 x 2 in. and 3 x 3 in. well crystals, there is an insignificant difference between the point and disk source values of  $\epsilon_{AT}$  for disks up to 0.8 cm. radius. Disks up to 1.0 cm. radius differ from on-axis point sources by less than 2% in  $\epsilon_{AT}$ . Figure II-11 represents the variation in  $\epsilon_{AT}$  as a disk of fixed radius (1.0 cm.) is moved axially from the well bottom of an 8F8 crystal.

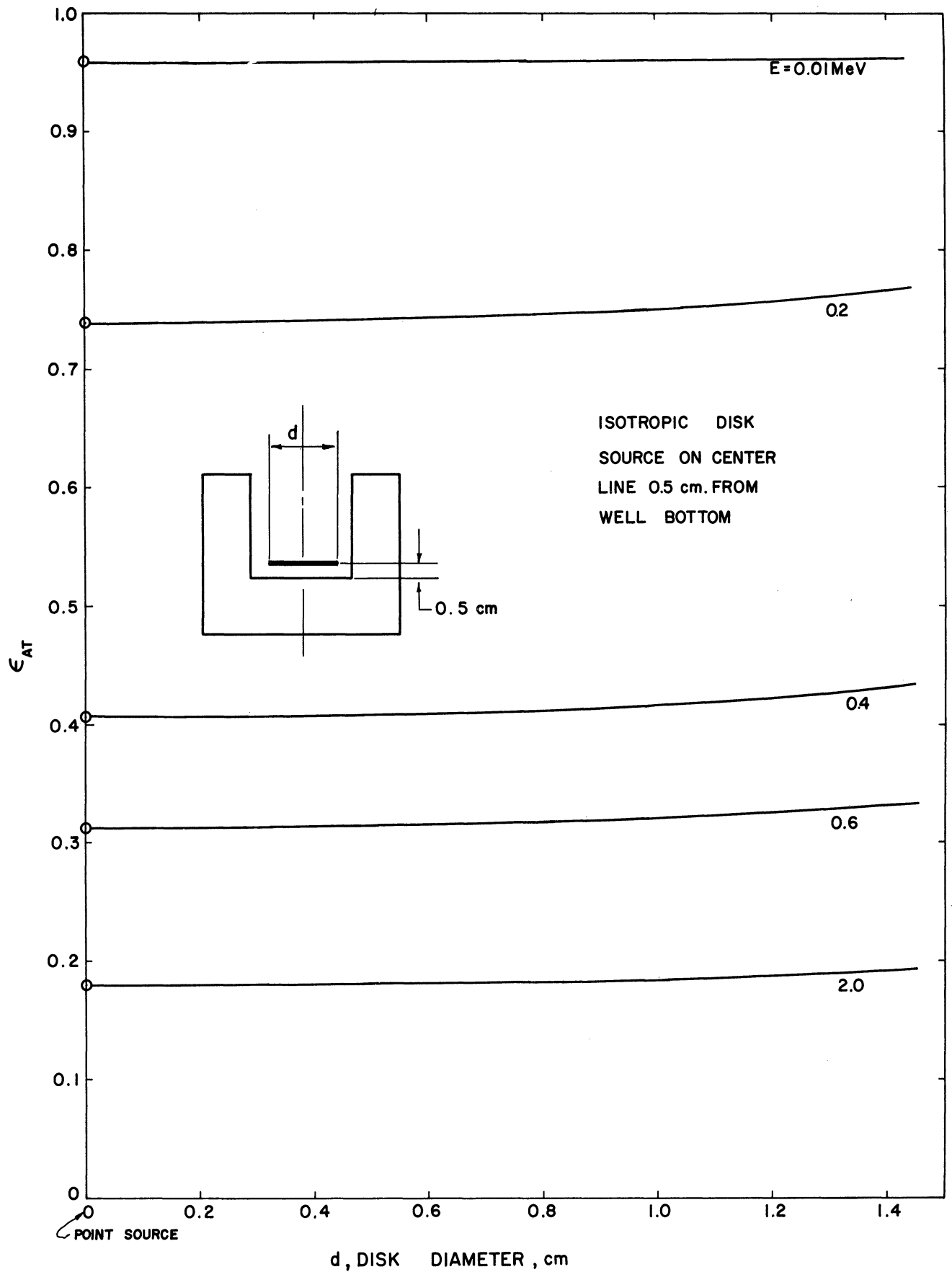


Figure II-9.  $\epsilon_{AT}$  Variation with Disk Diameter for 8F8 Well Crystal.

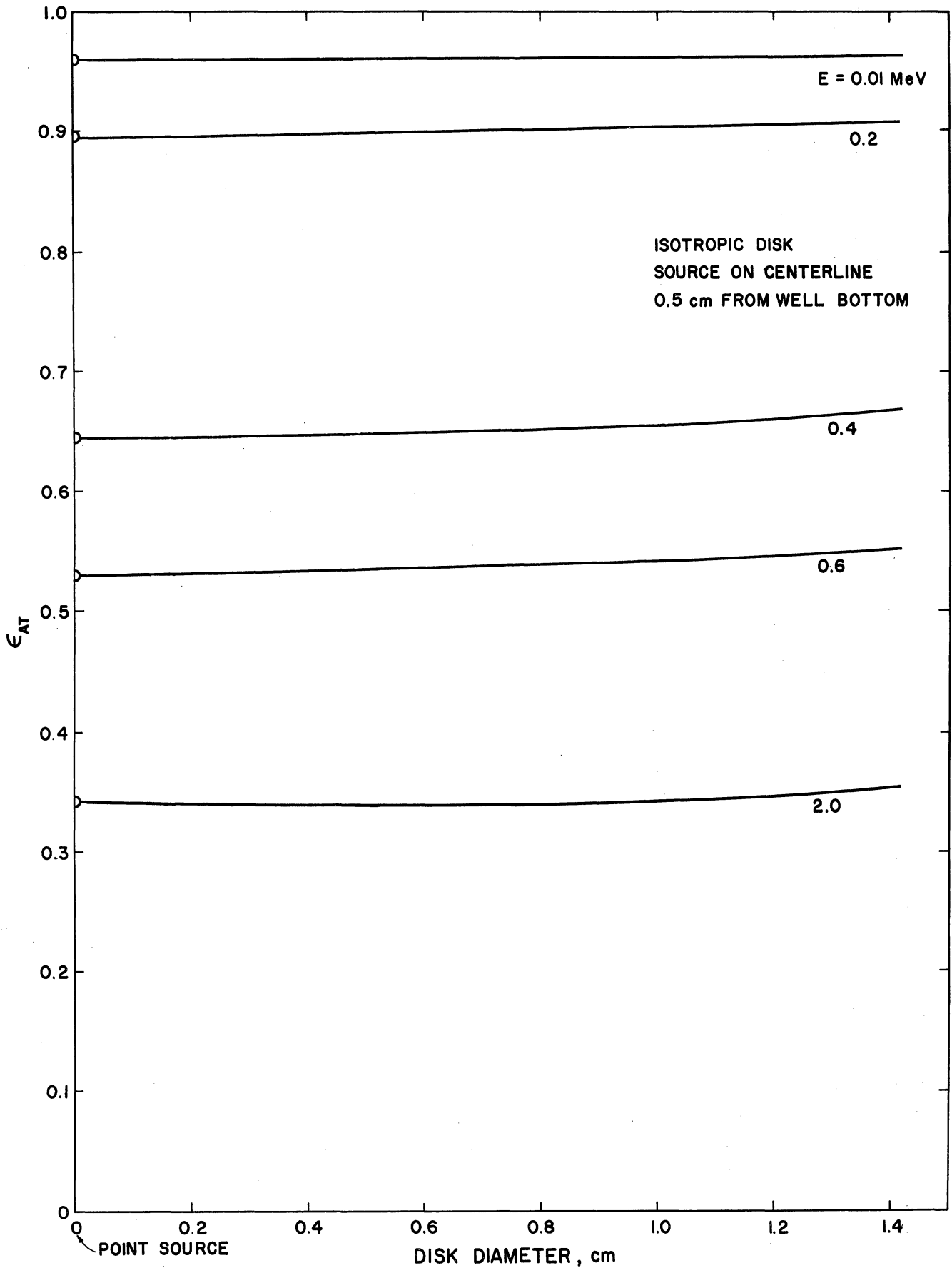


Figure II-10.  $\epsilon_{AT}$  Variation with Disk Diameter for 12AW12-W2 Well Crystal.

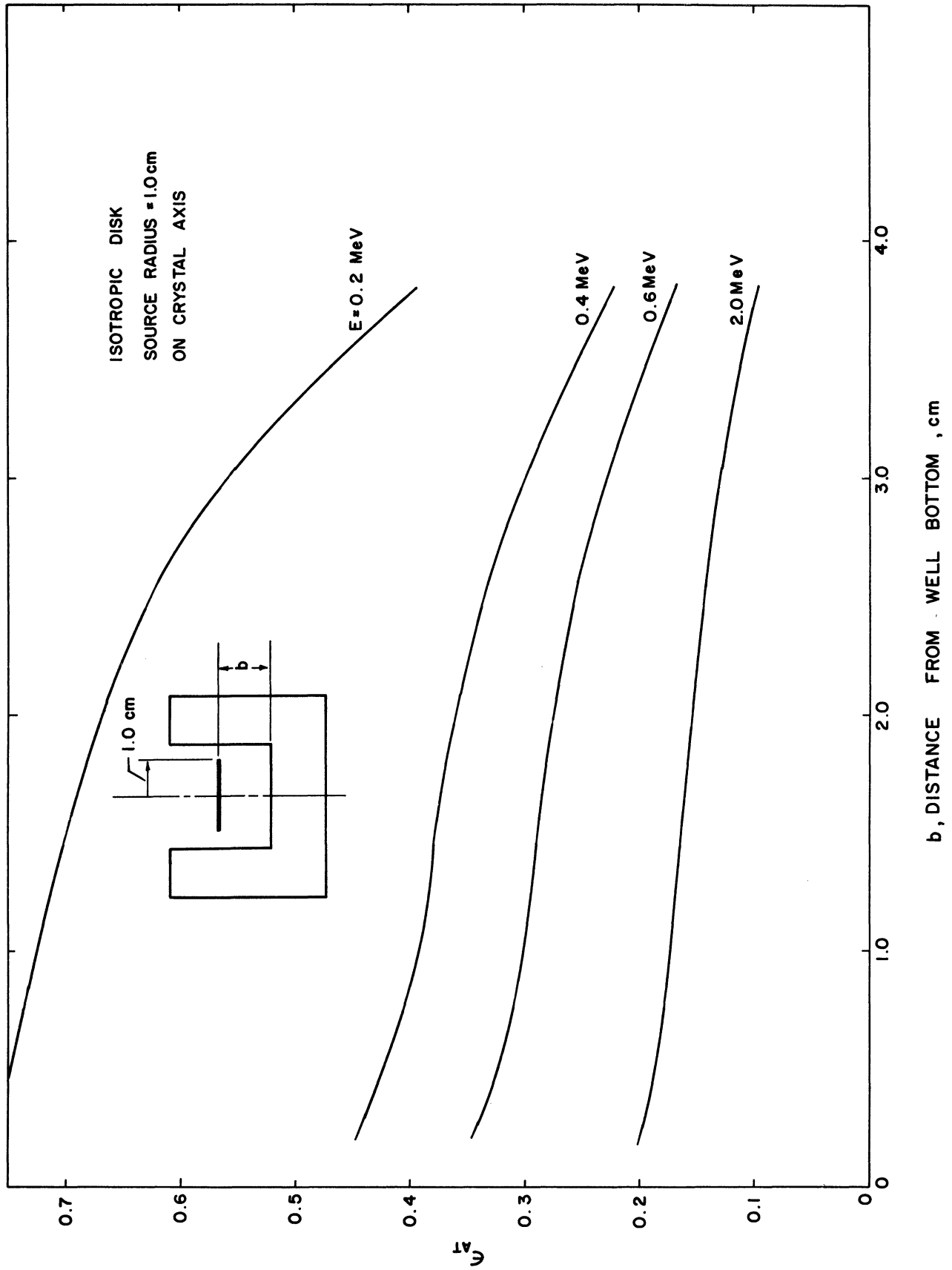


Figure II-11.  $C_{AT}$  Variation with Disk Position for 8F8 Well Crystal.

Figure II-12 gives results for disk sources of various radii, all at .412 MeV. The 8F8 well crystal, 2 x 2 in., and 3 x 3 in. solid crystals are compared in this figure. It should be noted that the total efficiency increases with disk size at a fixed axial position for the well crystal, and decreases for the solid crystal. This is a manifestation of the same effects previously discussed for the point source moved radially from the crystal axis. Also, the advantage in absolute total efficiency of a well crystal over a solid crystal of the same outside dimensions can be seen from this figure. The data for the two solid crystals indicate that for disks located close to the crystal, little deviation from a point source is found for disk radii up to 0.8 cm. For a disk close to the crystal and a radius of 1.5 cm., the decrease in  $\epsilon_{AT}$  is approximately 6% for the 2 x 2 in. solid crystal and 3% for the 3 x 3 in. solid crystal. At a disk-solid crystal distance of 100cm., it is seen that disks of 2.54 cm. radius cause no significant variation from the point source results. Thus for disks, as for off-axis points, the deviation from on-axis point source values of  $\epsilon_{AT}$  decreases and becomes negligible as the source-solid crystal distance increases.

Since it has been shown that only a small error results in using on-axis point source  $\epsilon_{AT}$  values for disks of less than 0.8 cm. radius, it was considered sufficient to limit extensive calculations, to point sources only. Where greater accuracy is desired, some tables for disks are given for a limited number of well and solid crystals. All these tables will be found in Appendix G.

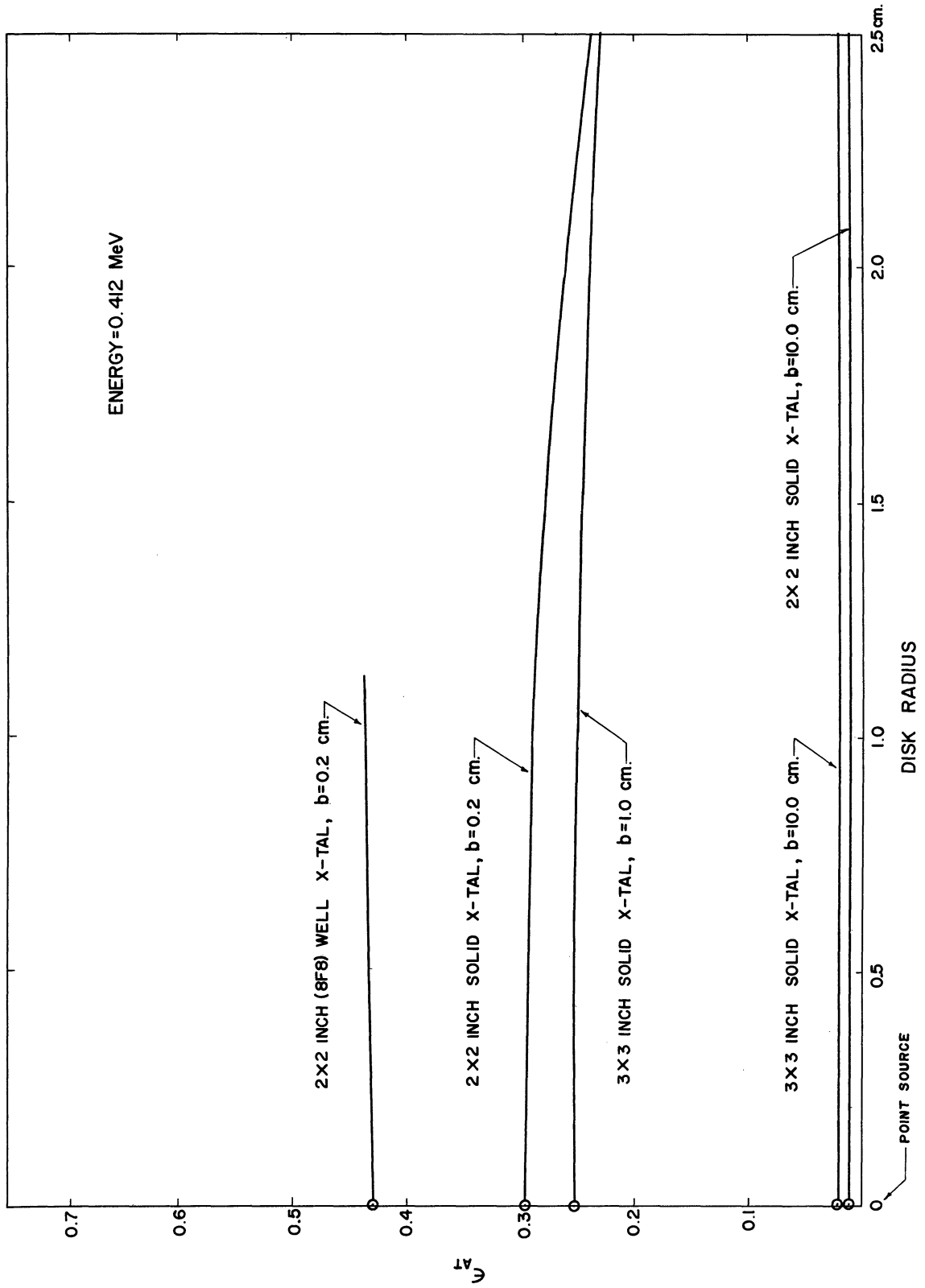


Figure II-12.  $\epsilon_{AT}$  Variation with Disk Radius.



#### 4. Cylindrical Volume Sources

Verheijki<sup>(18)</sup> has given the only previous results for cylindrical volume sources. His work was restricted to cylindrical sources and solid crystals of equal diameters. Again no data are available for well crystals, and therefore a computer program was developed to consider any sized cylindrical volume source located along the axis of either well or solid crystals.

All calculations for homogeneous, isotropic disk sources assume that the source is two-dimensional. The effect of finite source thickness has also been investigated. Some results are shown in Figures II-13 through II-17. Figures II-13 and II-14 give values of  $\epsilon_{AT}$  for a cylindrical source which is 0.3 cm. from the well bottom, to allow for the combined thickness of a glass test tube, and crystal canning and reflector. Again these figures confirm one aspect of the computer programs because they indicate a smooth asymptotic behavior as a cylindrical volume source approaches zero thickness, finally converging to the independently calculated disk source results. Figures II-13 and II-14 are for the 8F8 well crystal, and show that for cylinder thicknesses up to .05 cm. (approximately 20 mils), insignificant variation from disk source  $\epsilon_{AT}$  values results. For most neutron activation foils and other foil sources, this 20 mil foil thickness would not be exceeded. In fact, seldom are foils used which are greater than 1-2 mils in thickness. Thus, foils in general use can be considered to be two-dimensional sources, and if they are located at the well bottom and are well-approximated by a disk of radius less than 0.8 cm., they can be considered point sources.

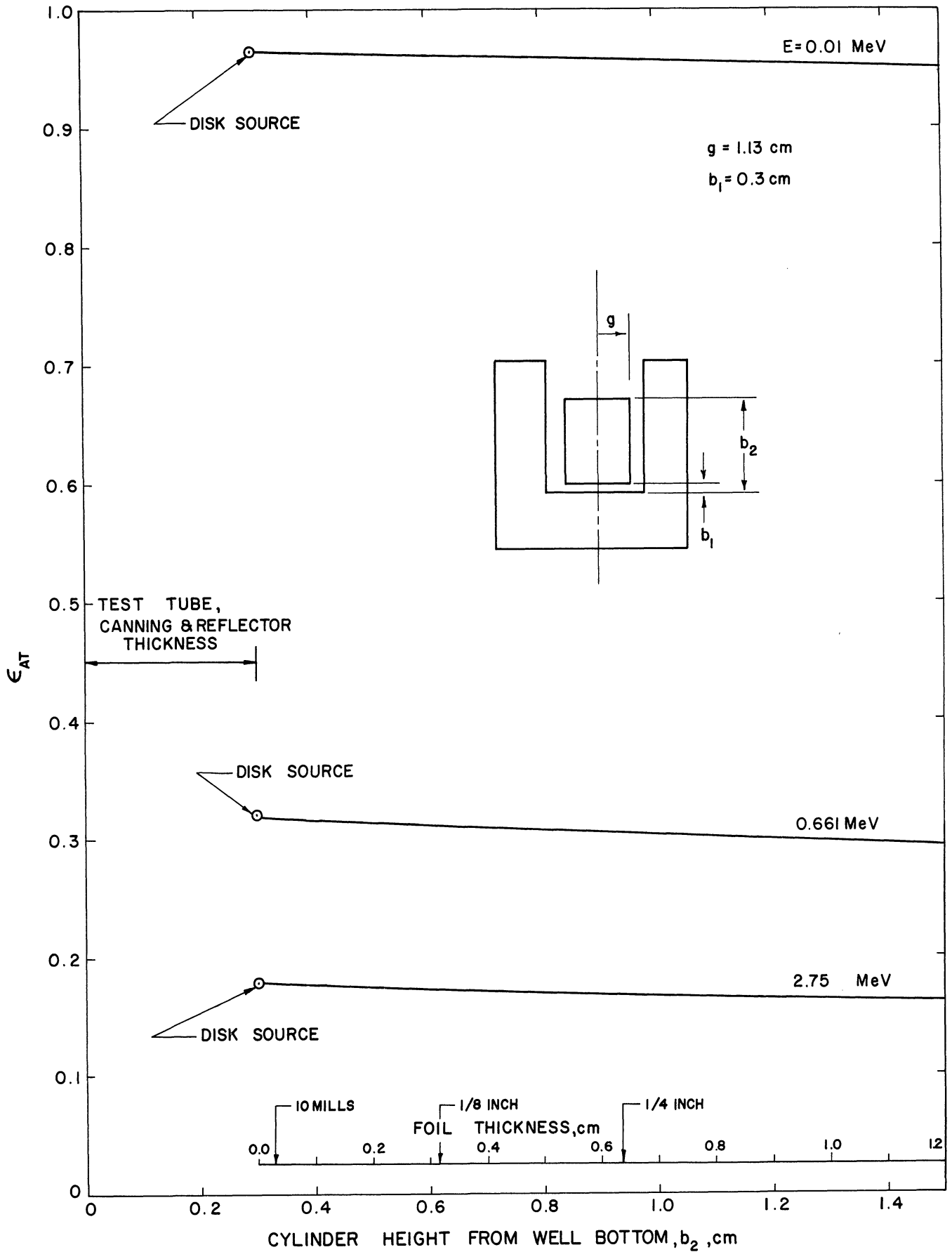


Figure II-13.  $\epsilon_{AT}$  Variation with Cylindrical Volume Source Height for  $^{8F8}$  Well Crystal.

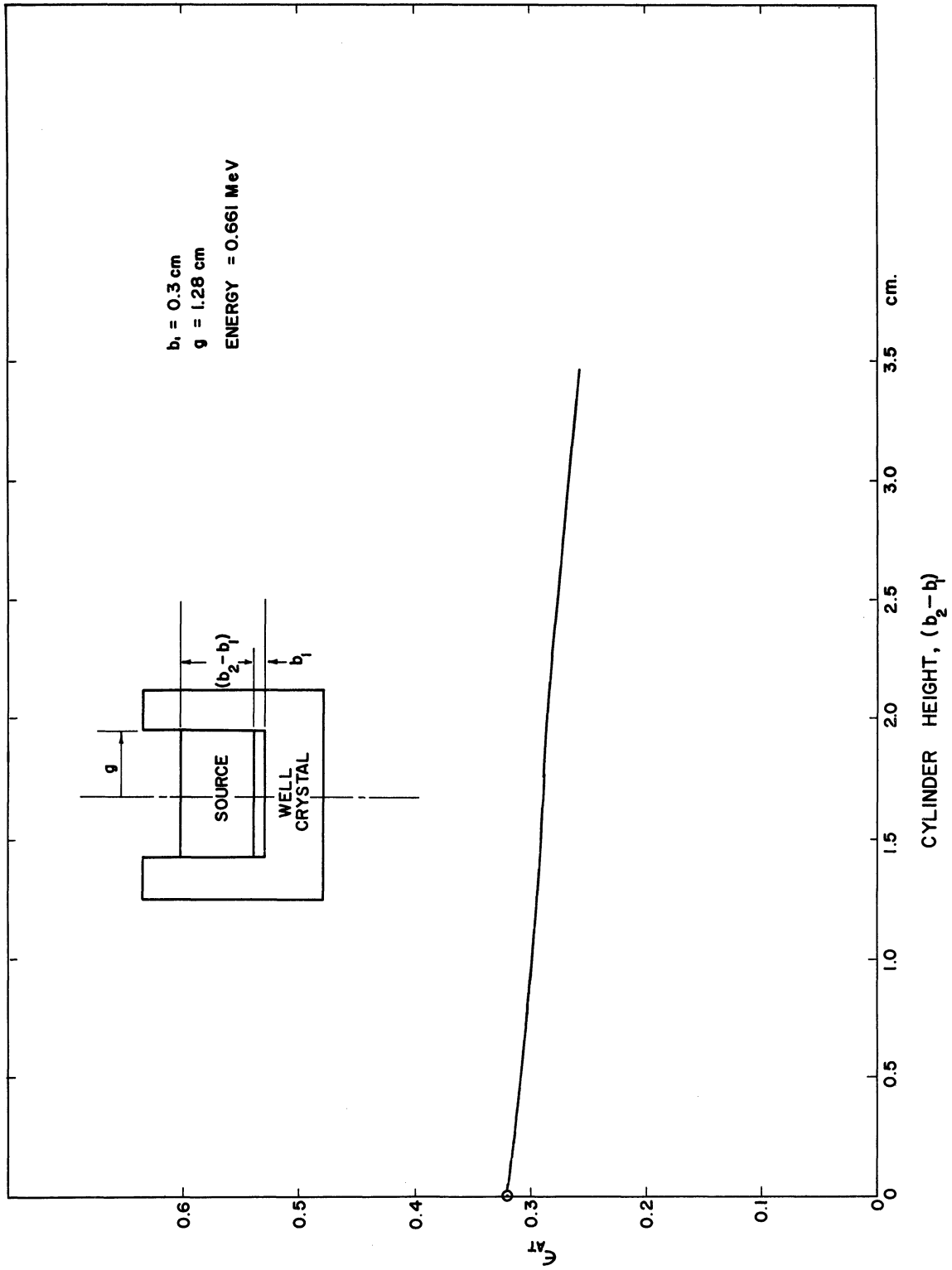


Figure II-14.  $\zeta_{AT}$  Variation with Volume Source Height for 8F8 Well Crystal.

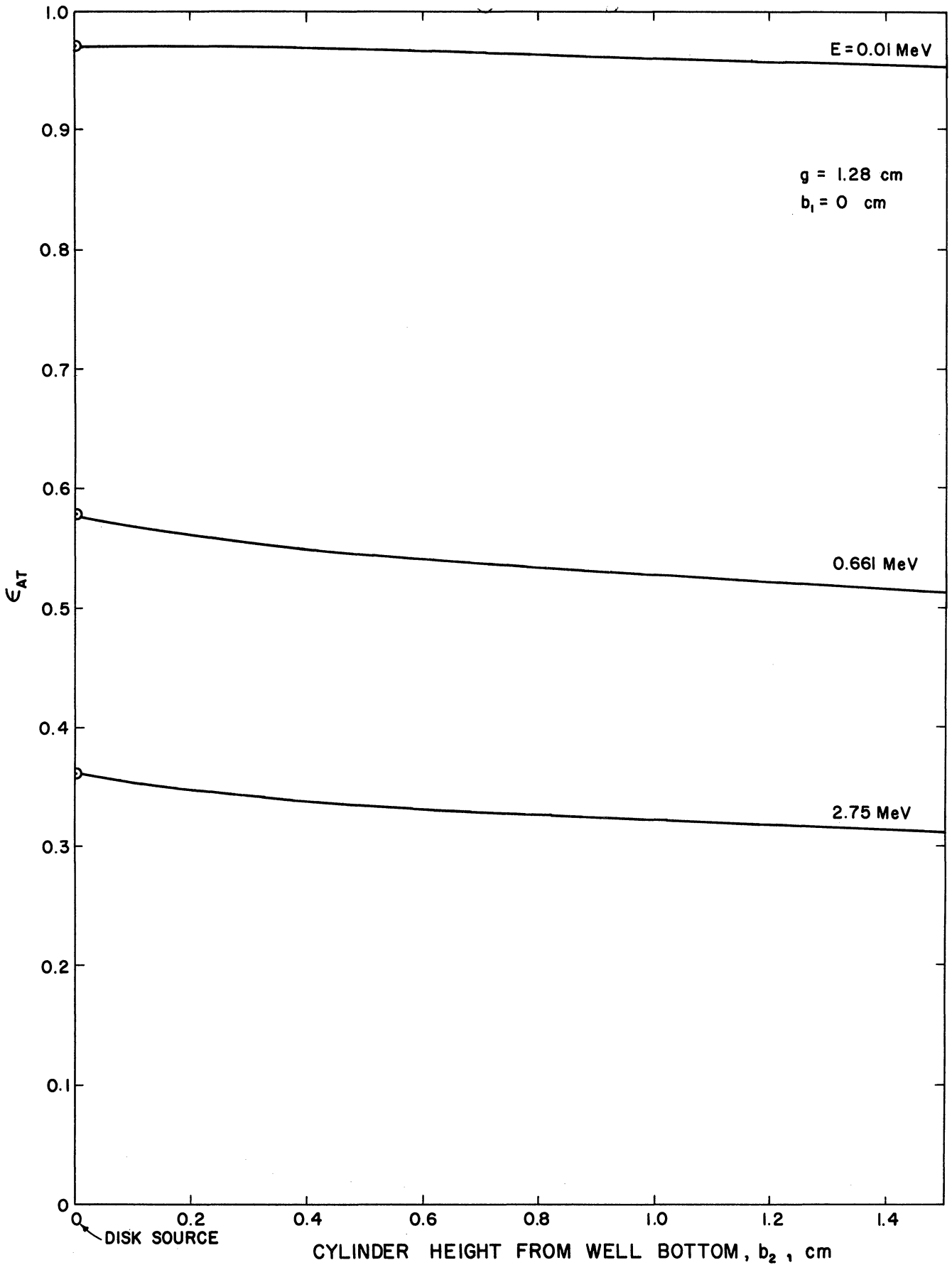


Figure II-15.  $\epsilon_{AT}$  Variation with Volume Source Height for 12AW12-W2 Well Crystal.

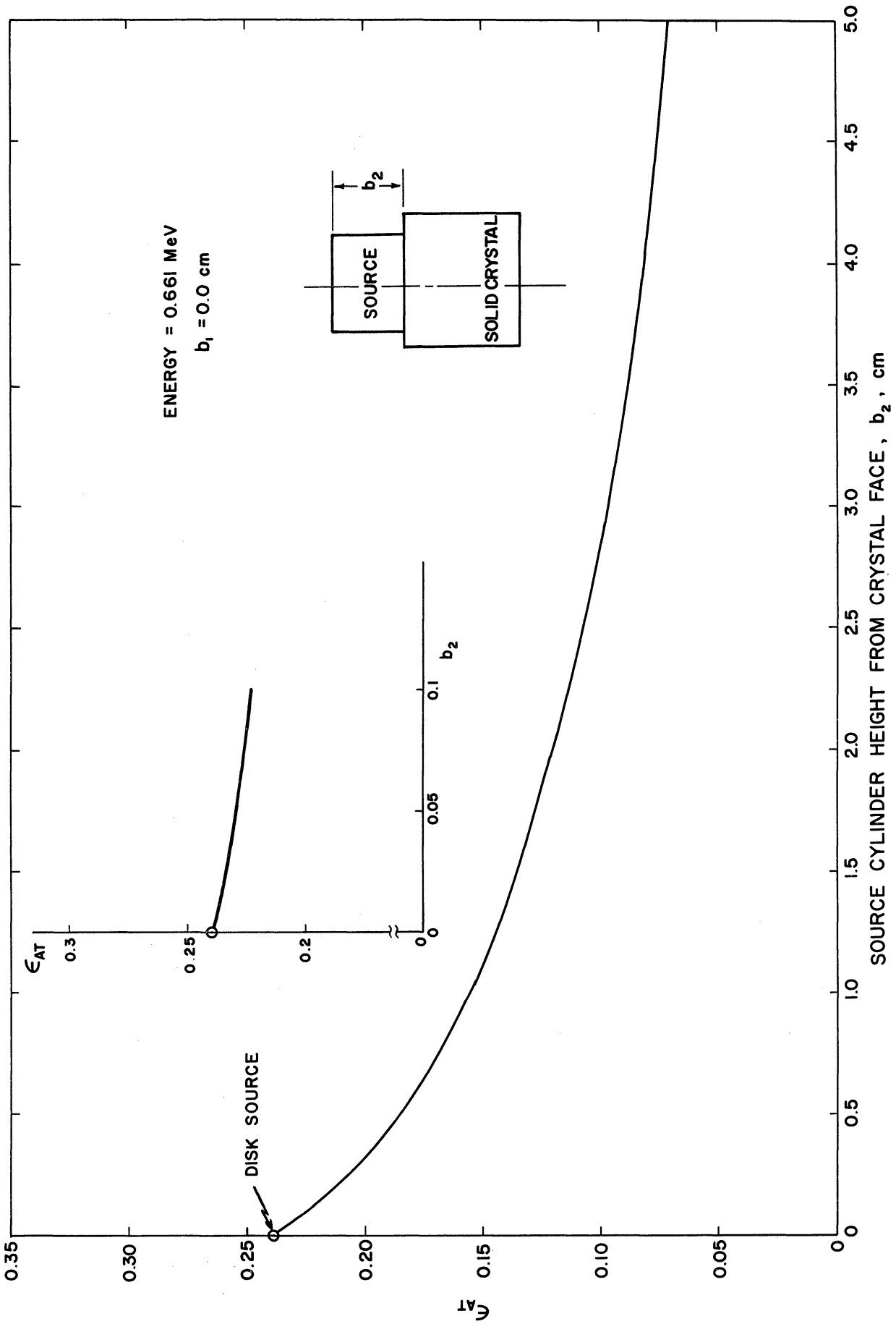


Figure II-16.  $\epsilon_{AT}$  Variation with Volume Source Height for 2 x 2 In. Solid Crystal.

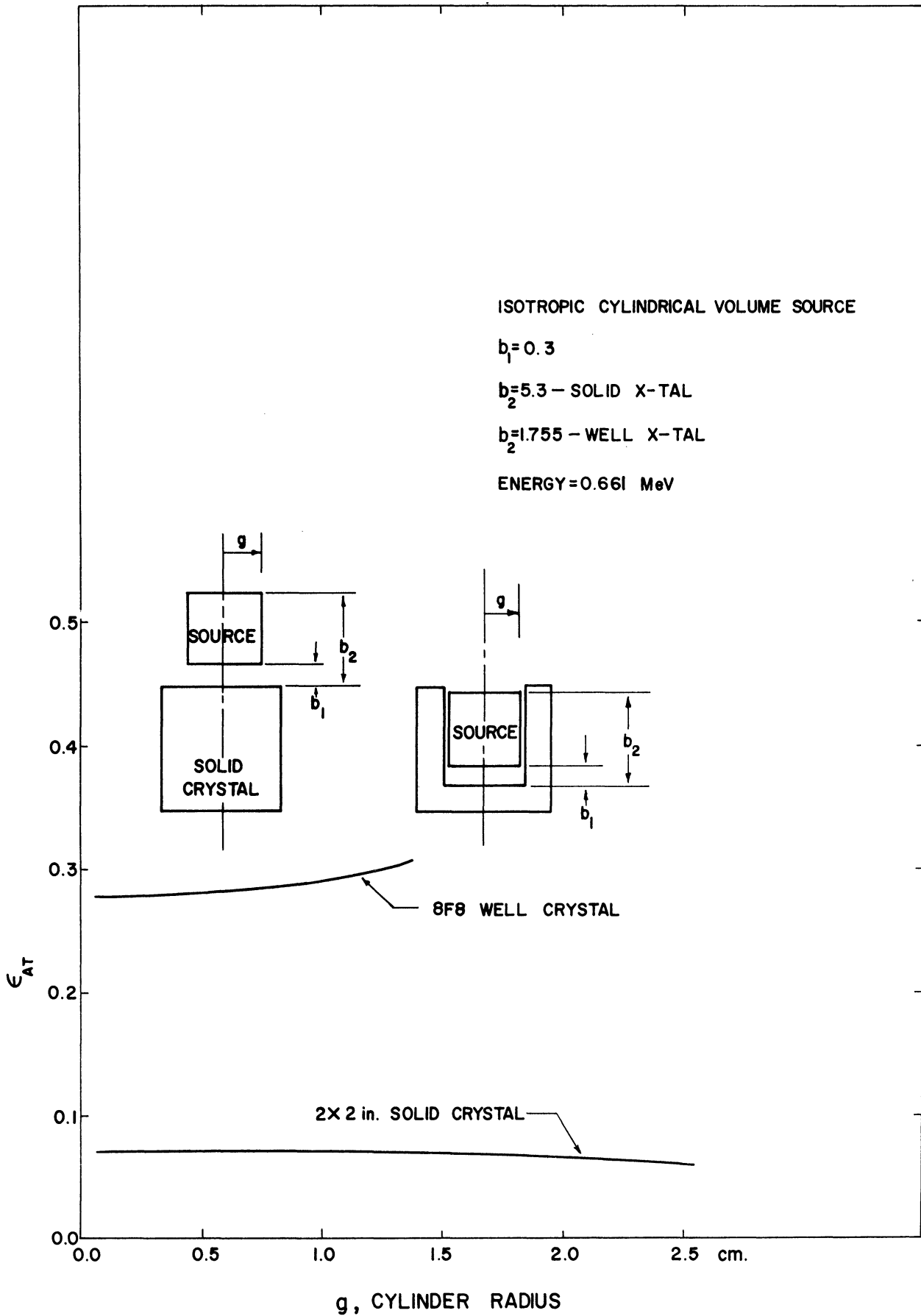


Figure II-17. Variation in  $\epsilon_{AT}$  with Source Cylinder Radius.

The rapid decrease in  $\epsilon_{AT}$  with source cylinder height is as expected since the upper annular portion of the well crystal contributes less to the attenuation of source gammas than does the solid lower portion, and also the fraction that escape out the top of the well increases. The decreasing efficiency with distance from the bottom of the well has been a characteristic seen in calculations for all source geometries. There is no available data for calculated values of volume source  $\epsilon_{AT}$ , except for Reference 18, so the results of some computations are tabulated for both solid and well crystals in Appendix G. These volume sources are assumed to be transparent to emergent gammas and no attenuation has been considered. For volume sources in which absorption and scattering of the source gammas is not negligible, a separate calculation has been made. This problem will be discussed in detail in Chapter IV, Section H. In order to take into account the combined thickness of the crystal casing, reflector, and source container, the tabulations for  $\epsilon_{AT}$  are made for various height cylinders which are placed 0.3 cm. from the crystal surface. Some calculations of the effect of varying the cylindrical source diameter have been made for a 2 x 2 in. (Harshaw No. 8F8) well crystal at 0.661 MeV. The results of these calculations are shown in Figure II-17. By comparison with Figure II-16, the decrease in  $\epsilon_{AT}$  for a solid crystal is negligible as the source diameter increases. From Figures II-15 and II-17 for well crystals, a slightly greater change in  $\epsilon_{AT}$  is seen with variations in source height than with increasing source diameter. Although not as pronounced for the well crystal, this trend for  $\epsilon_{AT}$  with radial and axial dimensional changes is the same as for point and disk sources.

E. Other Factors Effecting  $\epsilon_{AT}$

The final geometry variations were calculations to study the influence of crystal dimensions on  $\epsilon_{AT}$ . In particular, the influence of well crystal overall dimensional tolerances, and the effect of various well sizes were determined. Also, since Reference 19 indicates the thallium concentration in the central portion of a typical NaI(Tl) crystal can vary from 0.11% - .25% by weight (w/o) calculations were performed to study this effect on the absolute total efficiencies for 8F8 and 12AW12 crystals. The results obtained indicated that  $\epsilon_{AT}$  varied at most by 0.2% for a variation of thallium concentration from zero to 0.25 w/o. The effect of well crystal dimensional tolerances on the total efficiency calculations has been determined for a typical well crystal. According to Reference 16, a manufacturing tolerance of  $\pm .005$  in. is guaranteed. Using the worst combinations of this tolerance on all crystal dimensions causes a maximum deviation in the absolute total efficiency of 0.64% from a nominal sized crystal.

The influence that well diameter and height have on  $\epsilon_{AT}$  are shown in Figures II-18, II-19 and II-20. Figures II-18 and II-20 show how  $\epsilon_{AT}$  varies with well dimensions for an isotropic point source on the crystal axis, at the top of the well. These two figures are plotted from the same data, but using different coordinates. The source was located at the top of the well specifically to illustrate that the computer results for a well crystal converged to those for a solid crystal, as the well is made progressively smaller. This provides another independent check of the computer programs. Figure II-18 shows a rather



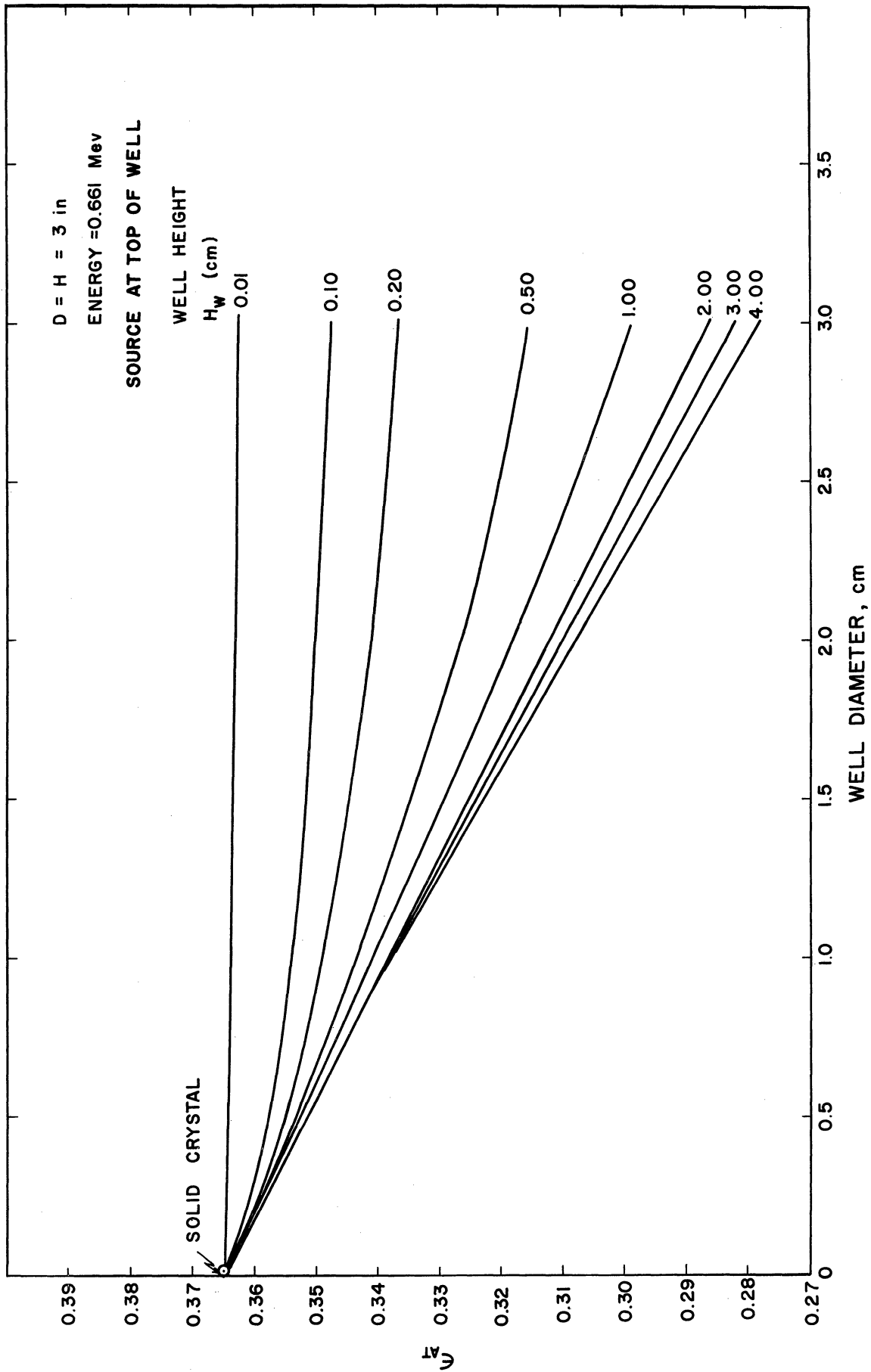


Figure II-18.  $\epsilon_{AT}$  Variation with Well Diameter.

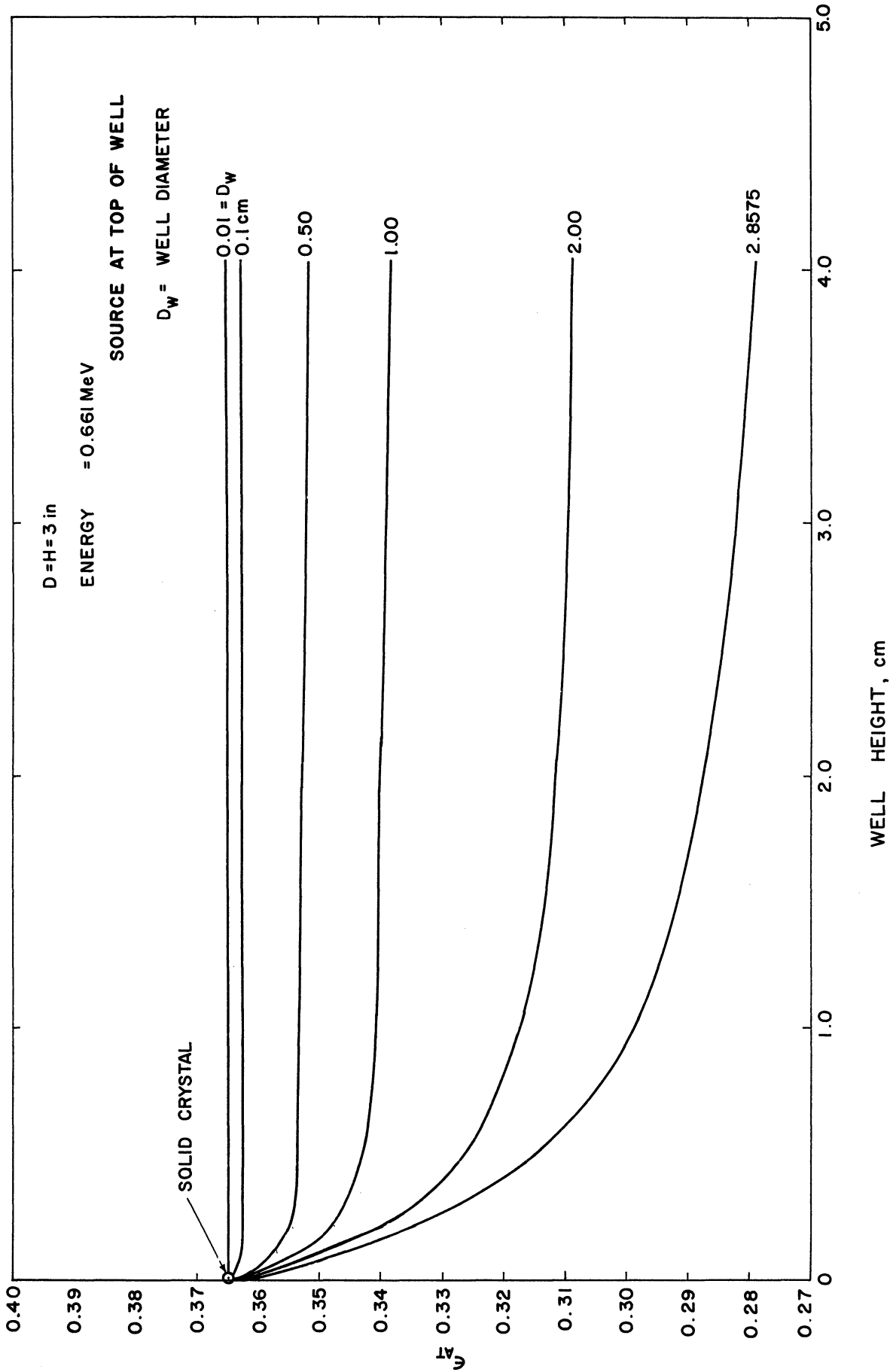


Figure II-19.  $C_{AT}$  Variation with Well Height.

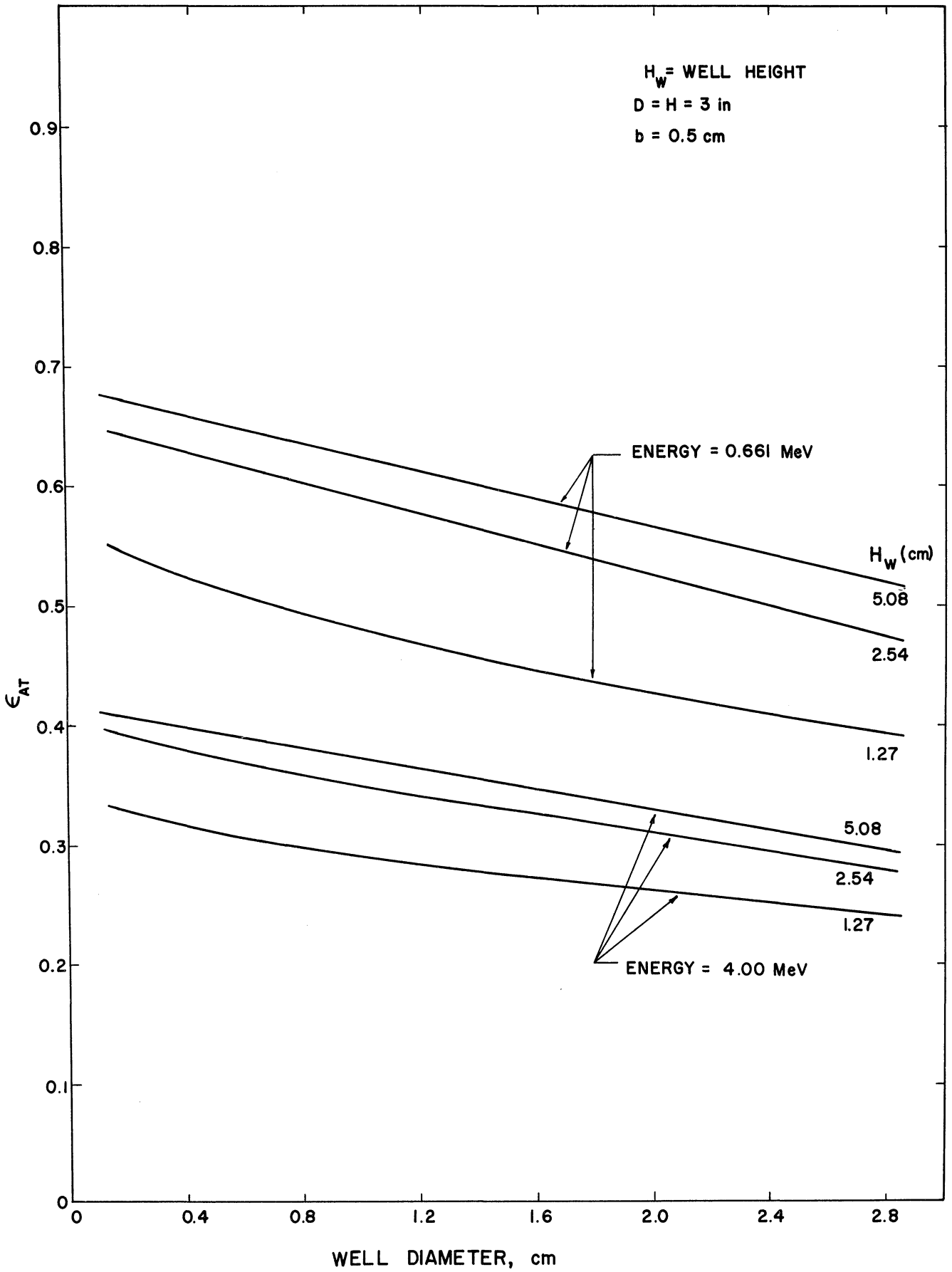


Figure II-20.  $\epsilon_{AT}$  vs. Well Size.

surprising linear variation of  $\epsilon_{AT}$  with increasing well diameter, for various values of well height. Although comparison of Figures II-18 and II-19 indicates that increases in well height beyond about 2.0 cm. have no further influence on  $\epsilon_{AT}$ , (for diameters < 2.0 cm.), it must be remembered that the source is located at the top of the well, and that the advantage of locating the source deeper within the crystal is not being considered. Figure II-20, to be discussed subsequently, does show this effect. However, one can conclude from a comparison of Figures II-18 and II-19 that variations in well diameter have a much greater effect on  $\epsilon_{AT}$  values than do variations in well height. That this is true, even when the source is located near the well bottom, can be seen in Figure II-20. In this figure, the same general trend is seen for two values of gamma ray energy, 0.661 MeV, and 4.00 MeV. The decrease in efficiency as the well diameter is increased is seen to be much greater than the change caused by decreasing the well height the same amount. This trend would be expected since of course the well volume goes as the square of the diameter, and is linear with height. However, calculations have shown that the change in  $\epsilon_{AT}$  does not correlate with well volume changes, i.e., for different diameter and height, but same volume wells, the efficiency is considerably different.  $\epsilon_{AT}$  is seen to depend on both the diameter and height of the well, independently.

#### F. Accuracy of $\epsilon_{AT}$ Results

Correct and accurate application of all these calculations is dependent upon many things. Primarily they are: accurate definition of

crystal dimensions, accuracy of total cross sections used, and accuracy of the numerical integration technique used. The effect of manufacturing tolerances was seen to be small, of the order of 0.6%. The Gaussian quadrature numerical integration technique has been optimized, with respect to the number of subintervals into which each integral is divided and the order of the approximating polynomial, such that the results are accurate to four decimal places.

The total gamma ray cross sections for NaI(Tl) included in the computer programs are taken from the National Bureau of Standards data given in References 20 and 21. References 20 and 21 give the most extensive summary and compilation of primary values of attenuation coefficients for photons on 29 materials. The summary of Reference 20 includes a detailed analysis of both theoretical and experimental results. These data were obtained primarily by theoretical calculations, with experimental data serving as a check. Reference 22 provides extrapolations and interpolations of older NBS data to include all elements up to atomic number 100.

The NBS data are reported to be accurate within 3 - 5% and this will cause some error in the application of any efficiency calculations to experimental results. Reference 5 presents some calculated results of the effect of an error in cross sections on detection efficiency. An estimate of the maximum percentage change in  $\epsilon_{IT}$  for a given percentage change in cross section can be made. The intrinsic total efficiency can be written approximately as:

$$\epsilon_{IT} \approx 1 - e^{-\tau x}$$

Since the average path length,  $x$ , in the crystal is of the order of the crystal height ( $x < 10$  cm. for most common crystals), two limiting cases are of interest. First, for low energy gammas ( $E < 0.2$  MeV) and an average path of about 4 cm. or more,  $\epsilon_{IT}$  is essentially unity, and changes in  $\tau$  will have no effect. Second, in limit of higher energy gammas ( $\tau$  generally decreases), the above expression can be expanded in a series and written approximately as:

$$\epsilon_{IT} \approx \tau x .$$

This case sets an upper limit to the effect of an error in cross section on the efficiency. The maximum effect is that a given percentage error in cross section causes, at most, the same percentage error in efficiency. Thus one can conclude that an error in cross section of 3% can cause no more than a 3% error in calculated efficiency.

The  $\epsilon_{AT}$  tabulations are presented with efficiency as a function of incident gamma ray energy, for convenience. As can be seen from Equation (2.1), the efficiency is a direct function of total cross section, and is related to energy only indirectly. If in the future improved cross sections become available, the tabulated data in Appendix G can be plotted as a function of total cross section, using the data of Table II-11, and the appropriate corrections made.

TABLE II-11

TOTAL GAMMA RAY CROSS SECTIONS IN PURE NaI<sup>(20,21)</sup> USED IN  
EVALUATING  $\epsilon_{AT}$  (NO COHERENT SCATTERING)

Energy, MeV	$\tau$ , cm <sup>-1</sup>	Energy MeV	$\tau$ , cm <sup>-1</sup>
0.01	564.718	1.0	0.212
0.015	178.950	1.5	0.171
0.02	81.041	2.0	0.151
0.03	26.806	3.0	0.135
0.03323	20.462		
0.03323	111.477	4.0	0.129
		5.0	0.127
0.04	66.739	6.0	0.127
0.05	37.037	8.0	0.128
0.06	22.625		
0.08	10.488	10.0	0.134
		15.0	0.147
0.10	5.757	20.0	0.158
0.15	2.083	30.0	0.176
0.20	1.118		
0.30	0.568		
0.40	0.407		
0.50	0.330		
0.60	0.289		
0.80	0.241		

G. Extrapolation of Tabulated Results

1. Other Crystal Sizes

The tabulated calculations for the absolute total efficiency given in Appendix G have been made for scintillation crystals found to be in most general use for laboratory gamma ray detection. Interpolation and extrapolation of these tables is possible for other crystal and source dimensions which are in the proportions dictated by the following scheme, which has been given by References 6 and 10. Although this method was originally given by References 6 and 10 for on-axis point sources, it can

be extended to any source geometry. Inspection of the expressions for  $\epsilon_{AT}$  given by Equations (2.4 - 2.9) shows that the crystal and source dimensions always occur as products with the total cross section,  $\tau$ , or in ratio with one another. Thus the absolute total efficiency calculated for a given set of crystal and source dimensions and cross section equals that for  $N$  times each of the dimensions and at a cross section corresponding to  $\tau/N$ , where  $N$  is any number.

## 2. Other Source Energies

The data tabulated in Appendix G may be readily interpolated for energy, as indicated in Figures II-21, II-22 and II-23. Figures II-21 and II-22 are for the 8F8 and 7F8 well crystals, respectively. Figure II-23 is for a 2 x 2 in. solid crystal. These figures give the variation of  $\epsilon_{AT}$  with energy, for different source-crystal distances. At the lowest energies (highest cross section) the intrinsic total efficiency,  $\epsilon_{IT}$ , is unity, so that  $\epsilon_{AT} = \frac{\Omega}{4\pi}$ . Any of the data given in Appendix G follows smooth curves such as these, so that accurately interpolated  $\epsilon_{AT}$  values may be obtained for energies not specifically tabulated.



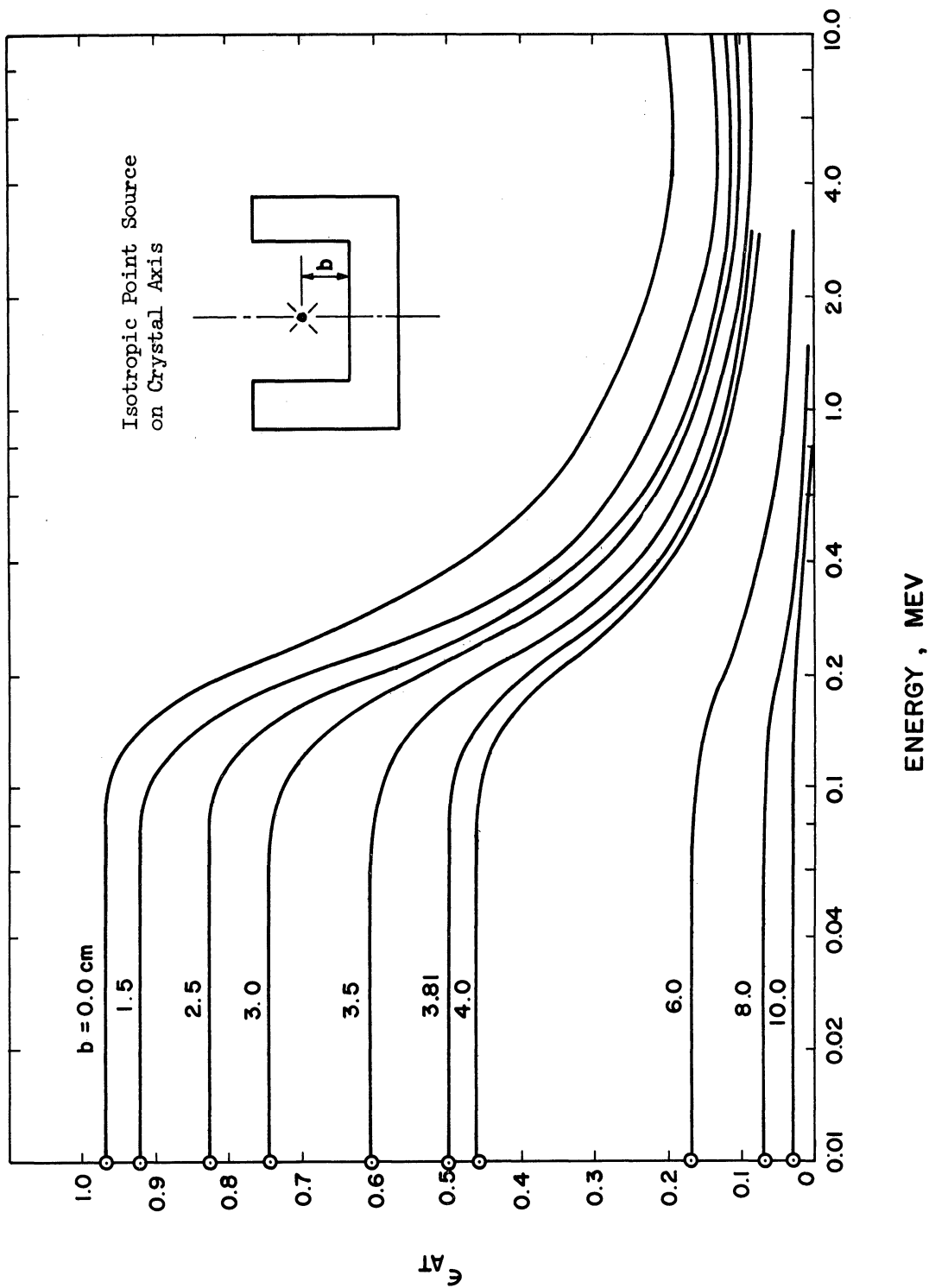


Figure II-21.  $C_{AT}$  Variation with Energy for 8F8 Well Crystal.

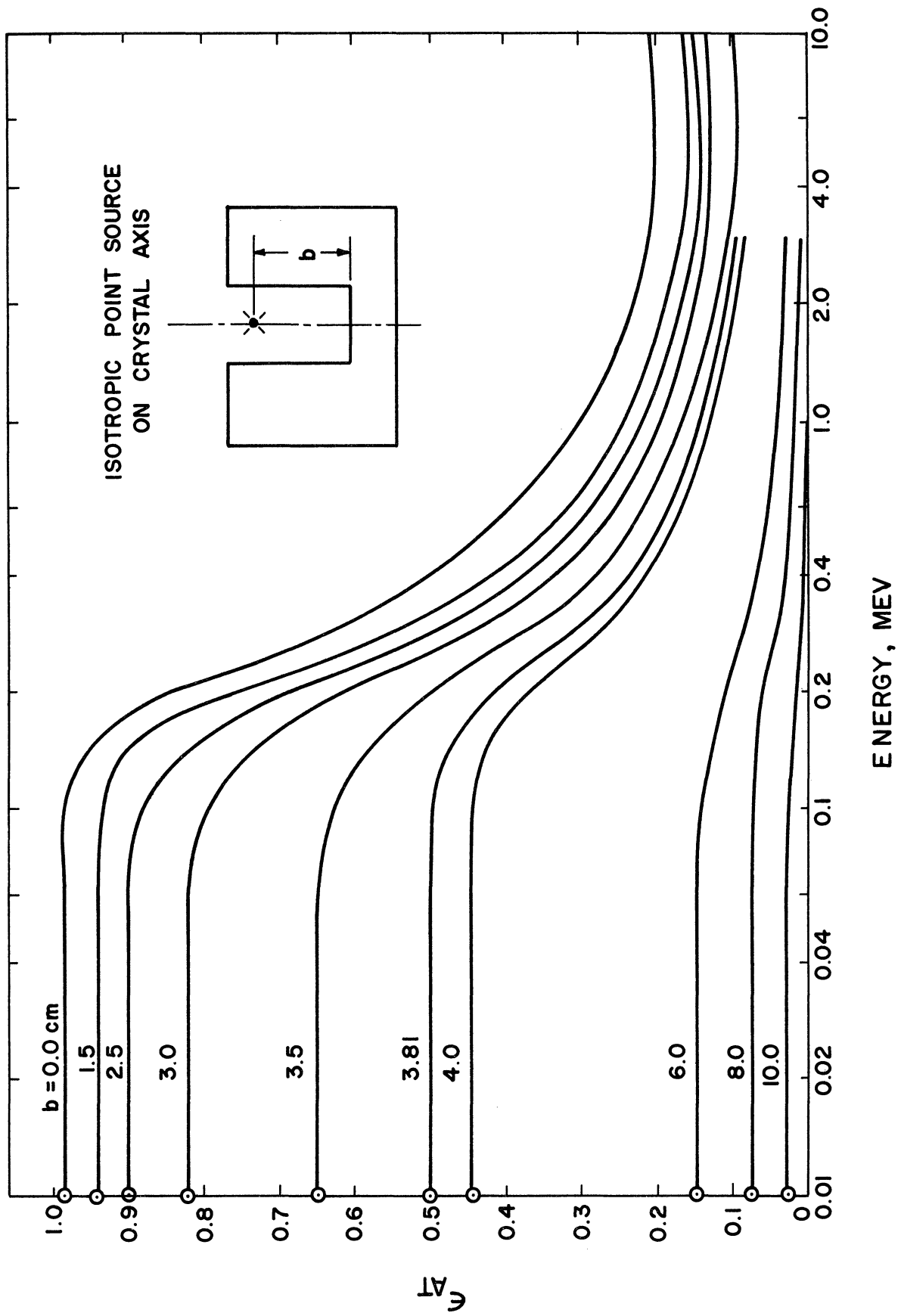


Figure II-22.  $\epsilon_{AT}$  Variation with Energy for 7F8 Well Crystal.

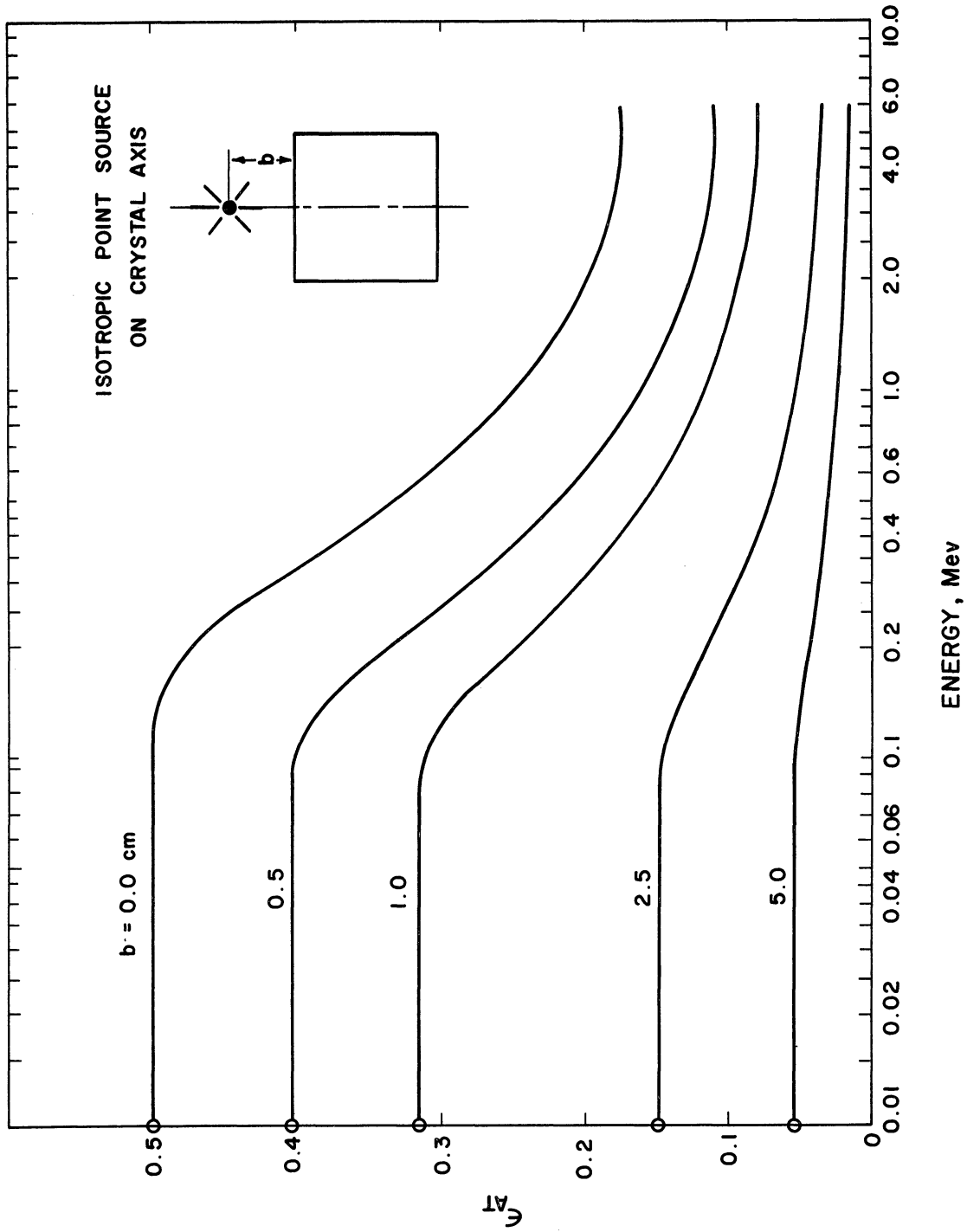


Figure II-23.  $C_{AT}$  Variation with Energy for 2 x 2 In. Solid Crystal.

## CHAPTER III

### APPLICATION OF MONTE CARLO TECHNIQUES TO THE CALCULATION OF PHOTOFRACTIONS

#### A. Principles of Monte Carlo Calculations

The principles of Monte Carlo calculations have been discussed elsewhere<sup>(23-29)</sup> and only a brief mention of some general methods used in these calculations will be given here. Monte Carlo methods involve statistical estimates of the fraction of a given number of source particles that can be expected to terminate in preassigned categories, after having undergone various interactions in media of known geometry and composition. Use of the method is only limited to those problems in which the probabilities of each interaction and the relevant physical laws are known. Since solution of the coupled set of equations describing these processes can not be obtained in general, Monte Carlo methods provide a powerful tool for the solution of practical problems involving particle transport. The method consists of calculating on the digital computer the mathematical equivalent of a low intensity experiment.

The basis of all Monte Carlo digital computer calculations is a set of random numbers, uniformly distributed between zero and one. In practice, however, such a set of numbers is not stored in the machine memory. Rather, upon demand, a so-called pseudo-random number is generated by any one of a number of techniques. The randomness of these generated numbers has been thoroughly tested,<sup>(25)</sup> such that the periodicity for their repetition is exceedingly large and that all digits have essentially an equal probability of appearing. The method of random number generation

employed in these calculations has a period of  $2^{35}$ .<sup>(30)</sup> Henceforth when a random number is referred to, it will mean one of these machine-generated pseudo-random numbers.

The discussion here is limited to a general outline of Monte Carlo techniques, as they are used in the present calculation of photo-fractions. The entire problem is treated here, without a detailed account of each of the physical processes and assumptions used, in order to provide an overall picture of primary photon and secondary particle transport through the crystal. Chapter IV will elaborate on methods of simulating each of these physical processes and source conditions.

Two events are of primary interest in calculating the photofractions; the number (I) of incident source gammas that interact at least once in the crystal, and the number (A) of incident source gammas that deposit their entire energy in the crystal. By definition, the photofraction is given as the ratio of these two numbers, (A/I). Thus, the principal objective of the Monte Carlo calculation is to determine the number of incident source gammas that interact, and how many of these are totally absorbed. Figure III-1 gives the general flow diagram for the computer program. Termination of a given problem occurs when a pre-specified number of primary interactions (I) occur in the crystal.

Starting with a monoenergetic source of specified geometry (e.g., isotropic point, collimated beam, etc.), a single gamma photon is chosen. If the photon interacts in the crystal, all the subsequent events involving the photon and its secondary particles constitute a history. The gamma is defined by seven variables: three rectangular coordinates (x,y,z),

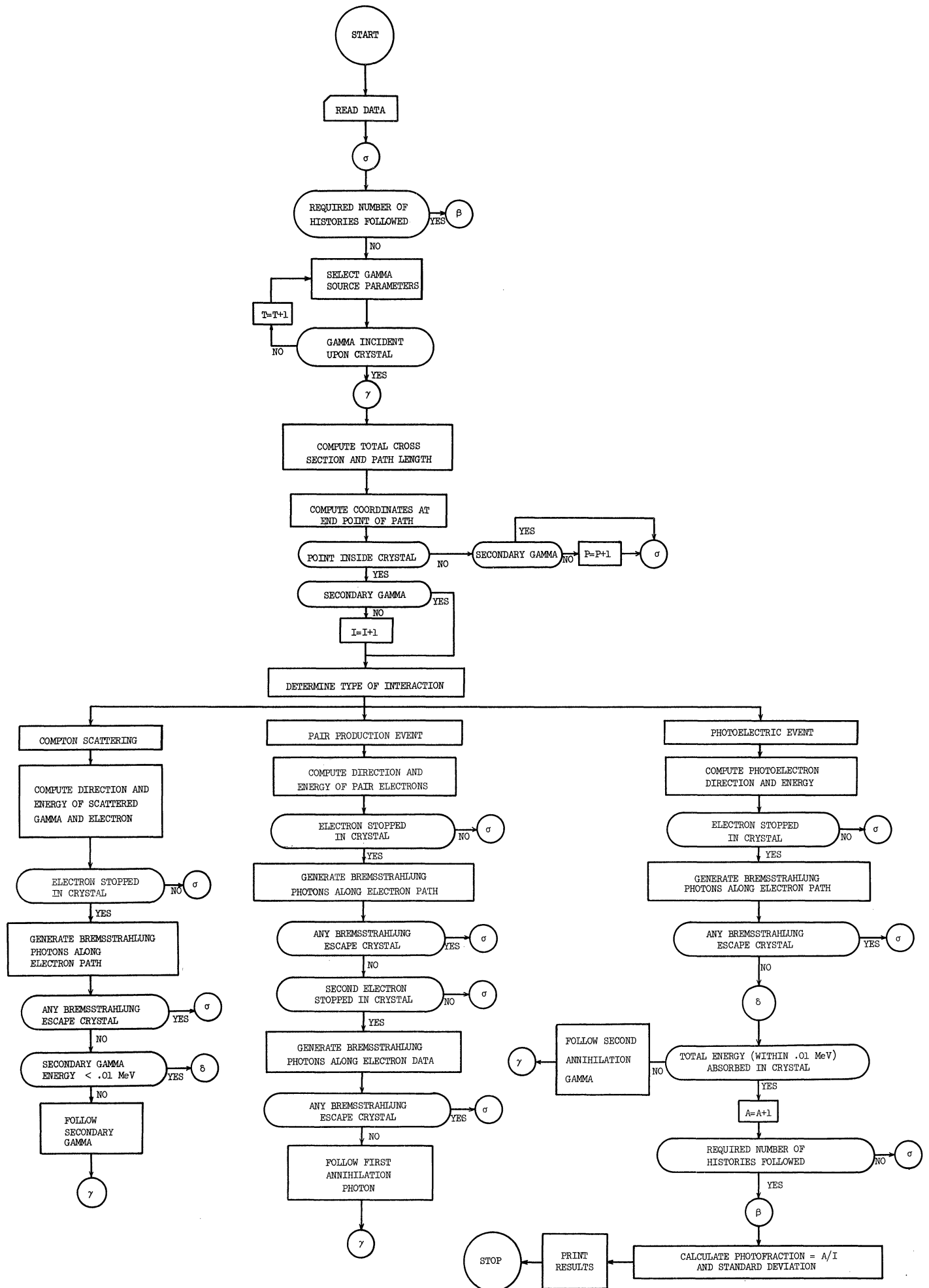
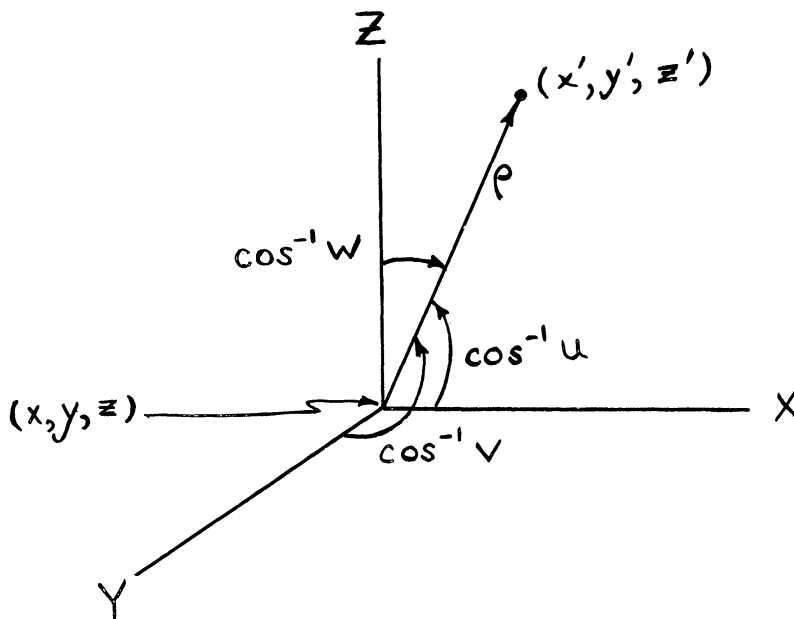


Figure III-1. Flow Diagram for Monte Carlo Calculation of Photofractions.

three direction cosines  $(u,v,w)$ , and energy  $(E)$ . Rectangular coordinates are used, even though the medium geometry is cylindrical, since the direction cosines remain constant under linear displacements. Thus one has:

$$\begin{aligned}x' &= x + u\rho \\y' &= y + v\rho \\z' &= z + w\rho\end{aligned}\tag{3.1}$$



The unprimed coordinates are initial values and the primed coordinates are final values after the gamma travels in a straight line radial distance  $\rho$ , in the direction  $u, v, w$ . Assuming that a source gamma is chosen by suitable sampling techniques to lie along a path which intersects the crystal, the distance traveled in the crystal will depend on the total macroscopic cross section,  $\mu$ . Calculation of this distance introduces

the first application of a fundamental principle of the Monte Carlo method, that of sampling from a properly normalized distribution function.

1. Cumulative Probability Technique

To sample from a given distribution, the transformation must be obtained between that distribution, and the uniform distribution of the random numbers. One such transformation is obtained by the defined connection between a probability distribution function (P.D.F.),  $f(x)$  and its cumulative distribution function (C.D.F.),  $F(X)$ . The P.D.F. is defined as a function that yields the probability that the random variable will assume any particular value (within a small increment) over its range of definition. The C.D.F. is the probability that the random variable takes on values less than or equal to some specified value. Then, by definition:

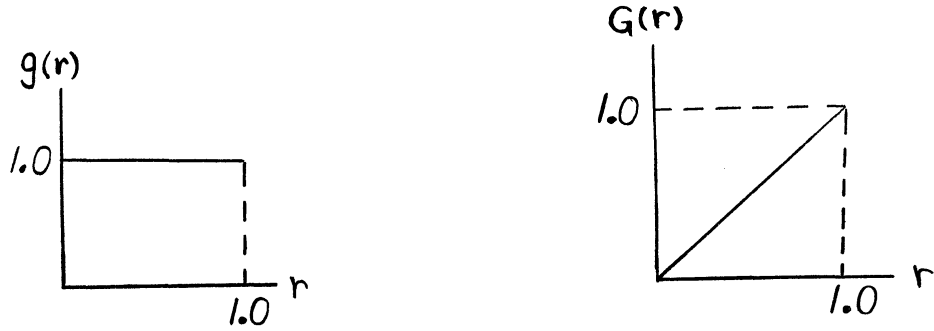
$$F(x) = \int_{-\infty}^x f(x') dx' \quad (3.2)$$

Consider now the P.D.F. and C.D.F. for the uniformly distributed random numbers over the range 0 - 1. Let  $g(r) =$  P.D.F., such that  $g(r)dr$  is the probability of obtaining a random variable in  $dr$  about  $r$ . Since the P.D.F. is a uniform (i.e., constant) distribution function, normalization requires that  $\int_0^1 g(r) dr = 1$ . Thus we have:

$$\text{C.D.F.} = G(r) = \int_0^r g(r') dr' = r \quad (3.3)$$

$$0 \leq r \leq 1 .$$





Consequently the C.D.F. for the random numbers is just the value of the random number. From Equation (3.2) it is seen that  $F(x)$  is a monotonically increasing, single-valued function of  $x$  for any  $f(x) \geq 0$ , and by definition  $f(x)$  is always positive. For a given value of the random number  $r$ , we wish to make the connection between Equations (3.2) and (3.3), such that we obtain a value of the variable  $x$  sampled from the distribution  $f(x)$ . This connection is given by:

$$r = F(x) = \int_0^x f(x') dx' \quad (3.4)$$

It may be seen that Equation (3.4) determines  $x$  uniquely as a function of  $r$ , in such a way that since  $r$  is uniformly distributed on the interval  $0 \leq r \leq 1$ ,  $x$  falls with the frequency  $f(x)$  in the interval  $dx$ . It has been arbitrarily assumed here that the lower limit of the interval of definition of  $f(x)$  is  $x = 0$ .

Therefore the so-called cumulative probability technique of Monte Carlo involves solving Equation (3.4) for  $x$  in terms of a random number  $r$ . Two objections to use of this method are immediately apparent.

First, no analytical evaluation of the integral may be possible, and second, even if the integral can be solved, the resulting expression may be so complicated that repetitive calculation with it may require too much computer time to be economical. For either case, other Monte Carlo techniques are available (e.g., rejection techniques).

## 2. Rejection Techniques

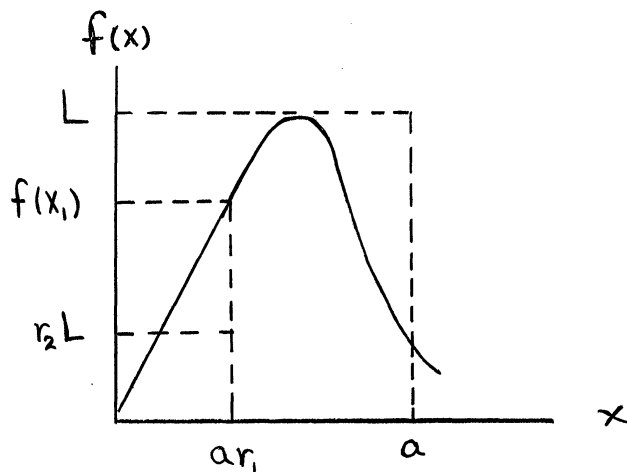
To avoid the problems presented by use of Equation (3.4), the rejection technique is commonly used. Given the normalized probability distribution function  $f(x)$  where  $0 \leq x \leq a$ , and that the maximum of  $f(x)$  is  $L$ , in the range definition of  $x$ , what is required is a choice of the variable  $x$  which lies within the area denoted by  $\int_0^a f(x')dx'$ . The procedure is to choose two random numbers  $r_1$  and  $r_2$ . Set  $x_1 = a \cdot r_1$  and test if  $r_2 L \leq f(x_1)$ . If this inequality is satisfied, accept  $x_1$  as a randomly obtained value for  $x$  from the function  $f(x)$ . If  $r_2 L > f(x_1)$ , then reject  $r_1, r_2$  and obtain two new random numbers, continuing the processes until the inequality  $r_2 L \leq f(r_1 a)$  is satisfied. The probability of accepting  $x_1$  is

$$\int_0^{f(x_1)/L} dr_2 = \frac{f(x_1)}{L}$$

which verifies that the frequency distribution from which the random variates are obtained is in fact the function  $f(x)$ . Rejection of sets of random numbers causes an inefficiency in the method, and for a normalized  $f(x)$ , the acceptance rate is  $1/aL$ . The acceptance rate may be

considered to be ratio of the area of interest to the total rectangular area being sampled given by

$$\frac{1}{aL} \int_0^a f(x) dx$$

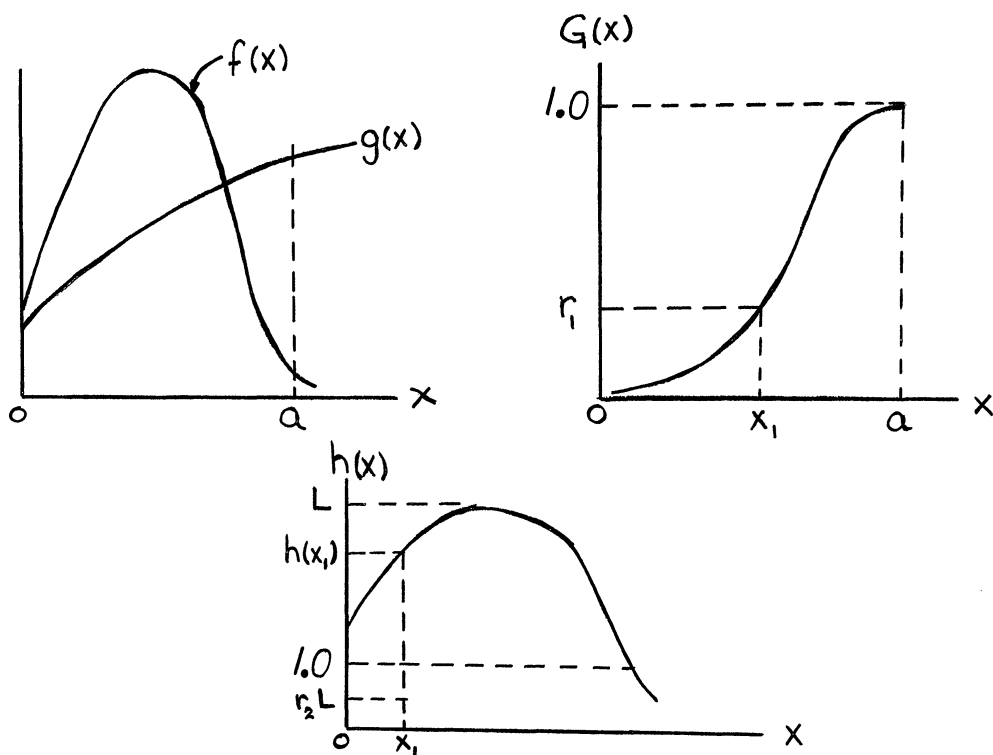


Most frequently the cumulative probability method and rejection techniques are combined (e.g., sampling from the Klein-Nishina formula used for Compton scattering in these calculations, see Appendix C). The advantage of combining these techniques is that if a simple approximation,  $g(x)$  can be found to a complicated function,  $f(x)$ , the cumulative probability method can be applied to  $g(x)$ . Then  $g(x)$  and  $f(x)$  can be related by use of the rejection technique. For a properly chosen  $g(x)$ , the acceptance rate in the rejection technique will be high and an efficient sampling procedure will be available for a given  $f(x)$ . Reference 24 gives an extensive compilation of such techniques for many distribution functions encountered in physical and mathematical problems.

To select a random variable  $x$  from a given  $f(x)$  for  $0 \leq x \leq a$ , one first obtains a value for  $x$  from an approximating  $g(x)$  by the cumulative probability technique. Thus one obtains  $x_1 = G^{-1}(r_1)$ , where  $r_1$  is a random number,

$$r_1 = G(x_1) = \int_0^{x_1} g(x') dx' ,$$

and  $x$  is easier to obtain from  $g(x)$  than solving Equation (3.4), with  $f(x)$ . The relationship between  $g(x)$  and  $f(x)$  is obtained from the rejection technique. Defining  $h(x) = f(x)/g(x)$ , and  $L =$  maximum of  $h(x)$  in the range  $0 \leq x \leq a$ , one obtains a second random number  $r_2$ . Rejection of the set  $r_1, r_2$  occurs until the inequality  $r_2 L \leq f(x_1)/g(x_1)$  is satisfied. When this is satisfied,  $x_1$  is accepted as the randomly chosen variable from the distribution  $f(x)$ . The process is depicted below.



The probability of accepting  $x_1$  from the rejection technique is

$$\int_0^{h(x_1)/L} dr_2 = \frac{h(x_1)}{L},$$

and the probability of obtaining  $x_1$  is  $g(x_1)$ , from the definition of a probability distribution function. Thus the combined probability of choosing and accepting  $x_1$  is the product of the independent probabilities

$$\frac{h(x_1)}{L} \cdot g(x_1) = \frac{f(x_1)}{L}$$

which again verifies that one is sampling from the correct distribution function,  $f(x)$ .

#### B. Path Length Sampling

Returning to the problem of determining the distance traveled by a gamma before any interaction occurs, we have the P.D.F.,  $f(\rho)$  given by:

$f(\rho)d\rho = e^{-\mu\rho}\mu d\rho =$  probability that a photon travels a distance  $\rho$  without interaction and then has an interaction in the interval between  $\rho$  and  $\rho + d\rho$ ,

$\mu =$  total cross section.

Applying Equation (3.4) we obtain:

$$\rho = -\left[\frac{\ln r}{\mu}\right] \tag{3.5}$$

$r =$  random number

Von Neumann<sup>(25)</sup> has given another method for obtaining the path length,  $\rho$ , without evaluating the logarithm of a random number. The incentive for using the von Neumann technique is to reduce the computer time, but a comparison between his method and Equation (3.5) with the Michigan computer give a negligible difference in computational time. Equation (3.5) was used throughout these calculations.

### C. Gamma Interactions

Having determined the path length of the source gamma in the medium, a check is made to determine if the gamma interacts within the crystal boundaries, by using Equations (3.1) and the crystal geometry. If the interaction occurs outside the crystal, then the gamma is counted in the appropriate termination category as having passed through the crystal with no interaction. Another source gamma is selected and the process is repeated. When a gamma has an interaction within the crystal, the event is recorded, and the elementary probabilities for the possible gamma ray interactions dictate which interaction occurred. The possible interactions considered are photoelectric absorption, Compton scattering, and pair production. The following macroscopic cross sections,  $[\text{cm}]^{-1}$ , are defined:

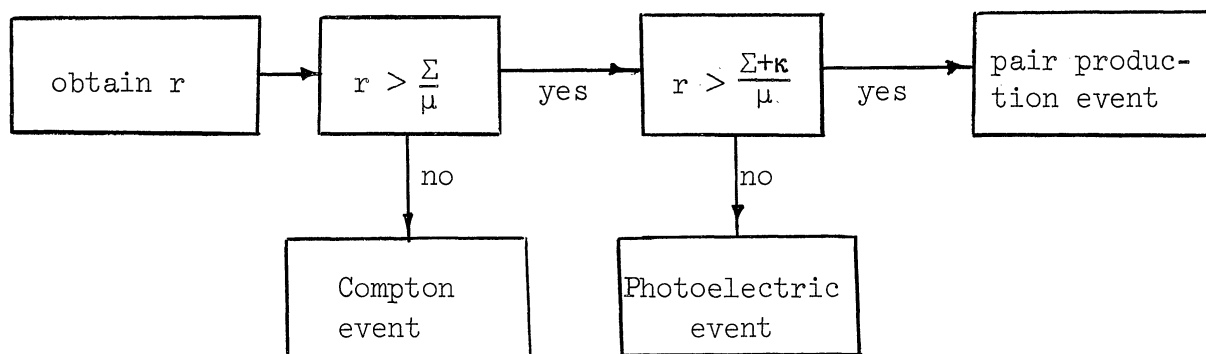
$$\Sigma(E) = \text{Compton scattering}$$

$$\kappa(E) = \text{photoelectric absorption}$$

$$\tau(E) = \text{pair production}$$

$$\mu(E) = \Sigma + \kappa + \tau = \text{total.}$$

Then  $\Sigma/\mu$  ,  $\kappa/\mu$  ,  $\tau/\mu$  at a given energy are the probabilities per interaction of Compton scattering, photoelectric absorption, and pair production, respectively. The Monte Carlo procedure for deciding which interaction occurred is shown by the following flow diagram, where  $r$  is another random number.



### 1. Photoelectric Absorption

Depending on which primary gamma interaction occurs, as determined by the technique shown in the sketch above, a different set of calculations must be made. If a photoelectric absorption takes place, the following sequence is followed. The photon is assumed to transfer all of its energy to a single target electron. The electron originates at the point of interaction and is ejected in a specific (energy dependent)

polar angle with respect to the incident photon direction. The azimuthal angle of ejection is uniformly distributed, and a transformation is made to refer the electron direction back to the coordinate system fixed in the crystal. Calculations are then made to determine if the electron escapes the crystal. If this occurs, the history is terminated. If not, then data for bremsstrahlung generation are sampled. These bremsstrahlung photons are followed through the crystal, undergoing all the same processes that primary photons do, except that electron and subsequent bremsstrahlung generation is considered negligible. If the bremsstrahlung photons are all absorbed, the total source energy has been absorbed, a record is made in the appropriate category, and another source gamma is chosen.

## 2. Compton Scattering

If a Compton scattering occurs, both the scattered gamma and free electron are followed. The polar angle for the scattered gamma ray is obtained by Monte Carlo sampling from the Klein-Nishina formula,<sup>(31)</sup> by the method given in Appendix C. The energy for the emergent gamma and electron, as well as the electron polar angle, are then calculated from the relationships given in Chapter IV. The scattered gamma and electron are assumed to be uniformly distributed in azimuthal direction. First the electron and subsequent bremsstrahlung are followed in an identical manner as described above. Then if the electron and bremsstrahlung are totally absorbed, the Compton scattered gamma is followed through the crystal in the same manner as for primary source gammas, with electrons being produced at every interaction. At each interaction in a



given history, a running summation is kept of the energy deposited in the crystal. Termination as a total absorption occurs when the difference between the source energy and the energy deposited is  $\leq 10$  Kev.

### 3. Pair Production

If a pair production event occurs, the two pair electrons are assumed to share equally the incident gamma kinetic energy excess over the rest mass of the two electrons. The electrons are ejected in an (energy dependent) forward direction, with a uniform azimuthal distribution given to one electron, the other one correlated in azimuth at  $180^\circ$ . The electrons and bremsstrahlung as followed, and if absorption of these secondaries occurs, one of the electrons is chosen at random to be the positron. The assumption is made that the positron comes to rest before annihilation, and this defines the position for emission of the two  $\sim 51$  MeV annihilation gammas. These gammas are assumed to be emitted isotropically in opposite directions, and they are followed through the crystal in the usual fashion, with electrons and subsequent bremsstrahlung being considered.

#### D. Secondary Gammas and Electrons

All of these gamma interactions give rise to secondary gammas and particles, i.e., scattered gammas and free electrons (positrons and negatrons). These gammas may interact further until they are absorbed, or escape from the crystal. In addition, the electrons produce positron annihilation gammas, bremsstrahlung gammas, and further electrons. Thus a sequence of gammas and charged particles is built up throughout the

crystal, which must be terminated at some point for any practical calculation. For usual applications of scintillation crystals, the sequence beyond the first few generations can be safely neglected with insignificant error. The termination of this sequence is discussed below. Gammas and particles from a given history are followed until either escape with more than 10 Kev energy, or the total source energy is absorbed. Whenever the former occurs, the history is immediately terminated since it is assumed that loss of 10 Kev energy removes the "count" from the total absorption peak. A count corresponds to the summation of the energy deposited in the individual events as discussed in Chapter I. The sequence of events from a primary source gamma is considered to be as follows:

- (a) Scattered gammas due to successive Compton events
- (b) Free negatrons from photoelectric and Compton events
- (c) Pair electrons (positrons and negatrons) from pair production events.

Further interactions of the above give:

- (a) Annihilation gammas from positron annihilations
- (b) Bremsstrahlung photons from energetic electrons.

It is assumed that electrons are slowed down by excitation and ionization of the target atoms, as well as by radiative losses (bremsstrahlung), but that the subsequent de-excitation photons and free electrons generated are totally absorbed in the crystal. Also it is assumed that the bremsstrahlung photons can undergo any of the three primary gamma interactions, but no electrons are generated. The justification for these assumptions is that for the high atomic number materials used for gamma scintillation

crystals, absorption of these low energy gammas and electrons occurs with a very high probability. Thus the sequence is terminated at this point.

#### E. Typical Histories

The tables given below summarize the number of primary events found to occur in a typical history of gammas from an isotropic source. Reference 32 gives similar results obtained from Monte Carlo calculations with a narrow collimated beam source normally incident on a solid crystal. Reference 32 ignored all electrons, bremsstrahlung, and annihilation gammas, including only Compton scattered gammas. Calculations were limited to a maximum source energy of 1.5 MeV. All of the data given below were obtained from the Monte Carlo program for a 2 in. dia. x 2 in. high cylindrical solid NaI crystal. The calculations were made for 1000 primary interactions at each source energy and neglects energy loss by escaping electrons and bremsstrahlung. Table III-1 compares the observed fraction of primary interactions with the elementary probabilities per interaction given by the cross sections. Agreement is seen to be excellent, considering the relatively few histories considered. Table III-2 indicates that for gammas which are absorbed, most absorptions occur after zero, one, or two scatterings; while from Table III-3, one sees that most escaping particles suffer only one scattering prior to escape. In general, the results tabulated here indicate that as a gamma suffers more scattering the probability of absorption increases. Physically this corresponds to reducing the source gamma energy by successive scatters, until the gamma energy is in the range where photoelectric absorption predominates. Table III-4 gives a

sequence of typical events when pair production occurs in the crystal. It should be noted that relatively few pair production events occur for a gamma that suffers an initial Compton scattering. Also, the number of times both annihilation gammas are absorbed is significantly less than the number of times one annihilation gamma is absorbed.

TABLE III-1  
FRACTION OF PRIMARY INTERACTIONS

Energy (MeV)	Photo- electric	$\frac{\kappa}{\mu}$	Compton	$\frac{\Sigma}{\mu}$	Pair Production	$\frac{\tau}{\mu}$
.51	.182	.174	.818	.826	0	0
2.0	.021	.025	.938	.915	.041	.059
3.0	.016	.017	.800	.808	.184	.174
4.0	.020	.013	.691	.703	.289	.285
5.0	0	.009	.614	.620	.386	.380

TABLE III-2  
FRACTION OF THE 1000 INTERACTING GAMMAS THAT HAVE  
EXACTLY X SCATTERINGS PRIOR TO ABSORPTION

Energy (MeV)	X = 0	X = 1	X = 2	X = 3	X = 4	X = 5	X = 6	X = 7
.51	.182	.212	.105	.033	.011	.004	0	0
2.0	.021	.076	.087	.033	.015	.003	.002	0
3.0	.016	.044	.063	.028	.002	0	0	0
4.0	.020	.041	.041	.033	.009	.002	0	0
5.0	0	.032	.032	.013	.007	.002	0	.001

TABLE III-3

FRACTION OF THE 1000 INTERACTING GAMMAS THAT HAVE  
EXACTLY X SCATTERINGS PRIOR TO ESCAPE

Energy (MeV)	X = 1	X = 2	X = 3	X = 4	X = 5
.51	.367	.073	.010	.003	0
2.0	.567	.121	.027	.007	0
3.0	.525	.106	.023	.003	.001
4.0	.471	.072	.012	.004	.001
5.0	.418	.084	.009	.006	0

TABLE III-4

TYPICAL PAIR PRODUCTION EVENTS  
(For 1000 Primary Interactions)

Energy (MeV)	Total No. Pair Events	No. Pair Events After Initial Compton	No. Times X Annihilation Gammas Totally Absorbed		
			X = 2	X = 1	X = 0
2.0	67	6	6	26	35
3.0	183	4	8	62	113
5.0	401	12	20	139	242

## CHAPTER IV

### DETAILS OF THE MONTE CARLO CALCULATIONS FOR PHOTOFRACTIONS

The Monte Carlo programs can be divided into sections consisting of:

- (a) Source selection routine
- (b) Particle interaction
- (c) Particle escape routine
- (d) Termination criteria and categories.

#### A. Source Geometries Considered

Two general types of monoenergetic gamma ray sources are considered. These are isotropic sources and monodirectional sources, the latter being collimated so that all rays are parallel to the crystal axis of symmetry. The isotropic sources are typical of small volume laboratory sources and are restricted to point sources (on and off the crystal axis), circular disk sources centered on the crystal axis, or right circular cylindrical sources located along the crystal axis. Self-absorption and scattering have been considered for the cylindrical volume source, and will be discussed in Section H of this chapter. The monodirectional source is the limiting case of a source at large distances from the detector, collimated to yield a parallel beam. Three degrees of collimation are considered: a narrow beam collimated to lie along the crystal axis, a beam collimated to any specified diameter, and a broad beam which provides full illumination of the crystal face. The

collimated beam sources are assumed to be normally incident upon the crystal face or well bottom. All of these seven sources have been considered for the solid cylindrical scintillation crystal, and for the well crystal except for the last two collimated sources.

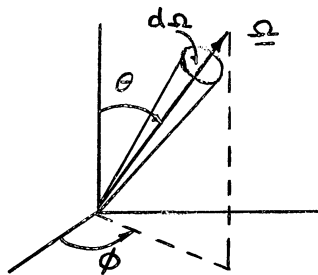
1. Isotropic Source Routines

The objective of any source routine is to obtain the direction of a source gamma and its coordinates at the point of intersection with the crystal surface. This point is determined by a line having the direction cosines  $u_0$ ,  $v_0$ ,  $w_0$  from the source to the crystal. An isotropic source is defined as one in which the probability,  $P(\Omega)$  of emission into any solid angle is a constant for all solid angles. Thus

$$P(\Omega)d\Omega = K d\Omega \quad K = \text{constant}$$

Expressing the solid angle in terms of an azimuthal angle  $\phi$ , and a polar angle  $\theta$  with respect to any one of the three rectangular coordinate axes, we have

$$\begin{aligned} P(\Omega)d\Omega &= P(u,\phi) du d\phi \\ &= K du d\phi \end{aligned}$$

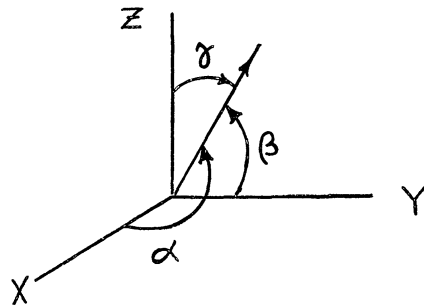


where  $\mu = \cos\theta$ , is the direction cosine relative to the arbitrary axis.

The probability is constant in azimuth about the arbitrarily chosen coordinate axis, and integrating over  $\varphi$  gives

$$P(\Omega) d\Omega = 2\pi K d\mu$$

Thus the probability of emission is a constant over all values of the direction cosine,  $\mu$ . Since the reference axis was arbitrarily chosen, this argument can be repeated for the other two rectangular coordinate axes. One concludes that isotropic emission can be described by obtaining the three direction cosines  $u_o$ ,  $v_o$ ,  $w_o$ , for a ray as shown below, from a constant distribution function such that all values from -1 to +1 have an equal probability of occurrence.



$$\begin{aligned} u_o &= \cos \alpha \\ v_o &= \cos \beta \\ w_o &= \cos \gamma \end{aligned} \tag{4.1}$$

These direction cosines may be obtained from a set of random numbers, uniformly distributed on the interval 0 - 1 by:

$$\begin{aligned} u_o &= 2r_1 - 1 \\ w_o &= 2r_2 - 1 \\ v_o &= \pm \sqrt{1 - (u_o^2 + w_o^2)} \end{aligned} \tag{4.2}$$

$r_1, r_2 =$  random numbers

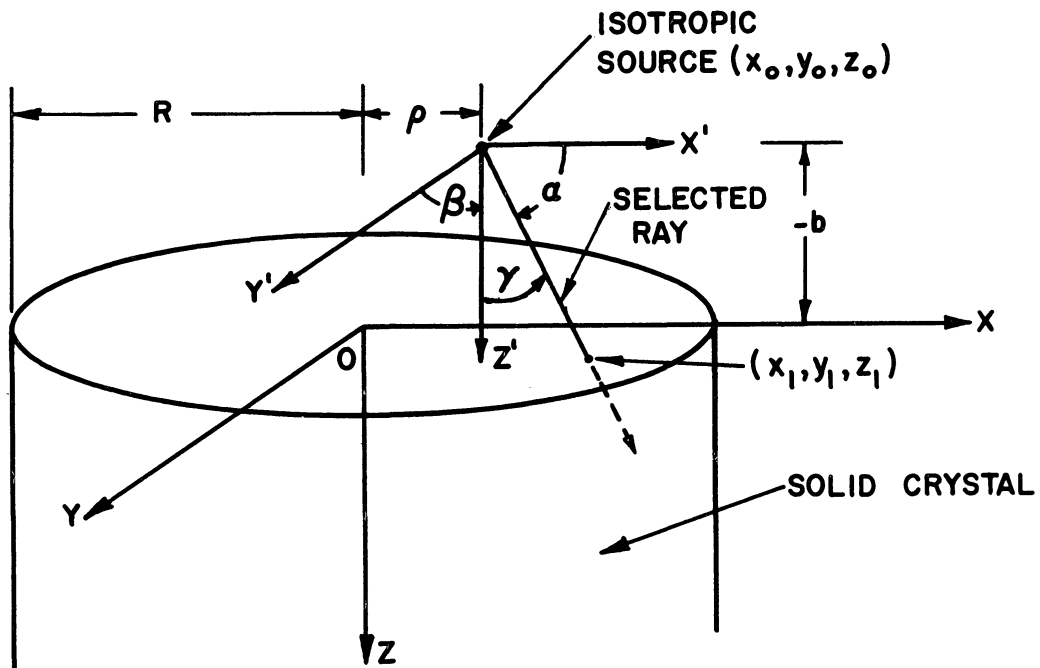


The last equation is a consequence of the definition of the direction cosines; with the + or - being chosen at random.

a. Solid Crystal - Point Source

For the solid crystal consider a point source located off the crystal axis as indicated below. The origin, 0, of the coordinate system is fixed in the crystal face, in contrast to that defined in Chapter II, and the initial coordinates for this point source are:

$$\begin{aligned}x_o &= \rho \\y_o &= 0 \\z_o &= -b .\end{aligned}$$



Rather than sample over all directions, as indicated by Equations (4.2), it is more efficient to restrict the directions of emission to randomly chosen vectors, uniformly distributed within the cone defined by:

$$1 \leq w_0 \leq \frac{b}{\sqrt{b^2 + (R+\rho)^2}} , \quad (4.3)$$

and then to reject any rays which do not intersect the crystal face.

Obviously as the distance  $\rho$  increases, the efficiency of this method will decrease since the fraction of the base of the cone which is covered by the crystal face decreases. In addition, it may appear that calculation of the square root may require more computer time than other methods, for example, sampling over the entire positive  $z$  direction and accepting only rays that intersect the crystal. However, for smaller distances  $\rho$ , the increase in efficiency due to the geometrical effect has been calculated to more than offset the time saved by use of more simple, but less efficient methods. In particular when  $\rho = 0$  (point source on axis), one has the case of greatest interest, and the conditions of Equation (4.3) require that every gamma strike the crystal face. Applying the cumulative probability technique of Equation (3.4) one gets:

$$w_0 = \left[ 1 - \frac{b}{\sqrt{b^2 + (R+\rho)^2}} \right] r_1 + \frac{b}{\sqrt{b^2 + (R+\rho)^2}} ,$$

and to obtain  $-1 \leq (u_0, v_0) \leq 1$  one uses:

$$u_0 = 2 r_2 - 1$$

$$v_0 = \pm \sqrt{1 - (u_0^2 + w_0^2)}$$

where  $r_1, r_2$  are random numbers and the + or - is chosen at random.

The coordinates in the plane of the crystal surface are:

$$x_1 = \rho + \frac{b}{w_0} u_0$$

$$y_1 = \frac{b}{w_0} v_0$$

$$z_1 = 0 \quad ,$$

and for intersection with the crystal, the above process is repeated until:

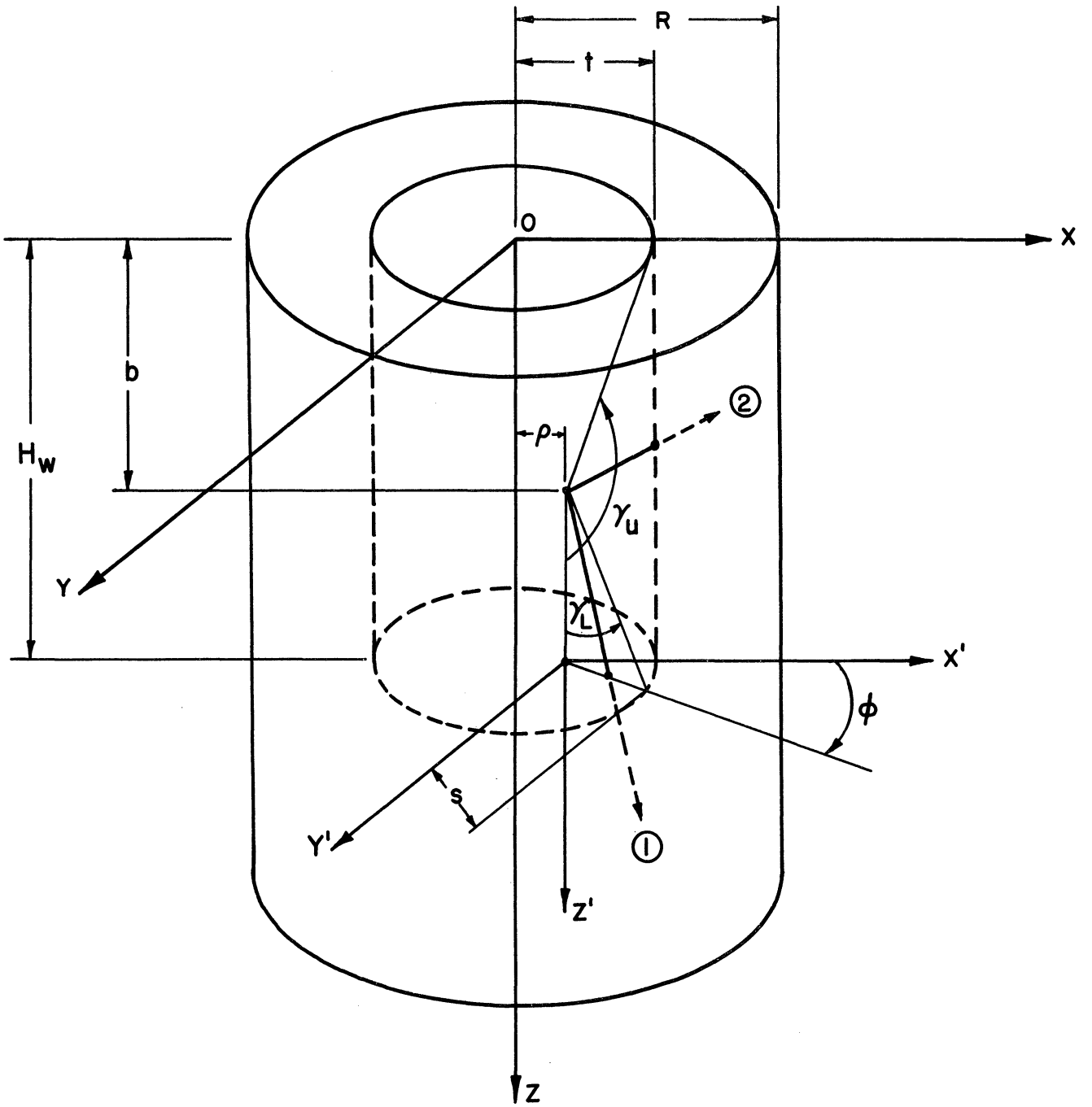
$$x_1^2 + y_1^2 < R^2 .$$

b. Well Crystal - Point Source

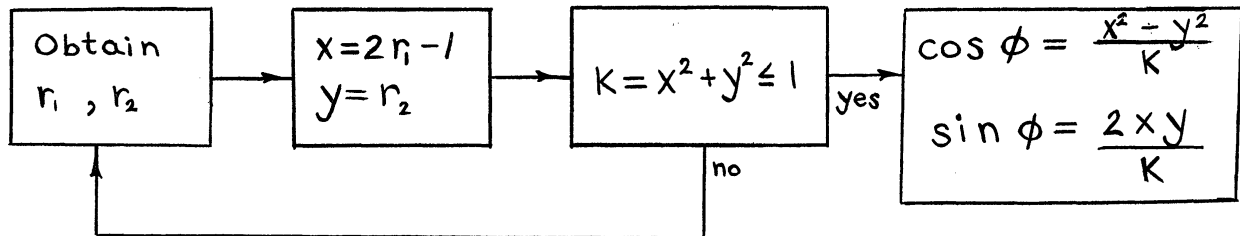
The procedure for the well crystal is somewhat more complicated, since gammas from an isotropic source can strike either the sides or the bottom of the well. Isotropic sources are limited to those contained within the well as shown below. (Again note that the origin of the coordinate system is different from that considered in Chapter II). The direction cosine  $w_0$  ( $w_0 = \cos \gamma$ ) is obtained from a uniform distribution ( $-1 \leq w_0 \leq 1$ ) by:

$$w_0 = 2 r - 1$$

$r$  = random number



Next the sine and cosine of a uniformly distributed azimuthal angle  $0 \leq \phi \leq 2\pi$  are obtained by the following technique first given by von Neumann.<sup>(25)</sup> (This procedure eliminates time-consuming series evaluation of the functions  $\sin\phi$ ,  $\cos\phi$ , where  $\phi = 2\pi r$ ).



The other two direction cosines,  $u_o$ ,  $v_o$ , defined in the sketch above Equations(4.1) are obtained from:

$$u_o = \cos\phi (1 - w_o^2)^{1/2}$$

$$v_o = \sin\phi (1 - w_o^2)^{1/2}$$

Then letting

$$w_L = \frac{H_w - b}{\sqrt{s^2 + (H_w - b)^2}} = \cos \gamma_L$$

and

$$w_u = \frac{-b}{\sqrt{s^2 + b^2}} = \cos \gamma_u$$

where

$$s = -\rho \cos\phi + \sqrt{t^2 - \rho^2 \sin^2\phi}$$

the tests are made

$$1 \geq w_o \geq w_L \quad (4.4)$$

and

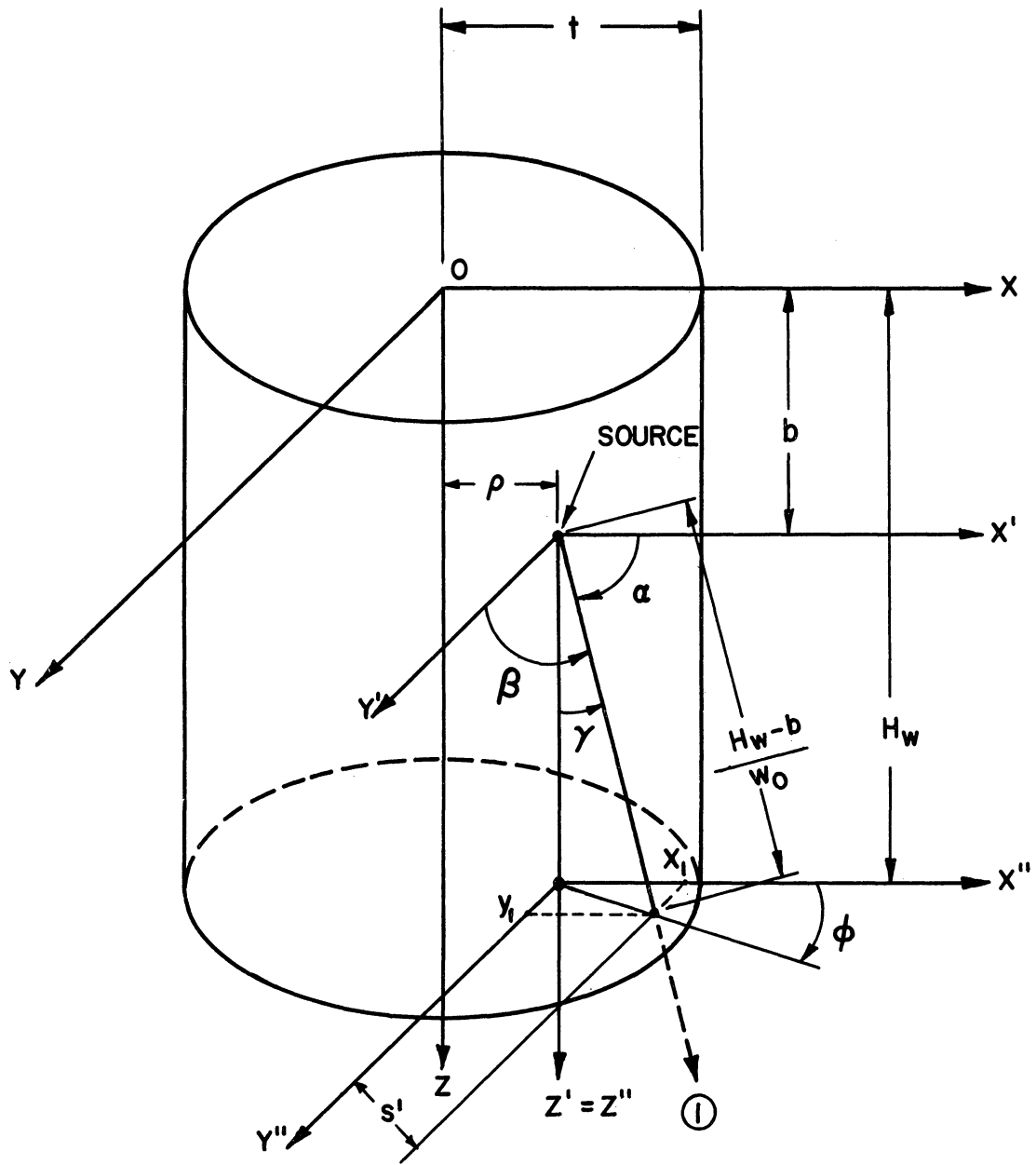
$$w_L > w_o \geq w_u \quad (4.5)$$

When (4.4) is satisfied the source gamma, labeled ray 1 in the sketch below, strikes the well bottom. The coordinates at the point of intersection with the bottom of the well are:

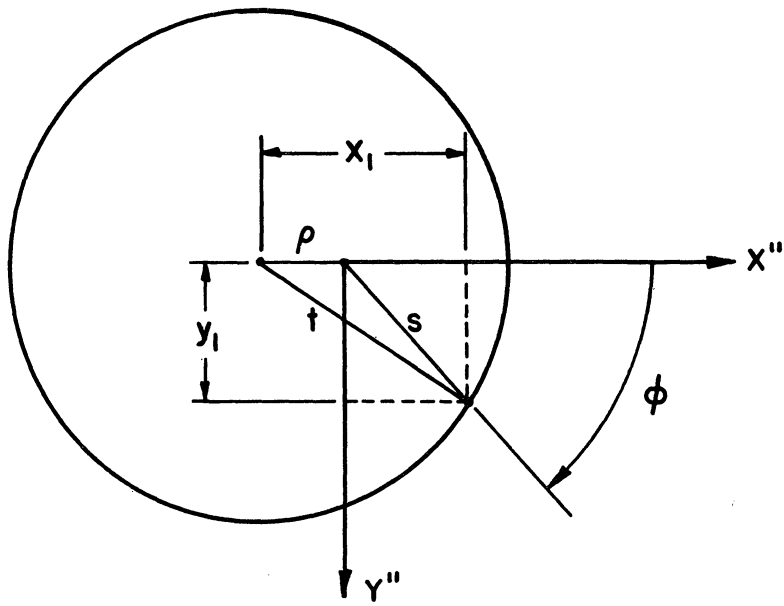
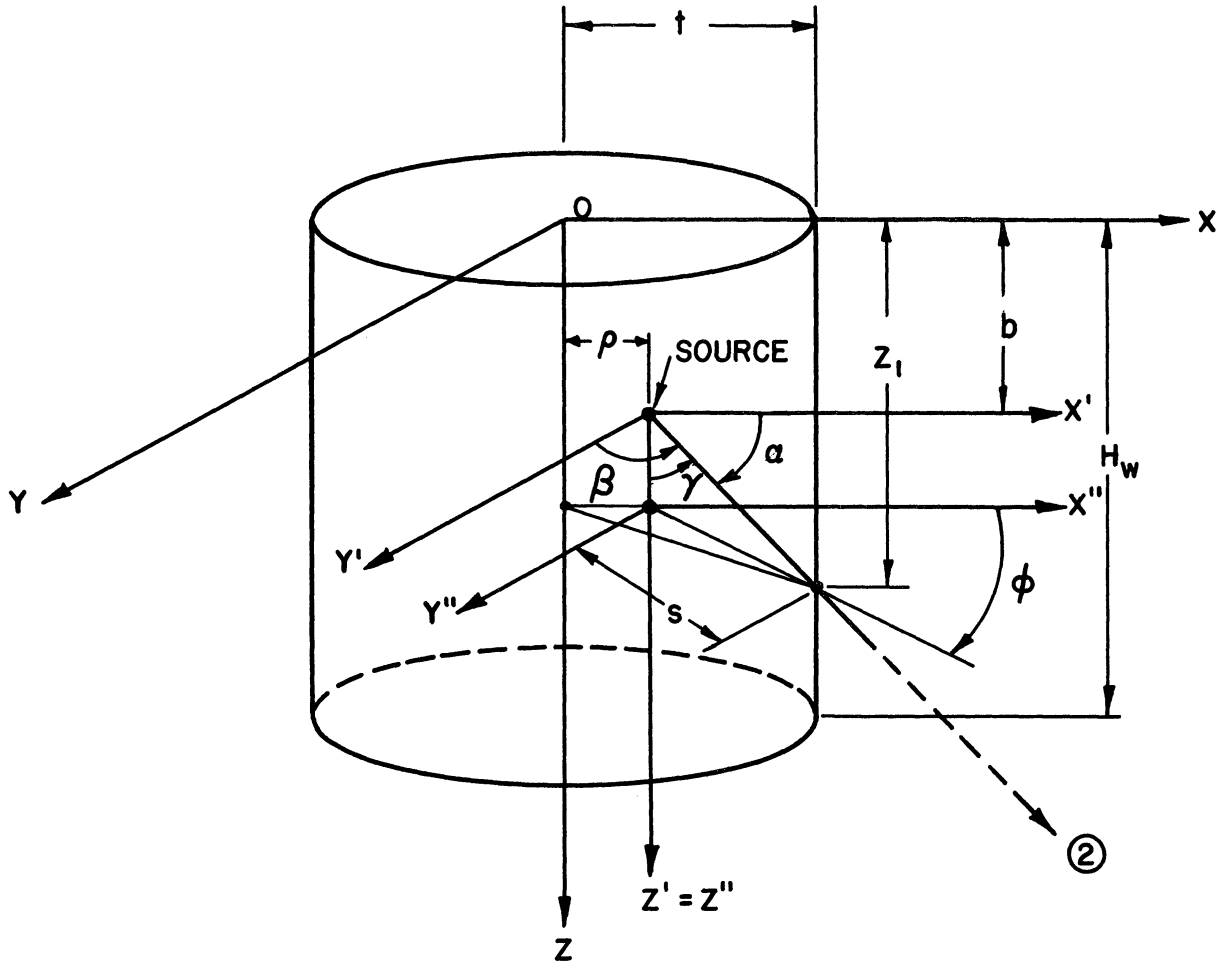
$$\begin{aligned} x_1 &= \rho + s' \cos\phi = \rho + (H_w - b)(1 - w_o^2)^{\frac{1}{2}} \frac{\cos\phi}{w_o} \\ &= \rho + (H_w - b) \frac{u_o}{w_o} \end{aligned}$$

$$y_1 = s' \sin\phi = (H_w - b)(1 - w_o^2)^{\frac{1}{2}} \frac{\sin\phi}{w_o} = (H_w - b) \frac{v_o}{w_o}$$

$$z_1 = H_w .$$



If (4.5) is satisfied the gamma, labeled ray 1 in the sketch below, strikes the side of the well.





The coordinates at the point of intersection with the side of the well are:

$$x_1 = \rho + S \cos \phi$$

$$y_1 = S \sin \phi$$

$$z_1 = b + \frac{w_0 S}{(1 - w_0^2)^{1/2}}$$

If neither (4.4) nor (4.5) are satisfied, then the gamma escapes through the top of the well without hitting the crystal. For this case, the entire process is repeated. For most practical well crystal geometries the efficiency for selection of a source gamma which strikes the crystal is very high, especially if the source is located deep within the well.

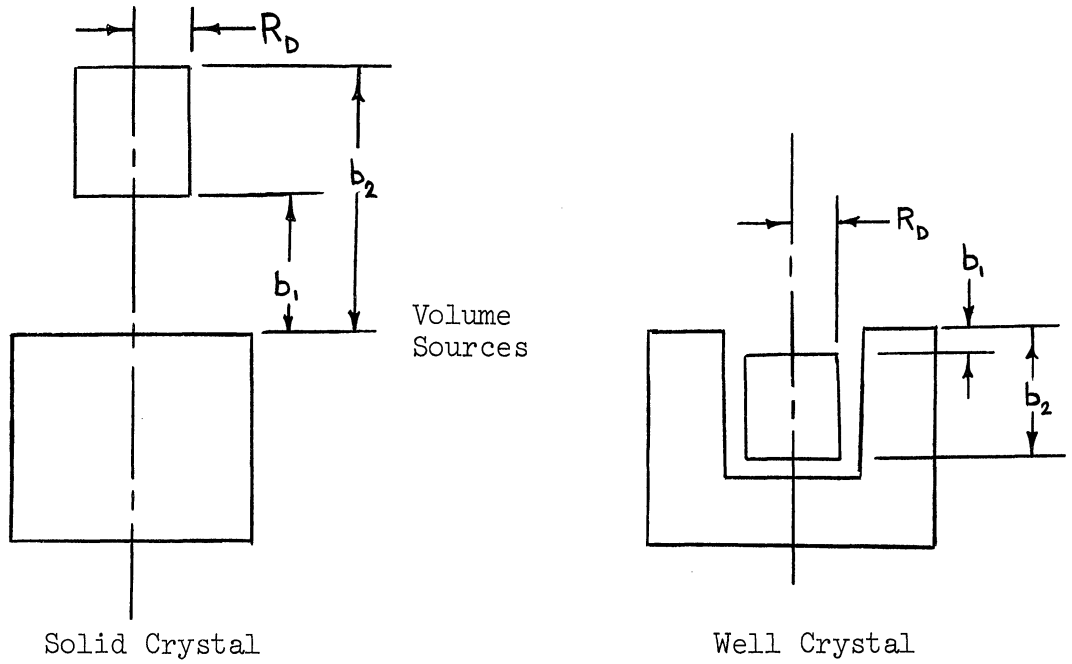
c. Extension to other Isotropic Sources

The above methods are readily extended to cover the other isotropic sources. For on-axis points,  $\rho = 0$  and the same procedures are used. For a disk source of radius  $R_D$ , the radial distance is sampled using the cumulative probability technique:

$$\rho = R_D \sqrt{r} \quad r = \text{random number}$$

This is extended to a cylindrical volume source of height  $b_2 - b_1$  by selecting

$$b = r(b_2 - b_1) + b_1, \quad r = \text{random number.}$$



2. Collimated Beam Sources

The monidirectional sources have by definition,

$$w_0 = 1$$

$$u_0 = v_0 = 0$$

For the narrow beam collimated along the crystal axis

$$x_1 = y_1 = 0$$

$$z_1 = 0, \text{ solid crystal}$$

$$z_1 = H_w, \text{ well crystal}$$

For a beam collimated to any diameter,  $D_s$  (solid crystal only)

$$x_1 = \frac{D_s}{2} \sqrt{r} \qquad r = \text{random number}$$

$$y_1 = z_1 = 0$$

and in particular for a broad beam,  $D_s = \text{crystal diameter}$ .

## B. Gamma Interactions

Having obtained the coordinates at the crystal surface  $x_1$ ,  $y_1$ ,  $z_1$ , given above for the appropriate source, the gamma travels into the crystal along a path in the direction  $(u_o, v_o, w_o)$ . As discussed in the preceding chapter, the radial distance traveled to the first interaction is obtained by sampling for the mean free path from the total cross section. The NaI cross section data of Grodstein and McGinnies<sup>(20,21)</sup> for Compton and photoelectric events, as well as the total cross section, are stored in the computer as an integral part of these programs, with interpolation for energy being performed when required. Table II-11 gives the energy increments used. As previously discussed, the type of interaction is determined by the relative probability for its occurrence. It is at this point that the various possible physical processes are simulated, based on assumptions made about the character of these processes.

### 1. Interaction Processes Considered

For gamma rays the only important interaction processes in the crystal, for usual applications of scintillation crystals, are photoelectric, Compton scattering, and pair production. Rayleigh (coherent) scattering has been ignored, as discussed in Chapter II. The fluorescent radiation and Auger electrons that are emitted in filling the vacancy in the inner shell following a photoelectric absorption are neglected since the energy released ( $\sim 28$  Kev for I) is so low. The photons will be absorbed essentially at the point of the photoelectric event for all crystals larger than  $\sim 1$  cm., since the absorption cross section in NaI for these

low energy photons is so high,  $\sim 32 \text{ cm}^{-1}$ . Nelms<sup>(44)</sup> indicates that electrons of this energy have a range  $< 10^{-3} \text{ cm}$ .

## 2. Secondary Gamma Treatment

Gammas interacting in Compton events are assumed to scatter according to the differential Klein-Nishina formula for free electrons.<sup>(31)</sup> Experimental confirmation of this formula has been reported by References 34 and 35. Since the Compton process occurs with the outer electron shell, the binding energy of these electrons (of the order of a few ev.) is negligible compared to the incident photon energy (of the order of 1.0 MeV.). Nelms<sup>(35)</sup> shows that the corrections required to this formula due to the electron binding energy are negligibly small. Polarization effects in Compton scattering were also ignored. Calculations made by Spencer and Wolff<sup>(36)</sup> indicate that when polarization effects are considered, the photon flux is only slightly increased ( $\sim 1\%$ ) over calculations made when polarization is neglected. Furthermore, these authors have shown the increase in photon flux occurs only for deep penetrations (i.e., many scatters), and photon energies in the range 0.1 - .2 MeV. Since typical histories for the present calculations, as given in the previous chapter, indicate that only 2 - 3 scatterings usually occur, and total penetration is only a few centimeters (typical crystal dimensions), polarization of Compton scattered gammas is negligible here.

As a photon is degraded in energy by successive Compton events, a cut-off energy has been chosen, below which the photon is assumed to be completely absorbed. This is required for proper termination of some

histories in the computer program and is chosen to be .01 MeV. Since the absorption cross section is so large ( $\sim 564 \text{ cm.}^{-1}$  in NaI), the probability for escape for a photon of energy  $\leq .01 \text{ MeV}$  is negligible.

In addition to Compton scattered gammas, the position created in the pair production events gives rise to secondary photons upon annihilation. These two annihilation photons each have a kinetic energy equal to the rest mass of an electron and are emitted from the location where the positron is essentially stopped. Heitler<sup>(37)</sup> has shown that for positron energies below 10 MeV, over 90% of the positrons will be reduced to essentially zero velocity before annihilation. The annihilation photons are assumed to be emitted isotropically, since there is no preferred orientation.<sup>(38)</sup> To conserve momentum the two photons are emitted in opposite directions.

### 3. Photoelectric Events

If a photoelectric event occurs, the gamma ray is totally absorbed and an electron is emitted with kinetic energy equal to the kinetic energy of the photon. This neglects the electron binding energy which is about 30 Kev for K or L shell electrons in iodine, as being negligible in comparison to the incident photon energy. The polar angle of photoelectron emission, relative to the incident photon direction, is assumed to be the average emission angle for the given electron energy. This average polar angle has been given by Davisson and Evans<sup>(39)</sup> as derived from the relativistic equation of Sauter.<sup>(40)</sup> Use of this data takes into account the

variation of emission angle with energy. For low energies, emission tends to be at right angles to the direction of incidence while the angular distribution shifts to the forward direction at higher energies. The photoelectrons are emitted in a uniform azimuthal distribution. These polar and azimuthal angles are measured relative to the directed line of the photon incidence and a transformation must be performed to relate these angles back to the coordinate system fixed in the crystal. The usual formulas for performing this transformation<sup>(23,32,38)</sup> involve computation with rather involved expressions. However Kleinecke<sup>(41)</sup> gives a highly efficient technique for performing the transformation. His method has been used throughout these calculations when it is desired to select a set of new direction cosines for a given set of original direction cosines and polar angle, knowing that the azimuthal angle is uniformly distributed. Kleinecke's method is given in Appendix F. Detailed treatment of the electron and bremsstrahlung will be given subsequently, in Sections C and D.

#### 4. Compton Events

If a Compton event occurs, the differential Klein-Nishina formula is sampled by the selection technique given by Kahn.<sup>(24)</sup> Appendix C gives details of the sampling procedure used. This method selects the cosine of the polar scattering  $\theta$  and then the energy of the scattered gamma is obtained from the Compton relationship:

$$E' = \frac{E_0}{1 + \frac{E_0}{m_0 c^2} (1 - \cos\theta)}$$

where  $E'$  = scattered gamma energy, MeV

$E_0$  = incident gamma energy, MeV

$m_0c^2$  = electron rest mass energy, MeV

The new direction cosines for the scattered gamma are obtained by the Kleinecke<sup>(41)</sup> technique, using  $\cos \theta$  and a uniform azimuthal distribution. Prior to following the scattered gamma ray through the crystal, calculations are performed to determine if the scattered electron, with energy  $E_e$  and polar angle  $\theta'$  given by

$$E_e = E_0 - E'$$

$$\tan \theta' = \frac{E' \sin \theta}{E_0 - E' \cos \theta} ,$$

is stopped in the crystal. Also prior to following the scattered gamma, it is determined that any bremsstrahlung photons generated by this electron have all been absorbed in the crystal. As previously discussed, escape of any of these electrons or photons terminates any further consideration of that history. Assuming that the electron and generated bremsstrahlung are absorbed, the scattered gamma is followed through the crystal in an identical procedure as that used for source particles. (See flow diagram, Figure III-1, of previous chapter.)

#### 5. Pair Production Events

If a pair production event occurs, the incident gamma energy, less twice the electron rest mass energy, is assumed to be shared equally between the negatron and positron. This neglects the slight asymmetry in

energy distribution between the position and negation. The mean polar angle for the emitted pair electrons is given by Bethe and Ashkin<sup>(42)</sup> as

$$\theta = \frac{m_0 c^2}{E_e} \quad (4.6)$$

where  $m_0 c^2$  = electron rest mass energy = .510976 MeV

and  $E_e$  = electron kinetic energy in MeV

The forward peaking predicted by Equation (4.6) for increasing electron energy, has been experimentally confirmed.<sup>(43)</sup> The azimuthal angles for the negatron-positron pair are uniformly distributed, 180° apart. No differentiation is made between positrons and negatrons when electron ranges and bremsstrahlung generation are considered (see Sections C and D, below). If both electrons are absorbed within the crystal, as well as any generated bremsstrahlung, then the two annihilation photons are followed. Since the pair electrons are treated in an identical manner, one is chosen at random to represent the positron for purposes of generating annihilation radiation. The two annihilation gammas originate at the point of stopping the positron, which was calculated to determine if the positron remained within the crystal, and are emitted in an isotropic angular distribution correlated at 180°, with an energy = 0.510976 MeV. One annihilation gamma is followed through the crystal and if absorbed the second gamma is followed. All Compton scattered and annihilation gammas are considered by the same computational procedure which includes generation of electrons and bremsstrahlung.



### C. Approximation of Electron Transport

All of the three gamma interaction processes give rise to electrons. The pair production events produce negatrons and positrons. However, many more negatrons are produced in the crystal by successive Compton and photoelectric events, and since Nelms<sup>(44)</sup> and Seliger<sup>(45)</sup> have indicated only a slightly greater range for positrons over negatrons, the assumption was made that both electrons would be treated as negatrons, as far as range calculations are concerned.

Slowing down and eventual absorption of electrons involves many interactions. Treatment of these electrons by the same techniques as used for gamma rays, which undergo a relatively small number of large energy-loss interactions, is not feasible for individual electron tracks. For the calculation of photofractions such detailed treatment of the electrons is not necessary because the important determination is whether the electron is stopped in, or escapes from, the crystal. This can be readily calculated by the following approximate method. Nelms<sup>(44)</sup> gives calculated data for NaI for the energy loss per unit path length (stopping power,  $-dE/dx$ ), and the integral:

$$R_o(E) = \int_0^E \frac{dE''}{|dE''/dx|} \quad (4.7)$$

which represents an average of the actual path lengths the electron follows from its origin to the end of its track. Nelms' data goes to  $E = 1.2$  MeV and Zerby<sup>(38)</sup> gives values for  $R_o(E)$  for  $2 \leq E \leq 10$  MeV.

The maximum radial penetration of an electron determines whether it passes through a given thickness of material and this distance is approximately related to the Nelms and Zerby data by the intercept of the electron transmission curve.

The transmission probability for electrons in sodium iodide is given in Figure IV-1. The data given in this figure has been calculated with the Monte Carlo program of K. Wainio<sup>(46)</sup> for an isotropic, monoenergetic electron source within sodium iodide. An isotropic source has been used to approximate the nearly random directions of electron incidence on the crystal boundary, after an electron has suffered many deflections. Also, by using an internal source within the medium, the effect of back scattered electrons is included in the transmission data of Figure IV-1. Conventional transmission curves, such as those of Seliger<sup>(45)</sup> and Agu,<sup>(48)</sup> are obtained with a source of normally incident electrons external to the medium and do not include back scatter effects. In Figure IV-1 the percent transmission is plotted versus the normalized range  $(\rho/R_0)$ , which is defined as the ratio of the mean penetration distance to the total path length traveled by the electron. This ratio is a measure of the range straggling that occurs. At  $\rho/R_0 = 0.7$ , the electron transmission is less than 3%. Plotting the data from the computer program of Wainio<sup>(46)</sup> in this manner, the transmission curve has been found to be nearly independent of energy for electron energies of interest. Other workers<sup>(45,47)</sup> have also reported that electron transmission data is nearly independent of energy, for low energy electrons, when plotted against the normalized range.

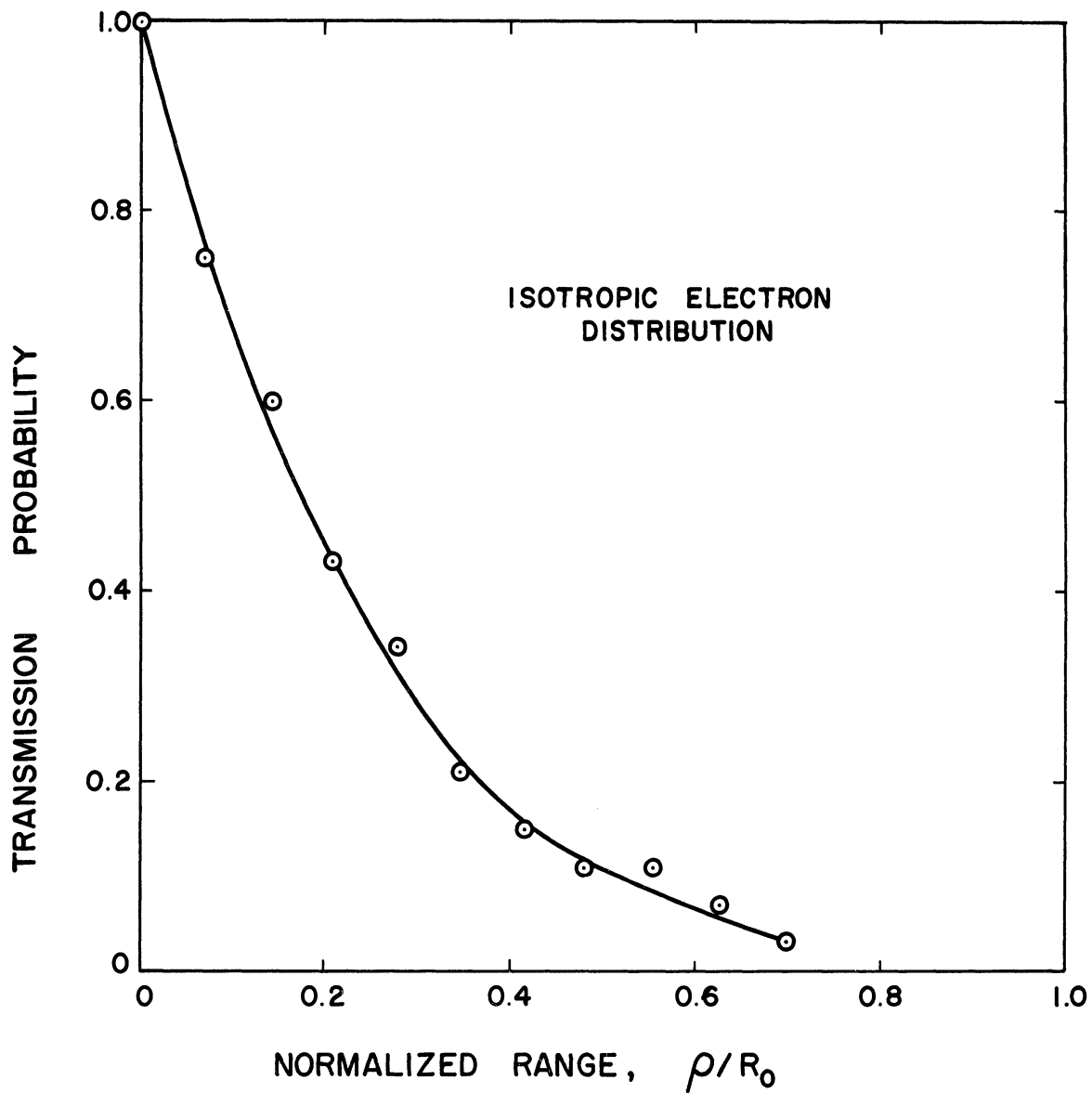


Figure IV-1. Electron Transmission in NaI. (46)

Empirical equations have been fitted to the data of Nelms<sup>(44)</sup> and Zerby<sup>(38)</sup> as follows:

$$\begin{aligned}
 R_0(E) &= .301 E^{1.625} \text{ cm.} , E \leq .2 \text{ Mev.} \\
 &= .200 E^{1.309} \text{ cm.} , .2 \leq E \leq 1.2 \text{ Mev.} \\
 &= .2154 E \text{ cm.} , E > 1.2 \text{ Mev.}
 \end{aligned}$$

Also the transmission data of Figure IV-1 are fitted by:

$$\begin{aligned}
 P_E(\rho/R_0) &= -2.05 \frac{\rho}{R_0} + .893 , \frac{\rho}{R_0} \leq .277 \\
 &= .172 \left(\frac{\rho}{R_0}\right)^{-1} + .293 \frac{\rho}{R_0} - .389 , \frac{\rho}{R_0} > .277
 \end{aligned}$$

Let  $\rho$  equal the distance along the directed line from the point of the free electron emission to the nearest crystal surface and consider the following cases:

- (1)  $\frac{\rho}{R_0(E)} \geq .7$
- (2)  $\frac{\rho}{R_0(E)} < .7$

For Case (1), the transmission probability from Figure IV-1 is essentially zero and the electron is assumed to be absorbed. The assumption is also made that the energy emitted by electron-induced excitation and ionization is absorbed in the crystal. For Case (2) the probability for electron escape is given by the function  $P_E(\rho/R_0)$  which has the form

of the transmission curve, where  $0 \leq P_E \leq 1$ . Sampling from the transmission curve can be performed by selecting a random number  $r$  and saying that escape from the crystal occurs when

$$r \leq P_E \left( \frac{\rho}{R_0} \right)$$

otherwise absorption occurs. Thus one approximately takes into account the decrease in escape probability as the distance to the crystal surface increases.

For those electrons which escape the crystal, a small fraction are returned to the crystal with nearly all their energy, due to small angle reflections from the casing of the crystal. Assuming the electrons are isotropically incident upon the casing, the number albedo and reflected energy spectrum data of Berger<sup>(47)</sup> have been used to determine the fraction of reflected electrons returned with approximately 98% of the incident energy. These electrons are assumed to deposit all their energy in the crystal. The number albedo data are stored in the program as a function of energy and the fraction of the returning spectrum that lies within about 98% of the incident energy has been determined to be approximately 0.08 by graphical integration of Berger's data for .51 MeV electrons isotropically incident upon aluminum. The shape of the energy spectrum for reflected electrons is expected to be nearly independent of incident electron energy, therefore this data of Berger has been used for all electron energies. The overall effect of electron reflection on the calculated photofractions is small enough so that these approximations are justified for all usual casing materials.

#### D. Bremsstrahlung Production

If the electron is stopped within the crystal boundaries, then the bremsstrahlung photons generated by these electrons are considered. In calculating the bremsstrahlung, the average bremsstrahlung spectrum generated by a monoenergetic electron of known initial energy has been used. This average spectrum is obtained by integrating over the entire electron path as the electron slows down, and is eventually stopped. The average spectrum, differential in photon energy, has been calculated by Zerby and Moran<sup>(49)</sup> for NaI and is given as Figure IV-2. This calculation is based on the Bethe-Heitler equation<sup>(51)</sup> for the bremsstrahlung cross section (includes screening effects of the atomic electrons), and the relativistic equation of Bethe<sup>(52)</sup> for energy loss by non-radiative collisions. No difference between the bremsstrahlung spectra generated by negatrons and positrons has been assumed, although a slight difference could be expected because of differences in energy loss by non-radiative collisions for positive and negative electrons. Zerby and Moran<sup>(49)</sup> have neglected any difference in their calculations, and Koch and Motz, in their review article,<sup>(50)</sup> point out that no data is available for positron bremsstrahlung spectra. The energy loss due to bremsstrahlung has assumed to be a small perturbation in comparison to the loss by all other mechanisms.

The Bethe-Heitler equation is based on the validity of the Born approximation. Due to this approximation the Bethe-Heitler equation is expected to be less reliable for high Z materials, and at

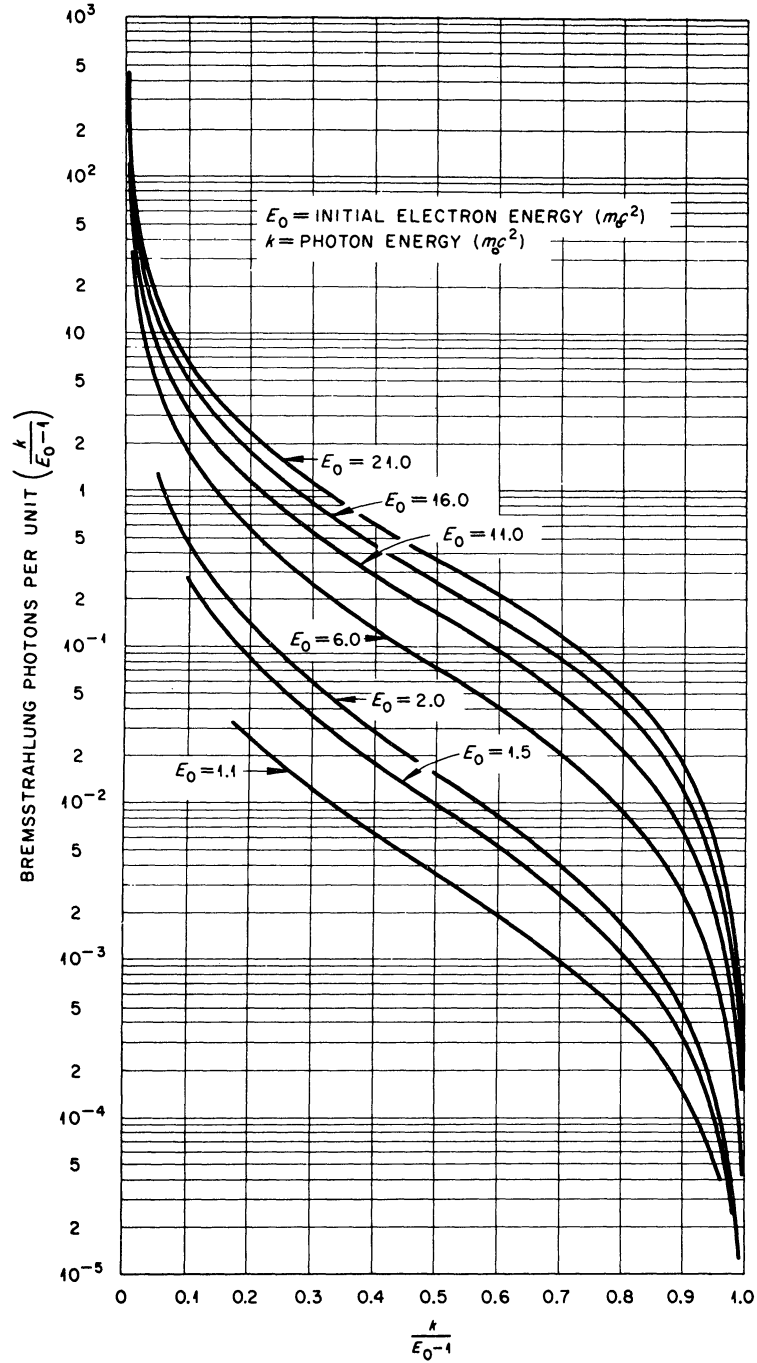


Figure IV-2. Bremsstrahlung Spectra from an Electron Slowing Down in Sodium Iodide. (Taken from Zerby and Moran.<sup>(49)</sup>)

lower initial or final electron energies. Koch and Motz<sup>(50)</sup> make comparisons between the differential cross section calculated from the Bethe-Heitler equation and experimental measurements in thin gold ( $Z = 79$ ) targets. The greatest difference between theory and experiment exists for electron initial kinetic energies in the range 0.1 - 2.0 MeV. The difference is as much as a factor of two for kinetic energies close to the electron rest mass energy, and less than 10% in the energy region above 4 MeV. The theoretical values are consistently lower than the experimental values and comparisons for aluminum indicate that the difference between theory and experiment is significantly reduced as  $Z$  decreases.

These comparisons made by Koch and Motz indicate that in calculations where bremsstrahlung radiation represents a major portion of the energy released, a large error can result when the only available formula (Bethe-Heitler) is used. However, in the calculations being made here the bremsstrahlung contributes a second order effect. For example, for 5 MeV source energy gammas, the average energy of the free electron from the first Compton scattering is 3.1 MeV. Evans,<sup>(53)</sup> page 616 gives the following semi-empirical formula for monoenergetic electrons, the energy fraction,  $\epsilon$ , converted to bremsstrahlung in a thick target:

$$\epsilon = .7 \times 10^{-3} ZE, \quad E \text{ in MeV.}$$



For 3.1 MeV electrons in NaI,  $\epsilon \approx 14\%$ . As Figure IV-2 indicates, the most probable radiative energy loss occurs by emission of a large number of low energy photons, most of which will be totally absorbed in the crystal. Even though  $\sim 14\%$  of the electron initial energy may be lost by bremsstrahlung emission, rarely will all this energy be concentrated in one or two high energy photons. Thus the error introduced by use of the Bethe-Heitler equation for NaI does not have a large effect on the overall calculation for the photofraction, for usual laboratory applications of scintillation detectors.

The differential spectra given in Figure IV-2 were calculated by Zerby and Moran,<sup>(49)</sup> assuming that the initial monoenergetic electrons lose energy in a continuous manner due to Coulomb scattering, and ionization and excitation of the target atoms. This continuous slowing down model is consistent with the previously discussed method of approximating electron transport in the crystal. Using the Bethe-Heitler equation,<sup>(51)</sup> Zerby and Moran<sup>(49)</sup> treated the bremsstrahlung events as a perturbation on the continuous energy loss model. Figure IV-2 gives their results for NaI, plotted as the average number of photons per unit photon energy versus normalized photon energy. Zerby<sup>(38)</sup> gives the total number of photons released, on the average, by integration of the differential spectra from a minimum photon energy of  $.04 m_0 c^2$  up to the maximum photon energy corresponding to the electron initial energy. The lower limit of integration is required because the spectrum has a singularity at zero photon energy. The assumption made here that all photons of energy less than  $.04 m_0 c^2$  will be totally absorbed is justified because

the photoelectric cross section is greater than  $80 \text{ cm.}^{-1}$  for these low energy photons. The results of Zerby are given in Table IV-1, below:

TABLE IV-1  
 INTEGRATION OF THE DIFFERENTIAL  
 BREMSSTRAHLUNG SPECTRA FOR NaI<sup>(38)</sup>

Electron Initial Total (Rest + Kinetic) Energy, $E_0 \text{ } m_0c^2$ units	Mean Number of Photons Released, $m(E_0)$ with Energy $> .04 \text{ } m_0c^2$
1.1	.0009
1.5	.0325
2.0	.0972
6.0	.8434
11.0	1.9770
16.0	3.1359
21.0	4.4144

The simulation of bremsstrahlung generation in the Monte Carlo programs is as follows. Of the electrons created in the three primary gamma interaction processes, only those stopped within the crystal are considered to generate some bremsstrahlung radiation along their path as they slow down in the crystal. (As previously discussed, if an electron escapes, the history is terminated.) For a given electron initial energy, the mean number of photons released is obtained by interpolation of the data of Table IV-1, using a third order interpolation formula. Given this mean number,  $m$ , of photons with energies  $> .04 \text{ } m_0c^2$  emitted over the electron path, the probability  $P(x)$  that exactly  $x$  photons will be emitted is assumed to be given by the Poisson distribution, since

the bremsstrahlung emission probability per electron interaction is small.

$$P(x) = \frac{e^{-m} m^x}{x!}$$

The probability that at most  $x_0$  photons will be emitted is given by the cumulative probability,

$$P(x_0) = \sum_{x=0}^{x_0} P(x) \tag{4.8}$$

which is a properly normalized cumulative distribution function (C.D.F.). The number of emitted bremsstrahlung photons,  $x_0$  is obtained from this C.D.F. whenever the inequality

$$P(x_0) \leq r \leq P(x_0+1) \tag{4.9}$$

is satisfied, where  $r$  is a random number. In these calculations, Equation (4.8) is evaluated for successive values of  $x_0$  and the inequality (4.9) is tested. By reference to Table IV-1, it is apparent that for low energy electrons, the inequality (4.9) will usually be satisfied for  $x_0 = 0$  or  $1$ . When  $x_0 = 0$ , no bremsstrahlung of energy  $> .04 m_0 c^2$  are generated. For  $x_0 \geq 1$ , a separate selection is made for the energy of each of the bremsstrahlung photons, by the following technique.

Making the definitions (energies in  $m_0c^2$  units):

$n(E_0, \epsilon)d\epsilon$  = mean number of photons with an energy between  $\epsilon$  and  $\epsilon + d\epsilon$ , emitted by an electron of incident total (rest + kinetic) energy,  $E_0$ .

Thus,  $n(E_0, \epsilon)$  versus  $\epsilon$  is the spectrum given in Figure IV-2.

Table IV-1 above gives values for:

$$m(E_0) = \int_{.04}^{E_0-1} n(E_0, \epsilon) d\epsilon =$$

mean number of photons with an energy  $> .04 m_0c^2$  released by an electron of total (rest + kinetic) energy  $E_0$ ;  $m_0c^2$ .

A normalized probability density function is obtained by:

$$f(E_0, \epsilon) d\epsilon = \frac{n(E_0, \epsilon) d\epsilon}{m(E_0)} =$$

fraction of photons with an energy between  $\epsilon$  and  $\epsilon + d\epsilon$ .

Using the cumulative probability technique, Equation (3.4), one obtains a random sample of the probability density function  $f(E_0, \epsilon) d\epsilon$ . No useful analytic expressions are available for  $f(E_0, \epsilon) d\epsilon$ , so that sampling must be performed from the function in a numerical form.

Letting:

$$B_i(E_0, \epsilon) = \int_{.04}^{\epsilon_i} f(E_0, \epsilon) d\epsilon = \frac{\int_{.04}^{\epsilon_i} n(E_0, \epsilon) d\epsilon}{\int_{.04}^{E_0-1} n(E_0, \epsilon) d\epsilon} \quad (4.10)$$

it is evident that:

$$B_i(E_o, \epsilon_i) = \begin{array}{l} \text{probability that an emitted photon will} \\ \text{have an energy } \leq \epsilon_i , \end{array}$$

and

$$0 \leq B_i \leq 1 .$$

Thus  $B_i(E_o, \epsilon_i)$  is the appropriate cumulative distribution function (C.D.F.), defined as the probability that a random variable (photon energy in this case) is less than or equal to some specified value.

Using the Monte Carlo technique of setting the C.D.F. equal to a random number,  $r$ , the selection of the bremsstrahlung energy is obtained from:

$$B_i(E_o, \epsilon_i) = r . \tag{4.11}$$

Values of  $B_i$  versus  $\epsilon_i$  have been computed from Equation (4.10) by integration of the bremsstrahlung spectrum<sup>(54)</sup> and are stored in the computer programs in discrete steps. Equation (4.11) is used to obtain a value for  $B_i(E_o, \epsilon_i)$ . A double linear interpolation scheme was devised to select the photon energy. First, an interpolation using the value of  $B_i(E_o, \epsilon_i)$  is made, and then an interpolation using the electron initial energy. The photons are uniformly distributed along the electron path in a random manner. This path is assumed to be a straight line starting from the creation of the electron (location of gamma interaction) to the greatest radial penetration. The radial penetration of some electrons goes beyond the crystal, yet sampling from the

transmission curve indicates that the electron actually does not escape. (See previous discussion of electron treatment.) For these electrons, the end of the path for purposes of bremsstrahlung emission, is considered to be at the nearest crystal boundary, along the direction of electron emission.

For typical applications of gamma ray scintillation crystals, the electrons produced in the crystal will be of sufficiently low energy to justify the assumption that the primary mechanisms causing electron slowing down are ionization and excitation losses. This assumption has been made by Zerby and Moran<sup>(49)</sup> in the calculation of the bremsstrahlung spectrum as a perturbation on the excitation and ionization processes of electron energy loss. The electron energy loss by radiative processes is assumed small compared to other mechanisms. Under these conditions, momentum is essentially shared between the target nucleus and deflected electron, with the bremsstrahlung photons emitted uncorrelated in angular distribution with respect to the scattered electron direction.<sup>(53)</sup> Only for extreme relativistic energies is the photon emitted preferentially in the forward direction.<sup>(55)</sup> Thus, for all of these calculations, the photon from the bremsstrahlung spectrum has been assumed to emerge with an isotropic angular distribution. As discussed in the previous chapter, the bremsstrahlung photons are treated in the same manner as primary gammas, except that no electrons or further bremsstrahlung are generated. The escape of any bremsstrahlung generated by the above technique causes termination of that history, since total absorption of the source gamma energy is not possible.

E. Escape Routines

Having considered the simulation of the interaction processes, one must next determine if a gamma or particle traveling a known distance in a given direction will escape the crystal. For the solid crystal, escape occurs whenever the coordinates at the end of the path satisfy any of the following inequalities:

$$x^2 + y^2 \geq R^2, \quad z \leq 0, \quad \text{or} \quad z \geq H \quad (4.12)$$

where  $R$  = crystal radius  
 $H$  = crystal height.

Although the same criteria applies for the well crystal, the problem is considerably more complicated. The derivation of the escape routine for the well crystal is given in Appendix D. Essentially it must be determined if the ray intersects the well, and if so, whether it re-enters the crystal or escapes out the top of the well. Postponing considerations of absorption and scattering in a three-dimensional source to a later section, the well volume is assumed to be a vacuum. The effect of adding a cylindrical vacuum within the crystal is to increase gamma ray escape through the crystal exterior surfaces, as well as escape out through the top of the well. Reduction of the photofraction, in comparison with that of a solid crystal, will be the net result. It is also assumed for those gamma rays that pass through the well, attenuation in the crystal canning material is negligible. Aluminum is most frequently used as a canning material; typical thickness being about 0.8 mm. In general, gammas will not be normally incident upon the canning, but the

directions of incidence will be nearly isotropic. Except for those few gammas which are incident at very large angles from the casing surface normal, the path length in aluminum will not be more than  $\sim 1$  mm. Attenuation through this thickness is appreciable only for that small fraction of gammas that cut through the well with energies less than about 80 Kev. Since the absorption cross section in scintillation materials at this energy is so high ( $\sim 10 \text{ cm.}^{-1}$  in NaI), only a small fraction of the gammas near the well surface will be effected, most being absorbed before reaching the well. Thus if the gamma cuts through the well and re-enters the crystal the total distance traveled is increased by the length of path through the well. Making this increase in the path length for these gamma rays, the above escape criteria is applied. Allowance is also made for escape out the top of the well.

#### F. Termination Categories

A photon history is recorded according to the method of termination. For off-axis isotropic point sources, and disk or volume sources some of the selected source gammas may miss the crystal entirely, and these are recorded in the termination category, T. Those source gammas which are incident upon the crystal, but pass through without any interaction are recorded in the category, P. For any source gammas which interact with the crystal at least once, a count is made in I category. Of these I photons, the number that deposit the entire source energy (i.e., totally absorbed) are recorded in the category, A. The photo-fraction is given by  $A/I$  and the intrinsic total efficiency,  $\epsilon_{IT}$  is



given by  $I/(I + P)$  . This later quantity has been calculated by numerical integration, as discussed in Chapter II, and thus provides a check on part of the Monte Carlo results.

#### G. Photofraction Standard Deviation

Estimates of the statistical significance of the Monte Carlo results for the photofraction may be obtained by calculation of the standard deviation. Statistical fluctuations occur in the number of source gammas totally absorbed in the crystal due to the random nature of the processes involved. For these calculations, the number of interacting source gammas,  $I$  , is a preassigned number. Of these  $I$  photons two events are of interest, either the total photon energy is absorbed, or not. The probabilities for either event are constant, and independent, thus satisfying the criteria for application of binomial statistics. It should be noted that the probability for total absorption is not always small, (the photofraction goes to 1.0 for low energies or very large crystals), so that application of the Poisson distribution is not justified, in general. One desires the variance of the ratio  $A/I$  , where  $I$  is a constant. It can be shown<sup>(56)</sup> that:

$$V\left[\frac{A}{I}\right] = \frac{1}{I^2} V[A]$$

Since in general the conditions for the binomial distribution are satisfied, the variance is given<sup>(56)</sup> by:

$$V[A] = I p (1-p)$$

where  $p$  = probability of total absorption.

Thus:

$$V\left[\frac{A}{I}\right] = \frac{p(1-p)}{I}$$

Since the definition of the photofraction corresponds to that given above for  $p$ ,

$$\begin{aligned} \frac{A}{I} &= p, \\ \sigma_p &= \sqrt{V\left[\frac{A}{I}\right]} = \left[\frac{p(1-p)}{I}\right]^{\frac{1}{2}} \end{aligned} \quad (4.13)$$

where  $\sigma_p$  = standard deviation of the photofraction. As is generally the case the standard deviation for an assumed constant photofraction varies as the inverse square root of the number of histories. Also one obtains the usual Poisson distribution result from:

$$\sigma_p = \frac{\sqrt{A}}{I} = \sqrt{\frac{p}{I}}, \quad p \ll 1.$$

Equation (4.13), being the general case, has been used in the Monte Carlo programs which calculate the photofraction and its standard deviation.

H. Absorption and Scattering in the Source

Up to this point in the present work, any interactions of the gamma rays within three-dimensional sources have been neglected. For some sources it will be desirable to consider these effects. In a review of the current literature, Reference 18 was found to give the only calculated results in which source interactions were considered. Reference 18 has given calculated results for the total efficiency of detecting, with a solid crystal detector, gammas from a homogeneous cylindrical volume source in which gamma attenuation occurs. The source was assumed to be an aqueous solution of a known energy gamma emitter. (A comparison is given in Table IV-2 between some of these results and those of the present work.) References 57 and 58 considered solution of a similar problem with an experimental approach. Unfortunately, the sources considered in References 57 and 58 were not homogeneous, and thus a comparison with the present work is not possible.

TABLE IV-2

ABSOLUTE TOTAL EFFICIENCIES SOURCE SELF ABSORPTION  
AND SCATTERING INCLUDED 2 x 2 IN. SOLID CRYSTAL

Energy MeV	<u>Present</u> $\epsilon_{AT}$	<u>Calc.</u> $\epsilon_{AT}'$	Ref. 18 $\epsilon_{AT}'$
0.20	.1490	.1373	.1380
1.00	.0499	.0453	.0457

Since for some volume sources it may be necessary to consider attenuation effects within the source, the following analysis was made. At lower energies, where the gamma ray cross sections are the highest, attenuation in the source may cause an appreciable reduction in the photo-fraction and total efficiency, and thus in the absolute peak efficiency,  $\epsilon_{AP}$ . We will designate as  $\epsilon_{AP}$  the absolute peak efficiency for an ideal source which has zero scattering and absorption cross sections, and  $\epsilon_{AP}'$  for the same source geometry which has non-zero source cross sections. Analogous definitions are made for the photofraction,  $p$  and absolute total efficiency,  $\epsilon_{AT}$ . Thus, by definition:

$\epsilon_{AT}'$  = fraction of source gammas that escape the source without interaction, and interact at least once in the crystal

then,

$$\epsilon_{AT}' = \frac{1}{V_s} \int_{\Omega} \int_{V_s} [1 - e^{-\tau x}] e^{-\mu y} d\Omega dV_s \quad (4.14)$$

where  $V_s$  = source volume, cm.<sup>3</sup>  
 $x(\Omega)$  = extrapolated path length in crystal, cm.  
 $y(\Omega)$  = extrapolated path length in source, cm.  
 $\tau(E)$  = total cross section of crystal, cm.<sup>-1</sup>  
 $\mu(E)$  = total cross section of source, cm.<sup>-1</sup>

An experimental measurement of the pulse height spectrum would indicate a lower photopeak and increased Compton continuum for a case in which gamma interactions occur in the source volume, as compared to a case

of identical geometry but the source being transparent to its radiation. This is because even with an initially monoenergetic source in the case of interactions in the source, the crystal has gammas of many different energies incident upon it since some variable fraction of the gamma energy can be lost in the source. Thus the experimental photofraction is reduced. Reference 59, page 87 gives a curve that shows this effect by comparing the pulse height spectra for a point source in air, and in water. This comparison approximates the situation considered here of a homogeneous source volume, with and without source absorption and scattering.

However, if the calculation for the photofraction  $p'$  is made for only those gammas which escape from the source unattenuated in energy, then the desired absolute peak efficiency is given by:

$$\epsilon'_{AP} = \epsilon'_{AT} \cdot p' \quad (4.15)$$

where  $p'$  = photofraction, given by the ratio  $A'/I'$

$A'$  = number of gammas that deposit the total source energy in the crystal

$I'$  = number of gammas that interact at least once in the crystal that could deposit the source energy in the crystal, i.e., those gammas that escape from the source without depositing any energy and interact with the crystal.

Thus, Equation (4.15) is equivalent to writing

$$\epsilon'_{AP} = \frac{I'}{N_0} \cdot \frac{A'}{I'} = \frac{A'}{N_0} \quad (4.16)$$

where  $N_0$  = source absolute gamma intensity.

This treatment of sources in which absorption and scattering occur is seen to be somewhat analogous to the treatment in Chapter I of the ideal total spectrum area  $A_T^*$  and the experimentally observed area  $A_T$ . In both cases, use of the absolute peak efficiency eliminates consideration of the observed total spectrum, since this quantity cancels out in Equations (1.7) and (4.16). Thus since  $\epsilon_{AT}'$  is obtained by numerical integration of Equation (4.14), the only parameter to be calculated is  $p'$ .

The photofraction  $p'$  will differ from the photofraction  $p$ , which is calculated for the transparent source case. However, this difference is due only to a geometrical effect, based on the above definition of  $p'$ . If the volume source could be considered to be concentrated at a point, then this "source point" would be located nearer the crystal for the source with non-zero scattering and absorption cross sections than for the transparent source. This is because in the non-transparent source, gammas being emitted nearer the crystal will have a greater probability of escaping uncollided from the source and then striking the crystal. In Chapter V, the effect of geometry on the photofraction will be shown to be small for regular source shapes of not too large an extent. By restricting considerations to cylindrical volume sources with dimensions no greater than approximately the crystal dimensions, one can take  $p' = p$ , to a very good approximation.

The above discussion is equally valid for solid and well crystals, even though the reentrant surface of the latter allows the possibility of a gamma which scatters in the crystal to reenter the source, depositing

some energy therein. The well crystal program was modified to study this effect, and for sources in an aqueous solution completely filling the well in less than 0.1% of the histories did such an event occur. Thus this possibility can be neglected, except for sources which are nearly "black" for their radiation.

The computer program, BURP-2 evaluates Equation (4.14) for any specified source total gamma ray cross section (without coherent scattering). Details of using this program to include source scattering and attenuation are given in Appendix E. Table IV-2 above gives a comparison of the present calculations with some results of Reference 18 for a solid crystal detector and a homogeneous aqueous solution of the gamma source. The source diameter is the same as the crystal diameter, with different source heights. Agreement is seen to be excellent. Since Reference 18 provides extensive tabulations for solid crystals, no further calculations for solid crystals are given in the present work. However, no results have been previously published for well crystals, and therefore Table IV-3 is given below. This table gives calculated  $\epsilon_{AT}'$  values for the Harshaw 8F8 well crystal with various energy sources in a homogeneous aqueous solution totally filling the well. Values of  $\epsilon_{AT}$ , in which source interactions are neglected, are also given in Table IV-3.

TABLE IV-3

ABSOLUTE TOTAL EFFICIENCIES SOURCE SELF ABSORPTION  
AND SCATTERING INCLUDED 8F8 WELL CRYSTAL,  
AQUEOUS SOURCE VOLUME EQUALS WELL SIZE

Energy MeV	$\epsilon_{AT}'$	$\epsilon_{AT}$	Energy MeV	$\epsilon_{AT}'$	$\epsilon_{AT}$
.01	.0697	.8760	.60	.2589	.2890
.015	.2388	.8760	.80	.2261	.2491
.02	.4158	.8758	1.00	.2049	.2234
.03	.5908	.8742	1.50	.1728	.1855
.04	.6539	.8756	2.00	.1567	.1667
.05	.6774	.8749	3.00	.1429	.1505
.06	.6883	.8737	4.00	.1385	.1444
.08	.7003	.8705	5.00	.1365	.1429
.10	.7051	.8652	6.00	.1371	.1429
.15	.6703	.8046	8.00	.1404	.1455
.20	.5698	.6725	10.00	.1452	.1499
.30	.4081	.4710	15.00	.1581	.1624
.40	.3284	.3750	20.00	.1689	.1731
.50	.2849	.3207	30.00	.1864	.1907



## CHAPTER V

### RESULTS FROM THE MONTE CARLO CALCULATIONS

#### A. Comparison of Experimental and Calculated Results

Both calculational and experimental approaches have been previously used to obtain photofractions for scintillation crystals. Nearly all published results are for solid crystals, with only a limited amount of data reported for well crystals. Early calculations emphasized determination of detector response spectra, and accurate photofractions were not reported. Typical of these were the work of Campbell and Boyle,<sup>(60)</sup> Foote and Koch,<sup>(61)</sup> and Maeder, Müller, and Wintersteiger.<sup>(62)</sup> Experimental determination of photofractions for solid crystals have been given in References 63 - 71. Calculations, using some type of Monte Carlo techniques with modern digital computers, have been reported in References 8, 9, 11, 32, 38, and 72 - 76. The recent papers of Miller and Snow,<sup>(9)</sup> and Zerby and Moran<sup>(38)</sup> are most noteworthy because their photofraction calculations for solid crystals cover a wide range of gamma energies. Trombka<sup>(77)</sup> has given some calculated values for photofractions (calculated by Miller and Snow) and absolute total efficiencies for a 2 in. spherical crystal. A limited amount of experimental data for well crystals have been reported in References 59 and 78 - 82. The only reported data for well crystals photofractions obtained by Monte Carlo calculations are given by Wächter,<sup>(74)</sup> but the geometry was restricted to spherical NaI crystals with empirical extrapolations used to approximately extend the data to cylindrical crystals.

1. Solid Crystals

Results for solid crystals have generally indicated larger values for calculated photofractions than those measured in experiments. Since the photofraction is a ratio of the area under the total absorption peak to the total response spectrum, it can be influenced by any experimental effects which change either of these areas. Photons may undergo an initial Compton event in surrounding media, and can enter the crystal. These scattered photons may then be absorbed in the crystal. This produces the familiar back-scatter peak in the response spectrum, as well as contributing to the rest of the Compton continuum. Even if the detector is well-removed from shielding and other external material such as room walls, contributions from back-scattered gammas will unavoidably be present in the experimentally observed Compton continuum, since some scattering will occur from the reflector and casing surrounding the crystal, as well as from the photomultiplier tube. For some isotopes that are difficult to prepare as point sources, absorption and scattering effects are present within the source. The above effects would tend to decrease the observed photofractions.

In the careful experiments of Heath, <sup>(67,83)</sup> measurements were made for point source geometry with the source and detector located in the center of a 5 ft. diameter plastic bag filled with helium to reduce air scattering. The experiments were done in a large open room, with minimum background present. Isotope sources were used in which electron-capture predominates over beta emission, so that no beta absorbers were needed, thus eliminating small-angle scattering from any beta absorber.

In References 67 and 83 a number of independent checks were made of the measured photofractions. By using the  $4\pi$   $\beta$ - $\gamma$  coincidence counting methods given in Reference 84, a number of suitable sources were calibrated and used with these detectors. The peak efficiencies obtained agreed within better than 2% in all cases when compared to the product of the directly measured photofractions and the absolute total efficiencies of Vegors.<sup>(5)</sup> Calibration of these sources was independently checked by the National Bureau of Standards and Chalk River Laboratories, and agreement within  $\pm 1\%$  was found. Data from References 67 and 83 are given in Figure V-1.

Photofractions obtained by Monte Carlo calculations are determined under idealized source-detector geometry, assuming no surrounding materials. Inherent errors are present in most of the previous Monte Carlo calculations primarily due to approximations made in treating secondary particles. At higher energies, deviation of calculated photofractions from experimental results, obtained under ideal conditions, has been about 10-20% probably because of these approximations. In addition, escape of secondary particles will have a greater influence on the photofractions for smaller crystals. In the previous Monte Carlo calculations only References 9 and 38 have considered electron production and subsequent bremsstrahlung generation. Miller and Snow<sup>(9)</sup> have treated electrons by simple range theory, which does not take into account the fractional leakage probability for electrons (see Chapter IV). On the other hand, Zerby and Moran<sup>(38)</sup> have neglected electron transport altogether. In data to be given in Section B below, it will be seen that electron escape has less of an effect on the calculated photofractions than does the bremsstrahlung escape.

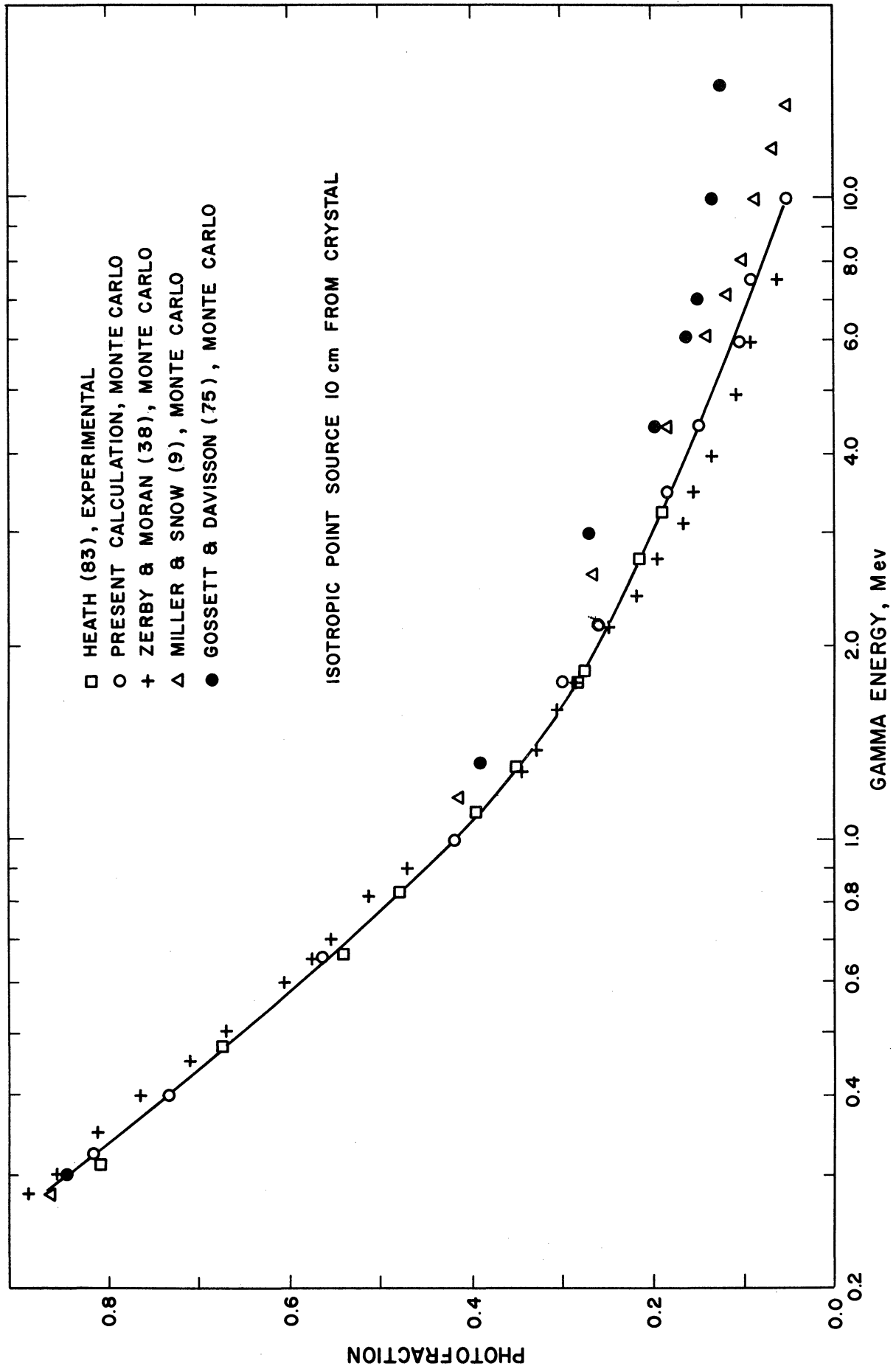


Figure V-1. Photofraction vs. Energy for 3 x 3 In. Solid Crystal.

Both References 9 and 38 have used the bremsstrahlung spectra calculated by Zerby and Moran.<sup>(49)</sup> No elaboration on the technique of using this data in the Monte Carlo calculations has been given in Reference 9, thus a comparison with the methods of treating bremsstrahlung given in Reference 38 is not possible. The method used in the present work to select bremsstrahlung photon energies (Chapter IV) is similar to that used in Reference 38. However, the assumption has been in Reference 38 that all electrons will give rise to some bremsstrahlung photons of energy  $> .04 m_0 c^2$ . In Reference 38 two bremsstrahlung photons are selected for every electron produced, and a statistical weight of  $m(E_0)/2$  is assigned to each, based on data given in Table IV-1. The photon is considered to be absorbed if its weight falls below a preassigned value. The method used in the present investigation, described in Chapter IV, obtains the number of bremsstrahlung photons emitted based on the mean values of Table IV-1 and sampling according to the Poisson distribution. By this method a fixed number of photons is not emitted for all electrons. The difference between these two approaches is that for low electron energies, the probability for photon emission with energy  $> .04 m_0 c^2$  is very low, and in most instances no bremsstrahlung will be generated in the present calculations. Bremsstrahlung effects on the calculated photofractions are nearly insignificant at these low energies. At higher energies, the methods used in Reference 38 and the present calculations give essentially the same number of bremsstrahlung photons and little difference is noted for the photofractions obtained (Figure V-1).

Figure V-1 gives a comparison made by Davisson and Gossett<sup>(75)</sup> of experimental and calculated results from References 9, 38 and 83 for photofractions of a 3 x 3 in. solid crystal, with an isotropic point source 10 cm. from the front crystal face. Results from the present work have also been included. The comparison in Figure V-1 is especially valid due to the large amount of data available for this geometry. The data of Reference 75 given in Figure V-1 is based on Monte Carlo calculations in which electrons and bremsstrahlung are neglected, and the divergence from the results of the more exact calculations can be seen at higher energies. However, the most significant aspect of this figure is the relatively poor agreement of References 9 and 38, especially at higher energies. Fairly good agreement is seen among the results of Zerby and Moran,<sup>(38)</sup> the experimental values of Heath,<sup>(83)</sup> and the present calculation. Results from the present work are seen to be in best agreement with the experimental values from Reference 83. The relatively large difference between Reference 9 results and the others, even though rather exact simulation methods were used, is unexplained. Zerby<sup>(73)</sup> has also mentioned this discrepancy and attributes it to the method of simulating bremsstrahlung emission.

Further doubt as to the validity of Reference 9 results, at higher energies, is given by the experimental values of Jarczyk,<sup>(70)</sup> some of which are listed in Table V-1 below. These values, obtained for collimated beam sources, were checked by three independent experimental methods which are discussed in detail in Reference 70. Considerable difference between References 9 and 70 is noted at these higher energies, at which the effects of

secondary particles would be expected to be more important. Excellent agreement with Reference 70 has been obtained with the present calculations. At lower energies, comparisons of experimental results with calculations from Reference 9 have been made by Roesch<sup>(85)</sup> and McCall.<sup>(86)</sup> For energies  $\leq 1.33$  MeV, the maximum difference between experiments and Reference 9 calculations was 9.3%, which is a considerable improvement over the large discrepancies seen at higher energies.

TABLE V-1

BROAD BEAM PHOTOFRACTIONS, 2 x 2 IN. SOLID NaI CRYSTAL

Energy, MeV	Miller and Snow <sup>(9)</sup>	Jarczyk, <u>et al.</u> <sup>(70)</sup>	Present Calculation
2.68	0.189	0.156	0.152
7.10	0.056	0.042	0.046
8.00	0.045	0.035	0.037

## 2. Well Crystals

The data given in References 59 and 78-82 provide a basis of approximate comparison between experimental values of peak efficiencies for well crystals and the calculations of the present work. References 59, 78 and 79, based on some early measurements at ORNL do not clearly specify the source configuration and its location in the well. One can infer from these references that the source was probably a volume source, in some cases with the isotope in an aqueous solution. If this were the case, scattering and attenuation in the source would tend to increase the Compton spectrum at the expense of a decreased photopeak causing a reduction of the photofraction. This effect is discussed in Chapter IV,

Section H. (Reference 59, p. 87, gives experimental response curves that show the effect of a reduced photopeak and increased Compton spectrum for a source located in water.) Since the comparison of the present work and References 59, 78 and 79 is intended to show approximate agreement only, calculations were made at the three lowest energies neglecting the effects of electron and bremsstrahlung escape. The calculation at 0.661 MeV was made including these effects. Table V-2 below gives this comparison for a 3 x 3 in. well crystal, 1/2 in. well dia. x 1-1/2 in. well height. For the calculations, the source was assumed to be a point isotropic source, 0.2 cm. from the well bottom. The values below from Reference 59 were taken from plotted data, and are only approximate. The standard deviation for the calculated results is that obtained from the variance in the Monte Carlo computations.

TABLE V-2

COMPARISON FOR POINT SOURCE  $\epsilon_{IP}$ , 3 x 3 IN. WELL CRYSTAL

Energy, MeV	References 78 and 79	Reference 59	Present Calculations
0.32	0.67	0.75	0.762 $\pm$ .003
0.364	0.60	0.64	0.677 $\pm$ .004
0.638	0.34	0.38	0.387 $\pm$ .004
0.661	0.33	0.36	0.370 $\pm$ .007

Gunnick and Stonner<sup>(82)</sup> have given values for experimentally determined absolute peak efficiencies for a 3 x 3 in. well crystal. The crystal dimensions for the well are not specifically given, but the well size including crystal casing and reflector has been given as



13/16 in. dia. x 1-29/32 in. height. Information obtained from the manufacturer (Isotopes, Inc.) indicated a probable canning thickness of 0.025 in. and reflector thickness of 1/16 in., which were used to determine the crystal well dimensions. Again the source position was unspecified and the assumption was made that it was an isotropic point at the well bottom, neglecting any source container. The comparison is given below for some of the values given in Reference 82.

TABLE V-3

COMPARISON FOR POINT SOURCE,  $\epsilon_{AP}$ , 3 x 3 IN. WELL CRYSTAL

Energy, MeV	Reference 82	Present Calculations
0.412	0.465	.520 $\pm$ .006
1.17	0.168	.180 $\pm$ .005
2.75	0.072	.079 $\pm$ .003

Comparison between the experimental results of Colby<sup>(80)</sup> and those calculated in the present work are given in Table V-4 below. The crystal size is 5 x 5 in., with 5/8 in. well dia. x 2-1/2 in. well height. For the calculations, the source was again assumed to be point isotropic, 0.2 cm. from the crystal well bottom.

TABLE V-4

COMPARISON FOR POINT SOURCE,  $\epsilon_{AP}$ , 5 x 5 IN. WELL CRYSTAL

Energy, MeV	Reference 80	Present Calculations
0.279	0.896	0.957 $\pm$ .002
0.662	0.614	0.594 $\pm$ .005
1.33	0.350	0.371 $\pm$ .005

Finally, Table V-5 gives a comparison made with the experimental data of Nablo<sup>(81)</sup> for two well crystals, Harshaw Nos. 7F8, and 8F8. In Reference 81 the experimental error is estimated to be about 3%, having used calibrated sources. The values given in Reference 81 were for photofractions and absolute total efficiencies,  $\epsilon_{AT}$  determined from a spectrometer response which included backscatter effects. As discussed in Chapter I, in the product of the photofraction and  $\epsilon_{AT}$  to give  $\epsilon_{AP}$ , the total spectrum area cancels. The absolute peak efficiencies,  $\epsilon_{AP}$  of Reference 81 are comparable to the calculations of the present investigation. For the calculations, the point isotropic source was again assumed to be 0.2 cm. from the well bottom.

TABLE V-5

COMPARISON FOR POINT SOURCE,  $\epsilon_{AP}$ , 8F8 AND 7F8 WELL CRYSTALS

Energy, MeV	7F8		8F8	
	Ref. 81	Present Calc.	Ref. 81	Present Calc.
0.080	0.97	0.983 $\pm$ .008	0.98	0.963 $\pm$ .008
0.279	0.49	0.557 $\pm$ .005	0.43	0.515 $\pm$ .005
0.412	0.24	0.294 $\pm$ .005	0.23	0.268 $\pm$ .005
0.662	0.12	0.147 $\pm$ .002	0.11	0.135 $\pm$ .002

The following conclusions are made, based on the comparisons given in Tables V-2 through V-5. A direct experimental check on the well crystal photofractions calculated in the present work is not possible because no careful experiments such as those of Heath<sup>(67,83)</sup> (for solid crystals) have been reported. However calculated values for  $\epsilon_{AT}$  have been shown to agree with independent calculations (Chapter II), and approximate agreement with

various experiments is seen for  $\epsilon_{AP}$  or  $\epsilon_{IP}$  values given in Tables V-2 through V-5. Thus an approximate check is given for the well crystal Monte Carlo calculated photofractions.

B. Effects of Bremsstrahlung and Electron Escape on Photofraction

In order to show the relative effects on the photofractions of the energy carried away by electrons and bremsstrahlung escaping the crystal, calculations were made in which these losses were ignored. (See Appendix E for the method of using the Monte Carlo programs without electrons and/or bremsstrahlung.) Table V-6 below gives some data for photofractions in which electrons and/or bremsstrahlung losses are neglected. This tabulation indicates that by neglecting electron losses only (Case 2), the photofractions for both the high and low energies considered here agree within one standard deviation with those obtained when electron losses are included (Case 1). However if only bremsstrahlung losses are neglected (Case 3), then a statistically significant increase in the photofraction occurs at the higher energy.

TABLE V-6

EFFECT OF ELECTRON AND BREMSSTRAHLUNG LOSSES ON  
PHOTOFRACTIONS, ISOTROPIC POINT SOURCES

Crystal	Case 1	Case 2	Case 3	Case 4	Energy, MeV
8F8 Well	.0515 $\pm$ .0049	.0530 $\pm$ .0050	.0829 $\pm$ .0064	.1000 $\pm$ .0042	6.00
8F8 Well	.2650 $\pm$ .0099	.2820 $\pm$ .0101	.2945 $\pm$ .0102	.2905 $\pm$ .0102	1.17
3x3 in Solid	.1010 $\pm$ .0114	.1055 $\pm$ .0069	.1535 $\pm$ .0081	.1705 $\pm$ .0084	6.00
3x3 in Solid	.3245 $\pm$ .0105	.3190 $\pm$ .0104	.3000 $\pm$ .0102	.3200 $\pm$ .0104	1.78

Case 1 - Electron and bremsstrahlung losses considered  
 Case 2 - No electron losses, bremsstrahlung only  
 Case 3 - No bremsstrahlung losses, electrons only  
 Case 4 - No electron or bremsstrahlung losses.

Additional calculations were made to determine at what energy bremsstrahlung and electron losses may be safely neglected for typical solid and well crystals. Figure V-2 shows the results for a 3 x 3 in. solid crystal. Below about 3 Mev the energy loss due to escaping electrons and bremsstrahlung are seen to have a negligible effect. Also included are some data of Miller and Snow.<sup>(9)</sup> It may be seen that the data of Reference 9 are in good agreement at low energies with the present calculations. However a significant divergence is noted at higher energies indicating that the probable difference from the present work is due to the methods of treating these secondary particles. Figure V-3 shows the results of similar calculations for the 8F8 well crystal. It may be seen that only for energies less than about 0.9 Mev may the electron and bremsstrahlung losses be neglected. As anticipated, these losses become significant at a lower energy for the well crystal, since it has a greater surface area to volume ratio and electron and bremsstrahlung leakage is more probable than for the solid crystal. These results are useful for making calculations because by neglecting electron and bremsstrahlung losses, computer time can be significantly reduced.

### C. Effect of Geometry on Photofractions

#### 1. Isotropic Sources

The effect of various source geometries on the photofraction has been studied with both the solid and well crystal Monte Carlo programs. Reference 83 gives additional data on this effect for solid crystals only.

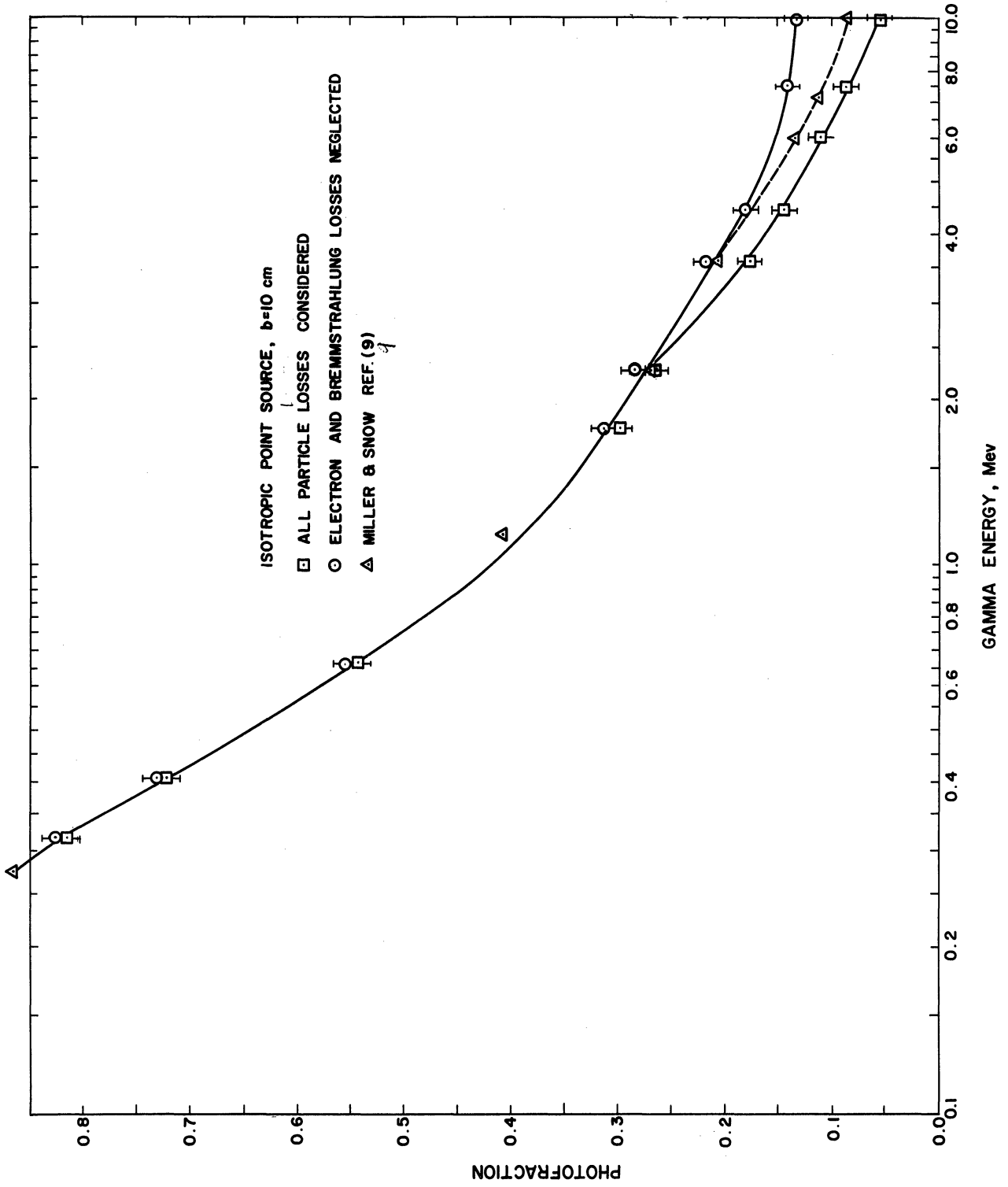


Figure V-2. Effect on Photofraction of Electron and Bremsstrahlung Escape from 3 x 3 In. Solid Crystal.

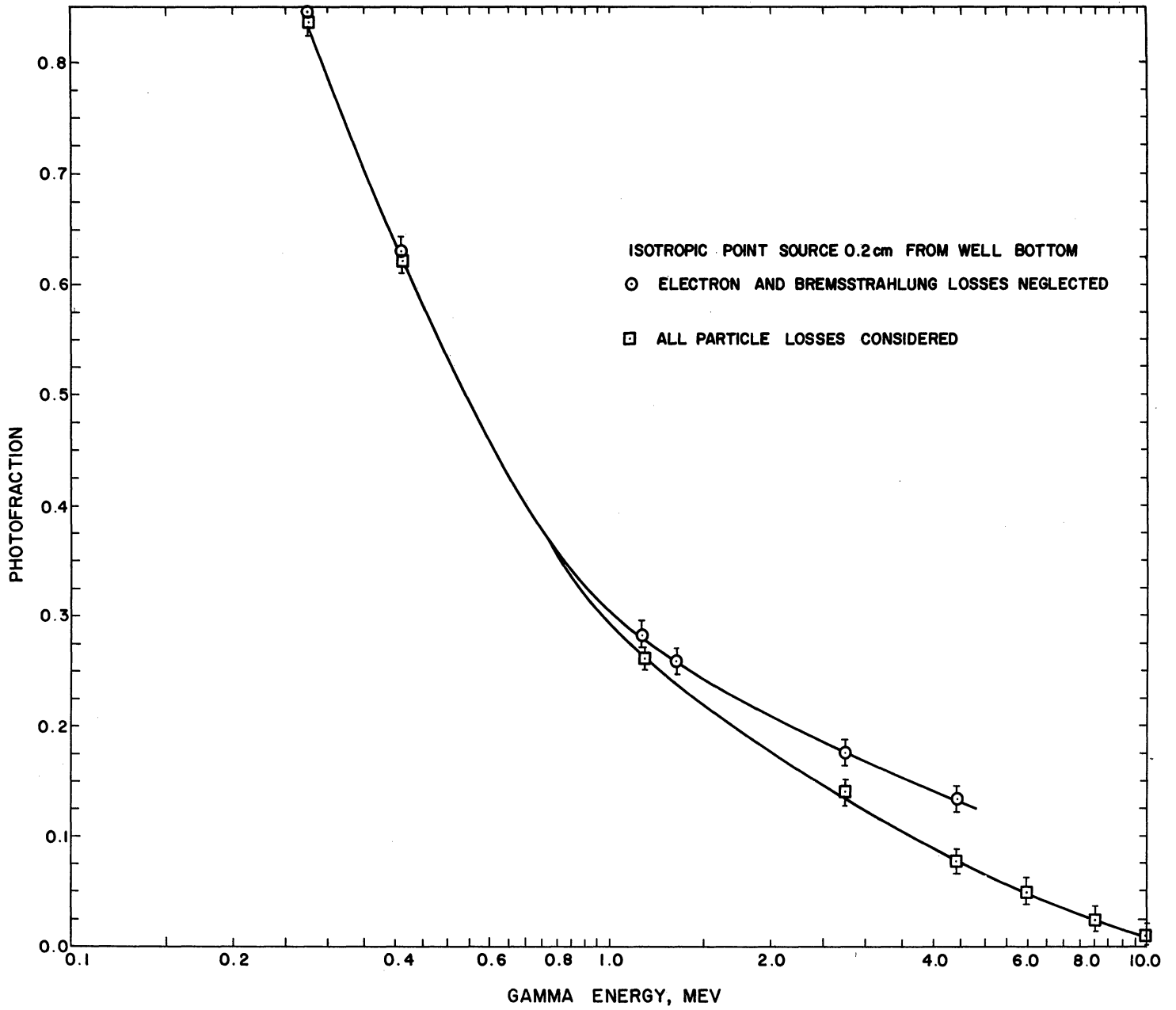


Figure V-3. Effect on Photofraction of Electron and Bremsstrahlung Escape from 8F8 Well Crystal.

From the data given in Tables V-7 and V-8 below, most isotropic source geometries can be well-approximated by a point source located on the crystal axis, eliminating the need for different Monte Carlo calculations when the source geometry is varied within reasonable limits. The geometrical effect on the photofraction consequently is small when point source results are used for a cylindrical volume source. The data given in Tables V-7 and V-8 are intended to illustrate that the relative photofractions for two typical crystals at two different energies are not significantly different from unity when the standard deviation are considered. For precise work, it would be preferable that photofractions be calculated for the exact experimental arrangement.

TABLE V-7

SOURCE GEOMETRY EFFECT - 3 x 3 IN. SOLID CRYSTAL

Isotropic Source	Relative Photofraction*	
	.412 Mev	4.45 Mev
Point, on-axis, b=10cm.	1.000	1.000
Point, on-axis, b=.2cm.	0.969 $\pm$ .012	1.000 $\pm$ .078
Point, off-axis, m=3.81cm., b=.2cm.	0.925 $\pm$ .012	0.850 $\pm$ .069
Point, off-axis, m=1.905cm., b=.2cm.	0.970 $\pm$ .012	1.014 $\pm$ .078
Disk, radius=3.81cm., b=.2cm.	0.939 $\pm$ .012	1.010 $\pm$ .078
Disk, radius=1.905cm., b=.2cm.	0.979 $\pm$ .012	1.040 $\pm$ .079
Cylinder, radius=3.81cm, b <sub>1</sub> =.2cm., b <sub>2</sub> =5.0cm.	0.985 $\pm$ .013	1.116 $\pm$ .084
Cylinder, radius=3.81cm, b <sub>1</sub> =.2cm., b <sub>2</sub> =10.0cm.	0.990 $\pm$ .013	1.055 $\pm$ .081

\* Values relative to on-axis point, b = 10 cm.

TABLE V-8

SOURCE GEOMETRY EFFECT - 8F8 WELL CRYSTAL

Isotropic Source	Relative Photofraction*	
	.412 Mev	4.45 Mev
Point, on-axis, b=.2cm.	1.000	1.000
Point, on-axis, b=1.2cm.	0.974 $\pm$ .015	1.000 $\pm$ .121
Point, off-axis, m=1.0cm., b=.2cm.	1.001 $\pm$ .016	1.142 $\pm$ .134
Point, off-axis, m=1.23cm., b=.2cm.	0.979 $\pm$ .016	1.182 $\pm$ .138
Disk, radius=.5cm., b=.2cm.	0.988 $\pm$ .016	1.200 $\pm$ .139
Cylinder, radius=1.0cm., b <sub>1</sub> =.2cm., b <sub>2</sub> =1.2cm.	0.974 $\pm$ .015	1.175 $\pm$ .137

\* Values relative to on-axis point, b = .2 cm.

## 2. Collimated Beam Source

An additional source geometry effect on the photofraction has been studied for the solid scintillation crystal. Varying degrees of collimation for monodirectional beams have been considered with the results given in Figure V-4. The photofraction for a narrow beam collimated along the crystal axis and incident on the crystal face is the largest possible value attainable for a given crystal size since leakage of scattered gammas through the crystal sides is minimized. As the beam diameter increases, this leakage increases and the photofraction correspondingly decreases. Thus the narrow beam source provides the most easily interpretable spectrum because the Compton continuum is minimized. From Figure V-4, for energies less than 6.13 Mev, less than 1% variation from narrow beam photofraction values are obtained for a beam diameter up to about one-half the crystal diameter. Also, the percent variations are not significantly different between the 2 x 2 in. and 3 x 3 in. solid crystals. References 68, 70 and 72 have also considered collimation effects. Berger and Doggett<sup>(72)</sup> have calculated this effect at 0.662 Mev and state that the relative change in photofraction with collimation could be applied at other energies with only slight error. However, as pointed out by Kreger and Brown<sup>(68)</sup> their experimental data indicate a strong energy dependence for beam diameter/crystal diameter  $\geq .25$ . Similar variation has been calculated in the present work and is given in Figure V-5. Since multiple scattering events are an increasingly important contribution to the total absorption peak as the energy increases (see Chapter III), one would expect that the effect of beam collimation on the photofractions would depend upon the source energy.



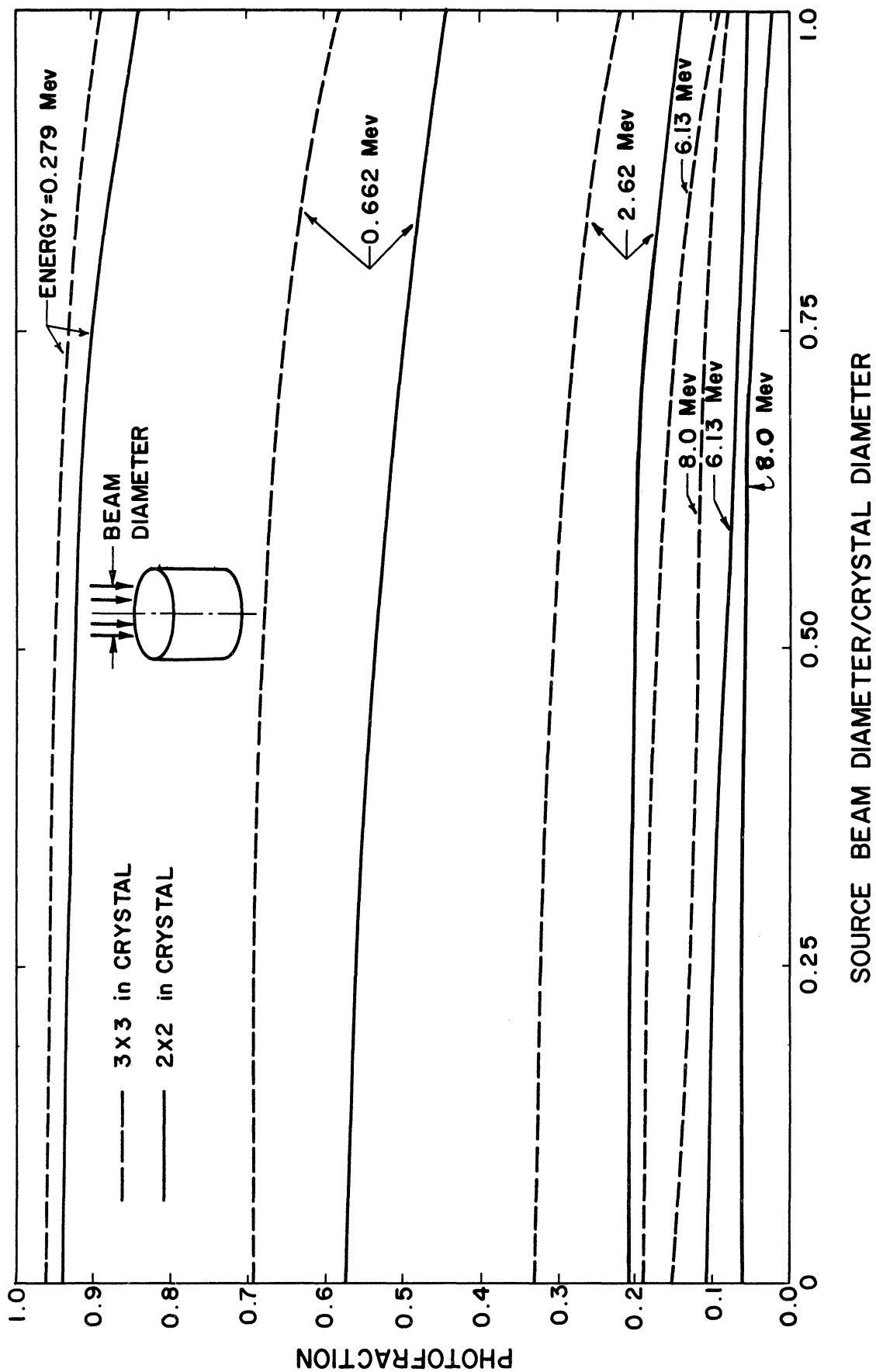


Figure V-4. Variation of Solid Crystal Photofraction with Collimation.

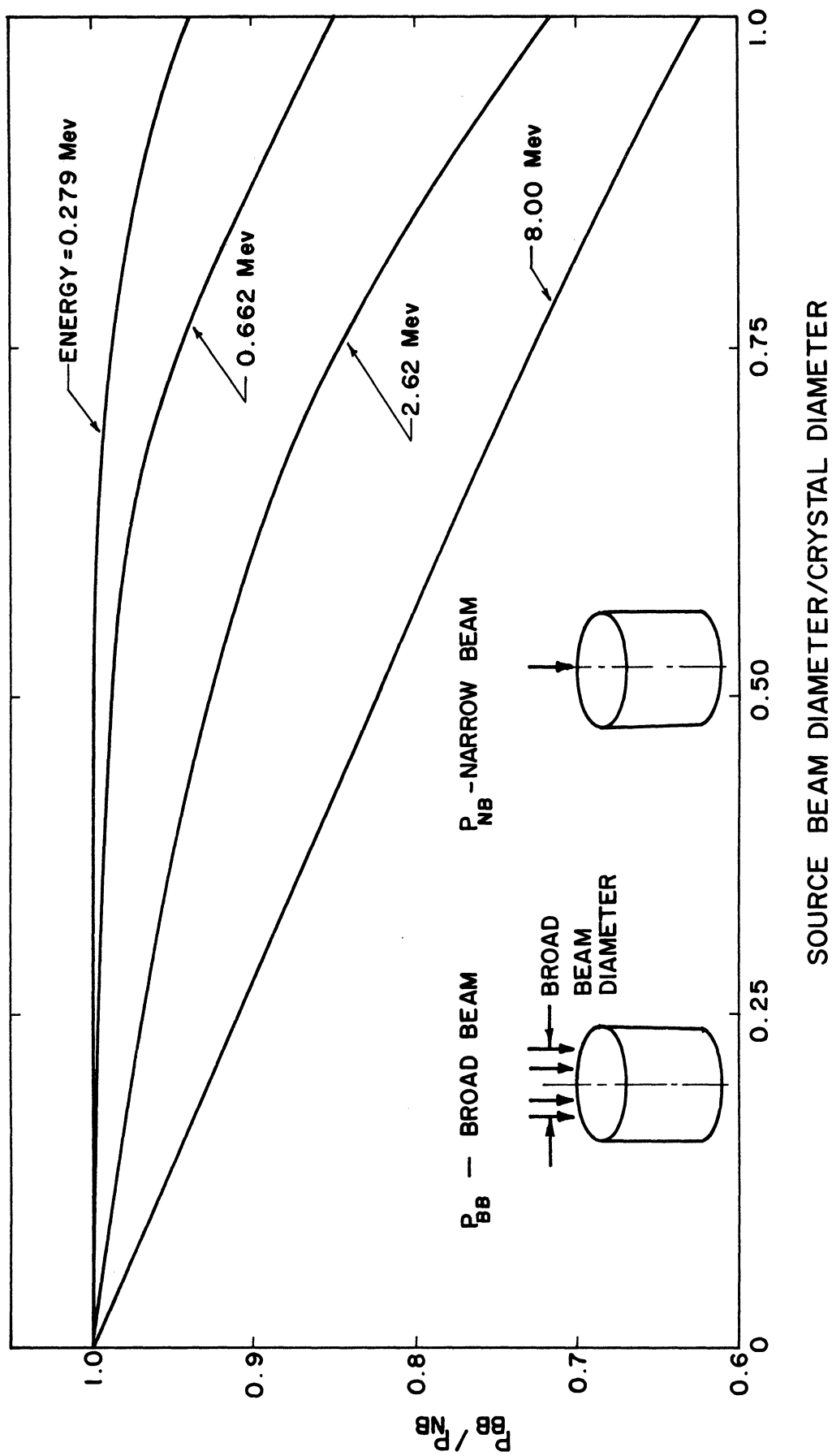


Figure V-5. Photofraction (Relative to Narrow Beam) Variation with Collimation for 3 x 3 In. Solid Crystal.

Jarczyk, <sup>(70)</sup> presents experimental results for broad beam and narrow beam measurements for energies up to 10.83 Mev, which are in agreement with those of the present work, within the experimental error given as  $\pm 8-12\%$ . Figure V-6, taken from Reference 70, includes the results of the present investigation.

### 3. Comparison of Solid and Well Crystal Photofractions

Reference 79, p. 57, indicates that the experimental intrinsic peak efficiency for a 3 x 3 in. well crystal (.5 in. well dia. x 1.5 in. well height) is nearly the same as that for a solid 3 x 3 in. crystal. Figure V-7 shows that the photofraction for well and solid crystals of the same outside dimension agree fairly well. A check has been made on the consistency of the separate Monte Carlo programs for well and solid crystals by calculating photofractions for progressively smaller well size. Convergence was obtained for the well crystal results, with sources at the top of the well, to the solid crystal photofraction for sources on the surface of the crystal.

### D. Comparison of Monte Carlo and Integration Results

As another check on the Monte Carlo calculations, a comparison was made with  $\epsilon_{IT}$  values obtained from direct calculation. The latter results for isotropic sources were obtained from  $\epsilon_{AT}$  values calculated by the numerical integration program, BURP-1, described in Chapter II. For monodirectional beam sources, normally incident upon a solid crystal face,  $\epsilon_{IT} = 1 - e^{-\tau H}$ . The comparison gave excellent agreement over a wide range of energies for both well and solid crystals, and confirms this portion of the Monte Carlo programs.

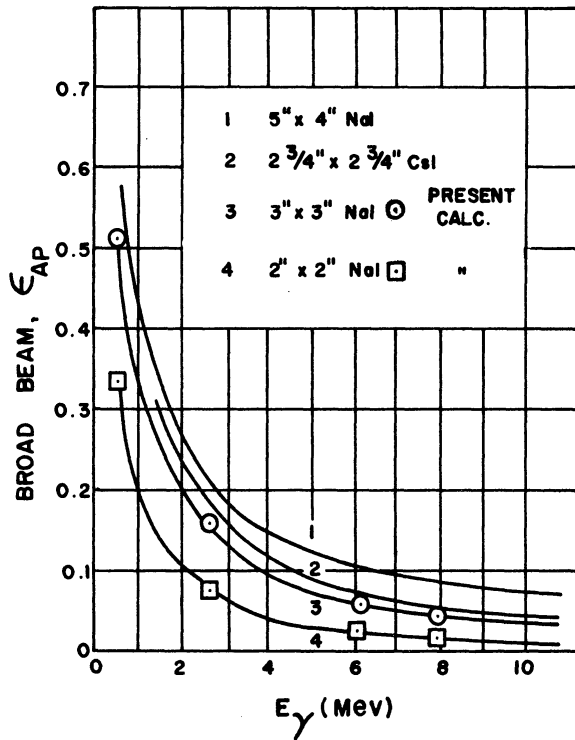
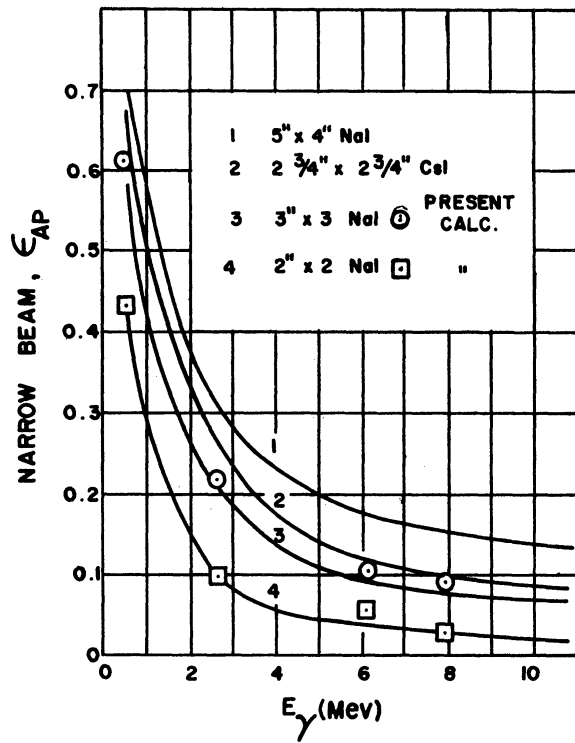


Figure V-6. Absolute Peak Efficiencies for Collimated Sources Compared with Experiments of Jarczyk. (70)

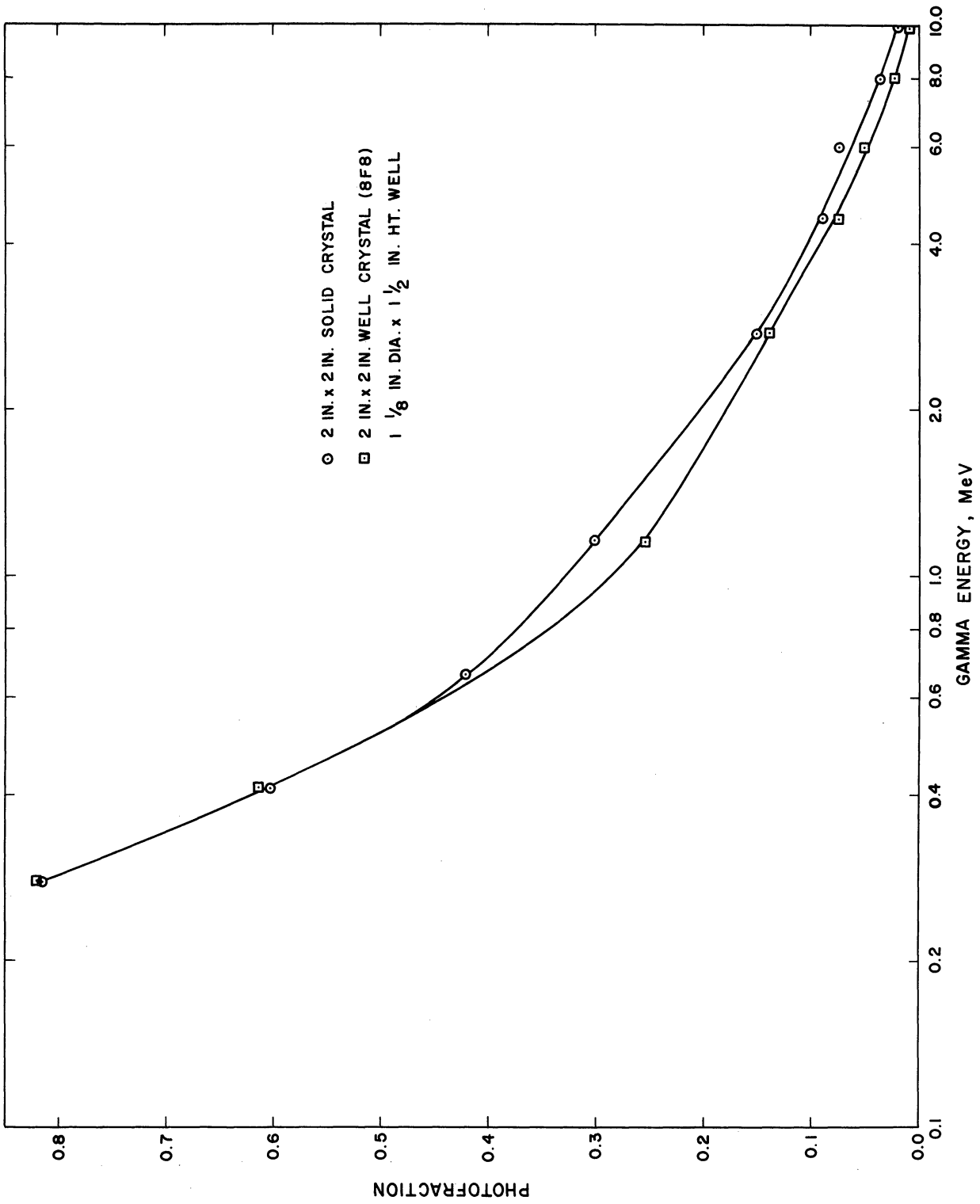


Figure V-7. Photofractions for Solid and Well-Type Crystals.

E. Photofractions Calculated for NaI

Values of photofractions for solid and well-type NaI crystals are given in Tables V-9 and V-10, respectively. These tabulated values have been calculated with the computer programs developed in this investigation. Calculations have been restricted to point isotropic sources, since photofractions have been shown to be only slightly dependent on isotropic source geometry.

The well crystal results are for the 7F8 and 8F8 crystals. The photofractions should be particularly useful since these two well crystals are the most commonly used, and no previous photofraction data have been available for well crystals.

TABLE V-9

SOLID CRYSTAL PHOTOFRACTIONS\*  
ISOTROPIC POINT SOURCE ON AXIS

Energy, Mev	2 x 2 in.**	3 x 3 in.***
0.279	.8315 ± .0084	
0.320		.8150 ± .0087
0.412	.6050 ± .0109	.7230 ± .0100
0.662	.4460 ± .0111	.5560 ± .0111
1.17	.3055 ± .0103	
1.78		.3245 ± .0105
2.14		.2685 ± .0099
2.75	.1565 ± .0081	
3.57		.1790 ± .0086
4.45	.0900 ± .0064	.1425 ± .0078
6.00	.0760 ± .0059	.1010 ± .0114
7.48		.0875 ± .0063
8.00	.0365 ± .0042	
10.00	.0180 ± .0030	.0530 ± .0050

\* For 2000 primary interactions

\*\* Source-crystal distance = 0.0 cm.

\*\*\* Source-crystal distance = 10.0 cm.

TABLE V-10

WELL CRYSTAL PHOTOFRACTIONS\*  
ISOTROPIC POINT SOURCE ON AXIS

Energy, Mev	7F8	8F8
0.279	.8590 ± .0078	.8365 ± .0083
0.412	.6460 ± .0107	.6225 ± .0108
0.662	.4305 ± .0111	.4520 ± .0111
1.17	.2775 ± .0100	.2650 ± .0099
2.75	.1420 ± .0078	.1210 ± .0073
4.45	.0785 ± .0060	.0815 ± .0061
6.00	.0445 ± .0046	.0515 ± .0049
8.00	.0235 ± .0034	.0215 ± .0032
10.00	.0185 ± .0030	.0125 ± .0025

\* For 2000 primary interactions,  
source 0.2cm. from crystal well bottom.

F. Photofraction for Materials other than NaI

Since scintillation materials other than NaI have been used for gamma ray detection, a limited investigation was made of the total absorption characteristics of CsI(Tl) and CaI<sub>2</sub>(Eu) relative to NaI(Tl), for a well crystal corresponding to the Harshaw 8F8 dimensions. Figure V-8 shows the NaI photofraction relative to the photofractions for CsI and CaI<sub>2</sub>. As previously mentioned, the Monte Carlo programs contain electron and bremsstrahlung data for NaI only and some error is introduced in the results for any other scintillation material at the higher energies. It can be seen that CsI has a significant advantage over NaI, in that the photofraction for the latter is only 40-65% of the former, over the energy range of most laboratory interest. This gives a better defined pulse height spectra

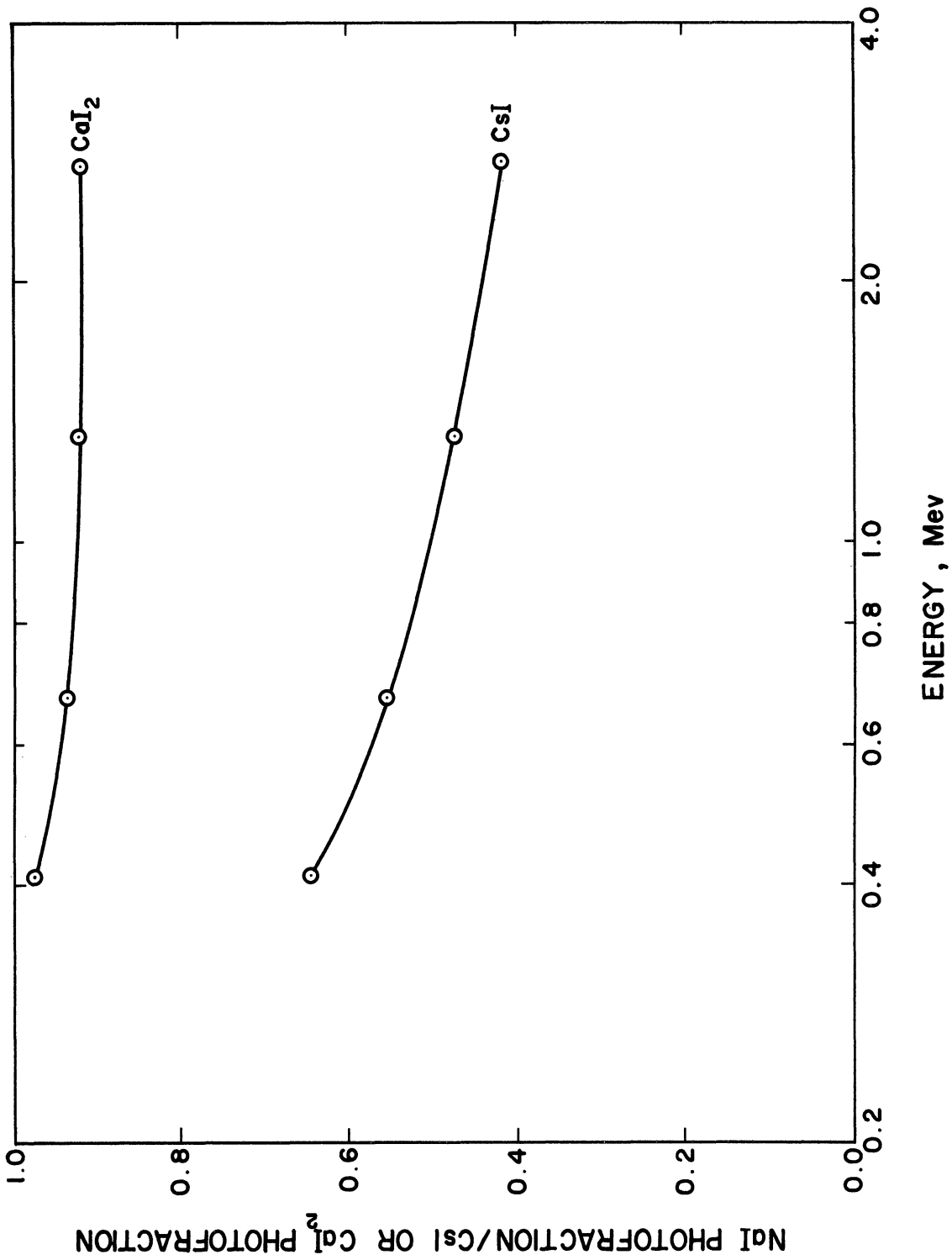


Figure V-8. Ratio of NaI Photofraction to CsI or CaI<sub>2</sub> Photofraction for 8F8 Well Crystal.



for CsI crystals. The comparison given here has been made on the basis of equal crystal dimensions and the greater density of CsI ( $4.510 \text{ gm/cm}^3$ ) over NaI ( $3.667 \text{ gm/cm}^3$ ) accounts for the major part of this advantage. Moran<sup>(73)</sup> has made a similar comparison between NaI and CsI, in which the two crystals were assumed to have linear dimensions inversely proportional to the crystal densities. On this basis the CsI volume is 0.665 that of the NaI, with the CsI weight 0.816 that of the NaI. On this basis Reference 73 found that CsI photo-fractions were slightly greater than those for NaI, while the intrinsic efficiencies were about the same, for the limited source energies and solid crystal sizes considered. A further advantage of CsI over NaI is that the former is non-hygroscopic, thus decreasing the manufacturing difficulties and allowing its use with no window between the source and crystal, for limited periods of time. CsI crystals are useful in applications where high shock-resistance is necessary since the material is not subject to cleavage. However, the material is relatively plastic and must be supported to prevent distortion during long periods of stress.<sup>(87)</sup> Special shapes can be bent from thin crystals for particular applications.<sup>(16)</sup> Resolution of CsI crystals is comparable to NaI,<sup>(73,87)</sup> but the light yield is considerably less.<sup>(16)</sup>

More recently Hofstadter<sup>(88)</sup> has developed a new scintillation material,  $\text{CaI}_2(\text{Eu})$ . Glos<sup>(89)</sup> has also reported information on this material. Measurements by Hofstadter have given promising results. Pulse heights 1.5-1.8 times those of NaI(Tl) were obtained, with resolution as good as the best NaI(Tl) values. To date only small-sized

crystals have been produced, 1-2cm<sup>2</sup> x .3 - .6 cm. thick. CaI<sub>2</sub> crystals have been found to cleave very easily when subjected to thermal or mechanical shock, and the material is highly deliquescent. Figure V-8 includes photofraction data calculated for comparison with NaI, and indicates less than a 10% advantage for CaI<sub>2</sub> over the energy range considered.

Appendix G contains some calculations of  $\epsilon_{AT}$  for CsI and CaI<sub>2</sub> crystals.

## CHAPTER VI

### CONCLUSIONS

#### A. Summary of Results

##### 1. Absolute Total Efficiencies ( $\epsilon_{AT}$ )

The analytical expressions for  $\epsilon_{AT}$  of solid and well crystals have been derived in the form of general point kernels. Integration of these kernels can be performed to reproduce any source geometry. Solutions have been obtained for point, disk, and cylindrical volume sources by numerical integration, and the accuracy of the results have been verified. Previously, solid crystal  $\epsilon_{AT}$  values had been available, <sup>(5,6)</sup> but except for the limited calculations of Verheijki, <sup>(14)</sup> no  $\epsilon_{AT}$  values for well crystals had been available. Using the computer programs developed in the present work, numerous quantitative studies have been carried out to investigate typical laboratory conditions for gamma ray detection by solid or well type scintillation detectors. Calculations have been made to determine the accuracy with which point sources can approximate disk or cylindrical volume sources. The errors introduced by applying on-axis point source  $\epsilon_{AT}$  values for points located off the crystal axis have been calculated. Also, the effect on  $\epsilon_{AT}$  values for variations in crystal dimensions and materials have been investigated.

The problem of calculating absolute peak efficiencies for scintillation detectors when absorption and scattering are present within a source has been considered. The treatment has been shown to be a

logical extension of  $\epsilon_{AT}$  calculations developed in the present investigation. Well crystal results are given in Chapter IV for homogeneous, monoenergetic sources in an aqueous solution.

The tabulated results for  $\epsilon_{AT}$  of different commercially available scintillation crystals for various source conditions given in Appendix G provide an extensive reference for experiments. The  $\epsilon_{AT}$  values are tabulated over a range of energies. If the  $\epsilon_{AT}$  values are plotted versus cross section (using the energy-cross section data of Table II-11), interpolation may be made for any future improvements in cross sections.

## 2. Photofractions

Monte Carlo methods have been used to simulate the transport of gamma rays, and the production of secondaries (electrons and bremsstrahlung) in solid and well type scintillation crystals. The general method of calculating photofractions by Monte Carlo techniques has been used previously for solid crystals. However, the present investigation has extended the calculations to cover well type crystals, for which no calculated photofraction values have previously been available in the literature. The present work also includes an improved simulation of electron transmission and bremsstrahlung generation through the crystal material. When compared with calculated data,<sup>(9,38)</sup> which were limited to solid crystals only, photofractions obtained in this investigation are in closer agreement with experiment.<sup>(83)</sup>

Isotropic and collimated sources used here cover the usual applications of gamma ray scintillation detectors. Numerous studies

were made using these Monte Carlo programs. Photofractions have been shown to be only mildly dependent on isotropic source position and thus the studies made of  $\epsilon_{AT}$  variations with source position are also valid for peak efficiencies,  $\epsilon_{AP}$ . Chapter V contains tabulation of calculated photofraction values for selected well and solid crystals which are commonly used in the laboratory.

#### B. Application of Results

Application of the results of this work for practical gamma ray scintillation detectors lie in two general areas. First, the absolute peak efficiencies obtained here may be used to calculate the absolute emission rate for gamma ray sources. Knowledge of the absolute source activity is required in many experimental studies, including absolute neutron flux measurements, activation analyses, etc. The second general area of application of the present work is in the choice of a gamma ray detection arrangement to serve a particular purpose. For example, one could obtain the minimum crystal size for a given efficiency or peak-to-total ratio in the detector pulse height spectrum.

#### C. Extension of Results

Since no tabulation of calculated results can ever cover all possible experimental arrangements that may arise in the laboratory, the values given here have been limited to typical situations. To permit extensions of these results, the computer programs are being made available through the Code Center of Argonne National Laboratory.

Quantitative information for specific experimental situations not included in these tabulations may be calculated by obtaining the programs from the Code Center. The ability to perform calculations for any scintillation materials make these computer programs useful as new materials are developed.

## APPENDIX A

### DERIVATION OF EXPRESSIONS FOR THE ABSOLUTE TOTAL EFFICIENCY

#### I. Isotropic Point Source Kernel

Using the notation previously defined in Chapter II, the general expression for the absolute total efficiency is

$$\epsilon_{AT} = \frac{1}{4\pi} \int_{\phi} d\phi \int_{\theta} \left[ 1 - e^{-\tau x(\phi, \theta)} \right] \sin\theta d\theta \quad (\text{A.1})$$

#### Solid Cylindrical Scintillation Crystal

Referring to the sketch below it is seen that integration over  $\theta$  must be performed in two steps, due to a discontinuity in the function  $x(\phi, \theta)$  when  $\theta = \theta_1$ . All gamma rays from the source enter the nearest face of the crystal, and as the polar angle,  $\theta$ , increases, the rays first leave the crystal through its lower face. For  $\theta > \theta_1$ , the rays leave the crystal through its cylindrical sides. Making the transformation  $\sin\theta d\theta = -d\mu$  ( $\mu = \cos\theta$ ), and referring to the sketch below, it is seen that:

$$\mu_1 = (H+b) / \left[ (H+b)^2 + S^2 \right]^{1/2}$$

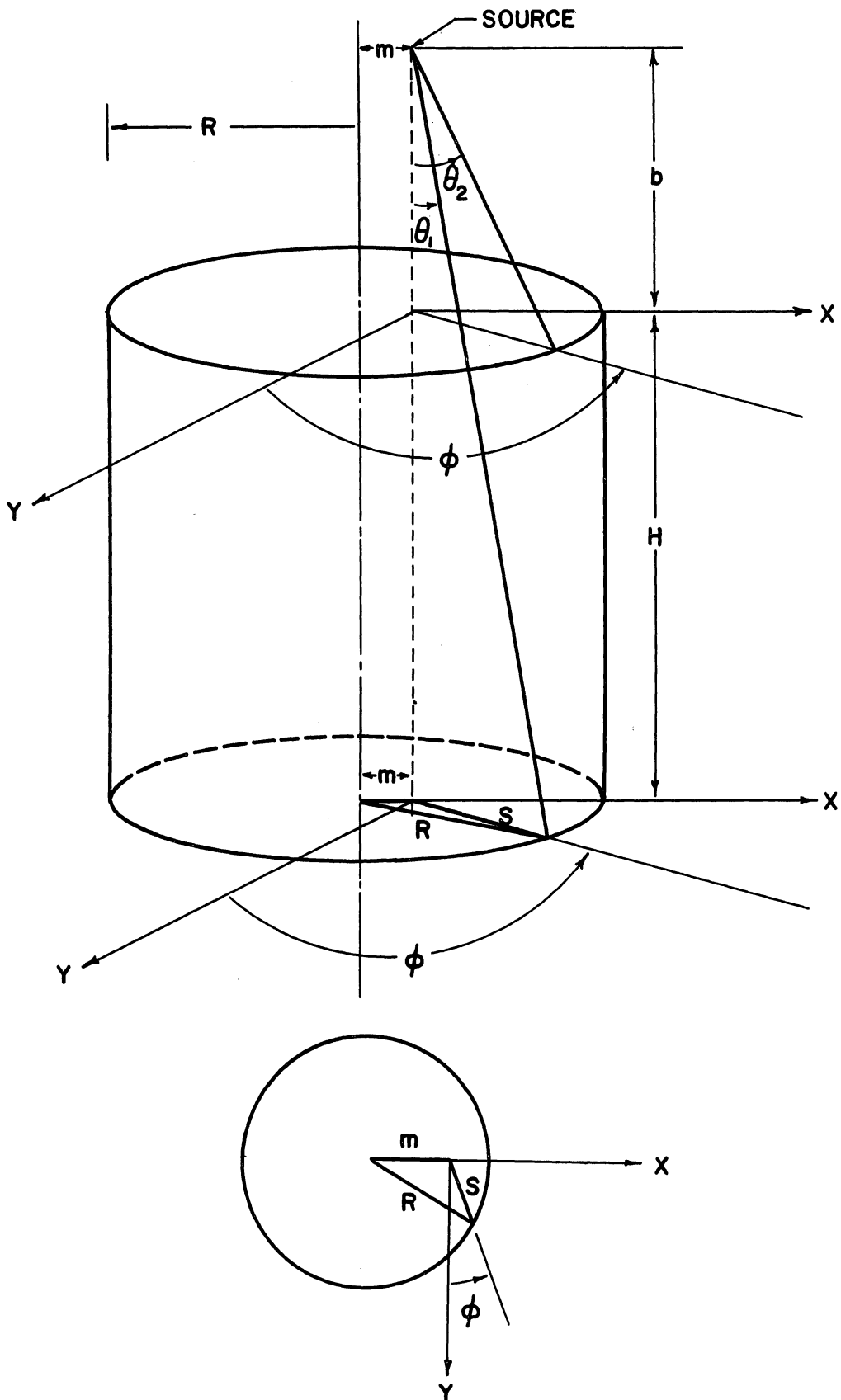
$$\mu_2 = b / (b^2 + S^2)^{1/2}$$

The distance  $s(m, \phi)$  may be determined from the sketch showing the lower crystal face.

$$s(m, \phi) = -m \sin\phi + \sqrt{R^2 - m^2 \cos^2\phi}$$

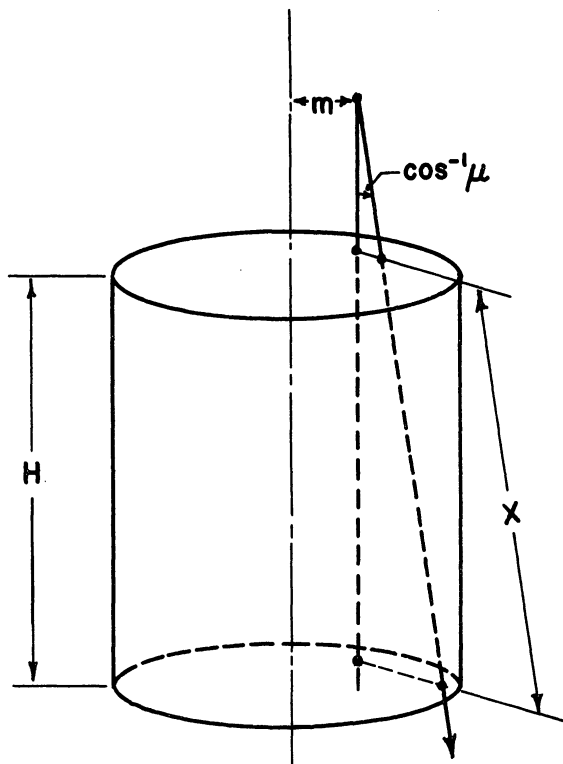
This expression is restricted to  $-\pi/2 \leq \phi \leq \pi/2$ , i.e., positive values of  $Y$ , in order to have a single functional form for  $s$ . Since the problem is symmetric about the X-axis, the integration is performed over

$-\pi/2 \leq \phi \leq \pi/2$  and a factor of 2 is introduced. The positive square root is required to insure  $s \geq 0$ .



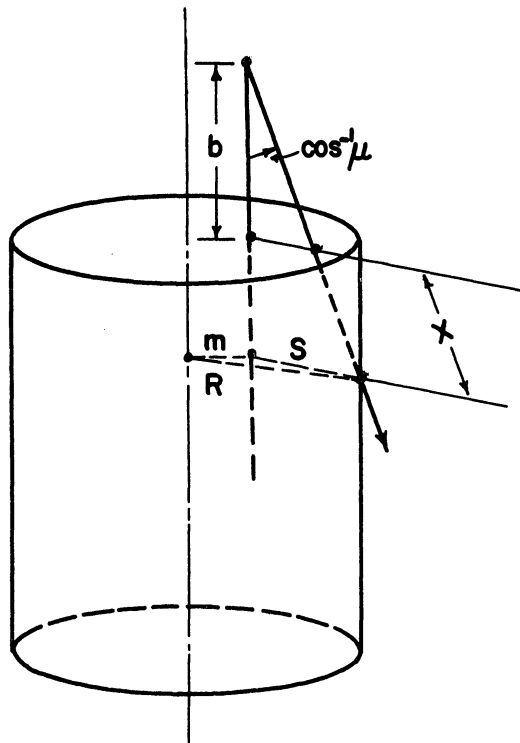


The path lengths  $x(\phi, \mu)$  may be determined from the following sketches:



$$1 \geq \mu \geq \mu_1$$

$$x = H/\mu$$



$$\mu_1 \geq \mu \geq \mu_2$$

$$x = \frac{s}{\sqrt{1-\mu^2}} - \frac{b}{\mu}$$

For an isotropic point source located off the solid crystal axis a radial distance  $m$ ,

$$\epsilon_{AT}(\text{off-axis pt.}) = \frac{1}{2\pi} \int_{-\pi/2}^{\pi/2} d\phi \left\{ \int_{\mu_1}^1 \left[ 1 - e^{-\tau H/\mu} \right] d\mu + \int_{\mu_2}^{\mu_1} \left[ 1 - e^{-\tau \left( \frac{s}{\sqrt{1-\mu^2}} - \frac{b}{\mu} \right)} \right] d\mu \right\}$$

which is Equation (2.4).

Well Type Scintillation Crystal

This crystal geometry is considerably more complicated because of the cylindrical well. The sketches below define the parameters to be used, and three discontinuities exist in the path length function  $x(\phi, \mu)$ . These discontinuities occur when the polar angle,  $\theta$ , equals  $\theta_1$ ,  $\theta_2$  and  $\theta_3$ , respectively. Again transforming to  $\mu$  we have:

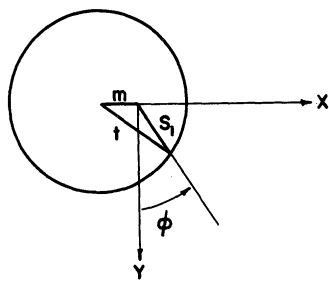
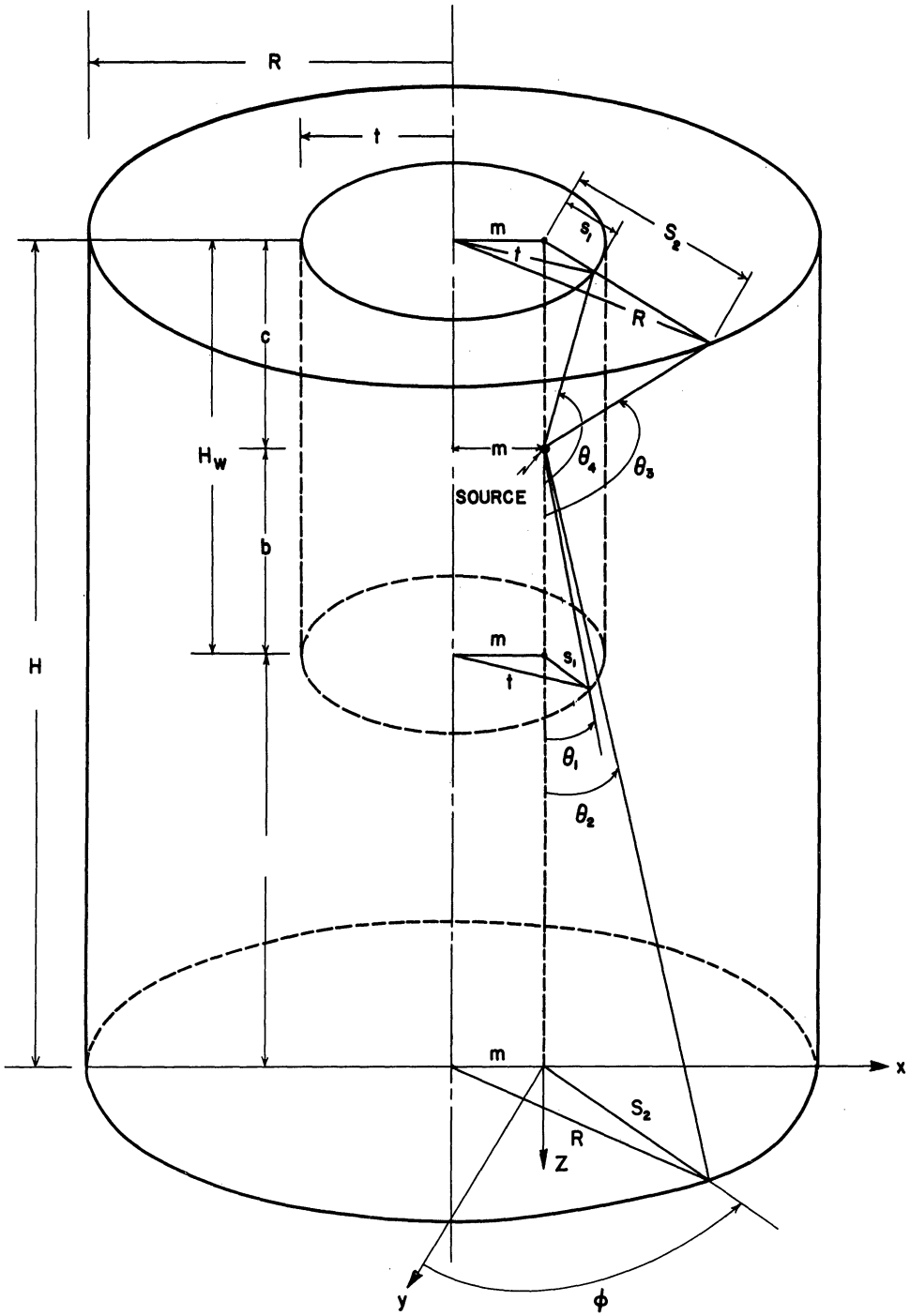
$$\begin{aligned}\mu_1^* &= b/(s_1^2 + b^2)^{1/2} \\ \mu_2^* &= (a+b)/[s_2^2 + (a+b)^2]^{1/2} \\ \mu_3 &= -c/(c^2 + s_2^2)^{1/2} \\ \mu_4 &= -c/(c^2 + s_1^2)^{1/2}\end{aligned}$$

Using the sketches showing the well bottom and the crystal lower face we have  $s_1$  and  $s_2$ , given as:

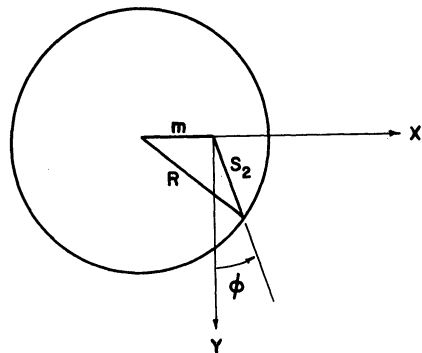
$$s_1(m, \phi) = -m \sin \phi + \sqrt{t^2 - m^2 \cos^2 \phi}$$

$$s_2(m, \phi) = -m \sin \phi + \sqrt{R^2 - m^2 \cos^2 \phi}$$

with the restriction  $-\pi/2 \leq \phi \leq \pi/2$ . Noting that  $\mu_1^*$  and  $\mu_2^*$  depend on the source-well bottom distance,  $b$ , two cases are possible, dependent upon whether  $\mu_1^* > \mu_2^*$  or  $\mu_1^* < \mu_2^*$ . Physically this means that as the integration proceeds over  $\mu$ , for  $\mu_1^* > \mu_2^*$ , rays from the source first strike the well bottom and emerge from the lower crystal face. Second, the rays strike the side of the well and emerge from the lower crystal face. Third, the rays strike the side of the well and emerge from the crystal side. However, when  $\mu_2^* > \mu_1^*$ , the rays for the second path



Well Bottom



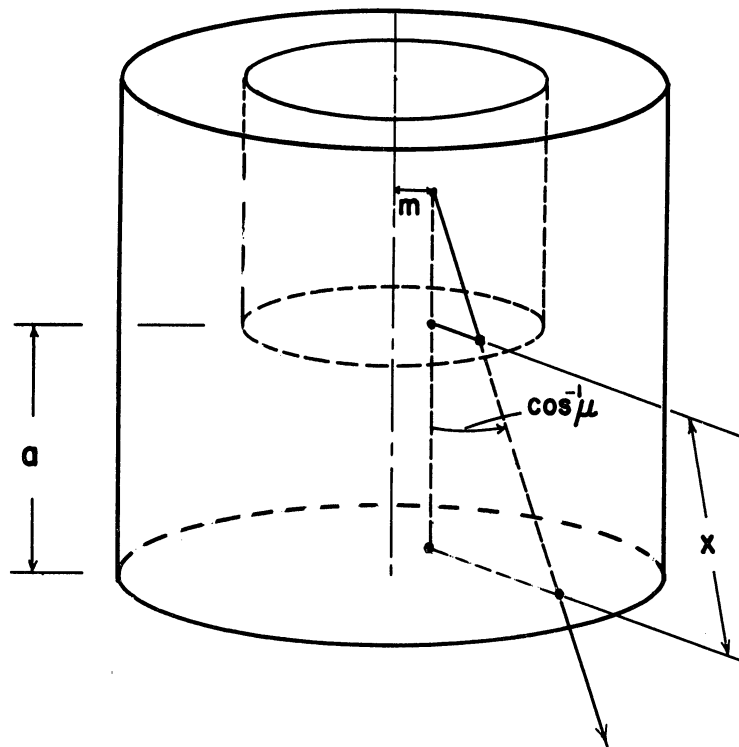
Lower Crystal Face

strike the bottom of the well, and then the side of the crystal. Writing the integrand in Equation (A.1) as a sum of four different functions,

$$\epsilon_{AT}(\text{off-axis pt.}) = \frac{1}{2\pi} \int_{-\frac{\pi}{2}}^{\frac{\pi}{2}} d\phi \left[ \int_{\mu_1}^{\mu_2} F_1(\phi, \mu) d\mu + \int_{\mu_2}^{\mu_3} F_2(\phi, \mu) d\mu + \int_{\mu_3}^{\mu_4} F_3(\phi, \mu) d\mu + \int_{\mu_4}^{\mu} F_4(\phi, \mu) d\mu \right] \quad (\text{A.2})$$

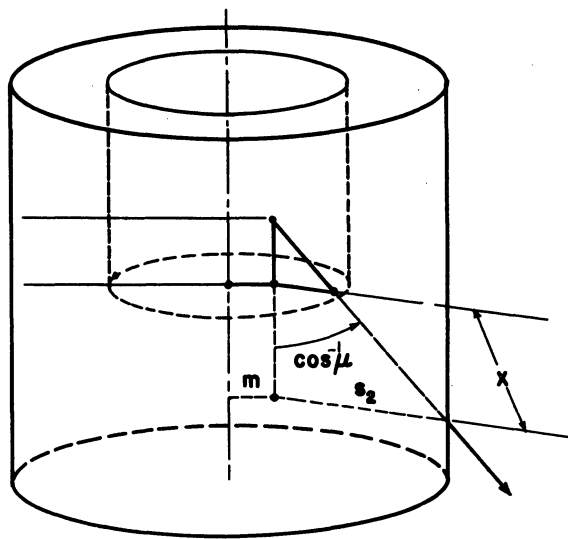
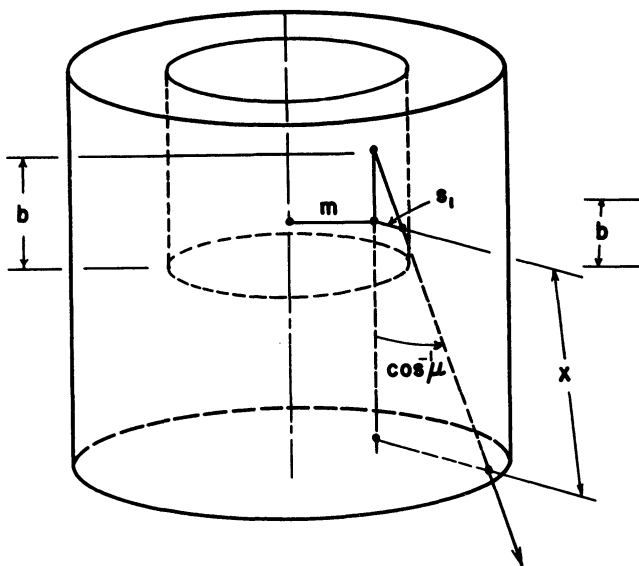
The form of  $F_2(\phi, \mu)$  depends on the inequalities  $\mu_1^* > \mu_2^*$  or  $\mu_1^* < \mu_2^*$ .

The derived path lengths,  $x(\phi, \mu)$  are shown in the following sketches.



$$1 \geq \mu \geq \mu_1$$

$$x = a/\mu$$

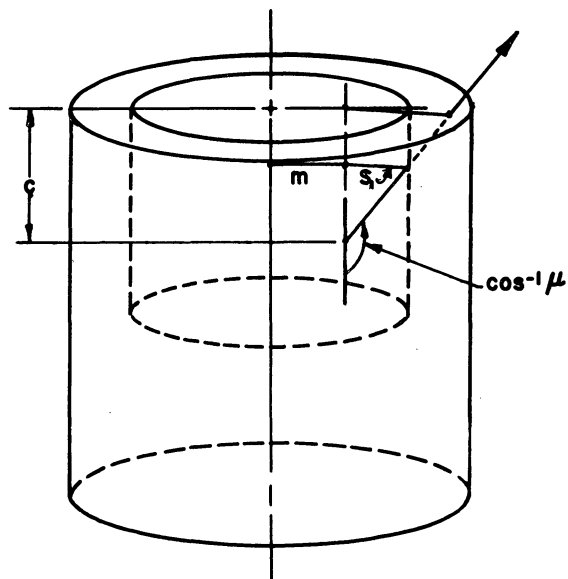
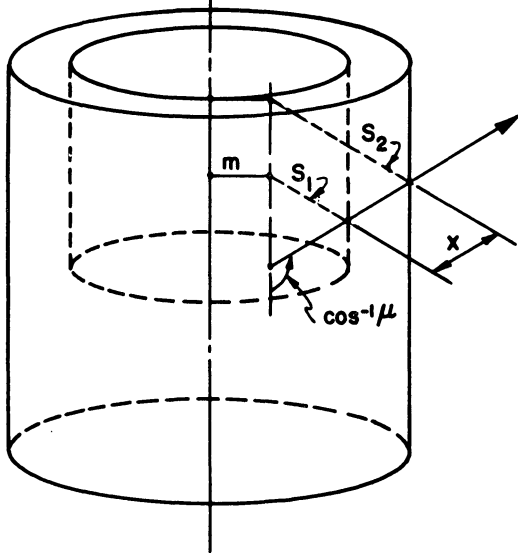


When  $\mu_1^* > \mu_2^*$   
 $\mu_1 \geq \mu \geq \mu_2$   

$$x = \frac{a+b}{\mu} - \frac{s_1}{\sqrt{1-\mu^2}}$$

or when  $\mu_1^* < \mu_2^*$   
 $\mu_1 \geq \mu \geq \mu_2$   

$$x = \frac{s_2}{\sqrt{1-\mu^2}} - \frac{b}{\mu}$$



$\mu_2 \geq \mu \geq \mu_3$   

$$x = \frac{s_2 - s_1}{\sqrt{1-\mu^2}}$$

$\mu_3 \geq \mu \geq \mu_4$   

$$x = -\frac{c}{\mu} - \frac{s_1}{\sqrt{1-\mu^2}}$$

Thus we have

$$F_1(\phi, \mu) = 1 - \exp(-\tau a / \mu)$$

and when  $\mu_1^* > \mu_2^*$  (i.e.  $\frac{s_1}{b} < \frac{s_2}{a+b}$ )

$$\mu_1 = \mu_1^* = b / (s_1^2 + b^2)^{1/2}$$

$$\mu_2 = \mu_2^* = (a+b) / [s_2^2 + (a+b)^2]^{1/2}$$

$$F_2(\phi, \mu) = 1 - \exp\left[-\tau \left(\frac{a+b}{\mu} - \frac{s_1}{\sqrt{1-\mu^2}}\right)\right]$$

or when  $\mu_1^* < \mu_2^*$  (i.e.  $\frac{s_1}{b} > \frac{s_2}{a+b}$ )

$$\mu_1 = \mu_2^* = (a+b) / [s_2^2 + (a+b)^2]^{1/2}$$

$$\mu_2 = \mu_1^* = b / (b^2 + s_1^2)^{1/2}$$

$$F_2(\phi, \mu) = 1 - \exp\left[-\tau \left(\frac{s_2}{\sqrt{1-\mu^2}} - \frac{b}{\mu}\right)\right]$$

and for both cases

$$F_3(\phi, \mu) = 1 - \exp\left[-\tau \left(\frac{s_2 - s_1}{\sqrt{1-\mu^2}}\right)\right]$$

$$F_4(\phi, \mu) = 1 - \exp\left[-\tau \left(-\frac{c}{\mu} - \frac{s_1}{\sqrt{1-\mu^2}}\right)\right]$$

This gives Equation (2.5).

## II. Isotropic Point Source On-axis

The expressions for on-axis points are readily obtained by letting  $m = 0$  in the previously derived results and performing the integration over  $\phi$ . In the above expressions for a solid crystal  $s = R$ ; and for a well crystal  $s_1 = t$ ,  $s_2 = R$ . It should be noted that the above derivation for the well crystal was for point sources within the crystal well. In order to check the results given in Reference 14, the solution for an on-axis isotropic point source was obtained for the point outside the well. Using arguments similar to those above, the results for the functions  $F(\mu)$ , and  $\mu$  to be substituted into Equation (A.2) are best summarized by the following table. (Note that  $F_i = 1 - e^{-\tau x_i}$ , for  $i = 1, 2, 3, 4$ ) This table includes all the limits of integration,  $\mu_i$ , and path lengths  $x_i$ , for on-axis points both inside (CASE 1) and outside the well (CASE 2), as well as the solid crystal (CASE 3).

## III. Two and Three-Dimensional Sources

Making the assumption that these sources are homogeneous and isotropic, the point kernel expressions can be integrated to cover any two or three-dimensional source. In particular, the disk and cylindrical volume sources were considered in this investigation. For a disk source consider first a ring coaxial with the crystal axis, with a width  $dm$ . The absolute total efficiency for this differential area is:

$$\frac{2\pi m dm [\epsilon_{AT} (\text{off-axis pt.})]}{2\pi m dm}$$

Case*	Conditions	$\mu_1$	$\mu_2$	$\mu_3$	$\mu_4$	$x_1$	$x_2$	$x_3$	$x_4$
1	$b < h - a$								
1a	$\frac{a+b}{((a+b)^2 + R^2)^{1/2}} = \frac{b}{(b^2 + t^2)^{1/2}}$	$\frac{a+b}{((a+b)^2 + R^2)^{1/2}}$	$\frac{a+b}{((a+b)^2 + R^2)^{1/2}}$	$\frac{-c}{(c^2 + t^2)^{1/2}}$	$\frac{-c}{(c^2 + t^2)^{1/2}}$	$\frac{a}{\mu}$	†	$\frac{R-t}{(1-\mu^2)^{1/2}}$	$\frac{-c}{\mu} - \frac{t}{(1-\mu^2)^{1/2}}$
1b	$\frac{a+b}{((a+b)^2 + R^2)^{1/2}} > \frac{b}{(b^2 + t^2)^{1/2}}$	"	$\frac{b}{(b^2 + t^2)^{1/2}}$	"	"	"	$\frac{R}{(1-\mu^2)^{1/2}} - \frac{b}{\mu}$	"	"
1c	$\frac{a+b}{((a+b)^2 + R^2)^{1/2}} < \frac{b}{(b^2 + t^2)^{1/2}}$	$\frac{b}{(b^2 + t^2)^{1/2}}$	$\frac{a+b}{((a+b)^2 + R^2)^{1/2}}$	"	"	"	$\frac{a+b}{\mu} - \frac{t}{(1-\mu^2)^{1/2}}$	"	"
2	$b > h - a$								
2a	$\frac{c}{t} = \frac{a+b}{R}$	"	$\frac{b}{(b^2 + t^2)^{1/2}}$	$\frac{a+b}{((a+b)^2 + R^2)^{1/2}}$	$\frac{c}{(c^2 + R^2)^{1/2}}$	"	†	$\frac{a+b}{\mu} - \frac{t}{(1-\mu^2)^{1/2}}$	$\frac{R}{\mu} - \frac{c}{(1-\mu^2)^{1/2}}$
2b	$\frac{a+b}{((a+b)^2 + R^2)^{1/2}} > \frac{c}{(c^2 + t^2)^{1/2}}$ and $\frac{b}{(b^2 + t^2)^{1/2}} > \frac{a+b}{((a+b)^2 + R^2)^{1/2}}$	"	$\frac{a+b}{((a+b)^2 + R^2)^{1/2}}$	$\frac{c}{(c^2 + t^2)^{1/2}}$	$\frac{c}{(c^2 + R^2)^{1/2}}$	"	$\frac{a+b}{\mu} - \frac{t}{(1-\mu^2)^{1/2}}$	$\frac{R-t}{(1-\mu^2)^{1/2}}$	"
2c	$\frac{b}{t} = \frac{a+b}{R}$	"	$\frac{b}{(b^2 + t^2)^{1/2}}$	"	"	"	†	"	"
2d	$\frac{b}{(b^2 + t^2)^{1/2}} < \frac{a+b}{((a+b)^2 + R^2)^{1/2}}$	$\frac{a+b}{((a+b)^2 + R^2)^{1/2}}$	"	"	"	"	$\frac{R}{(1-\mu^2)^{1/2}} - \frac{b}{\mu}$	"	"
2e	$\frac{c}{(c^2 + t^2)^{1/2}} > \frac{a+b}{((a+b)^2 + R^2)^{1/2}}$	$\frac{b}{(b^2 + t^2)^{1/2}}$	$\frac{c}{(c^2 + t^2)^{1/2}}$	$\frac{a+b}{((a+b)^2 + R^2)^{1/2}}$	"	"	$\frac{a+b}{\mu} - \frac{t}{(1-\mu^2)^{1/2}}$	$\frac{h}{\mu}$	"
3	Solid crystal	$\frac{a+b}{((a+b)^2 + R^2)^{1/2}}$	$\frac{b}{(b^2 + R^2)^{1/2}}$	-	-	"	$\frac{R}{(1-\mu^2)^{1/2}} - \frac{b}{\mu}$	-	-

\* All cases of same number must satisfy conditions  $b \leq h - a$ , as well as specific condition for cases a, b, etc. † Integral is zero.



and for a disk of radius  $g$

$$\epsilon_{AT}(\text{disk}) = \frac{2\pi \int_0^g m \epsilon_{AT}(\text{off-axis pt.}) dm}{2\pi \int_0^g m dm}$$

simplifying:

$$\epsilon_{AT}(\text{disk}) = \frac{2}{g^2} \int_0^g m \epsilon_{AT}(\text{off-axis pt.}) dm \quad (\text{A.3})$$

For a cylindrical volume source, consider a differential volume of radius  $g$ , and height  $db$  located coaxially with the crystal axis. The absolute total efficiency for this volume, assuming the source is transparent to the source gammas is:

$$\frac{\pi g^2 db \epsilon_{AT}(\text{disk})}{\pi g^2 db}$$

and performing the integration for a right circular cylinder extending between the axial dimensions  $b_1$  and  $b_2$  ( $b_1, b_2$  being measured from the same plane as  $b$  we have:

$$\epsilon_{AT}(\text{vol.}) = \frac{\pi g^2 \int_{b_1}^{b_2} \epsilon_{AT}(\text{disk}) db}{\pi g^2 \int_{b_1}^{b_2} db} ,$$

which gives

$$\epsilon_{AT}(\text{vol.}) = \frac{l}{(b_2 - b_1)} \int_{b_1}^{b_2} \epsilon_{AT}(\text{disk}) db$$

or

$$\epsilon_{AT}(\text{vol.}) = \frac{2}{g^2(b_2 - b_1)} \int_{b_1}^{b_2} db \int_0^g m \epsilon_{AT}(\text{off-axis pt.}) dm \quad (\text{A.4})$$

Equations (A.3) and (A.4) are the same as Equations (2.8) and (2.9), respectively.

APPENDIX B

SERIES SOLUTION FOR THE TOTAL EFFICIENCY

The following derivation, obtained by N. McCormick, is given for an on-axis isotropic point source located on the face of a solid crystal. Noting that  $\Omega/4\pi = 1/2$  for a solid crystal, with the source located at  $b = 0$ , the derivation will be given for the intrinsic total efficiency. By previous definition of parameters.

$$\epsilon_{IT} = \frac{\epsilon_{AT}}{\Omega/4\pi} ,$$

and for this case,

$$\epsilon_{IT} = 2\epsilon_{AT} = 1 - \int_{\frac{H}{(H^2+R^2)^{1/2}}}^1 e^{-\tau H/\mu} d\mu - \int_0^{\frac{H}{(H^2+R^2)^{1/2}}} e^{-\tau R/\sqrt{1-\mu^2}} d\mu$$

We introduce  $I_1, I_2$  for the first and second integrals, respectively.

Using the definition of the exponential integrals:

$$E_n(y) = y^{n-1} \int_y^\infty e^{-z} z^{-n} dz$$

we find

$$I_1 = \tau H \int_{\tau H}^\infty e^{-z} z^{-2} dz - \frac{H}{(H^2+R^2)^{1/2}} \tau (H^2+R^2)^{1/2} \int_{\tau(H^2+R^2)^{1/2}}^\infty e^{-z} z^{-2} dz$$

or

$$I_1 = E_2(\tau H) - \frac{H}{(H^2+R^2)^{1/2}} E_2(\tau \sqrt{H^2+R^2})$$

To obtain  $I_2$ ,

let  $f^2 = 1 - \mu^2$ , and rewrite  $I_2$

$$I_2 = \int_{\frac{R}{(H^2+R^2)^{1/2}}}^1 e^{-\tau R/f} \frac{f}{\sqrt{1-f^2}} df$$

since  $0 \leq \mu \leq 1$ , then  $0 \leq f \leq 1$ , and  $\frac{1}{\sqrt{1-f^2}}$  can be expanded in a binomial series:

$$\frac{1}{\sqrt{1-f^2}} = 1 + \frac{1}{2} f^2 + \frac{(\frac{1}{2})(\frac{3}{2})}{2!} f^4 + \frac{(\frac{1}{2})(\frac{3}{2})(\frac{5}{2})}{3!} f^6 + \dots$$

$$I_2 = \int_{\frac{R}{(H^2+R^2)^{1/2}}}^1 df e^{-\tau R/f} \left[ f + \frac{f^3}{2} + \frac{(\frac{1}{2})(\frac{3}{2})}{2!} f^5 + \frac{(\frac{1}{2})(\frac{3}{2})(\frac{5}{2})}{3!} f^7 + \dots \right]$$

let  $p = \frac{\tau R}{f}$

thus

$$I_2 = \int_{\tau R}^{\tau(H^2+R^2)^{1/2}} e^{-p} \left[ \frac{\tau R}{p} + \frac{1}{2} \left( \frac{\tau R}{p} \right)^3 + \frac{(\frac{1}{2})(\frac{3}{2})(\frac{\tau R}{p})^5}{2!} + \frac{(\frac{1}{2})(\frac{3}{2})(\frac{5}{2})(\frac{\tau R}{p})^7}{3!} + \dots \right] \frac{\tau R}{p^2} dp$$

This can be written as a summation:

$$I_2 = \sum_{m=0}^{\infty} \frac{(2m-1)!!}{2^m m!} (\tau R)^{2m+2} \int_{\tau R}^{\tau(H^2+R^2)^{1/2}} \frac{e^{-p}}{p^{2m+3}} dp$$

where

$$(2m-1)!! = (2m-1)(2m-3)(2m-5) \dots (3)(1)$$

$$(-1)!! = 1, \quad 0! = 1$$

This summation can be rearranged

$$I_2 = \sum_{m=0}^{\infty} \frac{(2m-1)!!}{2^m m!} \left[ (\tau R)^{2m+2} \int_{\tau R}^{\infty} \frac{e^{-p}}{p^{2m+3}} dp - \frac{R^{2m+2}}{(H^2+R^2)^{m+1}} \tau^{2m+2} (H^2+R^2)^{m+1} \int_{\tau(H^2+R^2)^{1/2}}^{\infty} \frac{e^{-p}}{p^{2m+3}} dp \right]$$

Again using the exponential integrals

$$I_2 = \sum_{m=0}^{\infty} \frac{(2m-1)!!}{2^m m!} \left[ E_{2m+3}(\tau R) - \frac{R^{2m+2}}{(H^2+R^2)^{m+1}} E_{2m+3}(\tau \sqrt{H^2+R^2}) \right]$$

Combining we finally obtain the desired solution.

$$\epsilon_{1T} = / - E_2(\tau H) + \frac{H}{(H^2+R^2)^{1/2}} E_2(\tau \sqrt{H^2+R^2}) -$$

$$\sum_{m=0}^{\infty} \frac{(2m-1)!!}{2^m m!} \left[ E_{2m+3}(\tau R) - \frac{R^{2m+2}}{(H^2+R^2)^{m+1}} E_{2m+3}(\tau \sqrt{H^2+R^2}) \right].$$

The above equation has been used to check the results of some calculations made with the BURP-1 Computer Program. Excellent agreement was found between results of the above equation and the computer program values.

## APPENDIX C

### DERIVATION OF KAHN'S METHOD FOR SAMPLING FROM THE KLEIN-NISHINA FORMULA

H. Kahn<sup>(24)</sup> has given a number of selection techniques for sampling from the Klein-Nishina formula, differential in polar angle, for Compton scattering events. The method used in these calculations has been shown by Kahn to be most efficient for photons below about 4 MeV, and even though source particles of greater energy are considered, most will be either degraded in energy below 4 MeV in the first or second scatterings, or will undergo a pair production event. Thus the technique used is the most efficient in the energy range where multiple Compton scatterings are the principal interaction mechanism.

The differential Klein-Nishina formula<sup>(31)</sup> for Compton collisions of incident unpolarized radiation is:

$$\frac{d\sigma}{d\Omega} = \frac{r_0^2}{2} \frac{(1 + \cos^2\theta)}{[1 + \alpha(1 - \cos\theta)]^2} \left[ 1 + \frac{\alpha^2(1 - \cos\theta)^2}{(1 + \cos^2\theta)[1 + \alpha(1 - \cos\theta)]} \right] \quad (C.1)$$

where  $\alpha$  = incident gamma energy,  $m_0c^2$  units

$$r_0 = \frac{e^2}{m_0c^2} \quad \text{classical electron radius}$$

The Compton energy-angle relationship is:

$$\alpha' = \alpha / [1 + \alpha(1 - \cos\theta)] \quad (C.2)$$

or 
$$\chi = 1 + \alpha(1 - \cos\theta)$$

where  $\alpha'$  = scattered gamma energy,  $m_0c^2$  units

$$x = \alpha/\alpha' .$$

Integration of Equation (C.1) over the azimuthal angle, and rearrangement using Equation (C.2) gives:

$$d\sigma(x, \theta, \alpha) = \frac{\pi r_0^2}{\alpha} \frac{dx}{x^2} \left( x + \frac{1}{x} + \cos^2 \theta - 1 \right) \quad (C.3)$$

Noting that in a rejection method, the normalization constant of the probability distribution need not be specified, one can define the P.D.F. for  $x$  as:

$$f(x, \theta, \alpha) = (\cos^2 \theta - 1 + x + \frac{1}{x}) \frac{1}{\alpha x^2} \quad (C.4)$$

The P.D.F. of Equation (C.4) is split into the sum of two other P.D.F.

$$f(x) = \frac{2\alpha+1}{2\alpha+9} \frac{1}{2\alpha} 4 \left( \frac{1}{x} - \frac{1}{x^2} \right) + \frac{8}{2\alpha+9} \frac{2\alpha+1}{2\alpha x^2} \frac{1}{2} \left( \cos^2 \theta + \frac{1}{x} \right) \quad (C.5)$$

let

$$g_1(x) = \frac{1}{2\alpha} \quad , \quad g_2(x) = \frac{2\alpha+1}{2\alpha x^2}$$

$$h_1(x) = 4 \left( \frac{1}{x} - \frac{1}{x^2} \right) \quad , \quad h_2(x) = \frac{1}{2} \left( \cos^2 \theta + \frac{1}{x} \right)$$

The procedure is to sample from  $f_1(x) = g_1(x)h_1(x)$  and  $f_2(x) = g_2(x)h_2(x)$  with relative frequencies  $\frac{2\alpha+1}{2\alpha+9}$  and  $\frac{8}{2\alpha+9}$ , respectively. Sampling is accomplished by applying the cumulative distribution function method to  $g_1(x)$  and  $g_2(x)$  and then applying the rejection method to  $h_1(x)$  and  $h_2(x)$ . The functions  $g_1(x)$  and  $g_2(x)$  are properly normalized for  $1 \leq x \leq 1 + 2\alpha$  and one obtains:

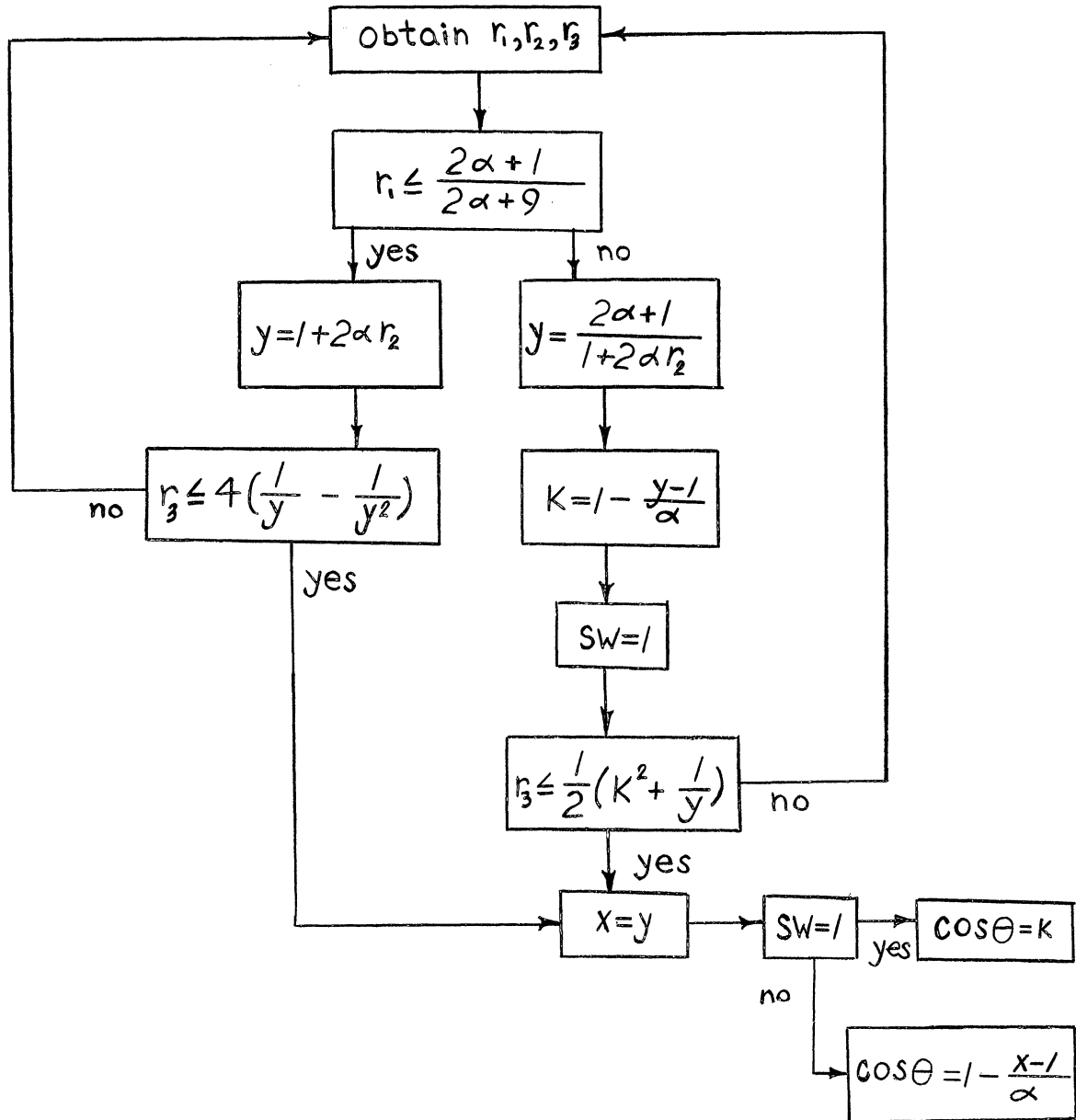
$$\text{for } g_1(x): \quad x = 2\alpha r_1 + 1$$

$$\text{for } g_2(x): \quad x = \frac{2\alpha + 1}{2\alpha r_2 + 1}$$

where  $r_1, r_2$  are random numbers.



The method is given in the following flow diagram:



APPENDIX D

WELL CRYSTAL ESCAPE ROUTINE

In the Monte Carlo calculation of photofractions for scintillation crystals with a coaxial cylindrical well, consideration must be given to those gamma rays which intersect the surface of the well. If a secondary gamma ray has (for any step in the calculation) its location in the crystal at the coordinates  $x, y, z$ , and then travels a radial distance,  $t$ , in the direction defined by the direction cosines  $u, v, w$ , its final coordinates are given by:

$$\begin{aligned}x' &= x + ut \\y' &= y + vt \\z' &= z + wt\end{aligned}\tag{D.1}$$

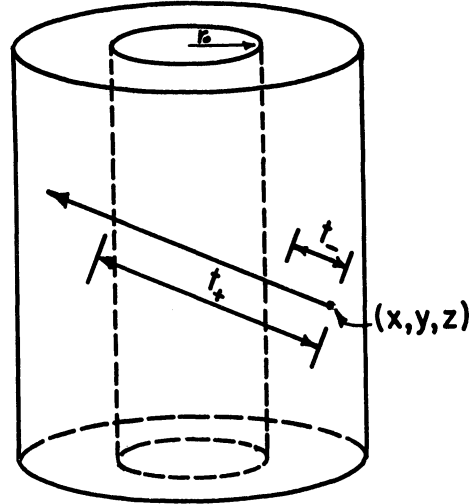
If the gamma ray path cuts the surface of an inner, coaxial cylinder of infinite height and radius  $r_0$ , then the radial distance to this surface is obtained by simultaneous solution of Equations (D.1) and

$$x'^2 + y'^2 = r_0^2\tag{D.2}$$

The radial distances to this inner cylindrical surface are given by:

$$t_{\pm} = \frac{-(ux+vy) \pm \sqrt{(ux+vy)^2 - (1-w^2)(x^2+y^2-r_0^2)}}{(1-w^2)}\tag{D.3}$$

The following sketch illustrates these distances.



Let:

$$\delta = ux + vy$$

$$\Delta = \delta^2 - (1-w^2)(x^2 + y^2 - r_0^2)$$

thus

$$t_{\pm} = \frac{-\delta \pm \sqrt{\Delta}}{(1-w^2)}$$

and note that for the coordinates  $(x, y, z)$  assumed in the above sketch

$$x^2 + y^2 \geq r_0^2 \tag{D.4}$$

For a given point of departure  $(x, y, z)$  and direction  $(u, v, w)$ , the gamma cuts through the inner cylinder only if both solutions to Equation (D.3) give different, positive, and real values for  $t_+$  and  $t_-$ . (Requiring different values for  $t_+$  and  $t_-$  excludes the case of a path tangent to the inner cylinder.) Thus for:

$$\Delta \leq 0, \text{ or } \delta \geq 0, \text{ or } |\delta| \leq \sqrt{\Delta} \tag{D.5}$$

no intersection occurs with the infinite height inner cylinder.

The actual well crystal geometry, in which the well depth is less than the crystal height, introduces a further consideration. Now a point of departure may be located below the well so that:

$$x^2 + y^2 < r_0^2 .$$

Except when  $w = \pm 1$ , all paths from this location intersect the extended cylindrical well surface, and the condition  $\Delta > 0$  is automatically satisfied. In addition the restrictions for intersection,  $\delta < 0$  and  $|\delta| > \sqrt{\Delta}$ , which insure that  $t_- \geq 0$ , are no longer applicable because  $t_+$  and  $t_-$  are measured in opposite directions and one of the roots of Equation (D.3) must be negative.

For points within the well crystal, three locations are possible and must be considered separately. These locations are characterized by the following conditions for a point of departure  $x, y, z$ , well radius,  $r_0$  and well height,  $H_w$ :

$$\text{Location A: } x^2 + y^2 < r_0^2 \quad \text{and} \quad z > H_w$$

$$\text{Location B: } x^2 + y^2 \geq r_0^2 \quad \text{and} \quad z > H_w$$

$$\text{Location C: } x^2 + y^2 \geq r_0^2 \quad \text{and} \quad z < H_w$$

Some preliminary considerations are applicable to all locations. If  $w = \pm 1$ , then no intersection with the well cylindrical surface is possible, and a test is made first for this condition. Next, if the path length obtained from Equation (3.5) is less than the distance to the nearest well surface, in the direction  $u, v, w$ , then the particle does not enter the well. In addition, when any of the conditions (D.5) are satisfied for Locations B and C, no intersection is made with the well cylindrical surface, extended. Assuming that a vacuum exists in the well, when a gamma does enter the well, no interactions occur. Under this assumption,

the gamma path length is increased by the distance traveled through the well. (Chapter IV, Section H, discusses the effect of absorption and scattering by a three dimensional source, considerations of which are ignored here.) Assuming all these conditions have been checked, then the calculation of the particle's escape through the well, or its increase in path length due to re-entry into the crystal after passing through the well, are summarized below.

Defining:

$$\begin{aligned}Z_{t_+} &= Z + t_+ w \\Z_{t_-} &= Z + t_- w \\l &= l_1 + l_2\end{aligned}$$

where  $l_1$  = path length in crystal from Equation (3.5)

$l_2$  = distance traveled through well

Thus the location of end point of the gamma path is:

$$\begin{aligned}x' &= x + lu \\y' &= y + lv \\z' &= z + lw\end{aligned}\tag{D.6}$$

and the criteria given in Equation (4.12) are applied. In the sketch below showing Location A, four different rays are possible and are identified as Cases 1-4, below:

LOCATION A

CASE	CONDITIONS	$l_2$	REMARKS
1	$z_{t_+} \leq 0$	-	Escape through well
2	$0 < z_{t_+} \leq H_w$	$t_+ - (H_w - z)/w$	Re-enters crystal
3	$z_{t_+} > H_w$	0	Does not enter well
4	$w > 0$	0	Does not enter well

In the following sketch which shows Location B, 5 different rays are identified as Cases 1-5 below:

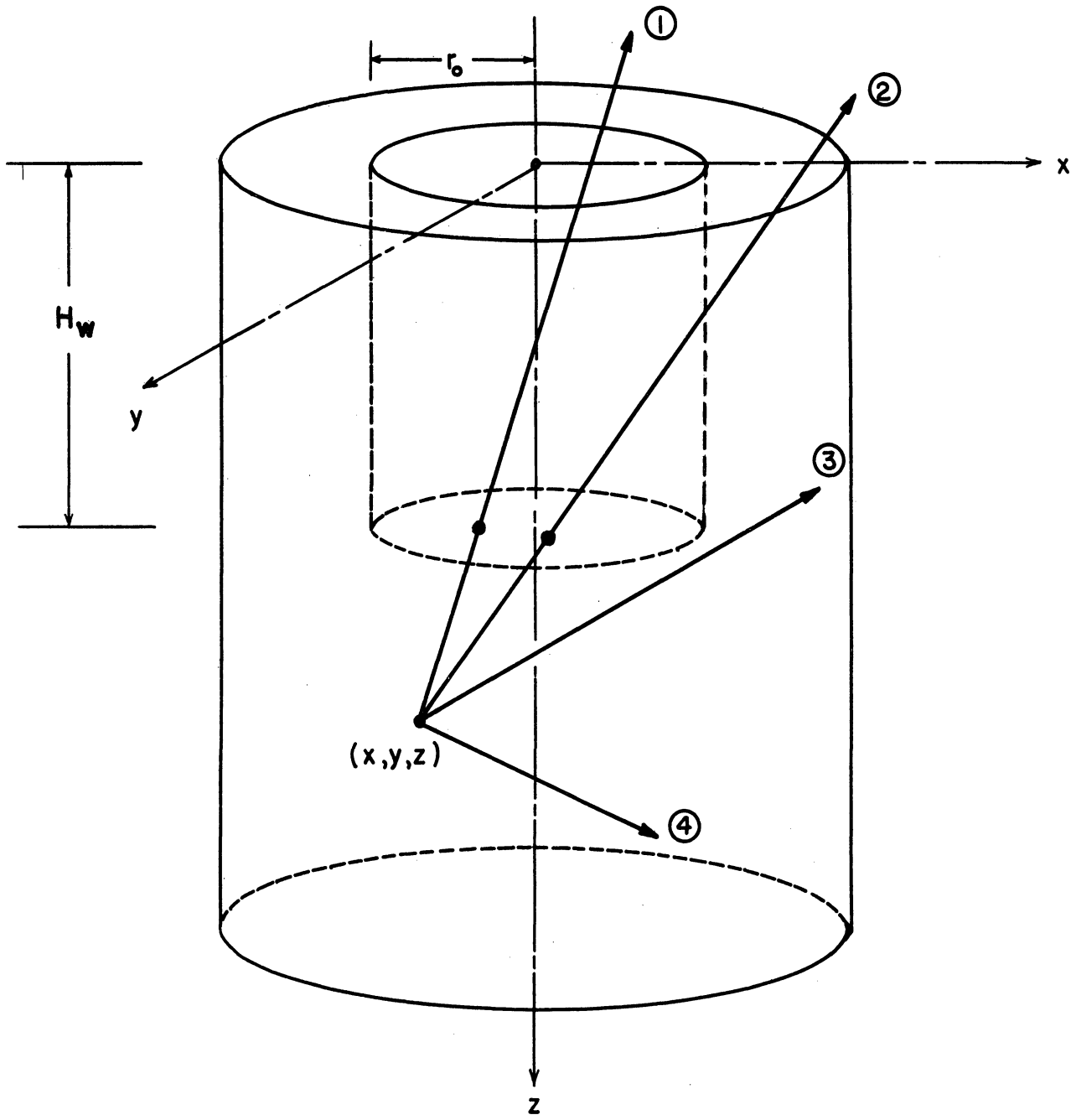
LOCATION B

CASE	CONDITIONS	$l_2$	REMARKS
1	$z_{t_-} < 0$	0	Does not enter well
2	$0 \leq z_{t_-} \leq H_w$ and $z_{t_+} \leq 0$	-	Escape through well
3	$0 < z_{t_-} < H_w$ and $0 < z_{t_+} \leq H_w$	$t_+ - t_-$	Re-enters crystal
4	$z_{t_-} \geq H_w$ and $0 < z_{t_+} \leq H_w$	$t_+ - (H_w - z)/w$	Re-enters crystal
5	$w > 0$	0	Does not enter well

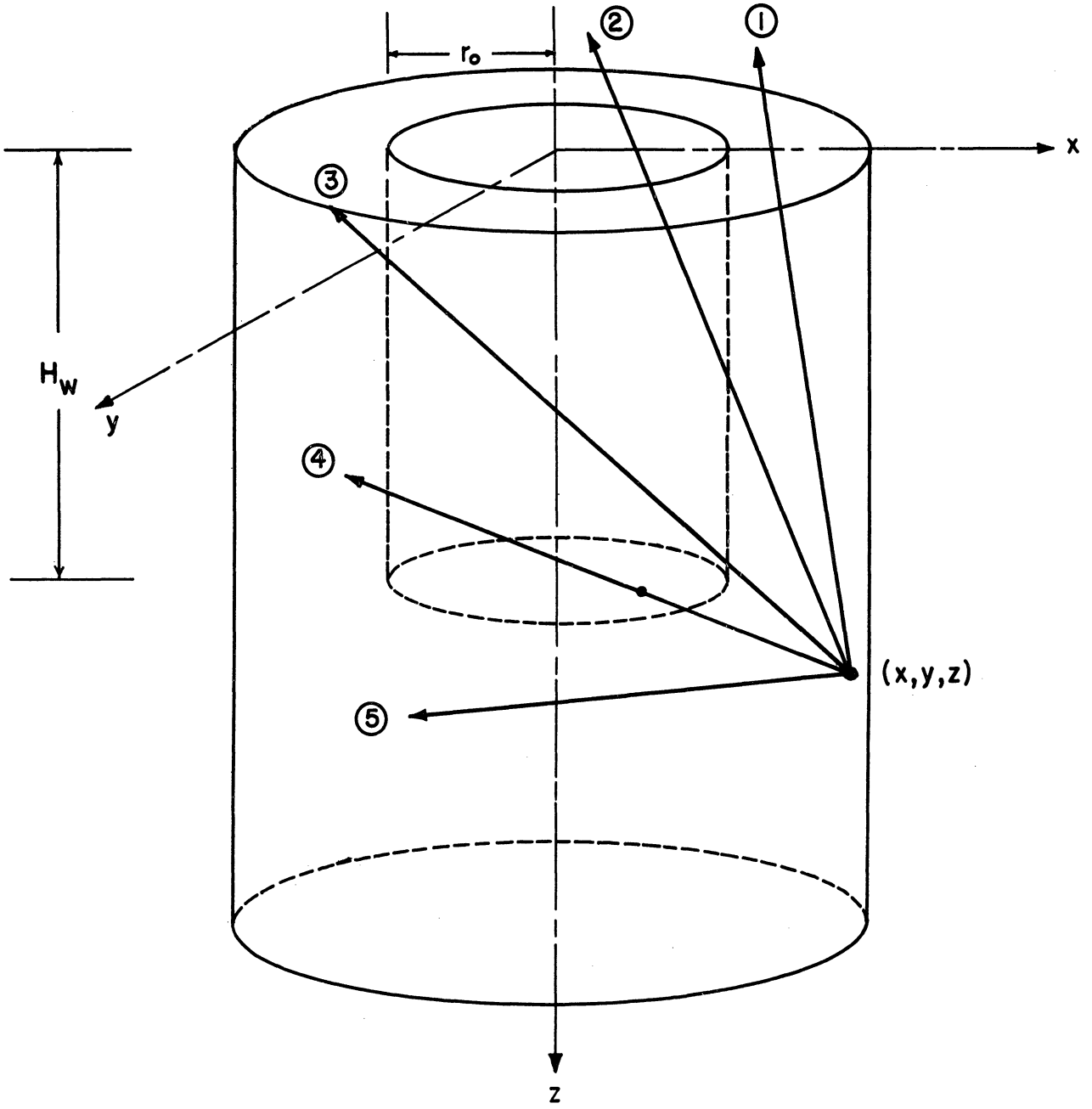
In the following sketch which shows Location C, 5 different rays are identified as Cases 1-5, below:

LOCATION C

CASE	CONDITIONS	$l_2$	REMARKS
1	$z_{t_-} < 0$	0	Does not enter well
2	$0 \leq z_{t_-} < H_w$ and $z_{t_+} \leq 0$	-	Escape through well
3	$0 \leq z_{t_-} < H_w$ and $0 \leq z_{t_+} < H_w$	$t_+ - t_-$	Re-enters crystal
4	$0 \leq z_{t_-} < H_w$ and $z_{t_+} \geq H_w$	$(H_w - z)/w - t_-$	Re-enters crystal
5	$z_{t_-} \geq H_w$	0	Does not enter well

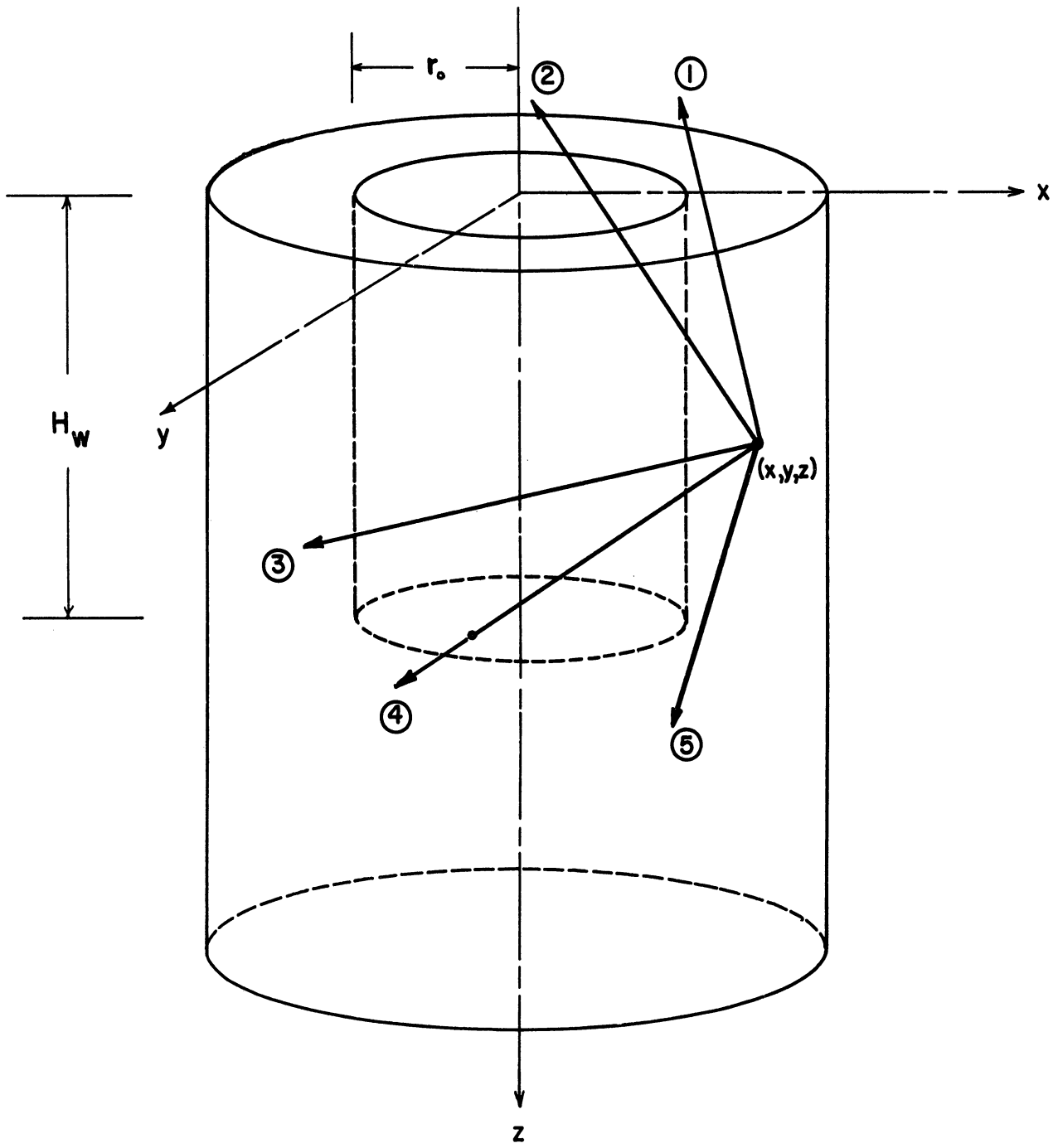


Location A



Location B





Location C

## APPENDIX E

### INSTRUCTIONS FOR COMPUTER PROGRAMS FOR CALCULATION OF THE ABSOLUTE TOTAL EFFICIENCY AND PHOTOFRACTIONS\*

#### Absolute Total Efficiency - BURP 1, 2, and 3

Three separate computer programs have been written to compute the absolute total efficiency,  $\epsilon_{AT}$ , of scintillation crystal detectors. Each of these programs will calculate  $\epsilon_{AT}$  for either solid or well type cylindrical crystals for various source geometries (see Figures II-1, II-2). The programs, and the equations that are solved are:

- BURP-1: Isotropic Point Source on Crystal Axis - Equations (2.6), (2.7).
- BURP-2: Isotropic, Homogeneous Disk, or Cylindrical Volume Sources Centered on Crystal Axis - Equations (2.8), (2.9).
- BURP-3: Isotropic Point Source Located Radially off the Crystal Axis - Equations (2.4), (2.5).

The programs are written in the Michigan Algorithm Decoder (MAD) language<sup>(90,91)</sup> for the University of Michigan IBM-7090 computer. The programs use a numerical integration technique to evaluate the integrals for  $\epsilon_{AT}$ . This technique, which forms a part of the available library system (Michigan Executive System Subroutines-MESS),<sup>(30)</sup> is a Gaussian quadrature formula. The subroutine allows selection of the power of the approximating polynomial and the number of interval sub-divisions for each integral, with no limit being placed on the multiplicity of integrals. For the numerical integration the order of the polynomial approximation and the number of subintervals have been optimized for maximum accuracy in a reasonable computational time. The procedure used was to sequentially

---

\* All computer programs are available from the Argonne National Laboratory Code Center, Argonne, Ill.

increase the order of the polynomial approximation and the number of sub-intervals until the results showed no change in the first four decimal places. These optimized values are included in the programs. In addition, the BURP programs use another MESS library routine for interpolation of the total cross section data at a specified energy. This subroutine is based on the iterative interpolation formula of Aitken.(92)

The general instructions are the same for use of each of these programs, although due to different source geometries there are some differences in the details of required input data. The required data is put in on punched cards and is in the so-called "simplified input" form, as opposed to format input.(90,91) Use of this simplified input provides greater flexibility in these programs and insures that these programs can be used with relative ease by those not familiar with digital computers. All data must have dimensions in cm., energies in MeV, and cross sections in  $\text{cm}^{-1}$ . For all programs, by proper choice of certain input parameters, various options are available. These options are: solid or well type crystal; evaluation of  $\epsilon_{AT}$  for NaI at a single energy or any number of energies; or calculation for any crystal material at a single energy. For all three programs the data may be given in any order, being punched in columns 1-72 on standard "IBM-Cards." The only requirements are that each value punched must be of the form, PARAMETER = value, separated from the next value by a comma, with the last value followed only by an asterisk. With this simplified input form, the first set of data must specify all numerical values required by the program for a given problem. However, subsequently run problems

for which only some of the values are changed, need contain only those values which are different. This saves considerable time when a large amount of input data is to be prepared. Since the most common material used for gamma ray scintillation crystals is NaI, the cross sections of Table II-11 have been incorporated in all these programs. However, provision has been made to read in any values of cross sections so that calculations can be performed for any material, or to take into account future improvements of the data given in Table II-11. To read in different values, one uses the form

$$\text{TAU}(1) = \text{xx.x}, \text{y.yy}, \text{etc.}$$

$$\text{E}(1) = \text{z.zz}, \text{zw.x}, \text{etc.}$$

where the corresponding numerical values of TAU and E are respectively the total cross section (without coherent scattering),  $\text{cm}^{-1}$  and energy, MeV. In addition, the integer number of cross section values read in must be specified as  $\text{KK} = \alpha$ , (no decimal point). When total cross sections are read in this manner, the NaI values stored in the program are automatically deleted. If subsequent calculations for NaI are desired in the same computer run, the NaI cross sections must be read in.

All three programs require input data of:

D = crystal diameter, cm

H = crystal height, cm

For well crystal:

CASE = 1 (no decimal point)

and WD = well diameter, cm

WH = well height, cm

or for solid crystal:

CASE = 2 (no decimal point)

Specified integer values of J (no decimal point), depending on the three options:

- 1) J = 0 calculation for NaI (or any other material if cross sections are supplied) at a single energy, which must be specified as:

E = incident gamma ray energy in MeV, where

$$.01 \leq E \leq 30 \text{ MeV}$$

- 2) J = 1 calculation for NaI (or any other material) over all energies given in Table II-11, except at K-edge of iodine (E = .03323 MeV), starting at E = .01 MeV. The calculation is repeated for every energy in sequence, up to and including the value specified by NUMBER, where:

NUMBER = number of gamma energies for which calculations will be performed (e.g., if NUMBER = 23, output will give calculations for  $.01 \leq E \leq 6.0$  MeV).

Other requirements for source geometry data will be discussed below.

- 3) J = 2 single calculation for any scintillation material for which the total cross section (without coherent scattering) must be specified as:

TAU = total cross section of crystal, cm. By specifying TAU = some large number (e.g. 500), one obtains the mean solid angle subtended by crystal at the source.

The output for  $J = 0$  or  $2$  is a single value for  $\epsilon_{AT}$ , designated as EFFAT, while for  $J = 1$ , the output is in a tabular form similar to the tables given in Appendix G. For BURP-1 only, the output for the solid crystal, when  $J = 0$  or  $2$  includes  $\text{EFFIT} = \epsilon_{IT}$ , and  $\text{OMEGA} =$  solid angle.

Each program also requires the following additional input data:

BURP-1

When  $J = 0$ , or  $J = 2$  options are specified, must also specify:

$B =$  source distance, cm. (see Figures II-1, II-2).

Or when  $J = 1$ , must also specify:

$B(1) = xx.x, y.yy, \dots$ , where the  $xx.x$  and  $y.yy$  are symbolic representation of the numerical values in cm. for the desired source distances. Also specify  $NN =$  integer number (no decimal point) of these source values read in.

Typical data for a 2 x 2 in. NaI well crystal (Harshaw No. 8F8) and solid crystal are:

- 1)  $D = 5.08, H = 5.08, \text{CASE} = 1, \text{WD} = 2.8575, \text{WH} = 3.81,$   
 $J = 0, E = .661, B = .2^*$
- 2)  $J = 1, B(1) = .5, 1.0, 2.0, \text{NUMBER} = 20, NN = 3^*$
- 3)  $J = 2, B = .5, \text{TAU} = 500^*$
- 4)  $\text{CASE} = 2, \text{TAU} = .519^*$

The problems to be calculated by this data are:

- 1)  $\epsilon_{AT}$  of a NaI well crystal for an isotropic point source of 0.661 MeV located 0.2 cm. from the well bottom.
- 2)  $\epsilon_{AT}$  for the same sized well crystal, for point sources located at 0.5, 1.0, 2.0 cm. from the well bottom having all energies  $.01 \leq E \leq 3.0$  MeV, tabular output.

- 3)  $\epsilon_{AT}$  for the same sized well crystal, with a total cross section  $TAU =$  some large number, (e.g., 500). For such a large value of  $TAU$ , the calculation will give the value for the geometry factor,  $\Omega/4\pi$ , for a point source 0.5 cm. from the well bottom.
- 4)  $\epsilon_{AT}$  for a 2 x 2 in. solid crystal, for energy corresponding to the total cross section  $TAU = .519 \text{ cm}^{-1}$ .

BURP-2

When  $J = 0$ , 2 must specify either:

- a)  $K = 3$  (no decimal point), disk source with:

$G =$  disk radius, cm.

$B =$  distance of disk from crystal, cm.

- b)  $K = 4$  (no decimal point), cylindrical volume source with:

$G =$  cylinder radius, cm.

$B1 =$  distance from crystal to bottom of cylinder, cm.

$B2 =$  distance from crystal to top of cylinder, cm.

When  $J = 1$ , must specify either:

- a)  $K = 3$  (no decimal point), disk sources of same radii,  
different source-crystal distances

$G =$  disk radii, cm.

$B(1) = x.xx, yy.y$ , etc. numerical values, in cm.,  
for desired disk source-crystal distances.

$NN =$  integer number (no decimal point) of these  
source distances.

b)  $K = 4$  (no decimal point), volume sources of same radii,  
different heights.

$G$  = cylinder radius, cm.

$B1$  = distance from crystal to bottom of source  
cylinder, cm.

$B2(1) = x.xx, y.yy, \dots$ , etc. numerical values, in  
cm., for desired source cylinder heights.

$NN$  = integer number (no decimal point) of these  
source cylinder heights.

Source absorption and scattering can be taken into account  
by evaluation of Equation (4.14), for the well or solid crystal. The  
source volume dimensions for the well crystal must be numerically equal  
to the well volume dimensions or for the solid crystal the source must  
have the same radius as the solid crystal with any desired values for  $B1$   
and  $B2$  allowed. The additional input data required is:

$SIGMA$  represents the source material total gamma cross  
section values  $cm^{-1}$  corresponding to the energy  
values,  $E$ .

(1) For  $CASE = 1$ , well crystal

$ABS = 1$

$G = WD/2$  (numerical value)

$B1 = 0$

(a) When  $J = 0$

$B2 = WH$  (numerical value)

$SIGMA(1) = x.x, y.y, \dots$ , etc.



(b) When  $J = 1$

$B2(1) = WH$  (numerical value)

$SIGMA(1) = x.x, y.y, \dots, \text{etc.}$

$NN = 1$

(c) When  $J = 2$

$B2 = WH$  (numerical value)

$SIGMA = x.x$

(2) For  $CASE = 2$ , solid crystal

$ABS = 1$

$G = D/2$  (numerical value)

(a) When  $J = 0, 1$

$SIGMA(1) = x.x, y.y, \dots, \text{etc.}$

(b) When  $J = 2$

$SIGMA = x.x$

BURP-3

When  $J = 0, 2$  specify:

$B =$  source-crystal axial distance, cm.

$M =$  radial distance of source from crystal axis, cm.

When  $J = 1$ , specify:

$B =$  source-crystal axial distance, cm.

$M(1) = x.xx, yy.y, \dots$ , numerical values, in cm., for desired  
off-axis radial distances.

$NN =$  integer number (no decimal point) of these off-axis  
distances.

The output for the J=1 option will give a column headed M=.00, which are the on-axis values of  $\epsilon_{AT}$ , and other columns headed M=x.xx, M=yy.y, etc. which are values of  $\epsilon_{AT}^{(M)}$  normalized to the on-axis value, at a given energy.

For all of these programs, the source dimensions must be no greater than the well dimensions for CASE=1, or the solid crystal diameter for CASE=2. The only exception is that BURP=1 will calculate for point sources located outside the well on the crystal axis.

#### PHOTOFRACTION - BURP 4,5 PROGRAMS

The input data for the Monte Carlo Programs are similar to that required for the previously described BURP 1-3 programs. The solid and well crystals are considered in two separate programs, designated BURP 4,5, respectively, but certain data are common to both. Again, both programs contain cross section data for NaI crystals (Table II-11), with provision being made for other materials. For other scintillation materials the following cross section (units of  $\text{cm}^{-1}$ ) and corresponding energy values must be read in:

MU(1) = x.xx, yy.y, etc. (total cross section)

KAPPA(1) = z.zz, ww.w, etc. (photoelectric cross section)

SIGMA(1) = x.yx, y.xx, etc. (Compton cross section)

E(1) = x.xy, x.yy, etc. (energy in MeV)

KK =  $\beta$  (no decimal point) - integer number of energy values read in.

As in the BURP 1-3 Programs, the NaI cross sections stored in the BURP 4,5 Programs are automatically deleted when cross sections for another material are read in in this manner. If subsequent calculations for NaI are desired in the same computer run, the NaI cross sections must be read in. When obtaining photofractions for scintillation crystal materials other than NaI, some error is introduced in the result because these programs use electron penetration data and bremsstrahlung spectra for NaI. The magnitude of these effects is reduced for lower energy incident gamma rays.

Termination of the calculation is based on a specified number of primary interactions occurring in the crystal. This number is read in as the integer value,  $N=\alpha$  (no decimal point). The incident gamma ray energy is specified by a single value  $E_0=z.xx$ , (MeV). The crystal dimensions in cm. are specified by D, H, WD, and WH as previously discussed. The various source configurations are given by reading in a numerical value for the parameter, SOURCE and other parameters, as summarized below:

SOURCE=1, B=x.xx: Isotropic point source on crystal axis, located B cm. from coordinate axes origin which is at the top of either the solid or well crystal. (Note difference from Figure II-2, for well crystal.)

SOURCE=2, B=x.xx, RHO=y.y: Isotropic point source off crystal axis a distance equal to RHO cm., located B cm. from coordinate axes origin.

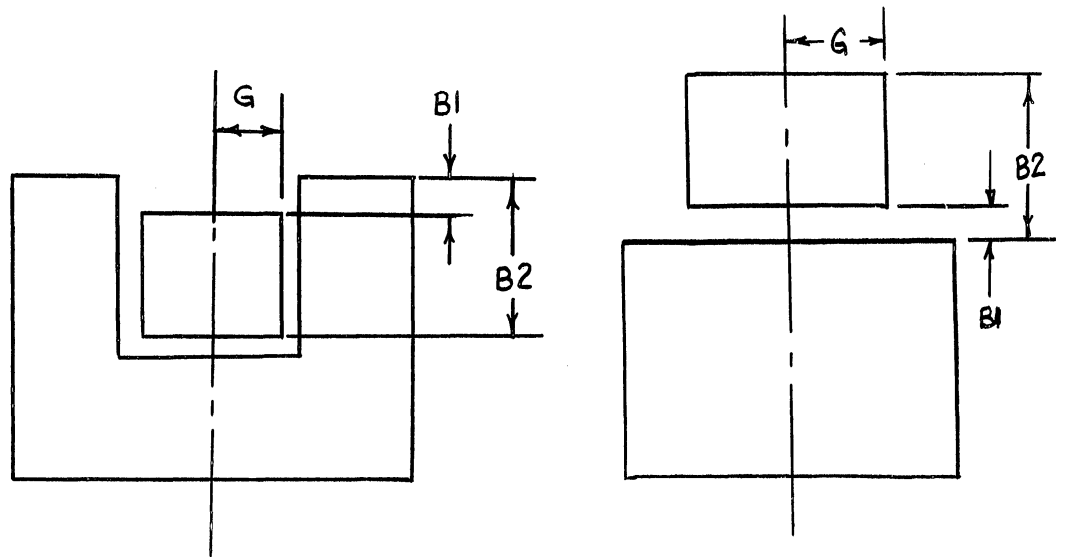
SOURCE=3, B=x.xx, DD=y.y: Isotropic disk source of diameter equal to DD cm., located B cm. from coordinate axes origin.

SOURCE=4, : Monodirectional beam source, collimated to solid crystal diameter.

SOURCE=5, DS=x.xy: Monodirectional beam source, collimated to diameter equal to DS cm., where  $DS \leq D$ .

SOURCE=6, : Monodirectional narrow beam source of zero divergence collimated to crystal axis.

SOURCE=7, G=x.x, B1=y.y, B2=z.z: Isotropic, homogeneous cylindrical volume source with radius equal to G cm., and distances B1, B2 measured to the source surfaces as shown below.



Well Crystal

Solid Crystal

The solid crystal program BURP-4 considers all seven of the above sources, while the well crystal program BURP-5 includes all sources except 4 and 5. All sources must be located within the crystal outside diameter for the solid crystal, or within the well dimensions for the well crystal.

In addition to specifying a value for SOURCE, a value must be read in for the parameter FORM. One must specify  $FORM=\beta$  and where:

$\beta = X =$  SOURCE value for first problem run

$\beta = 0$  for each subsequent problem run for which only the energy is changed

$\beta = XX$ , where  $X=$ SOURCE value for each subsequent problem run in which changes are made in the crystal or source dimensions, but retaining the same type of source.

Various options are provided by specifying values for the parameters BR and ELEC. If no values for BR or ELEC are specified in the input data, all electron and bremsstrahlung effects are considered. For low incident gamma energies, or when less accurate photofraction values are acceptable, computer time can be reduced by specifying any of the following values for these parameters:

ELEC=0 : Neither electrons, nor bremsstrahlung considered

ELEC=1 : No electron escape, bremsstrahlung considered to be distributed along electron path

BR=0 : Electrons produced and allowed to escape, no bremsstrahlung considered.

Finally, by specifying ALPHA=1, one will obtain an unbroadened energy deposition spectrum presented as a table of 128 values in the form of an  $8 \times 16$  matrix. These values represent the number of histories which result in energy deposition equal to  $n \times E_0/128$ , where  $n$  is the position in the  $8 \times 16$  matrix. Thus, the lowest deposited energy is given by the first row, first column position, and the last row, last

column position corresponds to the unbroadened photopeak. This spectrum is obtained, neglecting electrons and bremsstrahlung, and requires a relatively large amount of computer time.

The output from the Monte Carlo programs consists of columns headed by ENERGY, PHOTOFRACTION, A, P, I. For input data of SOURCE=2, 3, or 7 an additional column headed by the parameter T is given. The value for ENERGY is the incident gamma energy in MeV (read in as input data, EO), and the corresponding PHOTOFRACTION is given with its standard deviation. A is the number of totally absorbed source particles; P is the number of source particles incident upon the crystal that pass through with no interaction; I is the number of source particles that interact at least once in the crystal (I=N, where N is part of the input data); T is the number of source particles selected that are not incident upon the crystal.

Typical input data for the well crystal program might consist of:

- 1) N=5000, EO=.661, D=5.08, H=5.08, WD=2.8575, WH=3.81, SOURCE=1, FORM=1, B=3.61\*
- 2) FORM=0, EO=1.17\*
- 3) EO=2.75\*
- 4) FORM=11, B=3.51, EO=.661\*
- 5) SOURCE=3, FORM=3, B=3.61, DD=2.5\*
- 6) ELEC=0\*

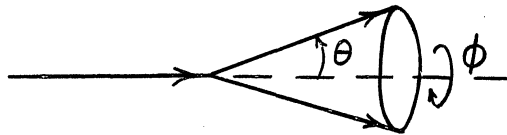
The photofractions calculated by this data are: (all calculations are for 5000 primary interactions in crystal)

- 1) 2 x 2 in. well crystal (8F8) for a .661 MeV point isotropic source located on the axis 0.2 cm. from well bottom.
- 2) Same crystal and source, for 1.17 MeV gammas.
- 3) Same as 2) for 2.75 MeV gammas.
- 4) Same crystal and source, but now located 0.3 cm. from well bottom for .661 MeV gammas.
- 5) Same crystal, .661 MeV disk source of 2.5 cm. dia., located .2 cm. from well bottom.
- 6) Same as 5), but electrons and bremsstrahlung are not considered.

## APPENDIX F

### METHOD OF SELECTING FROM A UNIFORM AZIMUTHAL DISTRIBUTION OF DIRECTIONS

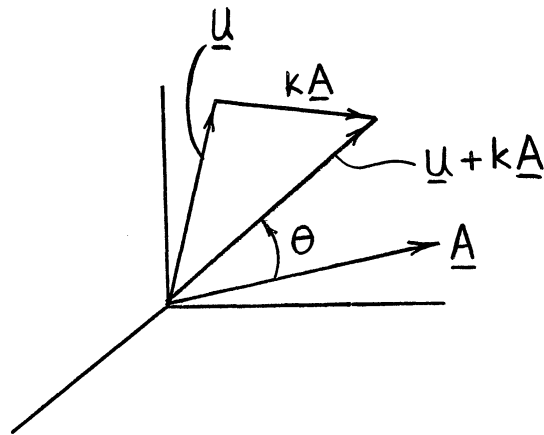
The following technique is due to Kleinecke.<sup>(41)</sup> In the transport of particles through a medium, the various physical laws give the cosine of the angle between the paths of the incident and emergent particles. This polar angle,  $\theta$  defines a cone of possible emergent directions.



When the assumption of azimuthal symmetry is made, one must select a direction from a uniform distribution over this cone. In the Monte Carlo calculation the direction cosines, relative to a fixed rectangular coordinate system are known for the incident path;  $\cos \theta$  is obtained from the physical laws; and the direction cosines for the emergent path are desired. We will denote the incident direction cosines by  $A_1, B_1, C_1$  and the desired emergent ones by  $A_2, B_2, C_2$  with  $\mu = \cos \theta$ .

Now suppose  $U, V, W$  are three numbers selected such that  $(U, V, W)$  is a point distributed uniformly within the unit sphere. The vector  $\underline{U}$  from the origin to the point  $(U, V, W)$  will be distributed with respect to the vector  $\underline{A}$  to  $(A_1, B_1, C_1)$  in a uniform azimuthal direction. Moreover, the vector  $\underline{U+kA} = (U+kA_1, V+kB_1, W+kC_1)$ , for any  $k$ , is also uniformly distributed in azimuth, with respect to  $\underline{A}$ .





The length of the vector  $\underline{u+kA}$  is

$$S = \left[ u^2 + v^2 + w^2 + 2k(uA_1 + vB_1 + wC_1) + k^2 \right]^{1/2},$$

since  $A_1^2 + B_1^2 + C_1^2 = 1$ .

Let  $Y = uA_1 + vB_1 + wC_1$ , and then the condition that the angle between the vectors  $\underline{u+kA}$  and  $\underline{A}$  has the cosine,  $\mu = \cos \theta$  gives

$$Y^2 + 2kY + k^2 = \mu^2 (u^2 + v^2 + w^2 + 2kY + k^2)$$

Solving, we obtain

$$k = -Y + \mu \left[ \frac{u^2 + v^2 + w^2 - Y^2}{1 - \mu^2} \right]^{1/2}$$

and also

$$S = \frac{Y+k}{\mu} = \left[ \frac{u^2 + v^2 + w^2 - Y^2}{1 - \mu^2} \right]^{1/2}$$

Thus the vector  $\underline{U+kA}$  is a vector uniformly distributed in azimuth about the vector  $\underline{A}$ , at the polar angle  $\theta$ . The direction vector,  $\frac{1}{s}(\underline{U+kA})$  defines the desired direction, and has the components  $(U+kA_1)/s$ ,  $(V+kB_1)/s$ ,  $(W+kC_1)/s$ . The desired direction cosines are thus

$$A_2 = (u+kA_1)Z = A_1\mu - Z(YA_1 - u)$$

$$B_2 = (v+kB_1)Z = B_1\mu - Z(YB_1 - v)$$

$$C_2 = (w+kC_1)Z = C_1\mu - Z(YC_1 - w)$$

where

$$Z = \frac{1}{s} = \left[ \frac{1 - \mu^2}{u^2 + v^2 + w^2 - Y^2} \right]^{1/2}$$

In summary, the procedure followed is:

- (1) Select  $U, V, W$  uniformly distributed in the unit sphere,

$$u^2 + v^2 + w^2 \leq 1.$$

(2) Let

$$Y = uA_1 + vB_1 + wC_1$$

$$Z = \left[ \frac{1 - \mu^2}{u^2 + v^2 + w^2 - Y^2} \right]^{1/2}$$

(3) Then

$$A_2 = A_1 \mu - Z(YA_1 - u)$$

$$B_2 = B_1 \mu - Z(YB_1 - v)$$

$$C_2 = C_1 \mu - Z(YC_1 - w)$$

APPENDIX G

TABULATED VALUES FOR ABSOLUTE TOTAL EFFICIENCIES\*

---

\* All calculations for NaI crystals, with dimensions in centimeters, and energies in MeV, unless otherwise noted. Well crystal numbers refer to Harshaw Chemical Co. Catalog<sup>(16)</sup> numbers.

ISOTROPIC POINT SOURCE ON CRYSTAL AXIS

2 x 2 IN. SOLID CRYSTAL

D = 5.080000, H = 5.080000

ENERGY	B = .00	.20	.50	1.00	2.50	5.00	10.00	20.00	50.00	100.00
.010	.5000	.4608	.4034	.3168	.1493	.0542	.0154	.0040	.0006	.0002
.015	.5000	.4608	.4034	.3168	.1493	.0542	.0154	.0040	.0006	.0002
.020	.5000	.4608	.4034	.3168	.1493	.0542	.0154	.0040	.0006	.0002
.030	.5000	.4608	.4034	.3168	.1493	.0542	.0154	.0040	.0006	.0002
.040	.5000	.4608	.4034	.3168	.1493	.0542	.0154	.0040	.0006	.0002
.050	.5000	.4608	.4034	.3168	.1493	.0542	.0154	.0040	.0006	.0002
.060	.5000	.4608	.4034	.3168	.1493	.0542	.0154	.0040	.0006	.0002
.080	.5000	.4608	.4034	.3168	.1493	.0542	.0154	.0040	.0006	.0002
.100	.5000	.4608	.4034	.3168	.1493	.0542	.0154	.0040	.0006	.0002
.150	.4988	.4471	.3776	.2833	.1276	.0475	.0142	.0038	.0006	.0002
.200	.4832	.4187	.3445	.2528	.1131	.0431	.0133	.0037	.0006	.0002
.300	.4172	.3479	.2794	.2019	.0909	.0359	.0116	.0033	.0006	.0001
.400	.3649	.3001	.2393	.1722	.0780	.0314	.0103	.0030	.0005	.0001
.500	.3287	.2686	.2134	.1534	.0698	.0283	.0094	.0028	.0005	.0001
.600	.3051	.2485	.1971	.1415	.0646	.0263	.0088	.0026	.0005	.0001
.800	.2729	.2213	.1752	.1257	.0576	.0236	.0080	.0024	.0004	.0001
1.000	.2506	.2027	.1603	.1150	.0528	.0218	.0074	.0022	.0004	.0001
1.500	.2153	.1737	.1371	.0983	.0453	.0188	.0064	.0019	.0003	.0001
2.000	.1968	.1585	.1250	.0897	.0414	.0172	.0059	.0018	.0003	.0001
3.000	.1801	.1448	.1142	.0819	.0378	.0158	.0054	.0016	.0003	.0001
4.000	.1739	.1398	.1102	.0790	.0365	.0153	.0052	.0016	.0003	.0001
5.000	.1724	.1385	.1092	.0783	.0362	.0151	.0052	.0016	.0003	.0001
6.000	.1724	.1385	.1092	.0783	.0362	.0151	.0052	.0016	.0003	.0001

ISOTROPIC POINT SOURCE ON CRYSTAL AXIS

3 x 3 IN. SOLID CRYSTAL

D = 7.620000,		H = 7.620000								
ENERGY	B = .00	.20	.50	1.00	2.50	5.00	10.00	20.00	50.00	100.00
.010	.5000	.4738	.4349	.3731	.2257	.1023	.0328	.0088	.0014	.0004
.015	.5000	.4738	.4349	.3731	.2257	.1023	.0328	.0088	.0014	.0004
.020	.5000	.4738	.4349	.3731	.2257	.1023	.0328	.0088	.0014	.0004
.030	.5000	.4738	.4349	.3731	.2257	.1023	.0328	.0088	.0014	.0004
.040	.5000	.4738	.4349	.3731	.2257	.1023	.0328	.0088	.0014	.0004
.050	.5000	.4738	.4349	.3731	.2257	.1023	.0328	.0088	.0014	.0004
.060	.5000	.4738	.4349	.3731	.2257	.1023	.0328	.0088	.0014	.0004
.080	.5000	.4738	.4349	.3731	.2257	.1023	.0328	.0088	.0014	.0004
.100	.5000	.4738	.4349	.3731	.2257	.1023	.0328	.0088	.0014	.0004
.150	.4999	.4690	.4240	.3550	.2051	.0922	.0304	.0085	.0014	.0004
.200	.4965	.4581	.4071	.3341	.1884	.0850	.0286	.0082	.0014	.0004
.300	.4641	.4153	.3601	.2887	.1597	.0731	.0256	.0076	.0013	.0003
.400	.4270	.3767	.3234	.2571	.1417	.0655	.0234	.0071	.0013	.0003
.500	.3969	.3475	.2969	.2351	.1294	.0603	.0218	.0067	.0012	.0003
.600	.3756	.3275	.2790	.2205	.1214	.0568	.0207	.0064	.0012	.0003
.800	.3444	.2989	.2538	.2001	.1102	.0519	.0191	.0059	.0011	.0003
1.000	.3216	.2782	.2358	.1857	.1023	.0483	.0179	.0056	.0010	.0003
1.500	.2833	.2441	.2064	.1622	.0895	.0425	.0159	.0050	.0009	.0002
2.000	.2623	.2256	.1905	.1496	.0826	.0394	.0148	.0047	.0009	.0002
3.000	.2427	.2084	.1758	.1380	.0762	.0364	.0137	.0044	.0008	.0002
4.000	.2353	.2019	.1703	.1336	.0738	.0353	.0133	.0043	.0008	.0002
5.000	.2334	.2003	.1689	.1325	.0732	.0350	.0132	.0042	.0008	.0002
6.000	.2334	.2003	.1689	.1325	.0732	.0350	.0132	.0042	.0008	.0002

ISOTROPIC POINT SOURCE ON CRYSTAL AXIS

7F8 WELL CRYSTAL

D = 4.445000, H = 5.080000

WD = 1.905000, WH = 3.810000

ENERGY	B= .00	.10	.20	.30	.40	.50	.75	1.00	1.25
.010	.9851	.9843	.9835	.9825	.9816	.9805	.9774	.9735	.9686
.015	.9851	.9843	.9835	.9825	.9816	.9805	.9774	.9735	.9686
.020	.9851	.9843	.9835	.9825	.9816	.9805	.9774	.9735	.9686
.030	.9851	.9843	.9835	.9825	.9816	.9805	.9774	.9735	.9686
.040	.9851	.9843	.9835	.9825	.9816	.9805	.9774	.9735	.9686
.050	.9851	.9843	.9835	.9825	.9816	.9805	.9774	.9735	.9686
.060	.9851	.9843	.9835	.9825	.9816	.9805	.9774	.9735	.9686
.080	.9851	.9843	.9835	.9825	.9816	.9805	.9760	.9718	.9664
.100	.9835	.9825	.9815	.9805	.9793	.9781	.9744	.9699	.9640
.150	.9492	.9423	.9375	.9336	.9303	.9275	.9214	.9151	.9076
.200	.8355	.8167	.8054	.7971	.7908	.7858	.7765	.7690	.7612
.300	.6186	.5926	.5781	.5679	.5604	.5547	.5447	.5377	.5313
.400	.5031	.4779	.4641	.4546	.4476	.4423	.4333	.4272	.4218
.500	.4351	.4114	.3986	.3898	.3834	.3785	.3703	.3649	.3601
.600	.3944	.3720	.3600	.3518	.3457	.3412	.3336	.3285	.3242
.800	.3424	.3220	.3111	.3036	.2982	.2941	.2872	.2828	.2790
1.000	.3086	.2895	.2795	.2726	.2676	.2638	.2575	.2534	.2500
1.500	.2579	.2413	.2326	.2266	.2223	.2190	.2137	.2102	.2073
2.000	.2325	.2173	.2093	.2038	.1998	.1969	.1920	.1888	.1862
3.000	.2102	.1962	.1889	.1839	.1802	.1775	.1730	.1701	.1678
4.000	.2021	.1886	.1815	.1767	.1732	.1705	.1662	.1634	.1611
5.000	.2001	.1866	.1796	.1748	.1714	.1688	.1645	.1617	.1595
6.000	.2001	.1866	.1796	.1748	.1714	.1688	.1645	.1617	.1595

ISOTROPIC POINT SOURCE ON CRYSTAL AXIS

8F8 WELL CRYSTAL

D = 5.080000, H = 5.080000  
 WD = 2.857500, WH = 3.810000

ENERGY	B=	.C0	.10	.20	.30	.40	.50	.75	1.00	1.25
.010	.9682	.9666	.9649	.9631	.9612	.9591	.9530	.9457	.9366	.9366
.015	.9682	.9666	.9649	.9631	.9612	.9591	.9530	.9457	.9366	.9366
.020	.9682	.9666	.9649	.9631	.9612	.9591	.9530	.9457	.9366	.9366
.030	.9682	.9666	.9649	.9631	.9612	.9591	.9530	.9457	.9366	.9366
.040	.9682	.9666	.9649	.9631	.9612	.9591	.9530	.9457	.9366	.9366
.050	.9682	.9666	.9649	.9631	.9612	.9591	.9530	.9457	.9366	.9366
.060	.9682	.9666	.9649	.9631	.9612	.9591	.9530	.9457	.9366	.9366
.080	.9667	.9651	.9633	.9613	.9593	.9570	.9506	.9428	.9330	.9330
.100	.9650	.9632	.9612	.9592	.9569	.9545	.9477	.9393	.9290	.9290
.150	.9205	.9130	.9065	.9006	.8951	.8900	.8781	.8664	.8537	.8537
.200	.8017	.7828	.7691	.7578	.7482	.7398	.7225	.7081	.6945	.6945
.300	.5916	.5646	.5473	.5339	.5229	.5137	.4960	.4825	.4710	.4710
.400	.4813	.4548	.4384	.4258	.4157	.4074	.3915	.3798	.3701	.3701
.500	.4165	.3914	.3761	.3646	.3553	.3477	.3333	.3229	.3143	.3143
.600	.3778	.3539	.3395	.3287	.3200	.3129	.2996	.2900	.2821	.2821
.800	.3282	.3062	.2932	.2834	.2756	.2693	.2574	.2488	.2419	.2419
1.000	.2959	.2754	.2633	.2543	.2471	.2413	.2304	.2226	.2163	.2163
1.500	.2475	.2295	.2190	.2112	.2050	.2000	.1907	.1841	.1788	.1788
2.000	.2232	.2067	.1970	.1899	.1842	.1796	.1711	.1651	.1604	.1604
3.000	.2019	.1866	.1778	.1712	.1661	.1619	.1541	.1487	.1443	.1443
4.000	.1942	.1794	.1708	.1645	.1595	.1555	.1480	.1427	.1386	.1386
5.000	.1922	.1776	.1691	.1628	.1579	.1539	.1464	.1412	.1371	.1371
6.000	.1922	.1776	.1691	.1628	.1579	.1539	.1464	.1412	.1371	.1371
8.000	.1956	.1807	.1721	.1658	.1607	.1567	.1491	.1438	.1396	.1396
10.000	.2014	.1862	.1773	.1708	.1657	.1615	.1537	.1483	.1440	.1440
15.000	.2176	.2014	.1919	.1849	.1794	.1749	.1666	.1608	.1561	.1561
20.000	.2316	.2145	.2046	.1972	.1914	.1866	.1778	.1716	.1667	.1667
30.000	.2542	.2359	.2251	.2171	.2108	.2057	.1961	.1894	.1840	.1840

(CONTINUED ON NEXT PAGE)



ISOTROPIC POINT SOURCE ON CRYSTAL AXIS (CONT'D)

8F8 WELL CRYSTAL

D =	5.080000,	H =	5.080000			
WD =	2.857500,	WH =	3.810000			
ENERGY	B=1.50	2.00	2.50	3.00	3.50	3.81
.010	.9252	.8925	.8379	.7466	.6060	.5000
.015	.9252	.8925	.8379	.7466	.6060	.5000
.020	.9252	.8925	.8379	.7466	.6060	.5000
.030	.9252	.8925	.8379	.7466	.6060	.5000
.040	.9252	.8925	.8379	.7466	.6060	.5000
.050	.9252	.8925	.8379	.7466	.6060	.5000
.060	.9252	.8925	.8379	.7466	.6060	.5000
.080	.9209	.8860	.8288	.7363	.6001	.5000
.100	.9162	.8796	.8207	.7280	.5955	.4996
.150	.8390	.8051	.7423	.6582	.5462	.4676
.200	.6804	.6461	.5986	.5327	.4477	.3890
.300	.4600	.4355	.4036	.3610	.3072	.2703
.400	.3610	.3415	.3166	.2837	.2426	.2144
.500	.3064	.2897	.2687	.2411	.2066	.1830
.600	.2750	.2599	.2411	.2164	.1857	.1647
.800	.2357	.2227	.2066	.1857	.1596	.1418
1.000	.2107	.1991	.1847	.1660	.1429	.1270
1.500	.1741	.1645	.1526	.1373	.1183	.1053
2.000	.1561	.1474	.1368	.1231	.1062	.0946
3.000	.1405	.1327	.1231	.1109	.0956	.0853
4.000	.1349	.1273	.1182	.1064	.0918	.0819
5.000	.1334	.1260	.1170	.1053	.0909	.0810
6.000	.1334	.1260	.1170	.1053	.0909	.0810

ISOTROPIC POINT SOURCE ON CRYSTAL AXIS

2 x 2 IN. WELL CRYSTAL

D =	5.080000,	H =	5.080000			
WD =	3.492500,	WH =	4.127500			
ENERGY	B= .00	.10	.20	.30	.40	.50
.010	.9605	.9587	.9569	.9549	.9528	.9505
.015	.9605	.9587	.9569	.9549	.9528	.9505
.020	.9605	.9587	.9569	.9549	.9528	.9505
.030	.9605	.9587	.9569	.9549	.9528	.9505
.040	.9605	.9587	.9569	.9549	.9528	.9505
.050	.9605	.9587	.9569	.9549	.9528	.9505
.060	.9605	.9587	.9569	.9549	.9528	.9505
.080	.9589	.9570	.9551	.9530	.9507	.9483
.100	.9547	.9525	.9501	.9476	.9450	.9423
.150	.8693	.8590	.8498	.8413	.8334	.8261
.200	.7201	.6982	.6818	.6678	.6557	.6451
.300	.5087	.4802	.4615	.4467	.4345	.4241
.400	.4078	.3804	.3632	.3498	.3390	.3299
.500	.3503	.3246	.3088	.2967	.2870	.2788
.600	.3164	.2922	.2774	.2662	.2571	.2496
.800	.2736	.2514	.2381	.2281	.2200	.2134
1.000	.2459	.2253	.2131	.2039	.1965	.1904
1.500	.2048	.1869	.1763	.1684	.1622	.1570
2.000	.1844	.1679	.1582	.1510	.1453	.1406
3.000	.1665	.1513	.1425	.1359	.1307	.1264
4.000	.1600	.1453	.1368	.1304	.1254	.1213
5.000	.1584	.1438	.1354	.1291	.1241	.1200
6.000	.1584	.1438	.1354	.1291	.1241	.1200

ISOTROPIC POINT SOURCE ON CRYSTAL AXIS

12AW(10)-W3 WELL CRYSTAL

D = 7.620000, H = 6.350000  
WD = 2.009140, WH = 5.080000

ENERGY	B= .00	.10	.20	.30	.40	.50
.010	.9905	.9901	.9897	.9893	.9889	.9884
.015	.9905	.9901	.9897	.9893	.9889	.9884
.020	.9905	.9901	.9897	.9893	.9889	.9884
.030	.9905	.9901	.9897	.9893	.9889	.9884
.040	.9905	.9901	.9897	.9893	.9889	.9884
.050	.9905	.9901	.9897	.9893	.9889	.9884
.060	.9905	.9901	.9897	.9893	.9889	.9884
.080	.9905	.9901	.9897	.9893	.9889	.9884
.100	.9905	.9901	.9897	.9893	.9888	.9884
.150	.9792	.9784	.9778	.9771	.9764	.9757
.200	.9298	.9263	.9241	.9225	.9213	.9203
.300	.7804	.7704	.7652	.7619	.7597	.7582
.400	.6732	.6610	.6549	.6511	.6487	.6471
.500	.6016	.5888	.5825	.5786	.5761	.5745
.600	.5559	.5430	.5367	.5328	.5304	.5288
.800	.4941	.4814	.4753	.4716	.4693	.4678
1.000	.4519	.4396	.4338	.4302	.4279	.4265
1.500	.3861	.3747	.3693	.3660	.3639	.3627
2.000	.3518	.3410	.3360	.3329	.3310	.3298
3.000	.3211	.3109	.3061	.3033	.3015	.3004
4.000	.3098	.2998	.2952	.2924	.2906	.2896
5.000	.3069	.2970	.2924	.2896	.2879	.2868
6.000	.3069	.2970	.2924	.2896	.2879	.2868

ISOTROPIC POINT SOURCE ON CRYSTAL AXIS

12AW(10)-W4 WELL CRYSTAL

D = 7.620000, H = 6.350000  
WD = 2.857500, WH = 5.080000

ENERGY	B= .00	.10	.20	.30	.40	.50
.010	.9813	.9806	.9799	.9791	.9782	.9773
.015	.9813	.9806	.9799	.9791	.9782	.9773
.020	.9813	.9806	.9799	.9791	.9782	.9773
.030	.9813	.9806	.9799	.9791	.9782	.9773
.040	.9813	.9806	.9799	.9791	.9782	.9773
.050	.9813	.9806	.9799	.9791	.9782	.9773
.060	.9813	.9806	.9799	.9791	.9782	.9773
.080	.9813	.9806	.9799	.9791	.9782	.9773
.100	.9801	.9792	.9784	.9775	.9766	.9756
.150	.9671	.9658	.9645	.9632	.9619	.9606
.200	.9088	.9038	.9001	.8971	.8944	.8920
.300	.7459	.7333	.7255	.7197	.7152	.7115
.400	.6360	.6211	.6124	.6060	.6011	.5972
.500	.5646	.5491	.5403	.5339	.5291	.5253
.600	.5196	.5042	.4955	.4892	.4845	.4809
.800	.4597	.4447	.4363	.4303	.4259	.4225
1.000	.4191	.4046	.3966	.3910	.3867	.3835
1.500	.3564	.3431	.3358	.3307	.3269	.3240
2.000	.3241	.3115	.3047	.2999	.2963	.2936
3.000	.2952	.2834	.2770	.2725	.2692	.2667
4.000	.2846	.2731	.2668	.2625	.2593	.2568
5.000	.2819	.2705	.2643	.2600	.2568	.2544
6.000	.2819	.2705	.2643	.2600	.2568	.2544

ISOTROPIC POINT SOURCE ON CRYSTAL AXIS

3 x 3 IN. WELL CRYSTAL

D =	7.620000,	H =	7.620000			
WD =	1.270000,	WH =	3.810000			
ENERGY	B= .00	.10	.20	.30	.40	.50
.010	.9932	.9928	.9924	.9920	.9915	.9910
.015	.9932	.9928	.9924	.9920	.9915	.9910
.020	.9932	.9928	.9924	.9920	.9915	.9910
.030	.9932	.9928	.9924	.9920	.9915	.9910
.040	.9932	.9928	.9924	.9920	.9915	.9910
.050	.9932	.9928	.9924	.9920	.9915	.9910
.060	.9932	.9928	.9924	.9920	.9915	.9910
.080	.9932	.9928	.9924	.9920	.9915	.9910
.100	.9932	.9928	.9924	.9920	.9915	.9910
.150	.9900	.9893	.9886	.9878	.9870	.9860
.200	.9725	.9692	.9671	.9653	.9636	.9619
.300	.8721	.8619	.8562	.8520	.8486	.8455
.400	.7778	.7648	.7577	.7526	.7486	.7451
.500	.7081	.6942	.6867	.6813	.6771	.6735
.600	.6614	.6473	.6397	.6343	.6300	.6264
.800	.5959	.5819	.5743	.5690	.5648	.5614
1.000	.5498	.5360	.5287	.5235	.5195	.5161
1.500	.4756	.4628	.4559	.4510	.4473	.4442
2.000	.4362	.4239	.4173	.4127	.4092	.4062
3.000	.4002	.3886	.3824	.3780	.3747	.3719
4.000	.3868	.3755	.3694	.3652	.3619	.3592
5.000	.3834	.3722	.3661	.3619	.3587	.3560
6.000	.3834	.3722	.3661	.3619	.3587	.3560

ISOTROPIC POINT SOURCE ON CRYSTAL AXIS

12AW(12)-W1 WELL CRYSTAL

D =	7.620000,	H =	7.620000			
WD =	2.009140,	WH =	3.810000			
ENERGY	B= .00	.10	.20	.30	.40	.50
.010	.9835	.9826	.9817	.9807	.9796	.9785
.015	.9835	.9826	.9817	.9807	.9796	.9785
.020	.9835	.9826	.9817	.9807	.9796	.9785
.030	.9835	.9826	.9817	.9807	.9796	.9785
.040	.9835	.9826	.9817	.9807	.9796	.9785
.050	.9835	.9826	.9817	.9807	.9796	.9785
.060	.9835	.9826	.9817	.9807	.9796	.9785
.080	.9835	.9826	.9817	.9807	.9796	.9785
.100	.9819	.9809	.9799	.9787	.9775	.9761
.150	.9770	.9755	.9739	.9722	.9705	.9686
.200	.9528	.9478	.9441	.9407	.9376	.9345
.300	.8418	.8287	.8202	.8134	.8077	.8025
.400	.7453	.7292	.7191	.7113	.7047	.6991
.500	.6758	.6588	.6484	.6403	.6336	.6279
.600	.6298	.6126	.6022	.5941	.5875	.5818
.800	.5658	.5489	.5387	.5309	.5244	.5190
1.000	.5211	.5047	.4947	.4872	.4810	.4758
1.500	.4496	.4344	.4252	.4182	.4125	.4077
2.000	.4118	.3973	.3886	.3820	.3767	.3722
3.000	.3775	.3638	.3556	.3494	.3443	.3401
4.000	.3647	.3513	.3434	.3373	.3324	.3283
5.000	.3615	.3482	.3403	.3342	.3294	.3253
6.000	.3615	.3482	.3403	.3342	.3294	.3253

ISOTROPIC POINT SOURCE ON CRYSTAL AXIS

12AW(12)-W2 WELL CRYSTAL

D = 7.620000, H = 7.620000  
WD = 2.857500, WH = 3.810000

ENERGY	B = .00	.10	.20	.30	.40	.50	.75	1.00	1.25
.010	.9682	.9666	.9649	.9631	.9612	.9591	.9530	.9457	.9366
.015	.9682	.9666	.9649	.9631	.9612	.9591	.9530	.9457	.9366
.020	.9682	.9666	.9649	.9631	.9612	.9591	.9530	.9457	.9366
.030	.9682	.9666	.9649	.9631	.9612	.9591	.9530	.9457	.9366
.040	.9682	.9666	.9649	.9631	.9612	.9591	.9530	.9457	.9366
.050	.9682	.9666	.9649	.9631	.9612	.9591	.9530	.9457	.9366
.060	.9682	.9666	.9649	.9631	.9612	.9591	.9530	.9457	.9366
.080	.9682	.9666	.9649	.9631	.9612	.9591	.9530	.9457	.9366
.100	.9654	.9637	.9618	.9597	.9575	.9552	.9484	.9401	.9298
.150	.9572	.9546	.9520	.9492	.9463	.9432	.9346	.9243	.9118
.200	.9240	.9172	.9116	.9064	.9014	.8966	.8845	.8717	.8572
.300	.8023	.7864	.7752	.7659	.7577	.7503	.7339	.7187	.7034
.400	.7049	.6861	.6733	.6629	.6540	.6460	.6290	.6140	.5996
.500	.6367	.6171	.6041	.5936	.5846	.5767	.5600	.5456	.5321
.600	.5920	.5724	.5595	.5491	.5403	.5326	.5163	.5025	.4896
.800	.5305	.5114	.4989	.4889	.4804	.4731	.4577	.4449	.4330
1.000	.4878	.4692	.4572	.4476	.4395	.4325	.4180	.4058	.3948
1.500	.4200	.4028	.3918	.3830	.3757	.3693	.3562	.3454	.3357
2.000	.3842	.3680	.3576	.3494	.3425	.3365	.3242	.3142	.3052
3.000	.3519	.3366	.3268	.3191	.3126	.3070	.2956	.2863	.2780
4.000	.3399	.3249	.3154	.3079	.3016	.2962	.2851	.2760	.2680
5.000	.3368	.3220	.3126	.3051	.2988	.2934	.2824	.2735	.2655
6.000	.3368	.3220	.3126	.3051	.2988	.2935	.2824	.2735	.2655
8.000	.3421	.3271	.3176	.3100	.3037	.2982	.2871	.2780	.2699
10.000	.3511	.3358	.3261	.3184	.3119	.3064	.2950	.2857	.2774
15.000	.3758	.3598	.3496	.3414	.3347	.3288	.3167	.3069	.2981
20.000	.3967	.3801	.3695	.3610	.3540	.3479	.3353	.3250	.3158
30.000	.4297	.4123	.4011	.3922	.3847	.3783	.3649	.3539	.3440

ISOTROPIC POINT SOURCE ON CRYSTAL AXIS

12AW(12)-W3 WELL CRYSTAL

D = 7.620000, H = 7.620000  
WD = 2.009140, WH = 5.080000

ENERGY	B= .00	.10	.20	.30	.40	.50
.010	.9905	.9901	.9897	.9893	.9889	.9884
.015	.9905	.9901	.9897	.9893	.9889	.9884
.020	.9905	.9901	.9897	.9893	.9889	.9884
.030	.9905	.9901	.9897	.9893	.9889	.9884
.040	.9905	.9901	.9897	.9893	.9889	.9884
.050	.9905	.9901	.9897	.9893	.9889	.9884
.060	.9905	.9901	.9897	.9893	.9889	.9884
.080	.9905	.9901	.9897	.9893	.9889	.9884
.100	.9905	.9901	.9897	.9893	.9889	.9884
.150	.9870	.9863	.9856	.9849	.9842	.9835
.200	.9630	.9592	.9567	.9547	.9531	.9516
.300	.8444	.8330	.8263	.8214	.8176	.8146
.400	.7429	.7287	.7205	.7147	.7102	.7067
.500	.6710	.6558	.6473	.6412	.6366	.6329
.600	.6237	.6084	.5998	.5937	.5891	.5855
.800	.5585	.5434	.5350	.5290	.5245	.5210
1.000	.5132	.4985	.4904	.4846	.4802	.4768
1.500	.4414	.4277	.4202	.4148	.4108	.4076
2.000	.4036	.3906	.3834	.3784	.3745	.3716
3.000	.3693	.3571	.3503	.3456	.3420	.3392
4.000	.3567	.3447	.3381	.3335	.3300	.3272
5.000	.3535	.3416	.3350	.3304	.3269	.3242
6.000	.3535	.3416	.3350	.3304	.3269	.3242

ISOTROPIC POINT SOURCE ON CRYSTAL AXIS

12AW(12)-W4 WELL CRYSTAL

D = 7.620000, H = 7.620000  
WD = 2.857500, WH = 5.080000

ENERGY	B= .00	.10	.20	.30	.40	.50
.010	.9813	.9806	.9799	.9791	.9782	.9773
.015	.9813	.9806	.9799	.9791	.9782	.9773
.020	.9813	.9806	.9799	.9791	.9782	.9773
.030	.9813	.9806	.9799	.9791	.9782	.9773
.040	.9813	.9806	.9799	.9791	.9782	.9773
.050	.9813	.9806	.9799	.9791	.9782	.9773
.060	.9813	.9806	.9799	.9791	.9782	.9773
.080	.9813	.9806	.9799	.9791	.9782	.9773
.100	.9801	.9793	.9784	.9776	.9766	.9756
.150	.9750	.9736	.9723	.9710	.9697	.9683
.200	.9420	.9367	.9327	.9293	.9262	.9234
.300	.8099	.7958	.7866	.7792	.7731	.7679
.400	.7057	.6888	.6780	.6695	.6626	.6568
.500	.6339	.6162	.6051	.5965	.5896	.5837
.600	.5875	.5697	.5587	.5502	.5433	.5375
.800	.5241	.5067	.4960	.4878	.4811	.4756
1.000	.4804	.4636	.4533	.4454	.4390	.4338
1.500	.4118	.3961	.3867	.3795	.3737	.3689
2.000	.3758	.3611	.3521	.3454	.3399	.3354
3.000	.3435	.3295	.3212	.3148	.3097	.3055
4.000	.3315	.3179	.3098	.3036	.2986	.2945
5.000	.3285	.3150	.3069	.3007	.2958	.2918
6.000	.3285	.3150	.3069	.3007	.2958	.2918

ISOTROPIC POINT SOURCE ON CRYSTAL AXIS

12AW(14)-W3 WELL CRYSTAL

D = 7.620000, H = 8.890000  
 WD = 2.009140, WH = 5.080000

ENERGY	B= .00	.10	.20	.30	.40	.50
.010	.9905	.9901	.9897	.9893	.9889	.9884
.015	.9905	.9901	.9897	.9893	.9889	.9884
.020	.9905	.9901	.9897	.9893	.9889	.9884
.030	.9905	.9901	.9897	.9893	.9889	.9884
.040	.9905	.9901	.9897	.9893	.9889	.9884
.050	.9905	.9901	.9897	.9893	.9889	.9884
.060	.9905	.9901	.9897	.9893	.9889	.9884
.080	.9905	.9901	.9897	.9893	.9889	.9884
.100	.9905	.9901	.9897	.9893	.9889	.9884
.150	.9874	.9866	.9859	.9853	.9846	.9838
.200	.9678	.9640	.9614	.9594	.9577	.9561
.300	.8627	.8509	.8438	.8385	.8343	.8308
.400	.7671	.7522	.7434	.7369	.7318	.7277
.500	.6972	.6813	.6721	.6652	.6599	.6555
.600	.6506	.6345	.6251	.6182	.6128	.6085
.800	.5855	.5696	.5603	.5535	.5482	.5439
1.000	.5398	.5242	.5152	.5086	.5034	.4993
1.500	.4665	.4520	.4436	.4374	.4326	.4287
2.000	.4276	.4138	.4058	.3999	.3954	.3917
3.000	.3922	.3791	.3715	.3660	.3617	.3582
4.000	.3790	.3662	.3589	.3535	.3493	.3459
5.000	.3757	.3630	.3557	.3503	.3461	.3427
6.000	.3757	.3630	.3557	.3503	.3461	.3427

ISOTROPIC POINT SOURCE ON CRYSTAL AXIS

12AW(14)-W4 WELL CRYSTAL

D = 7.620000, H = 8.890000  
 WD = 2.857500, WH = 5.080000

ENERGY	B= .00	.10	.20	.30	.40	.50
.010	.9813	.9806	.9799	.9791	.9782	.9773
.015	.9813	.9806	.9799	.9791	.9782	.9773
.020	.9813	.9806	.9799	.9791	.9782	.9773
.030	.9813	.9806	.9799	.9791	.9782	.9773
.040	.9813	.9806	.9799	.9791	.9782	.9773
.050	.9813	.9806	.9799	.9791	.9782	.9773
.060	.9813	.9806	.9799	.9791	.9782	.9773
.080	.9813	.9806	.9799	.9791	.9782	.9773
.100	.9801	.9793	.9784	.9776	.9766	.9756
.150	.9753	.9740	.9727	.9714	.9700	.9687
.200	.9469	.9415	.9374	.9339	.9308	.9279
.300	.8282	.8138	.8041	.7963	.7898	.7841
.400	.7299	.7122	.7008	.6917	.6842	.6778
.500	.6602	.6417	.6299	.6205	.6128	.6063
.600	.6144	.5958	.5839	.5747	.5670	.5605
.800	.5511	.5328	.5213	.5123	.5048	.4986
1.000	.5070	.4893	.4781	.4694	.4623	.4562
1.500	.4369	.4204	.4101	.4021	.3955	.3900
2.000	.3999	.3842	.3745	.3669	.3608	.3555
3.000	.3663	.3515	.3424	.3353	.3295	.3246
4.000	.3538	.3395	.3305	.3236	.3179	.3132
5.000	.3507	.3364	.3275	.3206	.3150	.3103
6.000	.3507	.3364	.3275	.3206	.3150	.3103

ISOTROPIC POINT SOURCE ON CRYSTAL AXIS

2 x 2 IN. SOLID CESIUM IODIDE CRYSTAL

D = 5.080000, H = 5.080000

ENERGY	B= .00	.20	.50	1.00	2.00	5.00	10.00	20.00
.010	.5000	.4608	.4034	.3168	.1907	.0542	.0154	.0040
.015	.5000	.4608	.4034	.3168	.1907	.0542	.0154	.0040
.020	.5000	.4608	.4034	.3168	.1907	.0542	.0154	.0040
.030	.5000	.4608	.4034	.3168	.1907	.0542	.0154	.0040
.040	.5000	.4608	.4034	.3168	.1907	.0542	.0154	.0040
.050	.5000	.4608	.4034	.3168	.1907	.0542	.0154	.0040
.060	.5000	.4608	.4034	.3168	.1907	.0542	.0154	.0040
.080	.5000	.4608	.4034	.3168	.1907	.0542	.0154	.0040
.100	.5000	.4608	.4034	.3168	.1907	.0542	.0154	.0040
.150	.4999	.4535	.3878	.2948	.1717	.0494	.0145	.0039
.200	.4954	.4382	.3660	.2719	.1562	.0458	.0138	.0038
.300	.4537	.3842	.3114	.2262	.1293	.0394	.0125	.0035
.400	.4047	.3361	.2694	.1944	.1114	.0348	.0113	.0032
.500	.3682	.3031	.2417	.1740	.0999	.0316	.0104	.0030
.600	.3433	.2812	.2237	.1609	.0925	.0295	.0098	.0029
.800	.3090	.2518	.1997	.1435	.0827	.0267	.0089	.0026
1.000	.2847	.2312	.1832	.1315	.0759	.0246	.0082	.0024
1.500	.2469	.1997	.1579	.1133	.0655	.0215	.0073	.0022
2.000	.2276	.1838	.1452	.1041	.0603	.0198	.0067	.0020
3.000	.2120	.1709	.1349	.0967	.0561	.0185	.0063	.0019
4.000	.2082	.1678	.1324	.0950	.0551	.0182	.0062	.0019
5.000	.2092	.1687	.1331	.0955	.0554	.0183	.0062	.0019
6.000	.2112	.1702	.1344	.0964	.0559	.0184	.0063	.0019

ISOTROPIC POINT SOURCE ON CRYSTAL AXIS

8F8 CESIUM IODIDE WELL CRYSTAL

D = 5.080000, H = 5.080000

WD = 2.857500, WH = 3.810000

ENERGY	B= .20	.40	.60	1.00	2.00	3.00	3.81
.010	.9649	.9612	.9568	.9457	.8925	.7466	.5000
.015	.9649	.9612	.9568	.9457	.8925	.7466	.5000
.020	.9649	.9612	.9568	.9457	.8925	.7466	.5000
.030	.9649	.9612	.9568	.9457	.8925	.7466	.5000
.040	.9649	.9612	.9568	.9457	.8925	.7466	.5000
.050	.9649	.9612	.9568	.9457	.8925	.7466	.5000
.060	.9649	.9612	.9568	.9457	.8925	.7466	.5000
.080	.9649	.9612	.9568	.9457	.8882	.7396	.5000
.100	.9629	.9588	.9541	.9421	.8845	.7342	.5000
.150	.9442	.9373	.9304	.9151	.8507	.7007	.4901
.200	.8578	.8421	.8293	.8077	.7420	.6106	.4391
.300	.6482	.6240	.6066	.5818	.5274	.4361	.3233
.400	.5186	.4944	.4777	.4550	.4102	.3402	.2554
.500	.4445	.4217	.4062	.3855	.3466	.2880	.2175
.600	.4003	.3788	.3642	.3449	.3097	.2575	.1952
.800	.3454	.3257	.3124	.2952	.2646	.2203	.1676
1.000	.3097	.2915	.2793	.2635	.2359	.1966	.1500
1.500	.2585	.2425	.2320	.2184	.1953	.1629	.1247
2.000	.2341	.2193	.2096	.1971	.1762	.1470	.1127
3.000	.2149	.2012	.1921	.1806	.1613	.1347	.1034
4.000	.2104	.1969	.1880	.1766	.1578	.1317	.1011
5.000	.2117	.1981	.1892	.1778	.1588	.1326	.1018
6.000	.2140	.2003	.1912	.1797	.1605	.1340	.1029

ISOTROPIC POINT SOURCE ON CRYSTAL AXIS  
2 x 2 IN. SOLID CALCIUM IODIDE CRYSTAL

D = 5.080000, H = 5.080000

ENERGY	B = .00	.20	.50	1.00	2.00	5.00	10.00	20.00
.010	.5000	.4608	.4034	.3168	.1907	.0542	.0154	.0040
.015	.5000	.4608	.4034	.3168	.1907	.0542	.0154	.0040
.020	.5000	.4608	.4034	.3168	.1907	.0542	.0154	.0040
.030	.5000	.4608	.4034	.3168	.1907	.0542	.0154	.0040
.040	.5000	.4608	.4034	.3168	.1907	.0542	.0154	.0040
.050	.5000	.4608	.4034	.3168	.1907	.0542	.0154	.0040
.060	.5000	.4608	.4034	.3168	.1907	.0542	.0154	.0040
.080	.5000	.4608	.4034	.3168	.1907	.0542	.0154	.0040
.100	.5000	.4608	.4034	.3168	.1907	.0542	.0154	.0040
.150	.4993	.4492	.3808	.2867	.1660	.0481	.0143	.0038
.200	.4878	.4251	.3512	.2586	.1481	.0439	.0135	.0037
.300	.4296	.3597	.2897	.2096	.1199	.0371	.0119	.0034
.400	.3785	.3122	.2493	.1796	.1030	.0325	.0106	.0031
.500	.3434	.2813	.2238	.1609	.0925	.0295	.0098	.0029
.600	.3198	.2610	.2072	.1489	.0857	.0276	.0092	.0027
.800	.2871	.2332	.1848	.1326	.0766	.0248	.0083	.0025
1.000	.2643	.2141	.1694	.1216	.0703	.0229	.0077	.0023
1.500	.2284	.1844	.1457	.1045	.0605	.0199	.0068	.0020
2.000	.2093	.1687	.1332	.0955	.0554	.0183	.0062	.0019
3.000	.1925	.1549	.1222	.0876	.0509	.0168	.0058	.0017
4.000	.1870	.1504	.1186	.0851	.0494	.0164	.0056	.0017
5.000	.1861	.1497	.1181	.0847	.0492	.0163	.0056	.0017
6.000	.1867	.1502	.1185	.0850	.0493	.0164	.0056	.0017

ISOTROPIC POINT SOURCE ON CRYSTAL AXIS  
8F8 CALCIUM IODIDE WELL CRYSTAL

D = 5.080000, H = 5.080000  
WD = 2.857500, WH = 3.810000

ENERGY	B = .20	.40	.60	1.00	2.00	3.00	3.81
.010	.9649	.9612	.9568	.9457	.8925	.7466	.5000
.015	.9649	.9612	.9568	.9457	.8925	.7466	.5000
.020	.9649	.9612	.9568	.9457	.8925	.7466	.5000
.030	.9649	.9612	.9568	.9457	.8925	.7466	.5000
.040	.9649	.9612	.9568	.9457	.8925	.7466	.5000
.050	.9649	.9612	.9568	.9457	.8925	.7466	.5000
.060	.9649	.9612	.9568	.9457	.8925	.7466	.5000
.080	.9634	.9595	.9548	.9430	.8866	.7372	.5000
.100	.9619	.9576	.9527	.9403	.8812	.7299	.4998
.150	.9194	.9094	.9003	.8825	.8165	.6718	.4753
.200	.7961	.7764	.7613	.7376	.6742	.5555	.4040
.300	.5782	.5536	.5364	.5124	.4631	.3835	.2863
.400	.4640	.4408	.4249	.4036	.3632	.3016	.2274
.500	.4004	.3788	.3642	.3450	.3098	.2576	.1952
.600	.3640	.3417	.3280	.3101	.2782	.2315	.1759
.800	.3131	.2947	.2824	.2665	.2386	.1988	.1516
1.000	.2815	.2645	.2531	.2385	.2135	.1780	.1360
1.500	.2351	.2203	.2105	.1980	.1769	.1477	.1132
2.000	.2118	.1982	.1893	.1779	.1589	.1327	.1018
3.000	.1920	.1794	.1712	.1608	.1435	.1199	.0922
4.000	.1856	.1734	.1654	.1553	.1386	.1158	.0890
5.000	.1846	.1725	.1646	.1545	.1379	.1152	.0886
6.000	.1853	.1732	.1652	.1551	.1385	.1157	.0889



ISOTROPIC DISK SOURCE ON CRYSTAL AXIS

3 x 3 IN. SOLID CRYSTAL

D = 7.620000,			H = 7.620000,			G = 2.000000			
ENERGY	B =	.50	1.00	1.50	2.00	3.00	5.00	10.00	30.00
.010	.5000	.4272	.3598	.3011	.2519	.1784	.0969	.0320	.0040
.015	.5000	.4272	.3598	.3011	.2519	.1784	.0969	.0320	.0040
.020	.5000	.4272	.3598	.3011	.2519	.1784	.0969	.0320	.0040
.030	.5000	.4272	.3598	.3010	.2518	.1783	.0968	.0320	.0040
.040	.5000	.4272	.3598	.3011	.2519	.1784	.0969	.0320	.0040
.050	.5000	.4272	.3598	.3011	.2519	.1784	.0969	.0320	.0040
.060	.5000	.4272	.3597	.3010	.2517	.1782	.0968	.0320	.0040
.080	.5000	.4270	.3588	.2994	.2498	.1763	.0957	.0317	.0040
.100	.5000	.4258	.3557	.2953	.2456	.1727	.0936	.0312	.0039
.150	.4994	.4148	.3394	.2786	.2302	.1612	.0877	.0297	.0039
.200	.4920	.3930	.3163	.2575	.2119	.1482	.0811	.0280	.0038
.300	.4521	.3432	.2719	.2198	.1804	.1264	.0701	.0251	.0035
.400	.4130	.3072	.2420	.1953	.1603	.1126	.0630	.0230	.0034
.500	.3827	.2817	.2214	.1785	.1466	.1032	.0581	.0215	.0032
.600	.3616	.2647	.2078	.1675	.1376	.0970	.0548	.0204	.0031
.800	.3310	.2407	.1887	.1521	.1250	.0883	.0501	.0188	.0029
1.000	.3087	.2236	.1752	.1412	.1161	.0821	.0467	.0176	.0027
1.500	.2718	.1958	.1532	.1235	.1016	.0720	.0412	.0157	.0024
2.000	.2515	.1807	.1414	.1140	.0938	.0665	.0381	.0146	.0023
3.000	.2329	.1670	.1306	.1053	.0867	.0616	.0353	.0136	.0021
4.000	.2255	.1616	.1264	.1019	.0839	.0596	.0342	.0132	.0021
5.000	.2237	.1603	.1253	.1011	.0832	.0591	.0340	.0131	.0020
6.000	.2237	.1603	.1253	.1011	.0832	.0591	.0340	.0131	.0020
8.000	.2269	.1626	.1271	.1025	.0844	.0600	.0344	.0132	.0021
10.000	.2322	.1665	.1302	.1050	.0865	.0614	.0352	.0135	.0021
15.000	.2466	.1771	.1385	.1117	.0920	.0652	.0374	.0143	.0022
20.000	.2586	.1860	.1455	.1173	.0966	.0685	.0392	.0150	.0023

ISOTROPIC DISK SOURCE ON CRYSTAL AXIS  
2 x 2 IN. SOLID CRYSTAL

D = 5.080000 H = 5.080000 G = 1.000000

ENERGY	B = .20	1.00	3.00	10.00	20.00	30.00	10.00	20.00
.010	.4583	.3084	.1146	.0153	.0040	.1146	.0153	.0040
.015	.4583	.3084	.1146	.0153	.0040	.1146	.0153	.0040
.020	.4583	.3084	.1146	.0153	.0040	.1146	.0153	.0040
.030	.4583	.3084	.1146	.0153	.0040	.1146	.0153	.0040
.040	.4583	.3084	.1146	.0153	.0040	.1146	.0153	.0040
.050	.4583	.3084	.1146	.0153	.0040	.1146	.0153	.0040
.060	.4583	.3084	.1146	.0153	.0040	.1146	.0153	.0040
.080	.4582	.3048	.1115	.0151	.0040	.1115	.0151	.0040
.100	.4575	.2983	.1083	.0148	.0039	.1083	.0148	.0039
.150	.4446	.2740	.0984	.0141	.0038	.0984	.0141	.0038
.200	.4123	.2440	.0878	.0132	.0037	.0878	.0132	.0037
.300	.3400	.1950	.0713	.0115	.0033	.0713	.0115	.0033
.400	.2929	.1666	.0615	.0103	.0030	.0615	.0103	.0030
.500	.2619	.1484	.0552	.0094	.0027	.0552	.0094	.0027
.600	.2422	.1371	.0512	.0088	.0026	.0512	.0088	.0026
.800	.2157	.1218	.0457	.0079	.0024	.0457	.0079	.0024
1.000	.1976	.1115	.0420	.0073	.0022	.0420	.0073	.0022
1.500	.1692	.0954	.0361	.0064	.0019	.0361	.0064	.0019
2.000	.1545	.0870	.0330	.0059	.0018	.0330	.0059	.0018
3.000	.1413	.0796	.0302	.0054	.0016	.0302	.0054	.0016
4.000	.1362	.0767	.0292	.0052	.0016	.0292	.0052	.0016
5.000	.1350	.0760	.0289	.0052	.0016	.0289	.0052	.0016
6.000	.1350	.0760	.0289	.0052	.0016	.0289	.0052	.0016

ISOTROPIC DISK SOURCE ON CRYSTAL AXIS  
2 x 2 IN. SOLID CRYSTAL

D = 5.080000 H = 5.080000 G = 2.000000

ENERGY	B = .20	1.00	3.00	10.00	20.00	30.00	10.00	20.00
.010	.4457	.2767	.1037	.0150	.0040	.1037	.0150	.0040
.015	.4457	.2767	.1037	.0150	.0040	.1037	.0150	.0040
.020	.4457	.2767	.1037	.0150	.0040	.1037	.0150	.0040
.030	.4455	.2758	.1034	.0150	.0040	.1034	.0150	.0040
.040	.4457	.2766	.1037	.0150	.0040	.1037	.0150	.0040
.050	.4456	.2763	.1036	.0150	.0040	.1036	.0150	.0040
.060	.4454	.2754	.1032	.0149	.0040	.1032	.0149	.0040
.080	.4437	.2716	.1012	.0148	.0039	.1012	.0148	.0039
.100	.4396	.2653	.0985	.0145	.0039	.0985	.0145	.0039
.150	.4156	.2423	.0901	.0138	.0038	.0901	.0138	.0038
.200	.3779	.2160	.0809	.0130	.0036	.0809	.0130	.0036
.300	.3080	.1740	.0664	.0113	.0033	.0664	.0113	.0033
.400	.2650	.1493	.0576	.0101	.0030	.0576	.0101	.0030
.500	.2370	.1335	.0518	.0092	.0027	.0518	.0092	.0027
.600	.2193	.1235	.0481	.0086	.0026	.0481	.0086	.0026
.800	.1954	.1100	.0430	.0078	.0022	.0430	.0078	.0022
1.000	.1791	.1008	.0396	.0072	.0022	.0396	.0072	.0022
1.500	.1536	.0865	.0341	.0063	.0019	.0341	.0063	.0019
2.000	.1402	.0790	.0312	.0058	.0018	.0312	.0058	.0018
3.000	.1284	.0723	.0286	.0053	.0016	.0286	.0053	.0016
4.000	.1238	.0697	.0276	.0051	.0016	.0276	.0051	.0016
5.000	.1227	.0691	.0274	.0051	.0015	.0274	.0051	.0015
6.000	.1227	.0691	.0274	.0051	.0015	.0274	.0051	.0015

ISOTROPIC DISK SOURCE ON CRYSTAL AXIS  
7F8 WELL CRYSTAL

D = 4.445000  
WD = 1.905000

H = 5.080000  
WH = 3.810000

G = 1.000000

ENERGY	R= .20	.50	.80	1.50	2.00	2.50	3.00	3.81
.010	.9843	.9817	.9783	.9662	.9506	.9227	.8676	.5000
.015	.9843	.9817	.9783	.9662	.9506	.9227	.8676	.5000
.020	.9843	.9817	.9783	.9662	.9506	.9227	.8675	.5000
.030	.9843	.9817	.9783	.9660	.9502	.9217	.8649	.5000
.040	.9843	.9817	.9783	.9662	.9505	.9226	.8673	.5000
.050	.9843	.9817	.9783	.9661	.9504	.9223	.8662	.5000
.060	.9843	.9816	.9783	.9659	.9499	.9212	.8640	.5000
.080	.9840	.9812	.9777	.9647	.9479	.9175	.8580	.5000
.100	.9831	.9801	.9763	.9623	.9442	.9117	.8487	.4999
.150	.9446	.9385	.9332	.9161	.8942	.8557	.7847	.4820
.200	.8213	.8099	.8031	.7857	.7639	.7266	.6615	.4222
.300	.5985	.5845	.5776	.5632	.5463	.5179	.4703	.3120
.400	.4836	.4703	.4640	.4520	.4381	.4151	.3771	.2539
.500	.4169	.4045	.3987	.3882	.3761	.3563	.3238	.2198
.600	.3772	.3655	.3602	.3505	.3396	.3217	.2924	.1994
.800	.3268	.3161	.3113	.3029	.2934	.2779	.2527	.1733
1.000	.2940	.2842	.2797	.2721	.2636	.2496	.2270	.1563
1.500	.2452	.2367	.2329	.2264	.2193	.2077	.1890	.1308
2.000	.2209	.2130	.2095	.2037	.1973	.1869	.1701	.1180
3.000	.1998	.1926	.1894	.1841	.1783	.1689	.1537	.1069
4.000	.1918	.1848	.1818	.1766	.1711	.1621	.1475	.1026
5.000	.1899	.1829	.1799	.1748	.1693	.1604	.1460	.1016
6.000	.1899	.1829	.1799	.1748	.1693	.1604	.1460	.1016
8.000	.1933	.1862	.1831	.1780	.1724	.1633	.1486	.1034
10.000	.1991	.1919	.1887	.1834	.1776	.1682	.1531	.1065

ISOTROPIC DISK SOURCE ON CRYSTAL AXIS  
8F8 WELL CRYSTAL

D = 5.080000  
WD = 2.857500

H = 5.080000  
WH = 3.810000

G = 1.000000

ENERGY	B= .20	.80	1.50	2.00	2.50	3.00	3.80
.010	.9665	.9544	.9310	.9027	.8560	.7749	.5044
.015	.9665	.9544	.9310	.9027	.8560	.7749	.5044
.020	.9665	.9544	.9310	.9027	.8559	.7747	.5044
.030	.9664	.9542	.9305	.9016	.8539	.7712	.5043
.040	.9665	.9544	.9310	.9026	.8558	.7744	.5044
.050	.9664	.9544	.9308	.9022	.8550	.7728	.5043
.060	.9663	.9541	.9302	.9012	.8532	.7702	.5043
.080	.9655	.9528	.9278	.8976	.8482	.7639	.5041
.100	.9635	.9499	.9236	.8919	.8405	.7547	.5035
.150	.9112	.8854	.8535	.8190	.7661	.6844	.4737
.200	.7755	.7340	.7003	.6691	.6241	.5580	.3976
.300	.5537	.5075	.4790	.4563	.4253	.3815	.2793
.400	.4441	.4017	.3775	.3593	.3349	.3009	.2225
.500	.3813	.3425	.3211	.3055	.2848	.2561	.1904
.600	.3443	.3081	.2885	.2744	.2558	.2302	.1716
.800	.2975	.2649	.2477	.2355	.2196	.1977	.1479
1.000	.2673	.2372	.2216	.2107	.1965	.1770	.1327
1.500	.2224	.1965	.1834	.1743	.1625	.1465	.1102
2.000	.2001	.1764	.1645	.1563	.1458	.1315	.0991
3.000	.1809	.1592	.1483	.1409	.1315	.1186	.0895
4.000	.1736	.1526	.1422	.1351	.1261	.1137	.0858
5.000	.1718	.1510	.1407	.1337	.1247	.1125	.0849
6.000	.1718	.1511	.1407	.1337	.1247	.1125	.0849
8.000	.1749	.1538	.1433	.1362	.1270	.1146	.0865
10.000	.1802	.1586	.1478	.1404	.1310	.1181	.0891
15.000	.1950	.1718	.1602	.1522	.1420	.1280	.0965
20.000	.2078	.1833	.1710	.1625	.1516	.1366	.1029
30.000	.2286	.2021	.1886	.1793	.1672	.1507	.1133

ISOTROPIC DISK SOURCE ON CRYSTAL AXIS

8F8 WELL CRYSTAL

D = 5.080000, H = 5.080000, B = .50

WD = 2.857500, WH = 3.810000

ENERGY	G = .00	.10	.15	.25	.50	.75	1.00	1.43
.010	.9591	.9591	.9591	.9592	.9596	.9602	.9611	.9632
.015	.9591	.9591	.9591	.9592	.9596	.9602	.9611	.9632
.020	.9591	.9591	.9591	.9592	.9596	.9602	.9611	.9632
.030	.9590	.9590	.9590	.9591	.9595	.9601	.9610	.9630
.040	.9591	.9591	.9591	.9592	.9596	.9602	.9611	.9632
.050	.9590	.9591	.9591	.9592	.9596	.9602	.9611	.9631
.060	.9589	.9589	.9589	.9590	.9594	.9600	.9609	.9629
.080	.9575	.9576	.9576	.9577	.9581	.9588	.9598	.9620
.100	.9547	.9547	.9548	.9549	.9554	.9563	.9574	.9600
.150	.8900	.8901	.8902	.8905	.8917	.8940	.8973	.9061
.200	.7398	.7399	.7400	.7404	.7422	.7455	.7507	.7668
.300	.5137	.5138	.5139	.5143	.5161	.5194	.5248	.5429
.400	.4074	.4075	.4076	.4079	.4095	.4124	.4172	.4338
.500	.3477	.3478	.3479	.3482	.3496	.3522	.3565	.3717
.600	.3129	.3130	.3131	.3133	.3147	.3171	.3211	.3353
.800	.2692	.2693	.2694	.2696	.2708	.2729	.2765	.2893
1.000	.2412	.2413	.2414	.2416	.2427	.2446	.2479	.2597
1.500	.2000	.2001	.2001	.2003	.2012	.2029	.2057	.2158
2.000	.1796	.1797	.1797	.1799	.1807	.1823	.1848	.1940
3.000	.1621	.1621	.1622	.1623	.1631	.1645	.1668	.1753
4.000	.1555	.1555	.1555	.1557	.1564	.1578	.1600	.1682
5.000	.1538	.1539	.1539	.1541	.1548	.1561	.1584	.1664
6.000	.1538	.1539	.1539	.1541	.1548	.1561	.1584	.1664
8.000	.1567	.1567	.1567	.1569	.1576	.1590	.1612	.1695
10.000	.1615	.1615	.1616	.1617	.1625	.1639	.1662	.1746
15.000	.1749	.1750	.1750	.1752	.1760	.1775	.1800	.1890
20.000	.1866	.1867	.1867	.1869	.1878	.1893	.1920	.2015
30.000	.2057	.2057	.2058	.2060	.2069	.2086	.2115	.2218

ISOTROPIC DISK SOURCE ON CRYSTAL AXIS

12AW(12)-W2 WELL CRYSTAL

B = .50

H = 7.620000,

D = 7.620000,

WH = 3.810000

WD = 2.857500,

ENERGY	G = .00	.15	.25	.50	.75	1.00	1.43
.010	.9591	.9591	.9592	.9596	.9602	.9611	.9632
.015	.9591	.9591	.9592	.9596	.9602	.9611	.9632
.020	.9591	.9591	.9592	.9596	.9602	.9611	.9632
.030	.9591	.9591	.9592	.9596	.9602	.9611	.9632
.040	.9591	.9591	.9592	.9596	.9602	.9611	.9632
.050	.9591	.9591	.9592	.9596	.9602	.9611	.9632
.060	.9591	.9591	.9592	.9596	.9602	.9611	.9632
.080	.9585	.9586	.9586	.9590	.9596	.9605	.9625
.100	.9564	.9564	.9565	.9570	.9577	.9588	.9611
.150	.9435	.9436	.9437	.9445	.9458	.9476	.9517
.200	.8967	.8968	.8971	.8983	.9005	.9037	.9118
.300	.7504	.7505	.7509	.7526	.7555	.7601	.7733
.400	.6461	.6462	.6466	.6483	.6513	.6559	.6700
.500	.5768	.5769	.5772	.5788	.5817	.5862	.6001
.600	.5326	.5327	.5331	.5346	.5374	.5417	.5552
.800	.4731	.4732	.4735	.4750	.4775	.4815	.4944
1.000	.4326	.4327	.4330	.4343	.4367	.4405	.4527
1.500	.3694	.3694	.3697	.3709	.3730	.3764	.3874
2.000	.3366	.3366	.3368	.3380	.3399	.3431	.3533
3.000	.3075	.3075	.3078	.3088	.3106	.3135	.3231
4.000	.2962	.2963	.2965	.2975	.2993	.3021	.3114
5.000	.2935	.2936	.2938	.2947	.2965	.2993	.3085
6.000	.2935	.2936	.2938	.2947	.2965	.2993	.3085
8.000	.2983	.2984	.2986	.2996	.3013	.3042	.3135
10.000	.3064	.3065	.3067	.3077	.3095	.3124	.3220
15.000	.3288	.3289	.3291	.3302	.3322	.3352	.3453

ISOTROPIC DISK SOURCE ON CRYSTAL AXIS

3 x 3 IN. SOLID CRYSTAL

D = 7.62  
H = 7.62  
B = .20  
G = 1.0

ENERGY	WD=2.009 WH=3.81	WD=2.8575 WH=3.81	WD=2.009 WH=5.08	WD=2.8575 WH=5.08
.010	.9826	.9665	.9900	.9804
.015	.9826	.9665	.9900	.9804
.020	.9826	.9665	.9900	.9804
.030	.9826	.9665	.9900	.9804
.040	.9826	.9665	.9900	.9804
.050	.9826	.9665	.9900	.9804
.060	.9826	.9664	.9900	.9803
.080	.9825	.9661	.9900	.9799
.100	.9820	.9647	.9899	.9740
.150	.9769	.9554	.9870	.9357
.200	.9504	.9167	.9605	.7917
.300	.8323	.7820	.8357	.6836
.400	.7327	.6801	.7320	.6108
.500	.6621	.6106	.6594	.5642
.600	.6158	.5658	.6120	.5013
.800	.5518	.5047	.5470	.4584
1.000	.5073	.4627	.5020	.3914
1.500	.4367	.3967	.4310	.3565
2.000	.3994	.3622	.3937	.3257
3.000	.3661	.3314	.3605	.3138
4.000	.3532	.3195	.3476	.3109
5.000	.3500	.3166	.3444	.3109
6.000	.3500	.3166	.3444	.3109
8.000	.3556	.3217	.3499	.3160
10.000	.3649	.3303	.3592	.3246
15.000	.3906	.3540	.3849	.3484
20.000	.4124	.3741	.4066	.3686
30.000	.4467	.4061	.4411	.4008

ISOTROPIC CYLINDRICAL VOLUME SOURCE ON CRYSTAL AXIS

2 x 2 IN. SOLID CRYSTAL

D = 5.080000, H = 5.080000  
G = 1.270000, B1 = .300000

ENERGY	B2=1.30	3.30	6.30	10.30	15.30
.010	.3400	.2218	.1408	.0928	.0630
.015	.3400	.2218	.1408	.0928	.0630
.020	.3400	.2218	.1408	.0928	.0630
.030	.3394	.2210	.1402	.0923	.0626
.040	.3400	.2218	.1408	.0927	.0630
.050	.3398	.2215	.1405	.0926	.0628
.060	.3391	.2206	.1399	.0921	.0625
.080	.3358	.2174	.1377	.0906	.0614
.100	.3302	.2128	.1346	.0885	.0599
.150	.3071	.1958	.1237	.0812	.0549
.200	.2759	.1749	.1106	.0727	.0493
.300	.2220	.1408	.0895	.0591	.0403
.400	.1900	.1207	.0770	.0510	.0348
.500	.1695	.1078	.0689	.0457	.0313
.600	.1566	.0997	.0638	.0424	.0290
.800	.1393	.0888	.0569	.0379	.0260
1.000	.1275	.0813	.0522	.0347	.0238
1.500	.1091	.0697	.0448	.0299	.0205
2.000	.0996	.0636	.0409	.0273	.0188
3.000	.0911	.0582	.0375	.0250	.0172
4.000	.0878	.0562	.0362	.0241	.0166
5.000	.0870	.0556	.0358	.0239	.0165
6.000	.0870	.0556	.0358	.0239	.0165

ISOTROPIC CYLINDRICAL VOLUME SOURCE ON CRYSTAL AXIS

2 x 2 IN. SOLID CRYSTAL

D = 5.080000, H = 5.080000  
 G = 2.540000, BI = .300000

ENERGY	B2=1.30	3.30	6.30	10.30	15.30
.010	.2801	.1824	.1173	.0778	.0533
.015	.2800	.1824	.1173	.0778	.0533
.020	.2798	.1823	.1172	.0778	.0533
.030	.2785	.1813	.1166	.0774	.0530
.040	.2797	.1823	.1172	.0778	.0533
.050	.2791	.1818	.1170	.0776	.0531
.060	.2780	.1810	.1164	.0772	.0529
.080	.2743	.1783	.1146	.0760	.0521
.100	.2686	.1743	.1121	.0744	.0509
.150	.2477	.1604	.1033	.0687	.0471
.200	.2227	.1443	.0932	.0622	.0428
.300	.1815	.1180	.0767	.0514	.0356
.400	.1567	.1021	.0666	.0448	.0310
.500	.1405	.0917	.0599	.0403	.0280
.600	.1302	.0851	.0556	.0375	.0261
.800	.1163	.0760	.0498	.0336	.0234
1.000	.1068	.0699	.0458	.0309	.0215
1.500	.0918	.0601	.0394	.0267	.0186
2.000	.0839	.0550	.0361	.0244	.0170
3.000	.0769	.0504	.0331	.0224	.0156
4.000	.0742	.0486	.0320	.0216	.0151
5.000	.0735	.0482	.0317	.0214	.0150
6.000	.0735	.0482	.0317	.0214	.0150

ISOTROPIC CYLINDRICAL VOLUME SOURCE ON CRYSTAL AXIS

3 x 3 IN. SOLID CRYSTAL

D = 7.620000, H = 7.620000  
 G = 1.000000, BI = 1.000000

ENERGY	B2=1.10	1.20	1.50
.010	.3641	.3582	.3410
.015	.3641	.3582	.3410
.020	.3641	.3582	.3410
.030	.3641	.3582	.3410
.040	.3641	.3582	.3410
.050	.3641	.3582	.3410
.060	.3641	.3581	.3409
.080	.3630	.3570	.3394
.100	.3596	.3534	.3356
.150	.3449	.3386	.3204
.200	.3233	.3169	.2990
.300	.2786	.2728	.2565
.400	.2479	.2426	.2280
.500	.2266	.2218	.2083
.600	.2126	.2080	.1953
.800	.1929	.1888	.1772
1.000	.1790	.1752	.1644
1.500	.1565	.1531	.1437
2.000	.1443	.1412	.1325
3.000	.1333	.1304	.1224
4.000	.1289	.1261	.1184
5.000	.1279	.1251	.1174
6.000	.1279	.1251	.1174
8.000	.1297	.1269	.1191
10.000	.1329	.1300	.1220
15.000	.1414	.1383	.1299
20.000	.1486	.1453	.1364
30.000	.1597	.1563	.1467

ISOTROPIC CYLINDRICAL VOLUME SOURCE ON CRYSTAL AXIS

3 x 3 IN. SOLID CRYSTAL

3 x 3 IN. SOLID CRYSTAL

		D = 7.620000, H = 7.620000, D = 7.620000, H = 7.620000				G = 1.905000, B1 = .300000, G = 3.810000, B1 = .300000					
		82=1.30		3.30		6.30		10.30		15.30	
ENERGY											
.010	.3883	.2850	.1962	.1362	.0972	.3272	.2347	.1626	.1137	.0814	
.015	.3883	.2850	.1962	.1362	.0972	.3272	.2347	.1626	.1137	.0814	
.020	.3883	.2850	.1962	.1362	.0972	.3271	.2347	.1626	.1137	.0814	
.030	.3882	.2847	.1960	.1360	.0970	.3261	.2340	.1622	.1134	.0812	
.040	.3883	.2850	.1962	.1362	.0972	.3270	.2346	.1626	.1137	.0814	
.050	.3883	.2849	.1962	.1362	.0971	.3266	.2344	.1624	.1136	.0813	
.060	.3881	.2846	.1958	.1359	.0969	.3258	.2338	.1620	.1133	.0811	
.080	.3870	.2826	.1941	.1346	.0959	.3234	.2317	.1604	.1122	.0803	
.100	.3843	.2791	.1913	.1326	.0943	.3192	.2283	.1580	.1105	.0790	
.150	.3705	.2655	.1812	.1253	.0890	.3032	.2160	.1494	.1045	.0748	
.200	.3489	.2472	.1682	.1163	.0825	.2826	.2008	.1390	.0973	.0698	
.300	.3028	.2124	.1445	.1001	.0711	.2450	.1739	.1206	.0848	.0610	
.400	.2704	.1892	.1289	.0895	.0637	.2198	.1561	.1085	.0765	.0551	
.500	.2477	.1732	.1182	.0821	.0586	.2022	.1436	.1000	.0706	.0509	
.600	.2326	.1626	.1111	.0773	.0551	.1904	.1353	.0943	.0666	.0481	
.800	.2114	.1478	.1011	.0704	.0503	.1738	.1236	.0862	.0610	.0441	
1.000	.1964	.1373	.0940	.0655	.0468	.1619	.1152	.0804	.0569	.0412	
1.500	.1718	.1202	.0824	.0575	.0412	.1424	.1013	.0708	.0502	.0364	
2.000	.1586	.1109	.0761	.0532	.0381	.1317	.0938	.0656	.0465	.0337	
3.000	.1465	.1025	.0704	.0492	.0353	.1220	.0869	.0608	.0431	.0313	
4.000	.1418	.0992	.0681	.0476	.0341	.1181	.0841	.0589	.0418	.0303	
5.000	.1406	.0984	.0676	.0472	.0339	.1172	.0835	.0584	.0415	.0301	
6.000	.1406	.0984	.0676	.0472	.0339	.1172	.0835	.0584	.0415	.0301	



ISOTROPIC CYLINDRICAL VOLUME SOURCE ON CRYSTAL AXIS ISOTROPIC CYLINDRICAL VOLUME SOURCE ON CRYSTAL AXIS

7F8 WELL CRYSTAL

8F8 WELL CRYSTAL

12AW(12)-W2 WELL CRYSTAL

7F8 WELL CRYSTAL				8F8 WELL CRYSTAL				12AW(12)-W2 WELL CRYSTAL			
D =	H =	B1 =	WH =	D =	H =	B1 =	WH =	D =	H =	B1 =	WH =
4.445000,	5.080000	.300000	3.810000	5.080000,	5.080000,	1.428750,	2.857500,	7.620000,	7.620000,	1.428750,	3.810000
.952500,	.300000			.300000				1.428750,			
1.905000,	3.810000			3.810000				2.857500,			
ENERGY	B2=1.30	2.30	3.81	ENERGY	B2=1.30	2.30	3.80	ENERGY	B2=1.30	2.30	3.81
.9777	.9667	.9054	.9667	.9565	.9390	.8688	.8688	.010	.9565	.9390	.8678
.9777	.9667	.9054	.9667	.9565	.9390	.8687	.8687	.015	.9565	.9390	.8678
.9777	.9667	.9054	.9667	.9565	.9390	.8684	.8684	.020	.9565	.9390	.8676
.9776	.9664	.9033	.9664	.9561	.9383	.8668	.8668	.030	.9563	.9386	.8661
.9777	.9667	.9049	.9667	.9565	.9389	.8683	.8683	.040	.9565	.9390	.8675
.9777	.9666	.9040	.9666	.9563	.9386	.8675	.8675	.050	.9564	.9388	.8668
.9775	.9662	.9028	.9662	.9559	.9380	.8663	.8663	.060	.9562	.9384	.8657
.9768	.9649	.8991	.9649	.9547	.9363	.8628	.8628	.080	.9551	.9366	.8622
.9753	.9626	.8932	.9626	.9524	.9331	.8572	.8572	.100	.9532	.9338	.8569
.9314	.9157	.8401	.9157	.8961	.8735	.7956	.7956	.150	.9424	.9193	.8358
.8001	.7839	.7154	.7839	.7547	.7315	.6632	.6632	.200	.8999	.8727	.7885
.5741	.5609	.5109	.5609	.5314	.5121	.4632	.4632	.300	.7586	.7298	.6564
.4608	.4498	.4097	.4498	.4236	.4074	.3683	.3683	.400	.6551	.6279	.5643
.3558	.3481	.3318	.3481	.3626	.3483	.3148	.3148	.500	.5857	.5603	.5033
.3575	.3486	.3177	.3486	.3268	.3138	.2836	.2836	.600	.5413	.5172	.4646
.3089	.3011	.2745	.3011	.2817	.2703	.2443	.2443	.800	.4813	.4592	.4124
.2775	.2705	.2466	.2705	.2528	.2424	.2191	.2191	1.000	.4403	.4198	.3770
.2309	.2250	.2052	.2250	.2099	.2011	.1818	.1818	1.800	.3763	.3583	.3217
.2078	.2024	.1846	.2024	.1887	.1807	.1634	.1634	2.000	.3430	.3263	.2931
.1878	.1829	.1669	.1829	.1704	.1632	.1475	.1475	3.000	2.000	3.000	2.677
.1602	.1555	.1401	.1555	.1635	.1565	.1415	.1415	4.000	3.000	4.000	2.931
.1783	.1737	.1585	.1737	.1618	.1549	.1400	.1400	5.000	3.000	5.000	2.981
.1783	.1737	.1585	.1737	.1618	.1549	.1400	.1400	6.000	3.000	6.000	2.981

## REFERENCES

1. R. Hofstadter, Phys. Rev., 74, 100 (1948); 75, 796 (1949); 79, 389 (1950).
2. W. J. Price, Nuclear Radiation Detection, McGraw-Hill, New York, 2nd Ed., 1964.
3. M. L. Verheijke, Nucl. Instr. and Methods, 30, 357 (1965).
4. D. Engelkemeir, Rev. Sci. Instr., 27, 589 (1956).
5. S. H. Vegors, L. L. Marsden, R. L. Heath, AEC Report IDO-16370, (1958).
6. E. A. Wolicki, R. Jastrow, and F. Brooks, Naval Research Laboratory Report No. 4833 (1956).
7. C. C. Grosjean, Nucl. Instr. and Methods, 17, 289 (1962).
8. W. F. Miller and W. J. Snow, Rev. Sci. Instr., 28, 717 (1957); and AEC Report ANL-5902 (1958).
9. W. F. Miller and W. J. Snow, Nucleonics, 11, 174 (1961); and AEC Report ANL-6318 (1961).
10. A. L. Stanford and W. K. Rivers, Rev. Sci. Instr., 29, 406 (1958).
11. C. D. Zerby and H. S. Moran, Nucl. Instr. and Methods, 14, 115 (1961); also AEC Reports ORNL-3169 (1962), and CF-60-5-72 (1960); see also Reference 38.
12. P. R. Bell, in Beta and Gamma Spectrometry, K. Siegbahn, ed., North-Holland Pub., Amsterdam, 1955.
13. C. E. Crouthamel, Applied Gamma Ray Spectrometry, Pergamon Press, New York, 1960.
14. M. L. Verheijki, Intern. J. Appl. Radiation and Isotopes, 13, 583 (1962).
15. A. H. Jaffey, AEC Report ANL-4875 (1953).
16. Harshaw Chemical Co., Scintillation Crystal Catalog, Cleveland, Ohio.
17. W. E. Mott and R. B. Sutton, in Handbuch der Physik, 45, Springer Verlag, Berlin, 1959.

18. M. L. Verheijke, Intern. J. Appl. Radiation and Isotopes, 15, 559 (1964).
19. J. A. Harshaw, AEC Report NYO-1577 (1952).
20. G. W. Grodstein, National Bureau of Standards, Circular-583 (1957).
21. R. T. McGinnies, National Bureau of Standards, Supplement to Circular-583 (1959).
22. E. Storm, AEC Report LA-2237 (1957).
23. E. D. Cashwell and C. J. Everett, The Monte Carlo Method for Random Walk Problems, Pergamon Press, New York, 1959.
24. H. Kahn, AEC Reports AECU-3259 (1954); RM-1237-AEC.
25. National Bureau of Standards, Applied Mathematics Series No. 12 (1951).
26. H. A. Meyer, ed., Monte Carlo Methods, Wiley, New York, 1956.
27. U. Fano, in Handbuch der Physik, 38, part 2, Springer Verlag, Berlin, 1959.
28. G. Goertzel and M. H. Kalos, in Progress in Nuclear Energy, 2, Series 1, Pergamon Press, New York, 1958.
29. Y. A. Shreider, Methods of Statistical Testing, Elsevier, Amsterdam, N. Y., 1964.
30. Michigan Executive Systems Subroutines for the IBM-7090 Computer, University of Michigan (1964).
31. O. Klein and Y. Nishina, Z. Physik, 52, 853 (1929).
32. C. M. Davisson and L. A. Beach, Naval Research Laboratory, Report No. 5408 (1959).
33. R. Hofstadter and J. A. McIntyre, Phys. Rev., 76, 1269 (1949); and 80, 631 (1950).
34. K. H. Spring, Photons and Electrons, Menthuen, London, 1960.
35. A. T. Nelms, National Bureau of Standards, Circular 542 (1953).
36. L. V. Spencer and C. Wolff, Phys. Rev., 90, 510 (1953).
37. W. Heitler, The Quantum Theory of Radiation, Oxford, 1954.

38. C. D. Zerby, in Methods in Computational Physics, 1, B. Alder, ed., Academic Press, New York, 1962.
39. C. M. Davisson and R. D. Evans, Rev. Mod. Phys., 24, 79 (1952).
40. F. Sauter, Ann. Physik, 11, 454 (1931).
41. D. C. Kleinecke, Civil Defense Research Project Report No. 182-102, Univ. of Calif., Berkeley (1962).
42. H. A. Bethe and J. Ashkin, in Experimental Nuclear Physics, 1, E. Segré, ed. Wiley, New York, 1953.
43. H. Klarmann and W. Bothe, Z. Physik, 101, 489 (1936).
44. A. T. Nelms, National Bureau of Standards, Circular 577 (1956), and Supplement (1958).
45. H. H. Seliger, Phys. Rev., 100, 1034 (1955).
46. K. Wainio, private communication (1965).
47. M. Berger, in Methods in Computational Physics, 1, B. Alder, ed., Academic Press, New York, 1962.
48. B.N.C. Agu, Proc. Roy. Soc. London, 72, 727 (1958).
49. C. D. Zerby and H. S. Moran, AEC Report ORNL-2454 (1958).
50. H. W. Koch and J. W. Motz, Rev. Mod. Phys., 31, 920 (1959).
51. H. A. Bethe and W. Heitler, Proc. Roy. Soc. (London), A146, 83 (1934).
52. H. A. Bethe, in Handbuch der Physik, 24, Springer Verlag, Berlin, 1933.
53. R. D. Evans, The Atomic Nucleus, McGraw-Hill, New York, 1955.
54. C. D. Zerby, private communication (1964).
55. L. Schiff, Phys. Rev., 70, 87L (1946).
56. K. A. Brownlee, Statistical Theory and Methodology in Science and Engineering, Wiley, New York, 1960.
57. D. Redon, Nucl. Instr. and Methods, 26, 18 (1964).
58. J. L. Crane and R. C. Doerner, Nucl. Sci. and Eng., 16, 259 (1963).
59. J. E. Francis, P. R. Bell, C. C. Harris, AEC Report ORNL-1975 (1955).

60. J. G. Campbell, A. J. F. Boyle, Australian J. Phys., 6, 171 (1953); and 7, 284 (1954).
61. R. S. Foote and H. W. Koch, Rev. Sci. Instr., 25, 746 (1954).
62. D. Maeder, R. Müller, and V. Wintersteiger, Helv. Phys. Acta, 27, 3 (1954).
63. R. L. Heath, et al., AEC Reports ORNL-1415 (1952); and IDO-16149 (1st Rev.) (1955).
64. R. Stephenson and P. R. Bell, AEC Report 1705 (1954).
65. F. K. McGowan, Phys. Rev., 93, 163 (1954).
66. W. E. Kreger, Phys. Rev., 96, 1554 (1954).
67. Proceedings of the Total Absorption Gamma Ray Spectrometer Symposium, AEC Report TID-7594 (1960); articles by W. E. Kreger and R. M. Brown, B. M. Branson, et al., W. H. Ellett, and R. L. Heath.
68. W. E. Kreger and R. M. Brown, Nucl. Instr. and Methods, 11, 290 (1961).
69. N. H. Lazar and H. B. Willard, AEC Report ORNL-2076 (1956).
70. L. Jarczyk, et al., Nucl. Instr. and Methods, 17, 310 (1962).
71. C. Weitkamp, Nucl. Instr. and Methods, 23, 10 (1963).
72. M. J. Berger and J. Doggett, J. Research National Bureau of Standards, 56, 355 (1956); and Rev. Sci. Instr., 27, 269 (1956).
73. Proceedings of the Total Absorption Gamma Ray Spectrometer Symposium, AEC Report TID-7594 (1960); articles by H. S. Moran, R. W. Pelle, M. H. Wächter, and C. D. Zerby, et al.
74. M. H. Wächter, Rev. Sci. Instr., 31, 626 (1960).
75. C. M. Davisson and G. R. Gossett, Naval Research Laboratory, Quarterly Progress Report, (Oct., 1961).
76. H. O. Anger and D. H. Davis, Rev. Sci. Instr., 35, 693 (1964).
77. J. I. Trombka, Ph. D. Thesis, Univ. of Michigan (1961).
78. N. H. Lazar, R. C. Davis and P. R. Bell, Nucleonics (April, 1956)
79. J. E. Francis, C. C. Harris and J. I. Trombka, AEC Report ORNL-2204 (1956).



80. L. J. Colby and J. W. Cobble, Anal. Chem., 31, 798 (1959).
81. S. V. Nablo and T. C. Martin, Intern. J. Appl. Radiation and Isotopes, 10, 55 (1961).
82. R. Gunnick and A. W. Stoner, Anal. Chem., 33, 1311 (1961).
83. R. L. Heath, AEC Reports IDO-16408 (1957); and IDO-16880 (1964).
84. U.S. National Academy of Sciences, National Research Council Publication No. 573 (1958).
85. W. C. Roesch, R. C. McCall, and H. E. Palmer, AEC Report HW-67045 (1960).
86. R. C. McCall and K. Liden, Arkiv för Fysik, 22, 497 (1962).
87. Isotopes, Inc., Scintillation Crystal Catalog, Westwood, N.J.
88. R. Hofstadter, E. W. O'Dell, and C. T. Schmidt, Rev. Sci. Instr., 35, 246 (1964).
89. M. B. Gloss, Nucleonics, 22, No. 5, 50 (1964).
90. Michigan Algorithm Decoder (MAD) Manual, University of Michigan, (1964).
91. E. I. Organick, A Computer Primer for the MAD Language, Cushing-Malloy, Ann Arbor, Michigan, 1962.
92. F. B. Hildebrand, Introduction to Numerical Analysis, McGraw Hill, New York, 1960.